GRID-ENHANCING TECHNOLOGIES IN POWER SYSTEM OPERATION AND PLANNING: MODELS, SOLUTION METHODS, AND MARKET MECHANISMS

by

Xinyang Rui

A dissertation submitted to the faculty of
The University of Utah
in partial fulfillment of the requirements for the degree of

Doctor of Philosophy

Department of Electrical and Computer Engineering

The University of Utah

May 2024

The University of Utah Graduate School

STATEMENT OF DISSERTATION APPROVAL

The dissertation of **Xinyang Rui**
has been approved by the following supervisory committee members:

Mostafa Ardakani ,	Chair(s)	__ Date Approved
Mingxi Liu ,	Member	__ Date Approved
Marc Bodson ,	Member	__ Date Approved
Mingyue Ji ,	Member	__ Date Approved
Hari Sundar ,	Member	__ Date Approved

by **Hanseup Kim** , Chair/Dean of
the Department/College/School of **Electrical and Computer Engineering**
and by **Darryl P. Butt** , Dean of The Graduate School.

ABSTRACT

Congestion in the transmission system hinders the utilization of efficient and clean renewable energy sources (RES). Upgrades in the transmission network are needed to alleviate congestion and ensure the delivery of cheap energy from generation to load centers. Such upgrades can be achieved by deploying grid-enhancing technologies (GETs), which unlock constraints of the transmission system by regulating its key parameters, thus improving flexibility and reducing congestion. GETs are regarded as an efficient alternative to constructing new transmission lines and their benefits are widely studied by the literature. However, increasing the deployment of GETs in the existing power grid faces some key barriers. First, utilizing GETs requires their integration into power system operation models. Their modeling must reflect the operating principles and be compatible with energy management systems. Additionally, GET integration requires efficient solution techniques to overcome the computational challenges caused by extra constraints and variables. Second, under the existing market structure, financial compensation to GET projects is minimal. Proper financial compensation to investors following a performance-based approach is essential to incentivize GET investments.

This dissertation focuses on facilitating the deployment of GETs in the power system by focusing on overcoming vital barriers. Extensive research has been conducted on incorporating GET operations in power system optimization. Newly developed and existing prominent algorithms are utilized to facilitate the solution process of various power system optimization problems with GET operation included. GETs are incorporated into optimization problems, including basic power system operation models, distributed control schemes, stochastic programs considering RES integration, and planning models. Additionally, proper and efficient modeling is proposed for prominent power flow controllers, allowing their smooth integration into power system operation and planning models. Furthermore, research is conducted on market mechanisms that provide adequate incentives to GET investments and operations. An incentive scheme for GETs

is developed, which uses an improved Shapley value for benefit allocation among market participants. Moreover, a market design utilizing shadow prices for GET payoff calculation is proposed, and revenue adequacy is proved with mathematical derivations. For both proposed mechanisms, financial rewards are based on the performance of GET operations in increasing social welfare. The effectiveness of the models, algorithms, and market designs in this project is tested by numerical studies on test systems of various sizes and operating conditions.

Dedicated to my parents.

CONTENTS

LIST OF FIGURES

LIST OF TABLES

ACKNOWLEDGEMENTS

First, I would like to express my deep appreciation to my Ph.D. advisor, Prof. Mostafa Ardakani. Working as a PhD student in his group has allowed me to gain tremendous knowledge in the research area of power systems. Over the years, he has provided me with valuable guidance and treated me with patience, and I have grown so much, not just as a young researcher but also as a person working with him.

I would also like to thank my Ph.D. committee members, Dr. Mingxi Liu, Dr. Marc Bodson, Dr. Mingyue Ji, and Dr. Hari Sundar, for their valuable feedback on my research, allowing me to strengthen my understanding of many important topics in my research area as well as related fields.

I would like to thank my coauthors, Prof. Ardakani, Dr. Liu, Dr. Sayed Abdullah Sadat, Dr. Thomas R. Nudell, Omid Mirzapour, and Brittany Pruneau. Collaboration with them made the publication during my Ph.D. studies possible.

I am also very grateful to former members of the Ardaknai Lab, Dr. Yuanrui Sang and Dr. Farshad Mohammadi. During the early stage of my Ph.D. studies, they generously shared their experiences as senior Ph.D. students and provided me with valuable mentorship.

My gratitude also goes to collaborators from the industry, Dr. Nudell, and his former employer, Smart Wires Inc., for whom I worked as a summer intern in 2019. The incredible industry experience provided by them will be valuable for me in the future as I continue to work in this field.

Finally, research conducted in this dissertation is supported by the National Science Foundation (NSF) under grant numbers 1756006 and 2146531.

CHAPTER 1

INTROCUTION

This dissertation focuses on facilitating the integration of grid-enhancing technologies (GETs) into power system operation and planning. GETs are capable of reducing congestion in the power grid by regulating key parameters of the transmission system. Improving the utilization of GETs is currently facing challenges. Research conducted for this dissertation seeks to address these issues.

1.1 Background and Motivations

The transition in the power sector towards more efficient and environmentally friendly renewable energy sources (RES) poses challenges to the transmission grid. Congestion in the transmission system, caused by insufficient transfer capability, hinders the delivery of RES. Additionally, congestion leads to immense costs, with 20.8 billion dollars across the U.S. in 2022 [2]. Therefore, transmission system upgrades that enhance the transfer capability are critical. Constructing new transmission lines is a straightforward approach to add more capacity to the system. However, it suffers from lengthy processes and high costs. Grid-enhancing technologies (GETs) offer an efficient alternative for transfer capability enhancement. GETs are hardware and software tools that improve the utilization of the existing grid [4]. Prominent examples of GETs include series flexible AC transmission systems (FACTS), dynamic line rating (DLR), phase-shifting transformers (PSTs), and transmission switching (TS). They can achieve congestion alleviation by regulating the parameters of the transmission systems, such as line reactance, thermal capacities, voltage phase angles, and system topology.

There are two significant challenges to increasing the deployment of GETs in the power grid. First, fully utilizing GETs requires integration into power system operation and planning models. For operation, integrating GET operating constraints in optimization problems such as the DC optimal power flow (DCOPF) is essential to achieve optimal

generation dispatch and GET setpoint. As for planning, it is critical to determine the optimal allocation, including location and sizing, of GETs in the transmission network. However, GETs introduce extra constraints and variables, which adds to the computational complexity of operation and planning problems, which can be already computationally demanding. Therefore, efficient modeling and solution methodologies are essential to overcome this problem. Second, proper financial incentives for GET investments are currently lacking. Adequate financial incentives are necessary to facilitate GETs proliferation. The research presented in this dissertation aims to tackle the challenges mentioned above.

1.1.1 GETs in Power System Optimization Models

Power system operation requires the frequent solution process of optimization models such as the DCOPF and its variants. The addition of GETs requires proper mathematical models to reflect the operating principles of the technologies. This includes the added variables and constraint formulations. GET modeling in DC power flow has been widely studied in previous research. A common approach is directly adding variables to the $b - \theta$ formulation of the DC power flow equation. For example, variable-impedance FACTS can be modeled with setting line susceptance b as a variable [13, 11]. Such modeling introduces bilinear terms that cause nonlinearity in the DC power flow equation. The nonlinearity issue can be addressed with mixed-integer reformulation using the big-M method [1, 10]. The $b - \theta$ formulation suffers from scalability issues [12]. Therefore, GET operations are also modeled as nodal injections, allowing compatibility with problem formulations using the injection shift factors (ISFs) or the power transfer distribution factors (PTDFs). These sensitivity factors are derived based on the topology of the transmission system and line susceptances. The nodal injection modeling introduces terms that separate GET operations from the original DC power flow equation, thus preserving system topology for the formulation and application of the original ISF matrix regardless of GET allocation. Previous studies have proposed GET modeling that facilitates the derivation of nodal injections for variable-impedance FACTS, PSTs, and TS [12, 15, 7]. Since different GETs operate based on a variety of principles, it is essential to ensure that the modeling is an accurate representation of their operating limits. Several previous studies failed to deliver this aspect due to generalization [11, 1, 5]. *In this dissertation, a comprehensive study is conducted*

on the linear modeling of FACTS in DC power flow to derive computationally efficient models based on device operating principles.

The integration of GETs into optimization models can lead to increased computational complexity due to added constraints and variables. For example, the mixed-linear reformulation of variable-impedance FACTS constraints, although addressing the nonlinearity issue, still introduces a binary variable for each line equipped with FACTS. The two-stage method presented in [11] aims to tackle this challenge with a flow direction enforcing approach that fixes the binary variables using the results from a base case DCOPF. An algorithm presented in this dissertation further advances this method, addressing the suboptimality issue of base case results and converging to optimality in almost all practical cases. Furthermore, the power grid faces increased complexities thanks to uncertainties, operational flexibilities, and distributed resources. With the increasing integration of RES in the power grid, their intermittency and variability cause challenges to power system operation. Implementation of distributed energy resources (DERs), demand-side management (DSM) programs, and GETs leads to flexibility in all sectors while also adding on complexities. All these factors lead to added complexities to the formulations of power system optimization models. For example, scenario-based stochastic unit commitment (SUC), which can bear immense computational burdens, is an essential model for uncertainty management under RES penetration. Such models require modeling to facilitate GET integration and efficient solution techniques to tackle the computational challenges. Research in this dissertation focuses on optimal GET operation in complex power system optimization models.

1.1.2 Incentivizing GET Investments

Proper incentives are critical in facilitating the deployment of GETs in the transmission grid. The existing market mechanism provides a regulated rate of return (RoR) for transmission investments based on capital expenditures [8]. This creates a bias against GETs as they involve far less capital investments compared to building transmission lines [3, 6]. Therefore, innovations in market mechanisms are desirable to provide proper incentives to GET investments. The changes should cover the following aspects. First, it is essential to adopt a performance-based approach to provide adequate financial compensation to

asset owners. Second, the market design needs to consider the full integration of GET operations. This is vital to harness the benefits of GET deployments and provide the basis for evaluating GET benefits. Moreover, to achieve optimal dispatches in power system operation, GET setpoints are required to be frequently adjusted in accordance with changes in the system, typically involving load profiles and RES variability. Therefore, it is key to incentivize socially optimal operations of GETs based on their integration into power system operation models.

Two main approaches fall into the performance-based category. First, asset owners can be directly rewarded with the whole or a portion of the social welfare increases created by the transmission projects. The WATT coalition has proposed shared-savings incentives for GETs [14], which rewards investors with a portion of the savings achieved by their projects. Second, a marginal price signal can be obtained from power system operation models and utilized to calculate the payoffs. An example of such a method is proposed in [9], where the dual variable of the DC power flow equation is used as a marginal value. This dissertation seeks to address critical challenges regarding each of these major approaches. The first approach raises the question of benefit distribution. GET deployments can belong to different asset owners, and the payoffs need to be fairly allocated among them. For the second approach, existing proposals failed to consider the full integration of GETs into power system operation models and did not address the potential revenue inadequacy. This dissertation presents two incentive schemes for GETs. The first one uses a game theory concept for allocating payoffs to different asset owners, and the second one shows a revenue-adequate market design considering GET operations and utilizing dual variables as marginal prices for GETs.

1.2 Contributions

The key contributions of this dissertation are summarized as follows:

- Effient linear models for various series FACTS devices are derived, with simulation studies validating the mathematical models and confirming their computational efficiency superiority.
- A successive flow direction enforcing algorithm is developed for optimal operation of variable-impedance FACTS devices. The proposed algorithm addresses the sub-

optimality issue of the method in previous research while still offering computational efficiency gains compared to directly solving problems formulated with the mixed-integer DC power flow equations.

- The effectiveness of prominent algorithms such as progressive hedging and the alternating direction method of multipliers (ADMM) in solving complex power system operation models considering GET operation is studied.

- The impact of GET operation on risk levels concerning unserved-load events is studied with a two-stage stochastic unit commitment model.

- A sensitivity-based method is developed to facilitate the planning of series FACTS devices. The sensitivities are derived based on the dual solution of DCOPF and the FACTS modeling presented in this dissertation.

- An incentive scheme is proposed, which utilizes an improved Shapley value approach to distribute the benefits to different GET owners. The proposed scheme provides adequate payoffs to GET owners and addresses the issue of benefit allocation when involving multiple market participants.

- A revenue-adequate market design is developed that provides payoffs to GET owners using shadow prices. The proposed mechanism is based on GET integration in power system operation and its effectiveness is demonstrated via a comparison with regulated RoRs.

1.3 Dissertation Outline

This dissertation consists of two parts, each presenting studies that focus on addressing one of the aforementioned major challenges to GET deployments. Part I, consisting of Chapters 2-7, advances the research on integrating GETs into power system optimization models. Linear modeling of various series FACTS devices in DC power flow is presented in Chapter 2. The modeling reflects the operating ranges of the devices while utilizing the simplifications of DC power flow. Chapter 3 presents the successive flow direction enforcing algorithm developed for the optimal operation of variable-impedance FACTS devices. Chapters 4-6 discuss GET operations in complex optimization problems, including SUC

and distributed DCOPF. The effectiveness of advanced algorithms such as progressive hedging and the alternating direction method of multipliers (ADMM) for these optimization models is studied, with results presented in Chapters 4 and 5. A risk-averse SUC model that includes GET operations is presented in Chapter 6 and is utilized to study the impact of these technologies on the risk of unserved load. Moreover, a sensitivity-based optimal placement method is proposed in Chapter 7 to facilitate the planning processes of FACTS devices.

Addressing the lack of proper incentives for GETs is the other key aim of this dissertation. Part II, consisting of Chapters 8-10, is dedicated to present research for incentivizing GET investments. A review of the proposals in the existing literature and current procedure regarding incentives for GETs by regulatory bodies and the industry is first presented in Chapter 8. Then, Chapter 9 presents an incentive scheme that utilizes an improved Shapley value approach for benefit allocation. Finally, a revenue-adequate market design for GETs is presented in Chapter 10. Results of comparison with the regulated RoR are presented for both proposed mechanisms.

Finally, Chapter 11 presents the conclusions of this dissertation and directions for future research.

1.4 References

[1] T. Ding, R. Bo, F. Li, and H. Sun, *Optimal power flow with the consideration of flexible transmission line impedance*, IEEE Transactions on Power Systems, 31 (2015), pp. 1655–1656.

[2] E. Howland, *US grid congestion costs jumped 56% to $20.8B in 2022: report*, July 2023. Accessed: 11-09-2023.

[3] Jay Caspary, *The Role for Grid-Enhancing Technologies*, January 2022. Accessed: 2023-07-25.

[4] S. Jenkins, *Grid-Enhancing Technologies: From R&D to Reality*, November 2023. Accessed: 02-26-2024.

[5] J. Mohammadi, G. Hug, and S. Kar, *Fully distributed DC-OPF approach for power flow control*, in 2015 IEEE Power & Energy Society General Meeting, IEEE, 2015, pp. 1–5.

[6] K. Rebane, K. Siegner, and S. Toth, *Cheaper, Cleaner, Faster - Four strategies utility regulators can use to accelerate new renewables interconnection.*, July 2023. Accessed: 02-27-2024.

[7] P. A. Ruiz, E. Goldis, A. M. Rudkevich, M. C. Caramanis, C. R. Philbrick, and J. M. Foster, *Security-constrained transmission topology control MILP formulation using sensitivity factors*, IEEE Transactions on Power Systems, 32 (2016), pp. 1597–1605.

[8] M. Sahraei-Ardakani, *Merchant power flow controllers*, Energy Economics, 74 (2018), pp. 878–885.

[9] M. Sahraei-Ardakani and S. A. Blumsack, *Transfer capability improvement through market-based operation of series FACTS devices*, IEEE Transactions on Power Systems, 31 (2015), pp. 3702–3714.

[10] M. Sahraei-Ardakani and K. W. Hedman, *Day-ahead corrective adjustment of FACTS reactance: A linear programming approach*, IEEE Transactions on Power Systems, 31 (2015), pp. 2867–2875.

[11] ——, *A fast LP approach for enhanced utilization of variable impedance based FACTS devices*, IEEE Transactions on Power Systems, 31 (2015), pp. 2204–2213.

[12] ——, *Computationally efficient adjustment of FACTS set points in DC optimal power flow with shift factor structure*, IEEE Transactions on Power Systems, 32 (2016), pp. 1733–1740.

[13] G. N. Taranto, L. Pinto, and M. V. F. Pereira, *Representation of facts devices in power system economic dispatch*, IEEE transactions on Power Systems, 7 (1992), pp. 572–576.

[14] WATT Coalition, *FERC Deep Dive on Performance Incentives Raises Few Challenges, No Alternatives*. Accessed: 08-01-2023.

[15] X. Zhang, D. Shi, Z. Wang, B. Zeng, X. Wang, K. Tomsovic, and Y. Jin, *Optimal allocation of series FACTS devices under high penetration of wind power within a market environment*, IEEE Transactions on Power Systems, 33 (2018), pp. 6206–6217.

PART I

GRID-ENHANCING TECHNOLOGIES IN POWER SYSTEM OPTIMIZATION

CHAPTER 2

LINEAR MODELLING OF SERIES FACTS DEVICES IN DC POWER FLOW

Harnessing the benefits of FACTS operation requires its integration into the energy management software tools. Therefore, linear modeling of FACTS is desirable. Additionally, as mentioned previously, FACTS models need to accurately reflect the technology principles utilized to achieve series compensation. However, generalizations have often been made in previous research regarding FACTS operation. This chapter includes a publication[1] that presents a comprehensive study on FACTS modeling in DC power flow. The models are developed based on the operating ranges of various FACTS technologies while adopting the simplifications in the DC power flow framework. In addition, FACTS operations are incorporated into the DC power flow problem formulations that are based on injection shift factors (ISFs), facilitating their smooth integration into existing market-clearing tools. The mathematical derivations and computational efficiency of the presented models are demonstrated via simulation studies conducted with various test systems.

[1]Reprinted, with permission, under a Creative Commons license, from Xinyang Rui and Mostafa Sahraei-Ardakani, "Linear modelling of series FACTS devices in power system operation", *IET Generation, Transmission & Distribution*, 16(6), 1047-1063, 2022.

Received: 2 July 2021 | Revised: 15 September 2021 | Accepted: 30 September 2021

IET Generation, Transmission & Distribution

DOI: 10.1049/gtd2.12348

The Institution of Engineering and Technology WILEY

ORIGINAL RESEARCH PAPER

Linear modelling of series FACTS devices in power system operation models

Xinyang Rui[1] | **Mostafa Sahraei-Ardakani**[1] | **Thomas R. Nudell**[2]

[1] Department of Electrical and Computer Engineering, University of Utah, Salt Lake City, Utah, USA

[2] Smart Wires Inc., Union City, California, USA

Correspondence
Mostafa Sahraei-Ardakani, 50 S Central Campus Dr., MEB 2218, Salt Lake City, UT, 84112.
Email: mostafa.ardakani@utah.edu

Funding information
National Science Foundation grant, Grant/Award Number: 1756006; National Science Foundation grant, Grant/Award Number: 1756006

Abstract

This paper presents injection-shift-factor-based linear modelling for various types of series flexible ac transmission system (FACTS) devices within the DC power flow framework. The presented models allow FACTS devices to be properly integrated in current operation and planning software tools, which is key to harnessing the power flow capabilities provided by FACTS technology. Although recent literature has attempted to develop linear models for FACTS devices, the existing models do not accurately reflect the actual operating range for many FACTS devices. Compared to the existing models, the modelling approach presented here reflects the principle of operation of each type of series FACTS device in adjusting transmission line reactance. Through mathematical derivation, linear constraints for FACTS operation are formulated, which are used to formulate power system operation models. The formulated problems are then analysed through simulation studies on various test systems. The results highlight the significant computational efficiency improvements provided by linear FACTS modelling in DC-based operation models.

1 | INTRODUCTION

The transmission system in the United States is outdated and needs to be upgraded [1]. High congestion costs in many parts of the US power grid is a strong economic signal for this need [2]. A robust transmission network is also central to reliability of the electric power grid [3]. Insufficient transfer capability leads to congestion in the transmission network, which may result in violations of network security limits [4]. Transfer capability enhancement, thus, improves economic efficiency and reliability of the bulk power network. Moreover, enhancing transfer capability facilitates penetration of higher levels of renewable generation in power systems. Renewable energy penetration is expected to rapidly grow and reach 42% of the total energy mix in the U.S. by 2050 [5]. However, congestion in the transmission network hinders the delivery of high levels of renewable generation [6], causing problems such as wind energy curtailment.

Transfer capability can be enhanced through construction of new transmission lines. However, the process of building new lines is lengthy and costly due to social and environmental issues, as well as new challenges such as market deregulation [7]. A faster alternative is improving the utilisation of the existing transmission network, which can be achieved through power flow control [8]. Note that the increase in transfer capability over the existing grid can be as large as 30% [8, 9]. One technology that enables power flow control is flexible AC transmission systems (FACTS). FACTS devices facilitate rerouting of power flow to avoid transmission bottlenecks and congested lines, which results in enhanced transfer capability and increased dispatch of cheaper generators. As an example, it is shown in [10] that the power flow control capabilities of FACTS devices can effectively reduce wind curtailment and reduce total generation cost. FACTS devices that are capable of effectively alter apparent impedance of transmission lines can be deployed for active power flow control. For the rest of this paper, the term "FACTS" is used to specifically refer to these types of devices. The impedance control can be either through direct addition of a controlled series impedance or injection of a controlled voltage, which emulates a controllable variable impedance.

While FACTS technology is a few decades old and there are numerous studies on a wide range of its benefits, the benefits can only be fully harnessed if FACTS devices are properly modelled in power system operation and planning models. Otherwise, the setpoint of these devices cannot be

adjusted dynamically based on the state of the system, leading to some level of underperformance. Unfortunately, due to the computational complexity of including FACTS devices in operation and planning software tools, this integration has not yet occurred, resulting in under-materialised benefits of current FACTS installations [11–13]. Moreover, the widely used representation of FACTS operating range in DC power flow in recent studies are inaccurate for many FACTS devices. In the following subsection, we present a review of the existing model and the usage of it in the literature.

1.1 | Review of existing models for the operating range of series FACTS in DC-based operation models

Independent system operators (ISOs) use DC-based market operations because of its robustness and operators' confidence in the quality of the solution [14]. Energy and market management system (EMS/MMS) software tools use one or another form of DC power flow models [15, 16]. Therefore, to enable integration of FACTS devices in EMS/MMS software tools, they should be modelled and integrated in DC-based operation models, often based on DC optimal power flow (DCOPF) and unit commitment (UC). The linearization in DC power flow is mostly on power flow equations, which results in a computationally tractable formulation.

With FACTS devices, line reactance or susceptance can be controlled. Therefore, susceptance of transmission lines equipped with FACTS should be represented as a variable, as is shown in the b-θ DC power flow equation in (1).

$$f_{ij} = \tilde{b}_{ij}\left(\theta_j - \theta_i\right) \tag{1}$$

An early study on the representation of FACTS in DCOPF models the operating range of FACTS devices that provide series reactance adjustment as a variable with constant variation bounds [17], as is shown in (2).

$$b_{ij}^{\min} \le \tilde{b}_{ij} \le b_{ij}^{\max} \tag{2}$$

In this paper, we refer to such modelling approach as the variable-susceptance model. It has alternative reactance-based representations in different studies that are essentially equivalent. Note that with (2), (1) is a nonlinear equation, due to the bilinear terms $\tilde{b}_{ij}\theta_j$ and $\tilde{b}_{ij}\theta_i$. The nonlinearity makes optimisation problems much more computationally demanding. Additionally, nonlinear models are not compatible with existing EMS/MMS software tools. Thus, linearization of (1) is essential for proper integration of FACTS devices in operation software tools. A number of recent research papers have focused on effectively reformulating (1) and (2) to linear or mixed-integer linear constraints [11–13, 18–20].

The variable-susceptance model of FACTS operating range is used in [11–13], where both the thyristor controlled series compensator (TCSC) and the unified power flow controller (UPFC) are presented as examples, where the model can be applied. However, according to the analysis in this paper, while the variable-susceptance model is an accurate representation for the TCSC, it cannot accurately reflect the operating range of UPFC devices because of the aforementioned difference in the impedance control methods. In [20], the type of series FACTS device is not clearly specified, when applying the variable-susceptance model. Similar issues reside in [21–23], where DC-based models with the distributed FACTS (D-FACTS) included are studied. However, the variable-susceptance model is used for modelling the operating range of D-FACTS devices, without specifying the type of FACTS technology.

In summary, the following gaps exist in the literature:

- Several studies simply apply the variable-susceptance model on devices, where the model cannot accurately reflect the impedance control method. As mentioned previously, depending on the type of FACTS device, different power electronic circuits are used to alter the apparent line impedance. The impacts are similar, yet the operating range of effective reactance injection may vary significantly, with some being highly nonlinear. The variable-susceptance model cannot accurately represent the true operating range of many FACTS devices.
- The variable-susceptance model is used as a general model in previous research without specifying the type of FACTS technology.
- The existing literature on the static synchronous series compensator (SSSC), the magnetic energy recovery switch (MERS), and the UPFC are by in large AC-based models [24–26]. Efficient and accurate linear modelling in DC-based software tools do not exist.
- A linear model for the emerging lightweight and compact modular FACTS (M-FACTS) devices is desirable.

1.2 | Contributions

This paper fills the aforementioned gaps in the existing literature by making the following contributes.

- This paper derives accurate and computationally efficient models for various types of series FACTS devices. The models, developed here, reflect the specific characteristics of different devices in operation. The models are formulated as linear or mixed-integer linear constraints, to enable appropriate integration with DCOPF and UC, while achieving computational tractability, allowing smooth integration within the existing operation and planning software tools. Specifically, this paper models the following FACTS devices: The SSSC, the MERS, the UPFC, and the TCSC.
- Operation and planning and models for the emerging lightweight and compact modular FACTS (M-FACTS) devices, particularly the modular SSSC (M-SSSC), are also included.
- The mathematical derivation for each type of device, in this paper, is based on the usage of injection shift factors (ISFs). The impact of series compensation is modelled as power

injections, with careful attention to the differences between each category of devices. ISF-based operation model formulations with each category of FACTS are presented at the end of the paper, which can serve as a reference for power system researchers that are interested in FACTS modelling, operation, and planning problems.
- The formulated problems are studied through simulations using the Texas 2000-bus system, the RTS-96 system, and the IEEE 14-bus system. The results show the computational efficiency of linear FACTS modelling, while also providing numerical verification for our mathematical derivations.

To the best of our knowledge, this is the first comprehensive study on efficient and accurate modelling of FACTS devices using ISFs in DC-based operation models.

1.3 | Paper layout

The rest of this paper is organised as follows: the derivation leading to formulation of power flow control constraints for each type of FACTS is presented in Section 2. Note that the term "power flow control constraints" is used to refer to the constraints that are directly related to FACTS series compensation. They include the constraints reflecting the operating range of FACTS, as wells the power flow equation with consideration of FACTS reactance adjustments. Formulations of DCOPF and UC problems with both linear and nonlinear FACTS modelling are presented in Section 3. In Section 4, the results of simulation studies are provided and analysed. Finally, a conclusion is drawn in Section 5.

2 | LINEAR FACTS MODELLING

In this section, we present the mathematical modelling of effective reactance injection operating range of FACTS devices including SSSC, M-SSSC, UPFC, TCSC, and MERS. The focus of this section is on (i) derivation of accurate models, based on the principles of operation for each type of FACTS device to adjust the apparent line reactance and (ii) discussion of how the models can be efficiently integrated in operation models. In DC power flow, only the active power flow is considered. Therefore, modelling in this section is solely focused on transmission line reactance adjustment, as well as changes in active power flow caused by FACTS.

2.1 | Injection modelling of FACTS compensation

In this section the derivations are based on b-θ power flow equation. However, due to its superior computational performance, all industry implementations of operation and planning problems use the ISF formulation [13]. The ISF for a transmission line represents the fraction of power injection at a certain bus that flows through this line. Using an ISF formulation eliminates the need for calculating bus voltage angles, thus, improving the scalability of DC-based models with respect to network size, compared to the b-θ formulation (1) [13]. This is the main reason that ISF-based models are widely used in industry practices. Thus, in order to enable smooth integration with existing energy and market management systems, this paper includes an injection model for each FACTS device, where the compensation is modelled as an injection pair at the two ends of the line, on which the FACTS device is installed [15]. The injection model, shown in Figure 1, preserves the offline calculated ISF matrix of the system even with FACTS deployment, and enhances computational tractability.

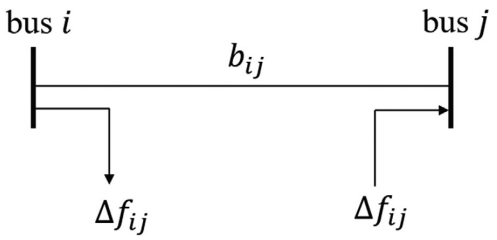

FIGURE 1 Nodal injection model of FACTS

For the transmission line in Figure 1, the DC power flow equation is formulated as follows:

$$f_{ij} = \left(b_{ij} + \Delta b_{ij}\right)\left(\theta_j - \theta_i\right). \tag{3}$$

(3) can be further derived to:

$$f_{ij} = b_{ij}\left(\theta_j - \theta_i\right) + \Delta b_{ij}\left(\theta_j - \theta_i\right) = \tilde{f}_{ij} + \Delta f_{ij}, \tag{4}$$

where

$$\tilde{f}_{ij} = b_{ij}\left(\theta_j - \theta_i\right), \tag{5}$$

$$\Delta f_{ij} = \Delta b_{ij}\left(\theta_j - \theta_i\right). \tag{6}$$

In (5), $\tilde{f}_{ij}$ only has the original susceptance of the line, allowing it to be calculated using the ISFs. The calculation is presented in Section 3 in the problem formulations. The impact of reactance injection is separated from the original line susceptance. The impact of FACTS adjustment, thus, can be modelled as injections, which is Δf_{ij}, at end buses of a transmission line [13].

2.2 | SSSC and M-SSSC

The SSSC is one of the most important FACTS devices for transmission line series compensation [27] and has been used as one of the M-FACTS devices in the industry. The SmartValve [28] by Smart Wires Inc. is an M-SSSC that provides the functionality of a series capacitor or series reactor. The

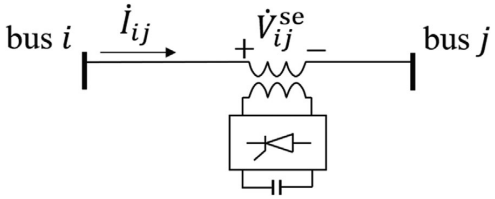

FIGURE 2 SSSC configuration [29]

configuration of the SSSC is presented in Figure 2, where the device consists of an inverter, a capacitor, and a coupling transformer. The SSSC is series connected with a transmission line through the coupling transformer [29].

Line reactance adjustment is achieved through a series injected voltage that is in quadrature with and independent of the line current. For line ij with the SSSC installed, the quadrature phase is defined as follows [29]:

$$\mathrm{Re}\left\{\dot{V}_{ij}^{se}\dot{I}_{ij}^{*}\right\}=0. \tag{7}$$

The magnitude of the voltage injection is constrained by its upper bound $V_{ij}^{\max}$. The operating range of voltage injection and effective reactance of the SSSC is shown in Figure 3. Note that the device requires a minimum line current to be powered up, since it depends on the line current to power the converter through a coupling transformer. We can see that the operating range in Figure 3b is highly nonlinear.

The effective reactance injection operating limits of SSSC devices are functions of the line current. For a transmission line, from bus i to bus j that is equipped with an SSSC, we have:

$$-V_{ij}^{\max}\le\Delta x_{ij}\left|I_{ij}\right|\le V_{ij}^{\max}. \tag{8}$$

The approximate equality between line current and active power flow in DC power flow is shown in (9) [30].

$$\left|I_{ij}\right|\approx\left|f_{ij}\right| \tag{9}$$

Using (9), while removing the absolute value sign, (8) can be reformulated as:

$$-V_{ij}^{\max}\le\Delta x_{ij}f_{ij}\le V_{ij}^{\max}. \tag{10}$$

With the effective reactance injection, we can formulate the corresponding line susceptance change as:

$$\Delta b_{ij}=-\frac{1}{x_{ij}+\Delta x_{ij}}-b_{ij}. \tag{11}$$

Solving Δx_{ij} from (11), we get:

$$\Delta x_{ij}=\frac{\Delta b_{ij}}{b_{ij}\left(b_{ij}+\Delta b_{ij}\right)}. \tag{12}$$

Next, consider the DC power flow Equation (3), we can further derive (12) to get:

$$\Delta x_{ij}=\frac{\Delta b_{ij}\left(\theta_j-\theta_i\right)}{b_{ij}\left(b_{ij}+\Delta b_{ij}\right)\left(\theta_j-\theta_i\right)}=\frac{\Delta f_{ij}}{b_{ij}f_{ij}}. \tag{13}$$

Thus, (10) can be reformulated as:

$$-V_{ij}^{\max}\le\frac{\Delta f_{ij}}{b_{ij}}\le V_{ij}^{\max}. \tag{14}$$

Therefore, we can get the following constraints on Δf_{ij}:

$$-V_{ij}^{\max}\left|b_{ij}\right|\le\Delta f_{ij}\le V_{ij}^{\max}\left|b_{ij}\right|, \tag{15}$$

where variation limits of FACTS power injection are imposed. The limits are determined by the maximum voltage injection of the SSSC device and the original line susceptance.

Thus far, we derived (15), which is a linear constraint, from the highly nonlinear constraint in (8). The linear model allows the effective reactance injection operating range to be efficiently included in the ISF-based DC models.

As is shown in Figure 3b, the variation bounds on Δx_{ij} are dependent on line current (or equivalently active power flow in DC power flow). Therefore, selecting variation limits on FACTS reactance/susceptance adjustment to apply the variable-susceptance model is nearly impossible, and the consequential inaccuracy in reflecting the power flow capabilities will be substantial. Furthermore, it is worth noting that, as mentioned previously, the variation of line susceptance in the b-θ formulation (1) makes the DCOPF problem a nonlinear program (NLP). If the variation range of line susceptance is simply modelled as in (2), assuming negative line susceptance, the constraint on FACTS nodal injection can be formulated as follows:

$$\text{For}\tilde{f}_{ij}\ge 0:\ \frac{\left(b_{ij}^{\max}-b_{ij}\right)}{b_{ij}}\tilde{f}_{ij}\le\Delta f_{ij}\le\frac{\left(b_{ij}^{\min}-b_{ij}\right)}{b_{ij}}\tilde{f}_{ij}, \tag{16}$$

$$\text{For}\tilde{f}_{ij}<0:\ \frac{\left(b_{ij}^{\min}-b_{ij}\right)}{b_{ij}}\tilde{f}_{ij}\le\Delta f_{ij}\le\frac{\left(b_{ij}^{\max}-b_{ij}\right)}{b_{ij}}\tilde{f}_{ij}. \tag{17}$$

The corresponding nonconvex feasible region, as well as the variation limits that are defined in (15), are presented in Figure 4.

The comparison between Figures 4a and 4b reveals that the appropriate modelling of the reactance injection operating range, developed in this paper, is convex. This is contrary to the nonconvex range that is calculated in the literature [11–13, 17, 20]. Linear FACTS modelling, thus, shows substantial superiority in both accuracy and computational efficiency of the operation models for the SSSC and similar devices.

The modular nature and lightweight enclosure of M-FACTS devices allow more efficient deployment and re-deployment compared to conventional devices, providing more flexibility in installation and planning [31]. Unlike conventional FACTS devices, sizing of an M-FACTS project will determine the

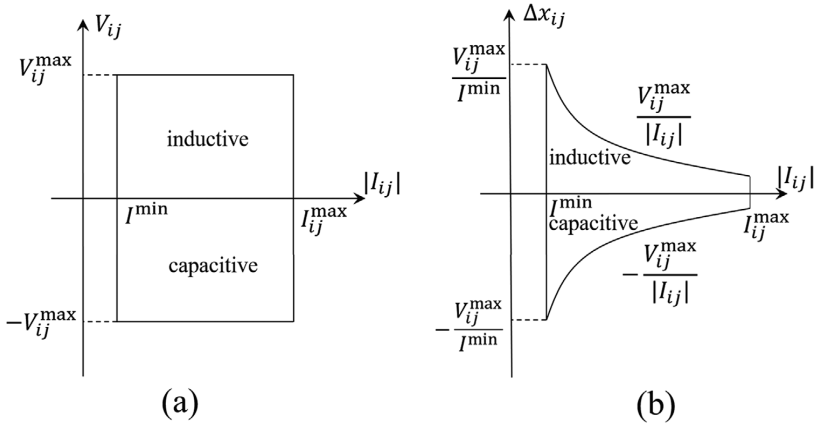

FIGURE 3 The SSSC operating range regarding: (a) Voltage–current (b) reactance-current

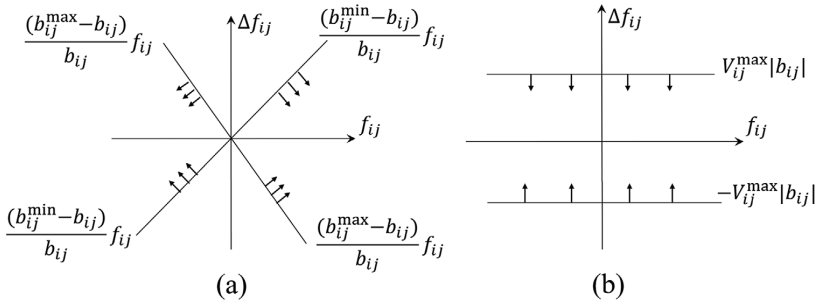

FIGURE 4 Feasible region (a) when SSSC operating range is modelled using the variable-susceptance model and (b) when considering the actual effective reactance injection operating range; arrows in the figure indicate the region defined by the corresponding constraints

number of modules that are deployed at each location. Therefore, in planning problems that involves M-FACTS, integer variables should be used to model the size of the project. Thus, for M-FACTS devices that are based on the SSSC, (15) can be rewritten as:

$$-N_{ij}^{\text{FACTS}}\bar{V}\left|b_{ij}\right| \le \Delta f_{ij} \le N_{ij}^{\text{FACTS}}\bar{V}\left|b_{ij}\right|, \qquad (18)$$

where an integer variable is added. Equation (18) is, thus, a mixed-integer linear constraint. Note that (18) should be specified for planning models. In operation models, (18) is equivalent to constraint (15) as the values of N_{ij}^{FACTS} will already be determined.

2.3 | MERS

The MERS is an alternative series compensator with advantages including simple configuration, low losses, low cost implementation, and zero turn-on current [32, 33]. The configuration of the MERS, which consists of a capacitor, four diodes, and four controllable switches, is shown in Figure 5 [33].

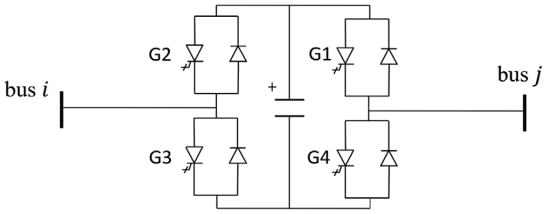

FIGURE 5 MERS configuration [33]

The MERS provides series compensation by injecting a capacitive series voltage that lags behind the line current by 90°. The size of the injected voltage can be controlled from zero to the rated voltage within the device current rating [32, 33]. Therefore, the operating range shown in Figure 6 is the same as the capacitive voltage operating range of the SSSC [33]. For line ij with MERS devices installed, the equivalent capacitive series injection provided by the MERS is subject to the following

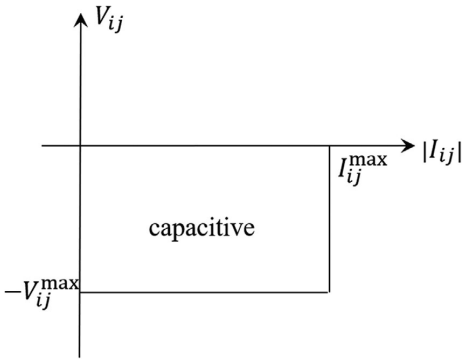

FIGURE 6 Voltage-current operating range for MERS

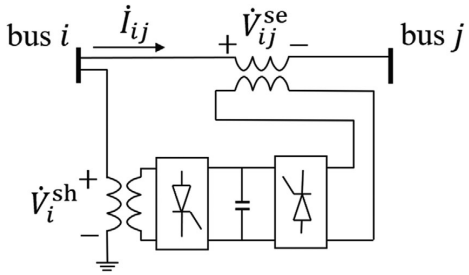

FIGURE 7 UPFC configuration [29]

constraints:

$$-V_{ij}^{\max} \le \Delta x_{ij} \left| f_{ij} \right| \le 0. \tag{19}$$

The variation limits of nodal injection of the MERS are, thus, similar to (15). However, because of the absolute value sign, they are dependent on flow direction. Combine (19) with (13), we get the following reformulated constraints.

$$\text{For } f_{ij} \ge 0 : -V_{ij}^{\max} \le \frac{\Delta f_{ij}}{b_{ij}} \le 0. \tag{20}$$

$$\text{For } f_{ij} < 0 : 0 \le \frac{\Delta f_{ij}}{b_{ij}} \le V_{ij}^{\max}. \tag{21}$$

The big-M method can used to obtain a mixed-integer linear reformulation of (20) and (21), which is presented as follows:

$$-z_{ij}M \le \frac{\Delta f_{ij}}{b_{ij}} \le V_{ij}^{\max} + z_{ij}M, \tag{22}$$

$$-V_{ij}^{\max} + \left(z_{ij} - 1\right) M \le \frac{\Delta f_{ij}}{b_{ij}} \le \left(1 - z_{ij}\right) M, \tag{23}$$

$$\left(z_{ij} - 1\right) M \le \Delta f_{ij} + \tilde{f}_{ij} \le z_{ij}M, \tag{24}$$

$$z_{ij} \in \{0, 1\}, \tag{25}$$

$$M \gg \max\left\{ f_{ij}^{\max}, V_{ij}^{\max} \right\}. \tag{26}$$

The binary variable, z_{ij}, is used to represent the power flow direction. The value of M can be set according to (26). The inclusion of binary variables adds more computational burden compared to (15).

2.4 | UPFC

The UPFC provides real-time control and dynamic compensation of the AC transmission systems [34] and is the most versatile FACTS device [35]. The configuration of the UPFC is shown in Figure 7 [29].

The series device of the UPFC is series connected with the transmission line through a coupling transformer. The shunt-connected transformer couples the shunt device to a local bus [29]. The series device of a UPFC can be regarded as a voltage source that is controllable in both magnitude and phase angle [36, 37]. UPFC devices provide the series compensation by regulating the series voltage injection to control the effective reactance of transmission lines [29]. Therefore, UPFC can be modelled as a controllable series voltage injection in power flow control, which is similar to the modelling of the SSSC. In addition, when comparing Figure 7 with Figure 2 we can see that the SSSC is the UPFC without the shunt device, which leads to the similarity in modelling.

Suppose a UPFC provides series compensation on a transmission line ij. Based on the modelling of the UPFC as a controllable voltage injection, the active power flow on the line can be formulated as:

$$\begin{aligned} f_{ij} &= \mathrm{Re}\left\{ \dot{V}_i \dot{I}_{ij}^{*} \right\} = \mathrm{Re}\left\{ \frac{\dot{V}_i \left(\dot{V}_i - \dot{V}_{ij}^{se} - \dot{V}_j \right)^{*}}{-jx_{ij}} \right\} \\ &= \mathrm{Re}\left\{ \frac{-\dot{V}_i \left(\dot{V}_j + \dot{V}_{ij}^{se} \right)^{*}}{-jx_{ij}} \right\} \end{aligned} \tag{27}$$

where $|\dot{V}_i| = |\dot{V}_j| = 1$ p.u., which is based on the assumptions in DC power flow [30]. Equation (27) can, then, be formulated as:

$$f_{ij} = \mathrm{Re}\left\{ \frac{-\dot{V}_i \left(\dot{V}_j + \dot{V}_{ij}^{se} \right)^{*}}{-jx_{ij}} \right\} = -\frac{1}{x_{ij}} \cos\left(\theta_i - \theta_j + \frac{\pi}{2} \right)$$

$$-\frac{\left|\dot{V}_{ij}^{se}\right|}{x_{ij}}\cos\left(\theta_i-\varphi_{ij}+\frac{\pi}{2}\right)=\frac{\sin\left(\theta_i-\theta_j\right)}{x_{ij}}$$
$$+\frac{\left|\dot{V}_{ij}^{se}\right|}{x_{ij}}\sin\left(\theta_i-\varphi_{ij}\right)=b_{ij}\left(\theta_j-\theta_i\right)$$
$$+\left|\dot{V}_{ij}^{se}\right|b_{ij}\sin\left(\varphi_{ij}-\theta_i\right). \quad (28)$$

The FACTS power injection in the nodal injection model is, then, formulated as:

$$\Delta f_{ij}=\left|\dot{V}_{ij}^{se}\right|b_{ij}\sin\left(\varphi_{ij}-\theta_i\right), \quad (29)$$

where $|\dot{V}_{ij}^{se}|$ and $\sin(\theta_i-\varphi_{ij})$ satisfy the following constraints:

$$0\le\left|\dot{V}_{ij}^{se}\right|\le V_{ij}^{max}, \quad (30)$$

$$-1\le\sin\left(\varphi_{ij}-\theta_i\right)\le 1. \quad (31)$$

The bounds on Δf_{ij} are, thus, determined as:

$$-V_{ij}^{max}\left|b_{ij}\right|\le\Delta f_{ij}\le V_{ij}^{max}\left|b_{ij}\right|, \quad (32)$$

which is exactly the same as (15). Therefore, UPFC and SSSC devices show consistency in flow variation limits for FACTS power injection. The SSSC operation can be considered as a specific case for the UPFC where the injected voltage is in quadrature with the line current. In addition, UPFC devices have been viewed as combinations of the SSSC and the static synchronous compensator (STATCOM) [38]. Consider the case where UPFC injects a voltage that is in quadrature with line current, with the phase angle of:

$$\varphi_{ij}=\frac{\theta_i+\theta_j\pm\pi}{2}. \quad (33)$$

Applying this phase angle to (29), we get:

$$\Delta f_{ij}=\left|\dot{V}_{ij}^{se}\right|b_{ij}\sin\left(\frac{\theta_i+\theta_j\pm\pi}{2}-\theta_i\right)$$
$$=\left|\dot{V}_{ij}^{se}\right|b_{ij}\left(\pm\cos\left(\frac{\theta_j-\theta_i}{2}\right)\right)=\pm\left|\dot{V}_{ij}^{se}\right|b_{ij}, \quad (34)$$

where the FACTS power injection has the same variation limits as in (15), considering the same operating range for the magnitude of the voltage injection.

2.5 | TCSC

A TCSC module consists of a capacitor that is in parallel with a thyristor-controlled inductor [29, 39, 40]. The configuration of a TCSC module is shown in Figure 8.

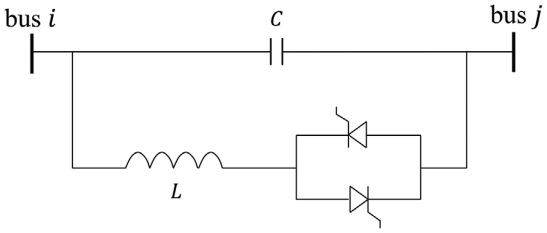

FIGURE 8 TCSC configuration [29]

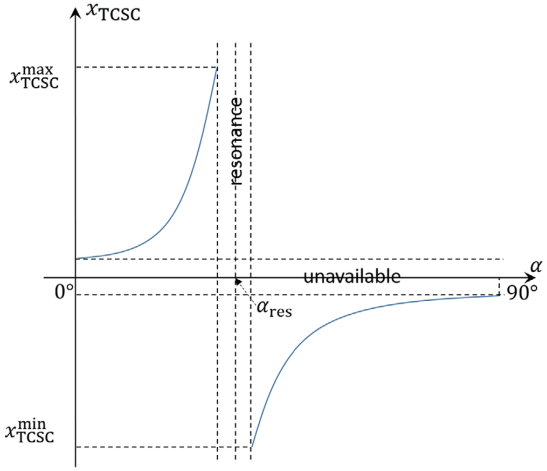

FIGURE 9 Reactance injection range of an individual module of TCSC as a function of the firing angle [41]

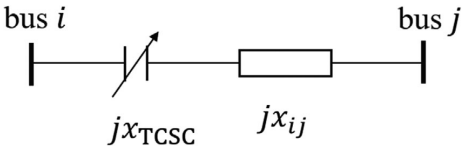

FIGURE 10 Static model of TCSC variable series reactance

The equivalent reactance injection of a single module TCSC is, thus, controlled by the firing angle of the thyristor. The operating range is shown in Figure 9 [41].

In Figure 9, α is the firing angle and α_{res} is the resonance angle. As multiple TCSC modules can be connected in series and operate independently, the unavailable band around zero reactance injection can be covered [41], allowing the TCSC to be modelled, in steady state, as a variable series reactance with continuous operating range. The static model of the TCSC is shown in Figure 10. Note that line resistance is neglected as it is not considered in DC power flow.

In several previous studies, the TCSC is considered to only provide capacitive reactance injection [42–44]. In this paper, we use a general model, where the TCSC can provide both inductive and capacitive series reactance compensation on transmission lines. The maximum inductive and capacitive series

compensation levels of the TCSC on transmission line ij are, typically, set as follows to avoid overcompensation [45, 46]:

$$-0.8\left|x_{ij}\right| \leq \Delta x_{ij} \leq 0.2\left|x_{ij}\right|. \tag{35}$$

The variation limits of adjusted line susceptance are, thus, determined as follows:

$$b_{ij}^{\min} = -\frac{1}{x_{ij} + x_{\text{TCSC}}^{\min}}, \tag{36}$$

$$b_{ij}^{\max} = -\frac{1}{x_{ij} + x_{\text{TCSC}}^{\max}}. \tag{37}$$

The constraint on FACTS nodal power injection for TCSC is, thus, the same as (16) and (17), assuming negative line susceptance. Using the big-M method and introducing the binary variable to represent flow directions, the constraint can be reformulated as:

$$\frac{(b_{ij}^{\max} - b_{ij})}{b_{ij}} f_{ij} - z_{ij}M \leq \Delta f_{ij} \leq \frac{(b_{ij}^{\min} - b_{ij})}{b_{ij}} f_{ij} + z_{ij}M, \tag{38}$$

$$(z_{ij} - 1)M + \frac{(b_{ij}^{\min} - b_{ij})}{b_{ij}} f_{ij} \leq \Delta f_{ij} \leq \left(1 - z_{ij}\right) M + \frac{(b_{ij}^{\max} - b_{ij})}{b_{ij}} f_{ij}, \tag{39}$$

$$-z_{ij}M \leq f_{ij} \leq \left(1 - z_{ij}\right) M, \tag{40}$$

$$z_{ij} \in \{0, 1\} \tag{41}$$

$$M \gg \max\left\{ f_{ij}^{\max}, \frac{(b_{ij}^{\min} - b_{ij}^{\max})}{b_{ij}} f_{ij}^{\max} \right\}. \tag{42}$$

The reformulation presented in (38)–(42) is equivalent to the ones in [11–13, 20]. Note that the linearity in the reformulation allows the DCOPF and UC problems involving TCSC to be solved more efficiently than problems formulated with the original nonlinear constraints.

3 | PROBLEM FORMULATION

In this section, we incorporate linear FACTS modelling into power system operation models DCOPF and UC. In addition, we formulate the DCOPF and UC problems with nonlinear FACTS modelling. For simplicity, we name each problem formulation according to the following format: device type_FACTS modelling (L: linear FACTS modelling; NL: nonlinear FACTS modelling)_operation model (OPF or UC). The formulated problems are studied through simulations in Section 4. As the nonlinear power flow control equations are formulated directly from the operating ranges of FACTS devices, the results of the problems with nonlinear formulations can be used for verifying the mathematical derivation leading to linear FACTS modelling. Moreover, the solution time are compared to show the computational efficiency improvement provided by the application of linear FACTS modelling.

Note that for devices that rely on current as source of power, an extra constraint may need to be considered:

$$\left|\tilde{f}_{ij} + \Delta f_{ij}\right| \geq f^{\min}. \tag{43}$$

Equation (43) is a not a linear constraint, which is undesirable for optimisation solvers. It can be reformulated to a mixed-integer linear constraint, using the big-M method, for which efficient solvers are available.

$$\tilde{f}_{ij} + \Delta f_{ij} + z_{ij}M \geq f^{\min} \tag{44}$$

$$\tilde{f}_{ij} + \Delta f_{ij} \leq -f^{\min} + \left(1 - z_{ij}\right) M \tag{45}$$

$$z_{ij} \in \{0, 1\} \tag{46}$$

$$M \gg \max\left\{ f_{ij}^{\max} + f^{\min} \right\} \tag{47}$$

Inclusion of (44)–(47) increases the computational complexity of power system operation models. However, power flow reaching the limits of (44) and (45) indicates that the line is very lightly utilised, which implies that it is an ineffective location for FACTS deployment in the first place. Therefore, it is unlikely for (44) and (45) to become active, if FACTS devices are allocated appropriately. The two constraints, thus, can usually be removed from the problem formulation, without affecting the solution.

For modular FACTS devices such as the M-SSSC, the number of modules deployed on each transmission line needs to be optimised as well. Therefore, the following constraints needs to be included in the problem formulation, along with (18):

$$N_{ij}^{\text{FACTS}} \leq N_{ij}^{\max}, \tag{48}$$

$$\sum_{i,j} N_{ij}^{\text{FACTS}} \leq N^{\max}. \tag{49}$$

Equation (48) is the constraint on the maximum number of devices allowed to be deployed on transmission line ij. Note that this limit is line specific and depends on a number of

factors, such as physical size and weight of M-FACTS, distance between transmission towers etc. (49) specifies the availability constraint of M-SSSC devices.

3.1 | Problem formulation with linear FACTS modelling

We first present the objective function and the constraints that are common for ISF-based DCOPF [13] with FACTS regardless of the choice of FACTS device type. The DCOPF problem without the power flow control constraints can be partially formulated as follows:

$$\text{minimise} \sum_{g\in G} c_g p_g \tag{50}$$

subject to:

$$f_{ij} = \sum_{n\in N} \Phi_{ij}^{n} \psi_n, \forall ij \notin K_{\mathrm{F}}; \tag{51}$$

$$\tilde{f}_{ij} = \sum_{n\in N} \Phi_{ij}^{n} \psi_n, \forall ij \in K_{\mathrm{F}}; \tag{52}$$

$$\psi_i = \sum_{g\in G(i)} p_g - d_i + \sum_{j\in N^+(i)} \Delta f_{ij} - \sum_{j\in N^-(i)} \Delta f_{ij}, \forall i; \tag{53}$$

$$p_g^{\min} \le p_g \le p_g^{\max}, \forall g; \tag{54}$$

$$\sum_{g\in G} p_g = \sum_{i\in N} d_i, \forall g, t; \tag{55}$$

$$-f_{ij}^{\max} \le f_{ij} \le f_{ij}^{\max}, \forall ij \notin K_{\mathrm{F}}; \tag{56}$$

$$-f_{ij}^{\max} \le \tilde{f}_{ij} + \Delta f_{ij} \le f_{ij}^{\max}, \forall ij \in K_{\mathrm{F}}. \tag{57}$$

Equation (50) is the objective function where the total generation cost is minimised, assuming linear marginal costs for generators. Power flows are calculated using ISFs in (51) and (52). Note that in (52), only the power flow without FACTS injection is calculated for lines with FACTS devices installed. In (53), power injection at each bus is calculated using generation, demand, and FACTS nodal injection. The generator operating capacities are specified in (54). (55) represents the power balance in the network. Thermal capacity limits of transmission lines are presented in (56) and (57).

We then need the power flow control constraints to formulate the full DCOPF problems. These constraints have been formulated in the mathematical derivations in Section 2. For each specific DCOPF problem formulation, the power flow control constraints are listed as follows:

SSSC_L_OPF & UPFC_L_OPF: (15).
MERS_L_OPF: (22)–(26).
TCSC_L_OPF: (38)–(42).
M-SSSC_L_OPF: (18), (48)–(49).

Linear FACTS modelling preserves the desirable characteristic of linearity of the original DCOPF problem. Both SSSC_L_OPF and UPFC_L_OPF are linear programs (LP) because (15) is a linear constraint. The other three formulations are mixed-integer linear programs (MILP) due to the presence of integer variables. The DCOPF formulations can be extended to other operation and planning applications, for instance, security-constrained optimal power flow (SCOPF).

The linear power flow control constrains can be utilised in ISF-based UC problems as well. Similarly, ISF-based UC problems can first be partially formulated as follows:

$$\text{minimise} \sum_{g\in G} \sum_{t\in T} (c_g p_{gt} + k_g u_{gt} + s_g v_{gt}) \tag{58}$$

s.t.

$$f_{ij,t} = \sum_{n\in N} \Phi_{ij}^{n} \psi_{nt}, \forall ij \notin K_{\mathrm{F}}, t; \tag{59}$$

$$\tilde{f}_{ij,t} = \sum_{n\in N} \Phi_{ij}^{n} \psi_{nt}, \forall ij \in K_{\mathrm{F}}, t; \tag{60}$$

$$\psi_{it} = \sum_{g\in G(i)} p_{gt} - d_{it} + \sum_{j\in N^+(i)} \Delta f_{ij,t} - \sum_{j\in N^-(i)} \Delta f_{ij,t}, \forall i, t; \tag{61}$$

$$u_{gt} p_g^{\min} \le p_{gt} \le u_{gt} p_g^{\max}, \forall g, t; \tag{62}$$

$$\sum_{g\in G} p_{gt} = \sum_{i\in N} d_{it}, \forall t; \tag{63}$$

$$-f_{ij}^{\max} \le f_{ij,t} \le f_{ij}^{\max}, \forall ij \notin K_{\mathrm{F}}, t; \tag{64}$$

$$-f_{ij}^{\max} \le \tilde{f}_{ij,t} + \Delta f_{ij,t} \le f_{ij}^{\max}, \forall ij \in K_{\mathrm{F}}, t; \tag{65}$$

$$-R_g^{-} \le p_{gt} - p_{g,t-1} \le R_g^{+}, \forall g, t; \tag{66}$$

$$\sum_{r=t-UT_g+1}^{t} v_{gr} \le u_{gr}, \forall g, t \ge UT_g; \tag{67}$$

$$\sum_{r=t+1}^{t+DT_g} v_{gr} \le 1 - u_{gr}, \forall g, t \le |T| - DT_g; \tag{68}$$

$$u_{gt} - u_{g,t-1} \le v_{gt}, \forall g, t; \tag{69}$$

$$u_{gt} \in \{0,1\}, \forall g,t; \tag{70}$$

$$0 \le v_{gt} \le 1, \forall g,t. \tag{71}$$

As is shown in (58), the objective of the UC problem is to minimise the summation of production cost, start-up cost, and no-load cost of the generators [47]. Equations (59)–(65) are interpreted similarly to (51)–(57), with differences being the added time index and binary commitment variables in (62). Equation (66) specifies the ramping constraints of generators. Minimum up and down time constraints are represented by (67) and (68) [48]. Equation (69) represents the relationship between commitment variables and start-up variables. Equation (70) specifies that commitment variables are binary. Equation (71) defines the upper and lower bounds of start-up variables. Note that start-up variables can be relaxed from being binary to being continuous as they will be forced to the extremes in the UC solutions.

Again, the power flow control constraints are needed to complete the UC problem formulations. Power flow control constraints with linear FACTS modelling for each specific problem formulation are presented as follows:

SSSC_L_UC & UPFC_L_UC:

$$-V_{ij}^{\max}\left|b_{ij}\right| \le \Delta f_{ij,t} \le V_{ij}^{\max}\left|b_{ij}\right|, \forall ij \in K_F, t; \tag{72}$$

MERS_L_UC: (26),

$$-z_{ij,t}M \le \frac{\Delta f_{ij,t}}{b_{ij}} \le V_{ij}^{\max} + z_{ij,t}M, \forall ij \in K_F, t; \tag{73}$$

$$-V_{ij}^{\max} + \left(z_{ij,t}-1\right)M \le \frac{\Delta f_{ij,t}}{b_{ij}} \le \left(1-z_{ij,t}\right)M, \forall ij \in K_F, t; \tag{74}$$

$$\left(z_{ij,t}-1\right)M \le \Delta f_{ij,t} + \tilde{f}_{ij,t} \le z_{ij,t}M, \forall ij \in K_F, t; \tag{75}$$

$$z_{ij,t} \in \{0,1\}, \forall ij \in K_F, t; \tag{76}$$

TCSC_L_UC: (42), (76),

$$\frac{(b_{ij}^{\max}-b_{ij})}{b_{ij}} f_{ij,t} - z_{ij,t}M \le \Delta f_{ij,t} \le \frac{(b_{ij}^{\min}-b_{ij})}{b_{ij}} f_{ij,t} + z_{ij,t}M, \forall ij \in K_F, t; \tag{77}$$

$$(z_{ij,t}-1)M + \frac{(b_{ij}^{\min}-b_{ij})}{b_{ij}} f_{ij,t} \le \Delta f_{ij,t} \le \left(1-z_{ij,t}\right)M + \frac{(b_{ij}^{\max}-b_{ij})}{b_{ij}} f_{ij,t}, \forall ij \in K_F, t; \tag{78}$$

$$-z_{ij,t}M \le f_{ij,t} \le \left(1-z_{ij,t}\right)M, \forall ij \in K_F, t; \tag{79}$$

M-SSSC_L_UC: (48) and (49),

$$-N_{ij}^{\text{FACTS}}\bar{V}\left|b_{ij}\right| \le \Delta f_{ij,t} \le N_{ij}^{\text{FACTS}}\bar{V}\left|b_{ij}\right|, \forall ij \in K_F, t. \tag{80}$$

The complete problems are then formulated by selecting the power flow control constraints based on the device type. As each of the formulations involves linear FACTS modelling as well as integer variables, all the problems are MILPs. We can expand the UC formulations to a variety of other more complicated models as well, including security-constrained unit commitment (SCUC) and stochastic unit commitment (SUC).

3.2 | Problem formulation with nonlinear FACTS modelling

The formulated problems, as mentioned previously, are solved in simulations for verification and exploring computational efficiency gains provided by linear FACTS modelling. Therefore, we need to formulate the DCOPF and UC problems using the nonlinear power flow control constraints as well. For these formulations, we use the original DCOPF formulations without shift factors because of the direct modelling of FACTS compensation in nonlinear power flow control constraints. Following a similar approach, we first present the partial formulation of DCOPF without power flow control constraints.

The objective function is, still, (50), and the operating capacity constraints for generators are specified in (54). The rest of the constraints, except for the power flow control constraints, are presented as follows:

$$-f_{ij}^{\max} \le f_{ij} \le f_{ij}^{\max}, \forall ij; \tag{81}$$

$$\sum_{g\in G(i)} p_g + \sum_{j\in N^+(i)} f_{ij} - \sum_{j\in N^-(i)} f_{ij} = d_i, \forall i; \tag{82}$$

$$f_{ij} = -\frac{\theta_j-\theta_i}{x_{ij}}, \forall ij \notin K_F; \tag{83}$$

$$\theta_1 = 0. \tag{84}$$

Equation (81) imposes the thermal capacity limits on transmission line ij. Equation (82) is the power balance constraint at bus i. Equation (83) is the DC power flow equation for lines without FACTS. Equation (84) ensures that the voltage angle at the reference bus is equal to zero.

The power flow control constraints with nonlinear FACTS modelling, along with the partial formulation discussed previously, are used to formulated complete DCOPF problems. The power flow control constraints involving each type of FACTS devices for DCOPF problems are presented as follows:

SSSC_NL_OPF: (10),

$$f_{ij} = -\frac{\theta_j-\theta_i}{x_{ij}+\Delta x_{ij}}, \forall ij \in K_F; \tag{85}$$

MERS_NL_OPF: (10), (85),

$$\Delta x_{ij} \le 0, \forall ij \in K_{\mathrm{F}}; \tag{86}$$

UPFC_NL_OPF: (30), (31),

$$f_{ij} = \frac{\theta_i - \theta_j}{x_{ij}} - \frac{\left|\dot{V}_{ij}^{\mathrm{se}}\right|}{x_{ij}} \sin\left(\varphi_{ij} - \theta_i\right), \forall ij \in K_{\mathrm{F}}; \tag{87}$$

TCSC_NL_OPF: (35), (85).
M-SSSC_NL_OPF: (48), (49), (85),

$$-N_{ij}^{\mathrm{FACTS}} \bar{V} \le \Delta x_{ij} f_{ij} \le N_{ij}^{\mathrm{FACTS}} \bar{V}, \forall ij \in K_{\mathrm{F}}. \tag{88}$$

Compared to (83), (85) has Δx_{ij} to represent the reactance injection by FACTS devices. The combination of (10) and (86) is equivalent to (19), thus allowing a more efficient formulation for the solver to compute with the removal of the absolute sign. In (87), as φ_{ij} is a free variable, we can simply regard $\sin(\varphi_{ij} - \theta_i)$ as a continuous variable with limits being 1 and -1 when implementing the problem involving UPFC in the solver. $|\dot{V}_{ij}^{\mathrm{se}}|$ is regarded as a continuous variable as well, with variation limits specified in (30). In (88), the inclusion of N_{ij}^{FACTS} shows that the voltage injection limits are dependent on the number of modules installed on the transmission line, which is different from that in (10).

Nonlinearity in the constraints makes the DCOPF problems with nonlinear FACTS modelling NLPs except for M-SSSC_NL_OPF, which is a mixed-integer nonlinear program (MINLP) as it contains integer variables.

We then formulate the UC problems with nonlinear FACTS modelling, starting with the partial formulation. The objective function is (58). Constraints (62), (66)–(71) are the same as in the UC problems with linear FACTS modelling. The rest of the constraints, except for the power flow control constraints, are formulated as follows:

$$-f_{ij}^{\max} \le f_{ij,t} \le f_{ij}^{\max}, \forall ij, t; \tag{89}$$

$$\sum_{g \in G(i)} p_{gt} + \sum_{j \in N^+(i)} f_{ij,t} - \sum_{j \in N^-(i)} f_{ij,t} = d_{it}, \forall i, t; \tag{90}$$

$$f_{ij,t} = -\frac{\theta_{jt} - \theta_{it}}{x_{ij}}, \forall ij \notin K_{\mathrm{F}}, t; \tag{91}$$

$$\theta_{1t} = 0, \forall t. \tag{92}$$

The interpretation of (89)–(92) is the same as that of (81)–(84), except for the added time index.

Nonlinear power flow control constraints are needed to complete the UC problem formulations. These constraints can be formulated by simply adding the time index to the previously formulated constraints. Nonlinear power flow control constraints for each specific UC problem formulation are presented as follows:

SSSC_NL_UC:

$$-V_{ij}^{\max} \le \Delta x_{ij,t} f_{ij,t} \le V_{ij}^{\max}, \forall ij \in K_{\mathrm{F}}, t; \tag{93}$$

$$f_{ij,t} = -\frac{\theta_{jt} - \theta_{it}}{x_{ij} + \Delta x_{ij,t}}, \forall ij \in K_{\mathrm{F}}, t; \tag{94}$$

MERS_NL_UC: (93), (94),

$$\Delta x_{ij,t} \le 0, \forall ij \in K_{\mathrm{F}}, t; \tag{95}$$

UPFC_NL_UC:

$$0 \le \left|\dot{V}_{ij,t}^{\mathrm{se}}\right| \le V_{ij}^{\max}, \forall ij \in K_{\mathrm{F}}, t; \tag{96}$$

$$-1 \le \sin\left(\varphi_{ij,t} - \theta_{it}\right) \le 1, \forall ij \in K_{\mathrm{F}}, t; \tag{97}$$

$$f_{ij,t} = \frac{\theta_{it} - \theta_{jt}}{x_{ij}} - \frac{\left|\dot{V}_{ij,t}^{\mathrm{se}}\right|}{x_{ij}} \sin\left(\varphi_{ij,t} - \theta_{it}\right), \forall ij \in K_{\mathrm{F}}, t; \tag{98}$$

TCSC_NL_UC: (94),

$$-0.8\left|x_{ij}\right| \le \Delta x_{ij,t} \le 0.2\left|x_{ij}\right|, \forall ij \in K_{\mathrm{F}}, t; \tag{99}$$

M-SSSC_NL_UC: (48), (49), (94),

$$-N_{ij}^{\mathrm{FACTS}} \bar{V} \le \Delta x_{ij,t} f_{ij,t} \le N_{ij}^{\mathrm{FACTS}} \bar{V}, \forall ij \in K_{\mathrm{F}}, t. \tag{100}$$

$|\dot{V}_{ij,t}^{\mathrm{se}}|$ and $\sin(\varphi_{ij,t} - \theta_{it})$ are regarded as continuous variables when the problems involving UPFC is implemented in the solver. Because of the nonlinear constraints and integer variables, all UC problems with nonlinear FACTS modelling are MINLPs.

3.3 | Incorporation of series FACTS into power system operation models using linear FACTS modelling

With the problem formulations using linear FACTS modelling, we can now summarise how series FACTS can be incorporated into DC-based operation models. Note that, as mentioned previously, the DCOPF and UC problem formulations can be further extended to more complicated models. The process of incorporating series FACTS devices into power system operation models using linear FACTS models is presented in Figure 11.

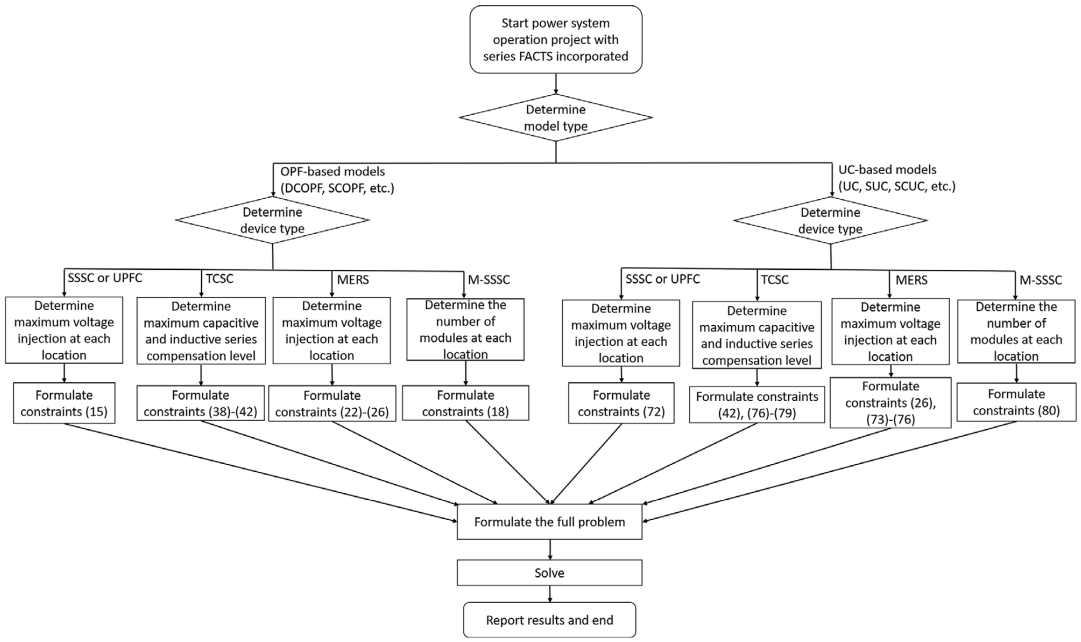

FIGURE 11 Incorporation of series FACTS into power system operation using linear FACTS models

TABLE 1 Solver selection in simulation studies

Problem type	Solver
LP	IBM ILOG CPLEX Studio 12.8 [49]
MILP	
NLP	IPOPT 3.11.1 [50]
MINLP	BARON 20.4.14 [51]

4 | SIMULATION STUDIES

Simulation studies are conducted to evaluate the effectiveness of the proposed modelling in improving computational efficiency. At the same time, the simulation results provide numerical verification for the mathematical derivations in Section 2. For the problems formulated in the previous section, we select prominent solvers that are well-suited for their problem types. Our solver selection is summarised in Table 1.

For MILPs and MINLPs, the optimality gap for both CPLEX and BARON solvers are set as 0.01%. Details of these parameters can be found in [52, 53]. Simulations are performed on a Windows Server with an Intel Xeon Gold 6136 CPU. The Texas 2000-bus system (ACTIVSg2000) [54] is used for DCOPF problems. The data for the test system is available at [55]. For UC problems, we use a smaller system, as the computational burden of UC plus the complexity of FACTS devices may lead to computational intractability with a large system. The system we use for UC is area 1 of the RTS-96 system [56], which is equivalent to a 24-bus test system. The test systems are modified to increase congestions, allowing them to be more suitable for studying operation models with FACTS included. The modifications are presented in the Appendix.

In the 2000-bus system, the ten lines are utilised the most are selected as locations for FACTS deployment. In the RTS-96 system, FACTS devices are deployed on each of the five lines with the largest reactance in the system, thus allowing diversity in FACTS allocation policy in the simulation studies. Note that optimal FACTS allocation is beyond the scope of this work. However, it is a key topic to be further studied in future work with the proposed modelling approach.

The sizing of FACTS at each location also needs to be specified. For the SSSC, we consider that each location has three SmartValve 10–3600 [57] devices installed, providing a maximum nominal voltage injection of 12006.67 V (0.087 p.u. for the RTS-96 system and 0.104 p.u. for the 2000-bus system). This value is used as the maximum voltage injection for MERS and UPFC devices as well. The maximum voltage injection for these three types of devices can be altered depending on the different need for power flow control capabilities in various scenarios. The setting for TCSC devices is the same as in (35), which, as mentioned previously, is a typical setting for TCSC operating range of series reactance adjustment.

Note that problem formulations involving M-SSSC has non-binary integer variables, making them computationally more demanding than other mixed-integer programs (MIP) in this paper. In addition, as mentioned previously, they are planning models, which is beyond the main focus of this paper which are operation models. Therefore, these problems are not studied

TABLE 2 Solutions and computational results of DCOPF with linear FACTS modelling

DCOPF	Obj. value (cost) ($)	Solution time avg. (s)	Solution time std. (s)
SSSC_L_OPF UPFC_L_OPF	882,782	2.508	0.164
MERS_L_OPF	887,295	1.826	0.140
TCSC_L_OPF	886,134	1.722	0.122

TABLE 3 Solutions and computational results of DCOPF with nonlinear FACTS modelling

DCOPF	Obj. value (cost) ($)	Solution time avg. (s)	Solution time std. (s)
SSSC_NL_OPF	882,782	4.423	0.193
UPFC_NL_OPF	882,782	3.681	0.143
MERS_NL_OPF	887,295	2.829	0.132
TCSC_NL_OPF	886,134	3.070	0.151

TABLE 4 Computational efficiency gain provided by linear FACTS modelling in DCOPF problems

FACTS device	Comp. efficiency gain
SSSC	176 %
MERS	155 %
UPFC	147 %
TCSC	178 %

through simulations in this paper and will be further explored in future research.

4.1 | DCOPF

The results of DCOPF problems with linear FACTS modelling are summarised in Table 2. Each problem is solved for 5 times and the results are used to obtain the average and standard deviation of solution time. The SSSC and the UPFC share the same linear modelling, thus their related problem formulations share the same results in Table 2.

The results of DCOPF problems with nonlinear formulations are presented in Table 3.

By comparing the objective function value results in Tables 2 and 3, we can see that both the linear and nonlinear formulations result in the same optima for every type of FACTS device discussed in this paper. The results, thus, provide a numerical verification the mathematical derivation leading to linear FACTS modelling.

We use the average solution time as the measurement for computational efficiency. Table 4 presents the comparison regarding computational efficiency between linear and nonlinear FACTS modelling for DCOPF problems.

TABLE 5 Solutions and computational results of UC with linear FACTS modelling

UC	Obj. value (cost) ($)	Solution time avg. (s)	Solution time std. (s)
SSSC_L_UC UPFC_L_UC	973,049	1.044	0.087
MERS_L_UC	973,170	1.100	0.066
TCSC_L_UC	973,464	16.858	0.549

TABLE 6 Solutions and computational results of UC with nonlinear FACTS modelling

UC	Obj. value (cost) ($)	Solution time avg. (s)	Solution time std. (s)
SSSC_NL_UC	973,049	141.328	17.525
UPFC_NL_UC	973,049	123.916	6.553
MERS_NL_UC	973,170	615.432	52.830
TCSC_NL_UC	Failed to converge after 100,000 s		

The results reveal that linear FACTS modelling provides computational efficiency gains for DCOPF models involving different types of FACTS devices. It is worth noting that DCOPF problems are inherently less computationally challenging and, thus, we expect more computational efficiency improvement from linear FACTS modelling in more complicated models. Computational efficiency improvement is further discussed with the results of UC problems, which are presented in the next subsection.

4.2 | UC

The results of UC problems with linear FACTS modelling are summarised in Table 5. Table 6 presents the results of UC problems with nonlinear formulations.

As is shown in Table 6, the solver failed to provide a solution for TCSC_NL_UC after the maximum time limit of 100,000 s. This emphasises the importance of linear FACTS modelling as the non-convexity and non-linearity of non-linear TCSC modelling leads to computational intractability for the basic UC problem implemented with a small test system. For the intuitiveness and explicitness of the results, we implemented TCSC_NL_UC and TCSC_L_UC with the smaller IEEE 14-bus test system [58]. The system data for the simulation studies is available in [59], and line thermal capacity data is obtained from [60]. Five lines with the largest reactance are selected as locations for FACTS deployment in the system. Again, we made modifications to the system to increase the congestion. The modifications are presented in the Appendix. The results are shown in Table 7.

The objective function value results in Tables 5–7 confirmed that both the linear and non-linear FACTS modelling achieve the same optima for UC models across all types of FACTS

TABLE 7 Solutions and computational results of UC with TCSC using the 14-bus system

UC	Obj. value (cost) ($)	Solution time avg. (s)	Solution time std. (s)
TCSC_ NL_UC	187,092	32.670	0.989
TCSC_L_UC	187,092	0.620	0.040

TABLE 8 Computational efficiency gain provided by linear FACTS modelling in UC problems

FACTS device	Comp. efficiency gain
SSSC	13,537%
MERS	55,948%
UPFC	11,869%
TCSC	5269%

devices studied in this paper. The UC results, thus, provide verification for linear FACTS modelling as well.

We again use the average solution time as the measurement for computational efficiency. Table 8 presents the comparison regarding computational efficiency between linear and nonlinear FACTS modelling.

The results in Table 8 show that the linear FACTS modelling provides significant computational efficiency improvement over nonlinear FACTS modelling in UC problems. Note that for UC problems involving the TCSC, the result in Table 8 is calculated using the results presented in Table 7. The computational efficiency gain is, thus, expected to be even more significant with a larger system.

The results of UC problems reveal that linear FACTS modelling will be valuable for a variety of related power system optimisation models, including previously mentioned SCUC and SUC, as well as planning models. These models inherently bear significant computationally burdens even without FACTS deployment. Therefore, linear FACTS modelling will be important for ensuring computational tractability for complex power system optimisation models involving FACTS deployment.

5 | CONCLUSIONS

This paper presents the linear modelling of series FACTS devices in power system operation models. Compared to the existing literature, the models presented here accurately captures the operating range of FACTS devices. In addition, this paper enables integration of FACTS devices within linear DC power flow models through derivation of an equivalent linear operating range. Finally, the paper shows how the constraints can be applied in injection-shift-factor-based DCOPF and UC, which are widely used in industry implementations of operation and planning software tools.

Simulation results verifies the mathematical derivation that leads to the proposed modelling. Moreover, linear FACTS modelling shows significant superiority in computational efficiency. The results underline the importance of linear FACTS modelling in combating the challenge of increased computational complexity due to FACTS deployment in the already computationally heavy optimisation models. Furthermore, linear FACTS modelling will be vital in facilitating FACTS technology deployment in the power gird. Linear FACTS modelling will be important for incorporating series FACTS into various operation and planning models, including SUC, SCOPF, and SCUC, allowing the utilization of power flow control capabilities of FACTS devices. The models presented in this paper is also vital for developing FACTS planning tools for optimal placement that are based on DC power flow models. Moreover, M-FACTS deployment problems, including optimal allocation, reinstallation scheduling etc., will be important topics as well. Studying these problems and models will be included in our future research.

NOMENCLATURE

$\dot{I}_{ij}$	Current phasor of transmission line ij
$\dot{V}_i$	Voltage phasor of bus i
$\dot{V}_i^{\mathrm{sh}}$	UPFC shunt voltage injection phasor for bus i
$\dot{V}_{ij}^{\mathrm{se}}$	FACTS series voltage injection phasor for transmission line ij
$\tilde{b}_{ij}$	Susceptance of transmission line ij with FACTS deployed
$\tilde{f}_{ij}$ ($\tilde{f}_{ij,t}$)	Partial power flow not including FACTS injection through transmission line ij (at time t)
$\mathbf{\Phi}_{ij}^{n}$	Injection shift factor associating bus n to transmission line ij
$I^{\min}$	Minimum current to power up FACTS devices
I_{ij}	Current on transmission line ij
$I_{ij}^{\max}$	Maximum current on transmission line ij
K_{F}	Set of transmission lines equipped with FACTS devices
$N^{-}(i)$	Set of buses that has a transmission line connected "from" bus i
$N^{+}(i)$	Set of buses that has a transmission line connected "to" bus i
$N^{\max}$	Total number of available M-FACTS devices
N_{ij}^{FACTS}	Number of M-FACTS devices installed on transmission line ij
$N_{ij}^{\max}$	Maximum number of M-FACTS allowed to be deployed on transmission line ij
R_g^{+}, R_g^{-}	Maximum hourly ramp rate of generator g
UT_g, DT_g	Minimum up and down time of generator g
$\tilde{V}$	Maximum voltage injection of a single M-SSSC device
$V_{ij}^{\max}$	Maximum voltage injection of SSSC or UPFC devices on transmission line ij
b_{ij}	Pre-injection susceptance of transmission line ij

$b_{ij}^{\min}$, $b_{ij}^{\max}$	Minimum and maximum susceptance of transmission line ij equipped with FACTS
$p_g^{\max}$, $p_g^{\min}$	Generator capacity limits
c_g	Marginal cost of generator g
d_i (d_{it})	Demand on bus i (at time t)
$f^{\min}$	Minimum flow to power up FACTS devices
f_{ij} ($f_{ij,t}$)	Active power flow through transmission lineij (at time t)
$f_{ij}^{\max}$	Capacity of transmission line ij
k_g	No-load cost of generator g
p_g (p_{gt})	Active power output of generator g (at time t)
s_g	Start-up cost of generator g
u_g (u_{gt})	Unit commitment variable of generator g (at time t)
v_g (v_{gt})	Start-up variable of generator g (at time t)
x_{TCSC}	TCSC reactance injection
$x_{\text{TCSC}}^{\min}$, $x_{\text{TCSC}}^{\max}$	Minimum and maximum reactance injection of TCSC devices
x_{ij}	Reactance of transmission line ij
z_{ij} ($z_{ij,t}$)	Binary variable representing flow direction of transmission line ij (at time t)
θ_i (θ_{it})	Voltage angle at bus i (at time t)
φ_{ij} ($\varphi_{ij,t}$)	Phase angle of UPFC voltage injection on transmission line ij (at time t)
ψ_i (ψ_{it})	Power injection at bus i (at time t)
Δb_{ij}	Susceptance change on transmission line ij
Δf_{ij} ($\Delta f_{ij,t}$)	FACTS power injection on transmission line ij (at time t)
Δx_{ij} ($\Delta x_{ij,t}$)	Effective reactance injection of FACTS devices on transmission line ij (at time t)
G	Set of all generators in the network
$G(i)$	Set of generators located at bus i
M	A very large positive number
N	Set of all buses in the network
T	Set of time periods
g	Index of generators
i, j, n	Index of buses
ij	Index of transmission line from bus i to j
t	Index of time

ACKNOWLEDGEMENTS

This research was funded by the National Science Foundation grant # 1756006.

CONFLICT OF INTEREST

Dr. Nudell works for Smart Wires Inc., a developer of modular flexible ac transmission system devices.

DATA AVAILABILITY STATEMENT

The data that support the findings of this study are openly available in: 'ACTIVSg2000: 2000-bus synthetic grid on footprint of Texas' at https://electricgrids.engr.tamu.edu/electric-grid-test-cases/activsg2000/, reference number [55];

'Power System Test Case Archive - Reliability Test System (RTS)-1996′ at http://labs.ece.uw.edu/pstca/rts/pg_tcarts.htm, reference number [56];

'SmartValve™ v1.04 Spec Sheet' at https://www.smartwires.com/download/20801/, reference number [57];

'Power Systems Test Case Archive - 14 Bus Power Flow Test Case' at https://labs.ece.uw.edu/pstca/pf14/pg_tca14bus.htm, reference number [58];

'Description of Case 14′ at https://matpower.org/docs/ref/matpower5.0/case14.html, reference number [59].

'A Data Sheet for IEEE 14 Bus System' at https://www.academia.edu/7781632/A_DATA_SHEETS_FOR_IEEE_14_BUS_SYSTEM, reference number [60].

ORCID

Mostafa Sahraei-Ardakani https://orcid.org/0000-0002-5770-8291

REFERENCES

1. Joskow, P.L.: Creating a smarter U.S. electricity grid. J. Econ. Perspect. 26(1), 29–48 (2012)
2. Sahraei-Ardakani, M.: Merchant power flow controllers. Energy Econ. 74, 878–885 (2018)
3. Ou, Y., Singh, C.: Assessment of available transfer capability and margins. IEEE Trans. Power Syst. 17(2), 463–468 (2002)
4. Del Rosso, A.D., Eckroad, S.W.: Energy storage for relief of transmission congestion. IEEE Trans. Smart Grid 5(2), 1138–1146 (2014)
5. Energy information administration: Annual energy outlook 2021. https://www.eia.gov/outlooks/aeo/ (2021). Accessed 1 June 2021
6. Zhang, X., Shi, D., Wang, Z., et al.: Optimal allocation of series FACTS devices under high penetration of wind power within a market environment. IEEE Trans. Power Syst. 33(6), 6206–6217 (2018)
7. Lumbreras, S., Ramos, A.: The new challenges to transmission expansion planning. Survey of recent practice and literature review. Electr. Power Syst. Res. 134, 19–29 (2016)
8. Marston, T.U.: The US electric power system infrastructure and its vulnerabilities. The Bridge 48(2), 31–39 (2018)
9. National Energy Technology Laboratory: Understanding the Benefits of the Smart Grid. https://netl.doe.gov/sites/default/files/Smartgrid/06-18-2010_Understanding-Smart-Grid-Benefits.pdf (2010). Accessed 20 November 2019
10. Sang, Y., Sahraei-Ardakani, M., Parvania, M.: Stochastic transmission impedance control for enhanced wind energy integration. IEEE Trans. Sustainable Energy 9(3), 1108–1117 (2018)
11. Sahraei-Ardakani, M., Hedman, K.W.: A fast LP approach for enhanced utilization of variable impedance based FACTS devices. IEEE Trans. Power Syst. 31(3), 2204–2213 (2016)
12. Sahraei-Ardakani, M., Hedman, K.W.: Day-ahead corrective adjustment of FACTS reactance: A linear programming approach. IEEE Trans. Power Syst. 31(4), 2867–2875 (2016)
13. Sahraei-Ardakani, M., Hedman, K.W.: Computationally efficient adjustment of FACTS set points in DC optimal power flow with shift factor structure. IEEE Trans. Power Syst. 32(3), 1733–1740 (2017)
14. Geng, G., Abhyankar, S., Wang, X., Dinavahi, V.: IEEE PES task force on interfacing techniques for solution tools: Solution techniques for transient stability-constrained optimal power flow – Part II. IET Gener. Transm. Distrib. 11(12), 3186–3193 (2017)
15. Yang, Z., Zhong, H., Bose, A., Zheng, T., Xia, Q., Kang, C.: A linearized OPF Model with reactive power and voltage magnitude: A pathway to improve the MW-only DC OPF. IEEE Trans. Power Syst. 33(2), 1734–1745 (2018)
16. Stott, B., Jardim, J., Alsac, O.: DC power flow revisited. IEEE Trans. Power Syst. 24(3), 1290–1300 (2009)

17. Taranto, G.N., Pinto, L.M.V.G., Pereira, M.V.F.: Representation of FACTS devices in power system economic dispatch. IEEE Trans. Power Syst. 7(2), 572–576 (1992)
18. Sahraei-Ardakani, M., Sang, Y.: Discussion on linear modeling of variable reactance in "co-optimization of transmission expansion planning and TCSC placement considering the correlation between wind and demand scenarios. IEEE Trans. Power Syst. 33(5), 5808–5809 (2018)
19. Ziaee, O., Alizadeh-Mousavi, O., Choobineh, F.F.: Co-optimization of transmission expansion planning and TCSC placement considering the correlation between wind and demand scenarios. IEEE Trans. Power Syst. 33(1), 206–215 (2018)
20. Ding, T., Bo, R., Li, F., Sun, H.: Optimal power flow with the consideration of flexible transmission line impedance. IEEE Trans. Power Syst. 31(2), 1655–1656 (2016)
21. Mohammadi, J., Hug, G., Kar, S.: Fully distributed DC-OPF approach for power flow control. In: Proceedings of 2015 IEEE Power & Energy Society General Meeting, Denver, Colorado, USA, pp. 1–5 (2015)
22. Li, B., Xiao, G., Lu, R., Deng, R., Bao, H.: On feasibility and limitations of detecting false data injection attacks on power grid state estimation using D-FACTS devices. IEEE Trans. Ind. Inf. 16(2), 854–864 (2020)
23. Liu, B., Wu, H.: Systematic planning of moving target defence for maximising detection effectiveness against false data injection attacks in smart grid. IET Cyber-Phys. Syst. 6(3), 151–163 (2021)
24. Yan, M., Shahidehpour, M., Paaso, A., Zhang, C., Abdulwhab, A., Abusorrah, A.: A convex three-stage SCOPF approach to power system flexibility with unified power flow controllers. IEEE Trans. Power Syst. 36(3), 1947–1960 (2020)
25. Rajabi-Ghahnavieh, A., Fotuhi-Firuzabad, M., Othman, M.: Optimal unified power flow controller application to enhance total transfer capability. IET Gener. Transm. Distrib. 9(4), 358–368 (2015)
26. Sadiq, A.A., Buhari, M., Adamu, S.S., Musa, H.: Coordination of multi-type FACTS for available transfer capability enhancement using PI–PSO. IET Gener. Transm. Distrib. 14(21), 4866–4877 (2020)
27. El Moursi, M., Sharaf, A.M., El-Arroudi, K.: Optimal control schemes for SSSC for dynamic series compensation. Electr. Power Syst. Res. 78(4), 646–656 (2008)
28. SMARTVALVE™. https://www.smartwires.com/smartvalve. Accessed 9 August 2019
29. Zhang, X.P., Rehtanz, C., Pal, B.: Flexible AC Transmission Systems: Modelling and Control. Springer Science & Business Media, Berlin (2012)
30. The Power Flow Equations. Available at http://home.eng.iastate.edu/~jdm/ee553/DCPowerFlowEquations.pdf. Accessed 1 July 2019
31. Sang, Y., Sahraei-Ardakani, M.: Effective power flow control via distributed FACTS considering future uncertainties. Electr. Power Syst. Res. 168, 127–136 (2019)
32. Wiik, J.A., T. Isobe, T. Takaku, et al.: Feasible series compensation applications using Magnetic Energy Recovery Switch (MERS). In: Proceedings of 2007 European Conference on Power Electronics and Applications, Aalborg, Denmark, pp. 1–9 (2007)
33. Wiik, J.A., Wijaya, F.D., Shimada, R.: Characteristics of the magnetic energy recovery switch (MERS) as a series FACTS controller. IEEE Trans. Power Delivery 24(2), 828–836 (2009)
34. Gyugyi, L., Schauder, C.D., Williams, S.L., Rietman, T.R., Torgerson, D.R., Edris, A.: The unified power flow controller: A new approach to power transmission control. IEEE Trans. Power Delivery 10(2), 1085–1097 (1995)
35. Guo, J., Crow, M.L., Sarangapani, J.: An improved UPFC control for oscillation damping. IEEE Trans. Power Syst. 24(1), 288–296 (2009)
36. Fujita, H., Watanabe, Y., Akagi, H.: Control and analysis of a unified power flow controller. IEEE Trans. Power Electron. 14(6), 1021–1027 (1999)
37. Noroozian, M., Angquist, L., Ghandhari, M., Andersson, G.: Use of UPFC for optimal power flow control. IEEE Trans. Power Delivery 12(4), 1629–1634 (1997)
38. Sen, D., Acharjee, P.: Optimal line flows based on voltage profile, power loss, cost and conductor temperature using coordinated controlled UPFC. IET Gener. Transm. Distrib. 13(7), 1132–1144 (2019)
39. Larsen, E.V., Clark, K., Miske, S.A., Urbanek, J.: Characteristics and rating considerations of thyristor controlled series compensation. IEEE Trans. Power Delivery 9(2), 992–1000 (1994)
40. Paserba, J.J., Miller, N.W., Larsen, E.V., Piwko, R.J.: A thyristor controlled series compensation model for power system stability analysis. IEEE Trans. Power Delivery 10(3), 1471–1478 (1995)
41. Glanzmann, G., Andersson, G.: Coordinated control of FACTS devices based on optimal power flow. In: Proceedings of 37th Annual North American Power Symposium, Ames, IA, USA, pp. 141–148 (2005)
42. Shanmukha Sundar, K., Ravikumar, H.M.: Selection of TCSC location for secured optimal power flow under normal and network contingencies. Int. J. Electr. Power Energy Syst. 34(1), 29–37 (2012)
43. Singh, J.G., Singh, S.N., Srivastava, S.C.: Enhancement of power system security through optimal placement of TCSC and UPFC. In: 2007 IEEE Power Engineering Society General Meeting, Tampa, FL, USA, pp. 1–6 (2007)
44. Duong, T., JianGang, Y., Truong, V.: A new method for secured optimal power flow under normal and network contingencies via optimal location of TCSC. Int. J. Electr. Power Energy Syst. 52, 68–80 (2013)
45. Gerbex, S., Cherkaoui, R., Germond, A.J.: Optimal location of multi-type FACTS devices in a power system by means of genetic algorithms. IEEE Trans. Power Syst. 16(3), 537–544 (2001)
46. Shafik, M.B., Chen, H., Rashed, G.I., El-Sehiemy, R.A.: Adaptive multi objective parallel seeker optimization algorithm for incorporating TCSC devices into optimal power flow framework. IEEE Access 7, 36934–36947 (2019)
47. Papavasiliou, A., Oren, S.S., O'Neill, R.P.: Reserve requirements for wind power integration: A scenario-based stochastic programming framework. IEEE Trans. Power Syst. 26(4), 2197–2206 (2011)
48. Papavasiliou, A., Oren, S.S.: Multiarea stochastic unit commitment for high wind penetration in a transmission constrained network. Oper. Res. 61(3), 578–592 (2013)
49. IBM CPLEX Optimizer. https://www.ibm.com/analytics/cplex-optimizer. Accessed 2 August 2020
50. IPOPT Documentation. https://coin-or.github.io/Ipopt/. Accessed 15 September 2020
51. BARON Solver. https://minlp.com/baron. Accessed 15 September 2020
52. relative MIP gap tolerance. https://prod.ibmdocs-production-dal-6099123ce774e592a519d7c33db8265e-0000.us-south.containers.appdomain.cloud/docs/en/icos/12.8.0.0?topic=parameters-relative-mip-gap-tolerance. Accessed 15 September 2020
53. Sahinidis, N.: BARON user manual v. 2021.1.13. https://www.minlp.com/downloads/docs/baron%20manual.pdf. Accessed 15 September 2020
54. Birchfield, A.B., Xu, T., Gegner, K.M., Shetye, K.S., Overbye, T.J.: Grid structural characteristics as validation criteria for synthetic networks. IEEE Trans. Power Syst. 32(4), 3258–3265 (2017)
55. ACTIVSg2000: 2000-bus synthetic grid on footprint of Texas. https://electricgrids.engr.tamu.edu/electric-grid-test-cases/activsg2000/. Accessed 1 February 2019
56. Power System Test Case Archive - Reliability Test System (RTS)-1996. http://labs.ece.uw.edu/pstca/rts/pg_tcarts.htm. Accessed 25 November 2020
57. Smart Wires Inc.: SmartValve™ v1.04 Spec Sheet. https://www.smartwires.com/download/20801/ (2021). Accessed 27 October 2020
58. Power Systems Test Case Archive - 14 Bus Power Flow Test Case. https://labs.ece.uw.edu/pstca/pf14/pg_tca14bus.htm. Accessed 18 March 2021
59. Matpower: Description of Case 14. https://matpower.org/docs/ref/matpower5.0/case14.html. Accessed 18 March 2021
60. A Data Sheet for IEEE 14 Bus System. https://www.academia.edu/7781632/A_DATA_SHEETS_FOR_IEEE_14_BUS_SYSTEM. Accessed 18 March 2021

How to cite this article: Rui, X., Sahraei-Ardakani, M., Nudell, T.R.: Linear modelling of series FACTS devices in power system operation models. IET Gener. Transm. Distrib. 2021;1–17.
https://doi.org/10.1049/gtd2.12348

APPENDIX

Our method to increase the congestion level in the test systems is through reducing the capacity of lines. The modifications in the 2000-bus system are summarised in Table 9.

In the RTS-96 system, the capacity of line 23, which is the most utilised line in the system, is altered from 500 MW to 315 MW. For the rest of the lines in the system, the capacity is reduced by 10%.

Similarly, in the 14-bus system, the capacity of line 15 is reduced by 40%. For the rest of the lines in the system, the capacity is reduced by 10%.

TABLE 9 Modifications of line capacities in the 2000-bus system

Line number	Capacity (MW)	Modified capacity (MW)
43	149	112
58	170	128
71	145	109
74	149	112
364	82	62
435	143.8	108
439	83	62
765	168	145
1038	150	113
1380	1450	1088
1381	1450	1088
2136	217.8	190
2382	1233	925
2389	220	165
2449	1600	1200
2450	1600	1200
2803	198	180
2911	280.8	220
2912	280.8	220
2913	280.8	220
2993	213	180
2994	213	180
2995	213	180

CHAPTER 3

A SUCCESSIVE FLOW DIRECTION ENFORCING ALGORITHM FOR OPTIMAL OPERATION OF VARIABLE-IMPEDANCE FACTS DEVICES

Variance-impedance FACTS devices offer power flow control capabilities by directly regulating line reactances. As mentioned in Chapter 1, the simple model of such devices by treating the reactance or susceptance as a variable leads to nonlinearity in the model. A mixed-integer reformulation, although eliminating the nonlinearity, still leads to added computational burdens. This issue can be addressed by following a flow direction approach. However, the method shown in previous research can lead to suboptimality due to directly using the base case DCOPF results. The published article[1] presented in this chapter seeks to tackle the problem of nonlinearity and extend the flow direction method application to unit commitment models. The successive flow direction enforcing algorithm is developed, which iteratively adjusts the enforced flow directions based on results from the previous iteration.

---

[1]Reprinted, with permission, from Xinyang Rui and Mostafa Sahraei-Ardakani, "A successive flow direction enforcing algorithm for optimal operation of variable-impedance FACTS devices", *Electric Power System Research*, 211, 108171, 2022.

Electric Power Systems Research 211 (2022) 108171

Contents lists available at ScienceDirect

Electric Power Systems Research

journal homepage: www.elsevier.com/locate/epsr

A successive flow direction enforcing algorithm for optimal operation of variable-impedance FACTS devices☆

Xinyang Rui, Mostafa Sahraei-Ardakani *

Department of Electrical and Computer Engineering, The University of Utah, 50 S. Central Campus Drive, 84112, Salt Lake City, Utah, USA

ARTICLE INFO

Keywords:
Power flow control
FACTS devices
Power system operation
DC power flow

ABSTRACT

This paper presents a novel successive flow direction enforcing (SFDE) algorithm for solving power system operation models with flexible AC transmission system (FACTS) devices. The power flow control capabilities of FACTS devices can improve the utilization of the existing transmission network. However, the added computational complexity of modeling FACTS devices in power system operation models is one of the primary challenges for FACTS deployment. A prominent component is the nonlinearity introduced by variable-impedance FACTS devices to the linear DC power flow equations. According to previous studies, such nonlinearity can be tackled by preassigning the power flow directions on lines equipped with FACTS to restore the linearity of DC power flow equations. However, this method has the issue of converging to suboptimal solutions in some cases, due to suboptimal flow direction assignment. The algorithm presented in this paper can address the issue of suboptimality, while still achieving computational efficiency improvements. Power system operation models with FACTS are solved iteratively with flow directions enforced, and the predetermined flow directions are adjusted successively based on the results of the previous iteration. Simulation studies confirm the effectiveness of the method in converging to the globally optimal solution within a few iterations in almost all practical cases.

1. Introduction

The annual revenue of the US electric power industry is more than 390 billion dollars [1]. As a result, it is important to improve the efficiency in power system operation. One of the causes of system inefficiency is congestion in transmission systems. Congestion occurs when power transfers reach or exceed the capacity of the existing transmission network [2]. Transmission congestion costs electricity consumers billions of dollars each year across the country [3]. Therefore, it is essential to enhance the transfer capability of transmission systems to address the congestion problem. Sufficient available transfer capability (ATC) should be guaranteed to maintain secure and economical system operation [4]. Besides, insufficient transfer capability is one of the challenges for the integration of higher levels of renewable energy into the power grid [5]. The integration of renewable energy sources (RES) is growing rapidly in the electricity sector and projected to support 36% of power demand worldwide in 2030 [6]. Additionally, the US has an ambitious goal of reaching a carbon-free grid by 2035 [7]. Increased penetration from RES will require further enhancement of transfer capability in the upcoming years.

One obvious approach to enhance transfer capability is upgrading and expanding the transmission system. However, this option is not attractive due to its lengthy process and high level of required investment. Improving utilization of the existing system is a faster and cheaper alternative, even though it cannot completely replace the need for new transmission lines. Regardless, utilization of the existing transmission system to its full capability is always paramount [8]. Utilization improvement can be achieved through the power flow control capabilities provided by the implementation of flexible AC transmission system (FACTS) technologies in the transmission network. It is worth noting that FACTS technology is a non-transmission alternative aligned with FERC order 1000 [9]. With power flow control, power can be rerouted to lines that are not congested to avoid transmission bottlenecks.

FACTS devices are power electronic devices that have the ability to control a variety of system properties, including voltage magnitude, voltage phase angle, shunt susceptance, and impedance of transmission lines [10], thus allowing them to have vital roles in various domains of power system operation and control [11]. With the fast operation and flexibility, they can be used to dampen low-frequency oscillation and deviations of wind power production [12,13]. FACTS devices can also

☆ This document is the results of the research projects funded by the National Science Foundation grant numbers 1756006 and 2146531.
* Corresponding author.
E-mail address: mostafa.ardakani@utah.edu (M. Sahraei-Ardakani).

https://doi.org/10.1016/j.epsr.2022.108171
Received 15 February 2022; Received in revised form 13 May 2022; Accepted 3 June 2022
Available online 1 July 2022

Nomenclature

Indices

g	Index of generators, $g \in G$
k	Index of transmission lines, $k \in K$
n	Index of buses, $n \in N$
t	Index of time periods, $t \in T$

Parameters

b_k	Susceptance of line k ($k \notin \mathcal{F}$)
$b_k^{\max}$	Maximum susceptance of line k ($k \in \mathcal{F}$)
$b_k^{\min}$	Minimum susceptance of line k ($k \in \mathcal{F}$)
c_g	Linear cost of generator g
$d_n(d_{nt})$	Demand at bus n (in time period t)
DT_g	Minimum down time of generator g
$f_k^{\max}$	Capacity of line k
FC_{C}	Capacitive FACTS capacity
FC_{L}	Inductive FACTS capacity
M	A very large positive number
N_{F}	The number of FACTS devices in the system
NL_g	No-load cost of generator g
$p_g^{\max}$	Maximum output of generator g
$p_g^{\min}$	Minimum output of generator g
RD_g	Ramp-down limit of generator g
RU_g	Ramp-up limit of generator g
SU_g	Start-up cost of generator g
UT_g	Minimum up time of generator g
x_k	Original reactance of line k ($k \in \mathcal{F}$)

Sets

$\delta^+(n)$	Set of lines that are connected "to" bus n
$\delta^-(n)$	Set of lines that are connected "from" bus n
$\mathcal{F}$	Set of lines equipped with FACTS, $\mathcal{F} \subset K$
$G(n)$	Set of generators connected to bus n
G	Set of generators
K	Set of transmission lines
N	Set of buses
T	Set of time periods

Variables

$\theta_{k,\mathrm{fr}}(\theta_{k,\mathrm{fr},t})$	Voltage angle at the "from" bus of line k (in time period t)
$\theta_{k,\mathrm{to}}(\theta_{k,\mathrm{to},t})$	Voltage angle at the "to" bus of line k (in time period t)
b_k	Susceptance of line k ($k \in \mathcal{F}$)
$f_k(f_{kt})$	Active power flow on line k (in time period t)
$p_g(p_{gt})$	Active power output of generator g (in time period t)
u_{gt}	Commitment of generator g in time period t
v_{gt}	Start-up of generator g in time period t
$z_k(z_{kt})$	Power flow direction on line k (in time period t)

help improve reliability and transient stability [14], as well as reduce loop flows in transmission systems [15].

There have already been deployment and planning of FACTS technology in the transmission network in the US and around the world. FACTS technology from Smart Wires Inc., a company that provides modular power flow control solutions, has been deployed in both the Tennessee Valley Authority and Southern Company networks to manage power flow, maintain reliability, and help integrate higher levels of renewable generation [16]. The UPFC Plus devices developed by Siemens can offer power flow capabilities in high-voltage transmission networks with desirable features such as fast response time. General Electric (GE) has deployed series compensation systems in Texas, Vietnam, and the California-Oregon Intertie to help increase transfer capability of existing transmission lines, improve reliability, and, thus, allowing higher level of renewable generation integration [17]. Following a $20 million contract signed in 2018, ABB has planned to install series compensation devices in the vicinity of Brasilia, Brazil to increase transmission capacity while maintaining system stability [18].

This paper focuses on variable-impedance FACTS devices, which has the ability to continuously regulate the reactance of transmission lines, in order to control active power flow [19]. DC power flow is, thus, a good approach for solving the planning and operation problems of variable-impedance FACTS devices. Devices such as the static var compensator (SVC) and the static synchronous compensator (STATCOM) are beyond the scope of this paper as proper modeling of voltage and reactive power is essential for their applications in voltage regulation and reactive power compensation. For the rest of this paper, we use the term "FACTS" to only refer to the types of devices that can provide continuous reactance adjustments with fixed variation limits, such as the thyristor-controlled series compensator (TCSC) and the continuously variable series reactor (CVSR). There are also modular-FACTS (M-FACTS) devices of such type deployed in the power grid, e.g., the PowerLine Guardian device by SmartWires Inc. [20]. Details about FACTS modeling in DC power flow are presented in Section 2.

The ability of FACTS devices to improve transfer capability is well-recognized [21]. However, the utilization of FACTS technology is still limited due to multiple reasons including the legacy operational philosophies that prefer minimal changes to the existing system, cost of devices, and the lack of economic incentives [21,22]. One main barrier is the computational complexity that FACTS devices introduce to the DC power flow equation. DC-based models are widely used in clearing day-ahead and real-time markets, contingency screening, transmission load relief, transfer capability analysis, and transmission planning [21,23]. Inclusion of FACTS devices adds nonlinearity to the DC power flow equation, which is linear in its original form. The nonlinearity makes solving power system operation models challenging within the limited time that is available to power system operation software [22].

Previous studies have proposed a mixed-integer reformulation of the DC power flow equation with FACTS included to eliminate the aforementioned nonlinearity [8,22,24]. Details of the reformulation is presented in Section 2. In this reformulation, if the flow directions or the signs of bus phase angle differences on transmission lines equipped with FACTS devices are known, the integer variables introduced by the reformulation in power flow equations are eliminated, thus further improving computational efficiency. Based on such reformulation, a two-stage linear program (LP) method is proposed in [8] to solve DC optimal power flow (DCOPF) with FACTS included, which is an nonlinear program (NLP) originally. In this method, the power flow directions can be obtained by solving a base case DCOPF problem (referred to as OPF_base for simplicity in this paper) that involves no FACTS device. Then, based on a key assumption that FACTS devices are often installed on transmission bottlenecks where the flow direction is unlikely to change [8], the results from OPF_base can be used to predetermine the flow directions, on the lines equipped with FACTS, to construct a second-stage linear program (LP) with FACTS devices included. We refer to this approach as the two-stage method for the rest of this paper. The two-stage method is also implemented with

large-scale systems in [25], where a DCOPF formulation with power transfer distribution factors (PTDF) is proposed, which eliminates the need for calculating bus voltage angles. Although simulation studies reveal impressive improvements in computational efficiency provided by the two-stage method, the issue of suboptimality exists in some cases as the power flow direction results from OPF_base can be suboptimal for formulating the second stage LP with FACTS. Furthermore, the two-stage method has been used in unit commitment (UC) models as well. In [26], the authors applied the two-stage method to solve a stochastic security-constrained unit commitment (SCUC) model, where a base case SCUC is solved for determining the flow directions on lines equipped with FACTS. However, no discussion on the optimality of the solutions and computational efficiency is provided.

Reviewing the two-stage method in the existing literature shows that there is a need for improving the flow direction enforcing approach to address the suboptimality issues, when solving power system operation models with FACTS included, while still providing computational efficiency gains. Additionally, the solution quality when applying the flow direction enforcing approach for UC models needs to be further analyzed. To fill these research gaps, this paper makes the following contributions.

- A novel successive flow direction enforcing (SFDE) algorithm is presented in this paper. The SFDE algorithm addresses the aforementioned suboptimality issue, while still providing computational efficiency improvements over directly solving the power system operation models with FACTS included. The first step of the SFDE algorithm is to initialize the flow directions of transmission lines equipped with FACTS devices. Then, the power system operation models are solved iteratively, with a simple check used to adjusts the enforced line flow directions based on the solution of the previous iteration. Simulation studies with different test systems show that the method converges within a limited number of iterations, and global optimality is achieved in almost all cases.
- The proposed SFDE algorithm is employed to solve more complicated UC model in this paper. Discussion on the solution quality and computational efficiency is presented, thus facilitating expanding the scope of application of the flow direction enforcing approach to UC-based models.

Note that energy and market management system software tools all rely on linear and mixed-integer linear optimization models, using one or another form of DC power flow. Therefore, the SFDE algorithm as a linear method provides compatibility with existing software tools, allowing for straightforward industry adoption.

The rest of this paper is organized as follows. Section 2 presents the methodology. Section 3 includes simulation studies that confirm the effectiveness of the developed method. A discussion on the convergence to optimality is presented in Section 4. Finally, Section 5 concludes this paper.

2. Methodology

The SFDE algorithm is proposed to solve power system operation models with FACTS included. Therefore, FACTS modeling, problem formulations, and the aforementioned mixed-integer reformulation are crucial for presenting the SFDE algorithm, and are, thus, presented first in this section. We then show the idea behind the design of the SFDE algorithm and its detailed steps.

2.1. FACTS modeling

In this paper, the parameter FACTS capacity is used to describe the compensation level of variable-impedance FACTS devices. For any line with FACTS installed, assuming positive line reactance, we have:

$$f_k - b_k(\theta_{k,\text{to}} - \theta_{k,\text{fr}}) = 0, k \in \mathcal{F}; \tag{1}$$

$$b_k^{\min} \le b_k \le b_k^{\max}, k \in \mathcal{F}; \tag{2}$$

$$b_k^{\min} = -\frac{1}{(1 - FC_{\text{C}})x_k}, k \in \mathcal{F}; \tag{3}$$

$$b_k^{\max} = -\frac{1}{(1 + FC_{\text{L}})x_k}, k \in \mathcal{F}. \tag{4}$$

(1) is the DC power flow equation for any transmission line with FACTS. (2) specifies that b_k is a continuous variable with variation limits calculated as in (3) and (4). Devices such as the TCSC and the CVSR provide continuous adjustments of transmission line reactance. The effective susceptance adjustments are within fixed operating ranges. Therefore, (1)–(2) is a proper model for such types of devices. Note that the reactance adjustment levels depend on the actual devices deployed.

2.2. Problem formulations

Due to the bilinear terms $b_k\theta_{k,\text{to}}$ and $b_k\theta_{k,\text{fr}}$, (1) is nonlinear. To address the issue of nonlinearity, (1) and (2) are first reformulated to linear constraints based on the sign of voltage angle differences [22]:

if $(\theta_{k,\text{to}} - \theta_{k,\text{fr}}) \ge 0$:

$$b_k^{\min}(\theta_{k,\text{to}} - \theta_{k,\text{fr}}) \le f_k \le b_k^{\max}(\theta_{k,\text{to}} - \theta_{k,\text{fr}}); \tag{5}$$

if $(\theta_{k,\text{to}} - \theta_{k,\text{fr}}) \le 0$:

$$b_k^{\max}(\theta_{k,\text{to}} - \theta_{k,\text{fr}}) \le f_k \le b_k^{\min}(\theta_{k,\text{to}} - \theta_{k,\text{fr}}). \tag{6}$$

Binary variables $z_k (z_k \in \{0, 1\})$ are then introduced to model the "if" conditions in (5) and (6) [22]. (1) and (2) can be further reformulated as:

$$b_k^{\min}(\theta_{k,\text{to}} - \theta_{k,\text{fr}}) - (1 - z_k)M \le f_k, k \in \mathcal{F}; \tag{7}$$

$$b_k^{\max}(\theta_{k,\text{to}} - \theta_{k,\text{fr}}) - z_k M \le f_k, k \in \mathcal{F}; \tag{8}$$

$$b_k^{\min}(\theta_{k,\text{to}} - \theta_{k,\text{fr}}) + z_k M \ge f_k, k \in \mathcal{F}; \tag{9}$$

$$b_k^{\max}(\theta_{k,\text{to}} - \theta_{k,\text{fr}}) + (1 - z_k)M \ge f_k, k \in \mathcal{F}; \tag{10}$$

$$\theta_{k,\text{to}} - \theta_{k,\text{fr}} \ge (z_k - 1)M, k \in \mathcal{F}; \tag{11}$$

$$\theta_{k,\text{to}} - \theta_{k,\text{fr}} \le z_k M, k \in \mathcal{F}; \tag{12}$$

$$M > \max_{k \in F}\{\frac{FC_{\text{C}} + FC_{\text{L}}}{1 - FC_{\text{C}}} f_k^{\max}\}. \tag{13}$$

Note that (13) specifies how the value of M should be set and is not a constraint as M is a parameter. In (7)–(12), z_k represents the flow direction on transmission line $k(k \in \mathcal{F})$ in the following manner:

$$z_k = 0 \iff f_k \ge 0, \tag{14}$$

$$z_k = 1 \iff f_k < 0. \tag{15}$$

The reformulation of (1)–(2) to (7)–(12) is the previously discussed mixed-integer reformulation of DC power flow equation for lines with FACTS installed using the big-M method [8,22,24]. The full formulation of DCOPF with FACTS (OPF_FACTS) after applying this reformulation is presented as follows:

OPF_FACTS :

$$\min \sum_{g \in G} c_g p_g \tag{16}$$

s.t.

(7)–(13);

$$p_g^{\min} \le p_g \le p_g^{\max}, g \in G; \tag{17}$$

$$-f_k^{\max} \le f_k \le f_k^{\max}, k \in K; \tag{18}$$

$$f_k = b_k(\theta_{k,\text{to}} - \theta_{k,\text{fr}}), k \notin \mathcal{F}, k \in K; \tag{19}$$

$$\theta_1 = 0; \tag{20}$$

$$\sum_{k \in \delta^+(n)} f_k - \sum_{k \in \delta^-(n)} f_k + \sum_{g \in G(n)} p_g = d_n, n \in N. \tag{21}$$

The objective is to minimize the total fuel cost of generators and is calculated using the linear function shown in (16). The generator operating capacities are specified in (17). (18) imposes thermal capacity limits on transmission lines. (19) is the DC power flow equation for lines without FACTS. (20) specifies that the voltage angle of the reference bus equals to zero. (21) represents the nodal power balance constraint at all the buses of the network.

Similarly, we can formulate the more complicated UC model with FACTS included (UC_FACTS). The formulation is presented as follows:

UC_FACTS :

$$\min \sum_{g\in G}\sum_{t\in T}(NL_g u_{gt} + c_g p_{gt} + SU_g v_{gt}) \tag{22}$$

s.t.

$$u_{gt}p_g^{\min} \le p_{gt} \le u_{gt}p_g^{\max}, g \in G, t \in T; \tag{23}$$

$$-f_k^{\max} \le f_{kt} \le f_k^{\max}, k \in K, t \in T; \tag{24}$$

$$f_{kt} = b_k(\theta_{k,\mathrm{to},t} - \theta_{k,\mathrm{fr},t}), k \notin \mathcal{F}, k \in K, t \in T; \tag{25}$$

$$\frac{\theta_{k,\mathrm{fr},t} - \theta_{k,\mathrm{to},t}}{(1+FC_\mathrm{L})x_k} - z_{kt}M \le f_{kt}, k \in \mathcal{F}, t \in T; \tag{26}$$

$$\frac{\theta_{k,\mathrm{fr},t} - \theta_{k,\mathrm{to},t}}{(1-FC_\mathrm{C})x_k} - (1-z_{kt})M \le f_{kt}, k \in \mathcal{F}, t \in T; \tag{27}$$

$$\frac{\theta_{k,\mathrm{fr},t} - \theta_{k,\mathrm{to},t}}{(1+FC_\mathrm{L})x_k} + (1-z_{kt})M \ge f_{kt}, k \in \mathcal{F}, t \in T; \tag{28}$$

$$\frac{\theta_{k,\mathrm{fr},t} - \theta_{k,\mathrm{to},t}}{(1-FC_\mathrm{C})x_k} + z_{kt}M \ge f_{kt}, k \in \mathcal{F}, t \in T; \tag{29}$$

$$\theta_{k,\mathrm{to},t} - \theta_{k,\mathrm{fr},t} \le z_{kt}M, k \in \mathcal{F}, t \in T; \tag{30}$$

$$\theta_{k,\mathrm{to},t} - \theta_{k,\mathrm{fr},t} \ge (z_{kt}-1)M, k \in \mathcal{F}, t \in T; \tag{31}$$

$$z_{kt} \in \{0,1\}, k \in \mathcal{F}, t \in T; \tag{32}$$

$$M > \max_{k\in\mathcal{F}}\{\frac{FC_\mathrm{C} + FC_\mathrm{L}}{1-FC_\mathrm{C}} f_k^{\max}\}; \tag{33}$$

$$\theta_{1t} = 0, t \in T; \tag{34}$$

$$\sum_{k\in\delta^+(n)} f_{kt} - \sum_{k\in\delta^-(n)} f_{kt} + \sum_{g\in G(n)} p_{gt} = d_{nt}, n \in N, t \in T; \tag{35}$$

$$-RD_g \le p_{g,t+1} - p_{gt} \le RU_g, g \in G, t \in T; \tag{36}$$

$$\sum_{r=t-UT_g+1}^{t} v_{gr} \le u_{gt}, g \in G, t \ge UT_g; \tag{37}$$

$$\sum_{r=t+1}^{t+DT_g} v_{gr} \le 1 - u_{gt}, g \in G, t \le |T| - DT_g; \tag{38}$$

$$0 \le v_{gt} \le 1, g \in G, t \in T; \tag{39}$$

$$u_{gt} - u_{g,t-1} \le v_{gt}, g \in G, t \in T; \tag{40}$$

$$u_{gt} \in \{0,1\}, g \in G, t \in T;. \tag{41}$$

(22) is the objective function of the UC problem, which minimizes the summation of fuel cost, start-up cost, and no-load cost of the generators. The constraints (23)–(34) are similar to (17)–(20) and (7)–(13), with differences being the commitment variables in (23) and the time period indices. (35) represents the nodal power balance constraints. The ramping constraints of generators are specified in (36). (37)–(38) represent the minimum up and down time constraints. (39) defines the upper and lower bounds of start-up variables. (40) represents the relationship between commitment variables and start-up variables. (41) specifies that commitment variables are binary. Note that start-up variables are continuous in this formulation, as they will converge to the bounds shown in (39) in the final solutions.

The power flow directions on lines equipped with FACTS can be assigned by determining the values of z_k in (7)–(12) and z_{kt} in (26)–(31), thus eliminating these binary variables and consequently improving computational efficiency. The results of a base case, which is a DCOPF or UC model without any FACTS device, can be used to predetermine the flow directions. The full formulations of the base cases (OPF_base and UC_base) are presented as follows:

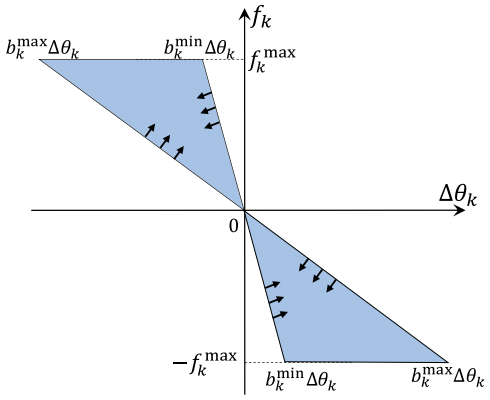

Fig. 1. The feasible set of power flow on transmission line k ($k \in \mathcal{F}$) [27].

OPF_base :

$$\min \sum_{g\in G} c_g p_g \tag{42}$$

s.t.

(17)–(18), (20)–(21);

$$f_k = b_k(\theta_{k,\mathrm{to}} - \theta_{k,\mathrm{fr}}), k \in K, \tag{43}$$

UC_base :

$$\min \sum_{g\in G}\sum_{t\in T}(NL_g u_{gt} + c_g p_{gt} + SU_g v_{gt}) \tag{44}$$

s.t.

(23)–(24), (34)–(41);

$$f_{kt} = b_k(\theta_{k,\mathrm{to},t} - \theta_{k,\mathrm{fr},t}), k \in K, t \in T. \tag{45}$$

2.3. SFDE algorithm design

As mentioned previously, the base case solutions can provide suboptimal flow directions for solving the power system operation model with FACTS included. Therefore, the two-stage method presented in [8] may suffer from suboptimaility in the final solution. The SFDE algorithm addresses the suboptimality issue by adjusting the enforced flow directions. The idea behind the design of the SFDE algorithm is first discussed in this subsection. Two versions of the SFDE algorithm that serve different purposes in the simulation studies are then presented.

The idea behind the SFDE algorithm is based on analyzing the feasible set identified from constraints (1) and (2) regarding f_k and $\Delta\theta_k = \theta_{k,\mathrm{to}} - \theta_{k,\mathrm{fr}}$, as shown in Fig. 1 [27].

The feasible set can be divided into two halves that are symmetric around the origin. Note that the sign of voltage angle difference determines the direction of power flow. By initializing the power flow direction, we are limiting the feasible set to only one of the halves. If the predetermined flow direction limits the feasible set to the suboptimal segment, the solution is expected to converge to the origin in Fig. 1, which is the point that connects the two halves of the feasible set and leads to the power flow being zero on the corresponding line. Based on this reasoning, once such a result is identified in the initial solution, or any iteration thereafter, we can change the direction of the power flow to the opposite of the previous iteration and proceed to a new iteration. Simulation results show that within just a few iterations of adjusting the enforced power flow directions and solving

the power system operation problems, the SFDE algorithm converges to the globally optimal solution in almost all practical cases.

The two important aspects regarding the performance of the SFDE algorithm are (i) convergence to global optimality and (ii) computational efficiency. We first traverse all possible initializations of power flow directions. Doing so allows us to create a variety of cases to demonstrate the effectiveness of SFDE in converging to global optimality. The SFDE algorithm with random initialization of flow directions is presented as follows:

Algorithm 1 The SFDE algorithm with random initialization of flow directions

1: *Initialization*–Randomly initialize power flow directions on lines with FACTS. Create $\Omega = \emptyset$;
2: *Parallel lines flow direction check*–If opposite directions are initialized on parallel lines, go back to step 1. If not, continue;
3: *Solve*–Solve the operation model with enforced flow directions;
4: *Feasibility check*–If this initialization of power flow directions causes infeasibility, go back to step 1. If not, record the result β and continue;
5: *Zero flow value check*–If active power flow results on lines with FACTS installed do not contain zero, go to step 8;
6: *Same results check*–If $\beta \in \Omega$, go to step 8. If not, $\Omega = \{\beta\} \cup \Omega$;
7: *Enforced flow direction adjustment*–If a line with FACTS installed has a power flow with value of zero, flip the enforced direction. Go back to step 3;
8: *Report and end*–Report the final results and end the algorithm.

It is worth noting that while traversing all possible power flow direction initializations, the results reveal that an arbitrary initialization of power flow directions does not guarantee feasibility. In fact, the majority of the initializations lead to infeasibility. The explanation is that based on the locations of the generating units and load in the system, forcing the flow directions on some transmission lines to be fixed may result in constraints that cannot be satisfied. In other words, changing the dispatch may not be able to change the flow direction on certain transmission lines.

In addition, there are multiple pairs of parallel lines connecting the same pair of buses in the test systems we use. Flow directions on parallel lines should not be initialized as opposite. Even though some of the cases where the flow directions on parallel lines are initialized as different are still feasible, the solutions are not optimal, and thus not useful. Feasibility in those cases are achieved only if the flow on the parallel lines, forced to have opposite flow directions, is zero. Such cases are eliminated when identified after initialization in our simulations.

In the actual implementation of SFDE, results of the base case, or state estimation, can be used for flow direction initialization to guarantee feasibility and improve computational performance. The SFDE algorithm with warm-start (Algorithm 2) is presented as follows:

Algorithm 2 The SFDE algorithm with warm-start

1: *Warm-start*–Solve a base case and enforce power flow directions on lines with FACTS installed based on the results and create $\Omega = \emptyset$;
2: *Solve*–Solve the operation model with enforced flow directions and record the result β;
3: *Zero flow value check*–If active power flow results on lines with FACTS installed do not contain zero, go to step 6;
4: *Same results check*–If $\beta \in \Omega$, go to step 8. If not, $\Omega = \{\beta\} \cup \Omega$;
5: *Enforced flow direction adjustment*–If a line with FACTS installed has a power flow with value of zero, flip the enforced direction. Go back to step 2;
6: *Report and end*–Report the final results and end the algorithm.

Compared to Algorithm 1, the step of parallel line flow direction checking is spared in Algorithm 2 as the base case solution will not have opposite flow directions on parallel lines. Both Algorithm 1 and Algorithm 2 stops when no power flow result is zero and no further adjustments of flow directions can be made. In addition, the design of both algorithms involve creating the set of Ω to record the result of each iteration. Then, in the later step of same results checking, exit the algorithm if the same result reappears. This design is to ensure an exit condition when the optimal solution involves zero power flows on lines equipped with FACTS. Due to the MIPgap in UC problems the results in the heuristic will show a cycling behavior. Therefore, it is necessary to record the results of each iteration.

In the simulation studies presented in Section 3, the SFDE algorithm is applied to solve OPF_FACTS and UC_FACTS. The total cost result will be compared to that of directly solving OPF_FACTS and UC_FACTS to show that the SFDE algorithm's convergence to global optimality. A comparison is also drawn between the solution time results to show that the SFDE algorithm provides computational efficiency improvements over directly solving OPF_FACTS and UC_FACTS.

3. Simulation studies

In this section, the method proposed in Section 2 is employed to solve power system operation models OPF_FACTS and UC_FACTS. The test systems used are the modified IEEE 118-bus system and the Texas 2000-bus system. Simulation results are presented to show the effectiveness of our algorithm. The effectiveness is evaluated through comparison with results of directly solving OPF_FACTS and UC_FACTS to see if the proposed method (i) has achieved optimality and (ii) can provide computational efficiency gains. Problems are solved using CPLEX 12.10 on an Intel Xeon Gold 6136 CPU with 128 GB RAM.

3.1. Implementation of SFDE for solving OPF_FACTS

We first implement the SFDE algorithm to solve OPF_FACTS. OPF_FACTS being a single-hour operation model allows us to implement Algorithm 1 when N_F is relatively small, thus, as mentioned previously, creating a variety of flow direction initializations to demonstrate the effectiveness of the SFDE algorithm in converging to optimality. Because of the presence of binary variables, OPF_FACTS is a mixed-integer linear program (MILP). In each iteration of the SFDE algorithm, the binary variables are effectively eliminated, thus LPs are being solved successively.

To demonstrate the robustness and effectiveness of the proposed algorithm under different FACTS device allocation schemes, we use two allocation policies (AP) which are presented as follows:

- AP1: FACTS devices are located on each of the lines that are utilized the most;
- AP2: FACTS devices are located on each of the lines with larger reactance.

Note that optimal allocation of FACTS devices is beyond the scope of this paper. We apply the two aforementioned simple, straightforward APs for the following reasons:

1. The most utilized lines in the system are very likely transmission bottlenecks. Therefore, FACTS devices deployed on these lines can "push power flow away" by increasing the line reactance, thus alleviate congestion;
2. FACTS devices deployed on the lines with larger reactance can reduce the reactance of these lines, thus "pull power flow in" to reduce congestion.

For FACTS capacity, the following settings are employed in simulation studies:

- Setting 1: $FC_C = FC_L = 0.5$;

Table 1
Simulation results of Algorithm 1 with 5 FACTS devices under AP1 in the 118-bus system.

FACTS setting	# Feasible cases	Average # iterations	Cost ($/h)	OPF_FACTS cost ($/h)
1	10	1.9	60 548.3	60 548.3
2	8	1.86	60 749.6	60 749.6

Table 2
Simulation results of Algorithm 1 with 5 FACTS devices under AP2 in the 118-bus system.

FACTS setting	# Feasible cases	Average # iterations	Cost ($/h)	OPF_FACTS cost ($/h)
1	14	2.71	60 745.7	60 745.7
2	14	2.71	60 588.7	60 588.7

Table 3
Simulation results of Algorithm 1 with 10 FACTS devices under AP1 in the 118-bus system.

FACTS setting	# Feasible cases	Average # iterations	Cost ($/h)	OPF_FACTS cost ($/h)
1	40	1.97	60 393.8	60 393.8
2	36	1.98	60 557.7	60 557.7

Table 4
Simulation results of Algorithm 1 with 10 FACTS devices under AP2 in the 118-bus system.

FACTS setting	# Feasible cases	Average # iterations	Cost ($/h)	OPF_FACTS cost ($/h)
1	136	2.4	60 698.9/60 699.2	60 698.9
2	136	3.4	60 532.9	60 532.9

- Setting 2: $FC_{\mathrm{C}} = 0.8, FC_{\mathrm{L}} = 0.2$;

Each of these settings are typical operating ranges of the widely used TCSC devices [28].

3.1.1. Modified IEEE 118-bus system

Algorithm 1 is first employed to solve OPF_FACTS for the modified IEEE 118-bus test system. The data is obtained from [29]. Because of the low congestion level in the original test system, modifications are made to thermal capacities of the most utilized lines to increase congestion, making the system more suitable for studying the impact of FACTS deployment. Details of the modifications are presented in Appendix.

Note that for each line k equipped with FACTS there are two initializations for power flow direction, corresponding to z_k in (7)–(12) taking the value of 1 or 0. As a result, there are $2^{N_{\mathrm{F}}}$ possible initializations of power flow directions on lines equipped with FACTS, which are traversed in the simulations. The number of feasible cases and average iterations in SFDE for each FACTS capacity setting is presented in the results. The average number of iterations presents the average number of LPs solved including solving the case with the flow direction initialization. Each "case" refers to a way that the power flow directions are initialized in Algorithm 1. The simulation results when 5 FACTS are installed in the system are presented in Tables 1–2.

The simulation results when 10 FACTS are installed in the 118-bus system are presented in Tables 3 and 4. More savings can be achieved with a larger number of FACTS devices installed.

We implement Algorithm 2 instead of Algorithm 1 when N_F is increased to 15 as it is impractical to traverse 2^{15} initializations. The results are presented in Tables 5–6.

We first discuss the effectiveness of the SFDE algorithm in converging to the same result as that of directly solving OPF_FACTS. Tables 1–6 include 389 feasible cases in total, out of which, 309 (79.4%) have successfully converged to the same result compared to that of OPF_FACTS. The exceptions occur with 10 FACTS devices of setting 1 deployed in the system under AP2 and results can be seen from Table 4. In these specific cases, 80 out of 136 feasible cases resulted in suboptimal results. However, we can see that the suboptimality is $0.3 (0.0005%) which is very minimal. The suboptimality occurs due to the nonconvexity of the feasible region shown in Fig. 1. A more detailed discussion of the limitation of the proposed algorithm is presented in Section 4. Overall, the results with the 118-bus system demonstrated the effectiveness of the SFDE algorithm in converging to global optimality in most of the practical cases even with random flow direction initialization in a limited number of iterations.

Table 5
Simulation results of Algorithm 2 with 15 FACTS devices under AP1 in the 118-bus system.

FACTS setting	# Iterations	Cost ($/h)	OPF_FACTS cost ($/h)
1	1	60 378.2	60 378.2
2	1	60 550.5	60 550.5

Table 6
Simulation results of Algorithm 2 with 15 FACTS devices under AP2 in the 118-bus system.

FACTS setting	# Iterations	Cost ($/h)	OPF_FACTS cost ($/h)
1	1	60 688.9	60 688.9
2	2	60 517.1	60 517.1

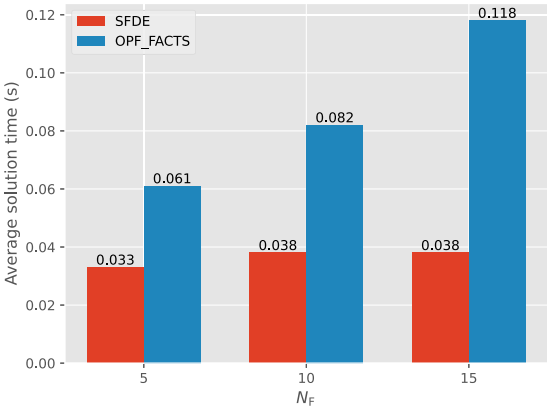

Fig. 2. Solution time of the SFDE algorithm and directly solving OPF_FACTS for the 118-bus system.

Table 7
Computational efficiency superiority of the SFDE algorithm over directly solving OPF_FACTS for the 118-bus system.

N_F	Computational efficiency improvement
5	84.1%
10	115.8%
15	210.5%

We then present the comparison of the average solution time results between applying the SFDE algorithm and directly solving OPF_FACTS. The results are presented in Fig. 2.

Table 7 shows the computational efficiency superiority of the SFDE algorithm over directly solving OPF_FACTS.

We can see that employing the SFDE algorithm is significantly more efficient than directly solving OPF_FACTS. The two factors contributing to such computational efficiency gain are (i) the LP in each iteration is much less computationally demanding than the MILP and (ii) the SFDE algorithm is capable of converging within a few iterations. Furthermore, higher computational efficiency gain is shown with more FACTS devices deployed in the system.

Table 8
Simulation results of Algorithm 2 with 45 FACTS devices under AP1 in the 2000-bus system.

FACTS setting	# Iterations	Cost ($/h)	OPF_FACTS cost ($/h)
1	1	889 613.4	889 613.4
2	1	891 347.4	891 347.4

Table 9
Simulation results of Algorithm 2 with 45 FACTS devices under AP2 in the 2000-bus system.

FACTS setting	# Iterations	Cost ($/h)	OPF_FACTS cost ($/h)
1	3	908 929.7	908 929.7
2	4	908 563.5	908 563.5

Table 10
Simulation results of Algorithm 2 with 60 FACTS devices under AP1 in the 2000-bus system.

FACTS setting	# Iterations	Cost ($/h)	OPF_FACTS cost ($/h)
1	2	884 754.2	884 754.2
2	2	887 654.5	887 654.5

Table 11
Simulation results of Algorithm 2 with 60 FACTS devices under AP2 in the 2000-bus system.

FACTS setting	# Iterations	Cost ($/h)	OPF_FACTS cost ($/h)
1	3	908 866.2	908 866.2
2	3	908 522.9	908 532.6

Table 12
Simulation results of Algorithm 2 with 75 FACTS devices under AP1 in the 2000-bus system.

FACTS setting	# Iterations	Cost ($/h)	OPF_FACTS cost ($/h)
1	2	884 752.2	884 752.2
2	2	887 652.2	887 652.2

Note that the computational efficiency improvement results are based on the total solution time reported by the solver. The solvers require a certain amount of time to construct the optimization models. The model construction time is not reported in this section as they are much smaller than the solution time, especially for complicated models. Additionally, the model construction time varies when using different programming languages.

3.1.2. Texas 2000-bus system

The Texas 2000-bus test system is first introduced in [30], and the data is available from [31]. Similar to the 118-bus system, modifications are made to the 2000-bus system to increase congestion so that it is more suitable for studying the influence of FACTS devices. Details of the modifications of the system are shown in the Appendix.

The 2000-bus system has 3206 transmission lines, which is significantly more than the 186 lines in the 118-bus system. Therefore, if we keep the number of FACTS devices the same in the 2000-bus system, the number of binary variables is scaling significantly less than the LP in each SFDE iteration. To better demonstrate the effectiveness of the proposed algorithm, we increased N_F to 45, 60, and 75 for the 2000-bus system. Note that such deployment can be carried out cost-efficiently and conveniently through distributed or modular FACTS (D-FACTS or M-FACTS), which is a light-weight version of FACTS devices [32] that offers better cost-effectiveness and re-allocation flexibility compared to conventional FACTS technologies [33].

As N_F is large for the 2000-bus system, Algorithm 2 is applied in this part of the simulation studies. Results of a total of 12 cases are included in Tables 8–13.

The results reveal the effectiveness of the SFDE algorithm to converge to global optimality after very few iterations of solving successive LPs in a large system with a significantly larger N_F. Note that the number of iterations shown in Tables 8–13 does not include solving the base case. The results also show consistency with the simulation results in Section 3.1.1: a larger N_F or greater FACTS capacity can lead to higher savings.

Table 13
Simulation results of Algorithm 2 with 75 FACTS devices under AP2 in the 2000-bus system.

FACTS setting	# Iterations	Cost ($/h)	OPF_FACTS cost ($/h)
1	3	908 810.9	908 810.9
2	3	908 429.7	908 532.6

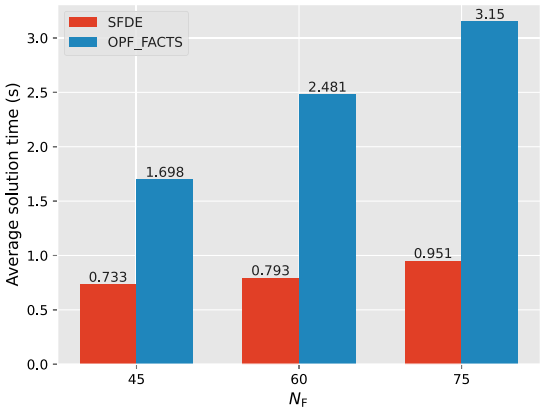

Fig. 3. Solution time of the SFDE algorithm and directly solving OPF_FACTS for the 2000-bus system.

Table 14
Computational efficiency superiority of the SFDE algorithm over directly solving OPF_FACTS for the 2000-bus system.

N_F	Computational efficiency improvement
45	131.7%
60	212.9%
75	231.2%

The solution time comparison between the SFDE algorithm and directly solving OPF_FACTS is presented in Fig. 3, and Table 14 shows the computational efficiency superiority of the SFDE algorithm over solving OPF_FACTS for the 2000-bus system.

The results again shows the significant computational efficiency improvement when the SFDE algorithm is applied, which is consistent with the results obtained using the 118-bus system. It is worth noting that even though the number of FACTS deployment is increased in the 2000-bus system, the lines equipped with FACTS devices is still a very small portion of the lines in the system. With the development of M-FACTS technology, a greater number of FACTS devices deployed in the system can be expected. The computational efficiency of the SFDE algorithm can be expected to be even more valuable under these circumstances.

3.2. Implementation of SFDE for solving UC_FACTS

In this subsection, we conduct simulation studies to demonstrate the computational efficiency gains provided by the SFDE algorithm, while still converging to global optimality with the UC model. We consider a typical day-ahead UC model with $|T| = 24$. Hourly load data for a winter weekday is obtained from [34]. For the day-ahead UC there are $2^{|T|N_F}$ possible initializations of power flow directions, and traversing

Table 15
UC simulation results of Algorithm 2 with 5 FACTS devices in the 118-bus system.

Iteration	SFDE cost ($)	UC_FACTS cost ($)
First Final (3)	1 127 676.3 1 127 331.0	1 127 177.5

Table 16
UC simulation results of Algorithm 2 with 10 FACTS devices in the 118-bus system.

Iteration	SFDE cost ($)	UC_FACTS cost ($)
First Final (4)	1 125 514.7 1 123 862.7	1 123 710.7

Table 17
UC simulation results of Algorithm 2 with 15 FACTS devices in the 118-bus system.

Iteration	SFDE cost ($)	UC_FACTS cost ($)
First Final (11)	1 125 224.1 1 123 583.0	1 123 265.3

Table 18
Comparing the results of the two-stage method and the SFDE algorithm to the result of UC_FACTS.

N_F	Method	
	Two-stage	SFDE
5	0.044%	0.014%
10	0.161%	0.014%
15	0.174%	0.046%

all of them is certainly impractical. Therefore, Algorithm 2 is applied for the UC problems. UC_base is solved and the solutions are used to determine the values of z_{kt}. Because of the significant computational complexity of UC models, the 118-bus system is used in this part of the simulation studies. For brevity, only AP1 and setting 1 are used for UC simulations, and setting 1 is used as it has been shown to be more cost-efficient under this allocation policy by the results in the previous subsection. Simulation results with 5, 10, and 15 devices in the system are presented in Tables 15–17.

In Tables 15–17, the results of both the first iteration and the final iteration of the SFDE algorithm are presented. The cost of the first SFDE iteration is equivalent to the result that would be achieved if the two-stage method proposed in [8,26] is employed. The objective function values of the final iterations are the eventual results reported by the SFDE algorithm. We compare both sets of results to the costs achieved by directly solving UC_FACTS, and the differences are shown in Table 18.

Note that the MIPgap used for UC problems is 0.1%. Therefore, the results in the "SFDE" column in Table 18 shows the convergence of the SFDE algorithm to optimality, as the difference is smaller than the defined MIPgap. The results of the two-stage method, however, suffer from significant suboptimality that is equivalent to 161% and 174% of the MIPgap with 10 or 15 FACTS devices deployed in the system. The results in Table 18 reveal the superiority of the SFDE algorithm over the two-stage method in the quality of final solutions.

We then compare the solution time of the SFDE algorithm to that of directly solving UC_FACTS to demonstrate the computational efficiency improvement. The results are presented in Fig. 4 and the computational efficiency gains of the SFDE algorithm are shown in Table 19.

It can be seen that the SFDE algorithm is significantly more efficient than directly solving UC_FACTS. Similar to the results in Section 3.1, the SFDE algorithm shows more computational efficiency superiority with a larger N_F. Note that for $N_F = 15$, the SFDE algorithm converges after 11 iterations and still provides huge computational efficiency gain, which shows the significant impact of FACTS operation on computational complexity, as well as the benefit of alleviating it through flow direction enforcing.

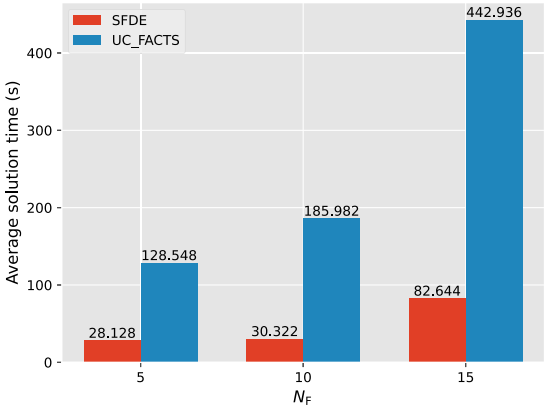

Fig. 4. Solution time of the SFDE algorithm and directly solving UC_FACTS for the 118-bus system.

Table 19
Computational efficiency superiority of the SFDE algorithm over directly solving UC_FACTS for the 118-bus system.

N_F	Computational efficiency improvement
5	357.0%
10	513.4%
15	536.0%

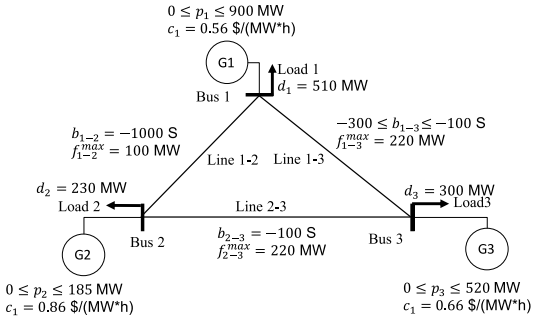

Fig. 5. Example in a 3-bus system to demonstrate the mathematical limitation of the SFDE algorithm.

4. Discussion on convergence

It should be noted that even though simulation studies show the practical effectiveness of the SFDE algorithm, it still does not theoretically guarantee global optimality due to the non-convexity of the problem. Here we present an example in a simple 3-bus system, shown in Fig. 5, to demonstrate the limitation of the algorithm. Variables and parameters are labeled in the figure. For the sake of simplicity, we consider a linear cost function in this example as well.

Line 3–1 is the only transmission line equipped with FACTS in the above system, which results in two possible ways of initializing of power flow direction on this line when using the algorithm introduced in this paper. The generation dispatch and power flow results in both cases are presented in Table 20.

We can see that if the flow direction on line 3–1 is initialized as from bus 1 to bus 3 in the system, the subsequent LP converges to a suboptimal cost with a non-zero power flow on line 3–1. In this case, the SFDE method will stop and report the solution. This example shows

Table 20
Results of the counterexample case.

Results	Initialization	
	Flow direction on Line 3-1 from 1 to 3	Flow direction on Line 3-1 from 3 to 1
f_{1-2} (MW)	100	100
f_{2-3} (MW)	50	−105
f_{3-1} (MW)	−180	95
p_1 (MW)	780	505
p_2 (MW)	200	45
p_3 (MW)	70	500
Cost ($/h)	642.9	638.9

that the method cannot theoretically guarantee global optimality. However, multiple conditions need to be satisfied simultaneously to allow such an example to occur. First, the flow on line 3–1 in this case is very sensitive to changes in dispatch that would keep the total cost constant (i.e., increase of p_3 and decrease of p_1 and p_2, by 2/3 and 1/3 of the increase in p_3). Therefore, two very similar solutions in terms of total cost, can lead to drastically different flows on line 3–1. This is not very likely in real world systems. Moreover, in this example the FACTS device is not placed on line 1–2, which is a better location as it is the most utilized and constrained line in the system. Therefore, we believe it will be rare for the method to converge to a suboptimal solution in a realistically large system with FACTS devices that are properly allocated.

A previous study [35] states that if only one transmission line is equipped with FACTS, the two-stage method in [8] will converge to the globally optimal solution. The example above clearly counters this theorem.

5. Conclusion

FACTS devices can effectively enhance the transfer capability over the existing transmission networks. Unfortunately, however, it has been shown that the inclusion of FACTS devices increases the computational burden of power system operation models. This paper presents a successive flow direction enforcing (SFDE) algorithm to solve power system operation models and optimize FACTS operation. Recent studies have proposed a mixed-integer reformulation of the DC power flow equation with FACTS, which is nonlinear. Based on this reformulation, power flow directions on lines equipped with FACTS can be preassigned to achieve computational efficiency improvements. The SFDE algorithm iteratively adjusts the preassigned flow directions to practically guarantee optimality, thus addressing the suboptimality issue of methods in the existing literature, while providing computational efficiency gains compared to directly solving operation models with FACTS included. Simulation results on different test systems confirm that the proposed SFDE algorithm converges to the globally optimal solution for almost all practical cases within a few iterations. Simulation studies also show that, compared to directly solving power system operation models with FACTS included, implementing the SFDE algorithm can achieve up to 231.2% and 536.0% computational efficiency improvement in for OPF and UC problems respectively.

Due to its linear nature, the algorithm developed in this paper can be integrated within the existing energy and market management systems, without substantially adding to the computational demands of the existing software tools. Even though global optimality is not guaranteed theoretically, the effectiveness of this method is expected to be satisfactory from a practical standpoint. Future work will include employing the proposed algorithm in more complex power system operation and planning models, such as security-constrained optimal power flow (SCOPF) and stochastic unit commitment (SUC).

Table 21
Modifications of line capacities in the 118-bus system.

Line num.	Line cap. (MW)	Modified line cap. (MW)
5	175	87.5
8	500	225
37	175	61.25
38	500	250
41	140	35
54	175	122.5
78	175	43.75
96	500	225
104	500	125
131	175	78.75
133	500	175
134	500	125
135	175	87.5

Table 22
Modifications of line capacities in the 2000-bus system.

Line num.	Line cap. (MW)	Modified line cap. (MW)
43	149	112
58	170	128
71	145	109
74	149	112
112	230	200
364	82	62
435	143.8	108
439	83	62
556	230	172.5
557	230	172.5
558	250	213
765	168	145
935	2295	1721
1038	150	113
1222	1379	1035
1380	1450	1088
1381	1450	1088
2136	217.8	190
2449	1600	1200
2450	1600	1200
2453	523	392
2803	198	180
2911	280.8	220
2912	280.8	220
2913	280.8	220
2993	213	180
2994	213	180
2995	213	180

CRediT authorship contribution statement

Xinyang Rui: Methodology, Validation, Formal analysis, Investigation, Writing, Visualization. **Mostafa Sahraei-Ardakani:** Conceptualization, Methodology, Validation, Supervision, Project administration, Funding acquisition.

Declaration of competing interest

One or more of the authors of this paper have disclosed potential or pertinent conflicts of interest, which may include receipt of payment, either direct or indirect, institutional support, or association with an entity in the biomedical field which may be perceived to have potential conflict of interest with this work. For full disclosure statements refer to https://doi.org/10.1016/j.epsr.2022.108171. Xinyang Rui, Mostafa Sahraei-Ardakani reports financial support was provided by National Science Foundation.

Appendix

Our method to increase the congestion level in the test systems is through reducing the thermal limit of lines that are utilized the most.

For the 118-bus system, we first decrease the capacities of all lines by 20%. Then, some of the heavily utilized lines' capacities modified further, and the modifications are presented in Table 21.

The modifications for the 2000-bus system are presented in Table 22.

References

[1] Electric power annual 2020, 2021, accessed: 2021-12-20. URL https://www.eia.gov/electricity/annual/pdf/epa.pdf.

[2] M. EL-Azab, W. Omran, S. Mekhamer, H. Talaat, Congestion management of power systems by optimizing grid topology and using dynamic thermal rating, Electr. Power Syst. Res. 199 (2021) 107433.

[3] Y. Sang, M. Sahraei-Ardakani, The link between power flow control technologies: Topology control and FACTS, in: 2017 North American Power Symposium (NAPS), IEEE, 2017, pp. 1–6.

[4] Y. Xiao, Y. Song, C.-C. Liu, Y. Sun, Available transfer capability enhancement using FACTS devices, IEEE Trans. Power Syst. 18 (1) (2003) 305–312.

[5] X. Zhang, D. Shi, Z. Wang, B. Zeng, X. Wang, K. Tomsovic, Y. Jin, Optimal allocation of series FACTS devices under high penetration of wind power within a market environment, IEEE Trans. Power Syst. 33 (6) (2018) 6206–6217.

[6] M.S. Alam, F.S. Al-Ismail, A. Salem, M.A. Abido, High-level penetration of renewable energy sources into grid utility: Challenges and solutions, IEEE Access 8 (2020) 190277–190299.

[7] White House, FACT SHEET: President biden sets 2030 greenhouse gas pollution reduction target aimed at creating good-paying union jobs and securing u.s. leadership on clean energy technologies, 2021, accessed: 2021-12-20. URL https://www.whitehouse.gov/briefing-room/statements-releases/2021/04/22/fact-sheet-president-biden-sets-2030-greenhouse-gas-pollution-reduction-target-aimed-at-creating-good-paying-union-jobs-and-securing-u-s-leadership-on-clean-energy-technologies/.

[8] M. Sahraei-Ardakani, K.W. Hedman, A fast LP approach for enhanced utilization of variable impedance based FACTS devices, IEEE Trans. Power Syst. 31 (3) (2015) 2204–2213.

[9] Federal Energy Regulatory Commission, Order no. 1000 - transmission planning and cost allocation, 2011, accessed: 2018-12-01. URL https://www.ferc.gov/electric-transmission/order-no-1000-transmission-planning-and-cost-allocation.

[10] Y. Sang, M. Sahraei-Ardakani, The interdependence between transmission switching and variable-impedance series FACTS devices, IEEE Trans. Power Syst. 33 (3) (2017) 2792–2803.

[11] P. Singh, N. Senroy, Steady-state models of STATCOM and UPFC using flexible holomorphic embedding, Electr. Power Syst. Res. 199 (2021) 107390.

[12] W. Yao, L. Jiang, J. Wen, Q. Wu, S. Cheng, Wide-area damping controller of FACTS devices for inter-area oscillations considering communication time delays, IEEE Trans. Power Syst. 29 (1) (2013) 318–329.

[13] A. Nasri, A.J. Conejo, S.J. Kazempour, M. Ghandhari, Minimizing wind power spillage using an OPF with FACTS devices, IEEE Trans. Power Syst. 29 (5) (2014) 2150–2159.

[14] M.M. Eladany, A.A. Eldesouky, A.A. Sallam, Power system transient stability: An algorithm for assessment and enhancement based on catastrophe theory and FACTS devices, IEEE Access 6 (2018) 26424–26437.

[15] K. Habur, D. O'Leary, FACTS-Flexible Alternating Current Transmission Systems: for Cost Effective and Reliable Transmission of Electrical Energy, Siemens-World Bank Document–Final Draft Report, Erlangen 46, 2004.

[16] Caitlin Marquis, This is advanced energy: flexible alternating current transmission systems, 2016, accessed: 2019-09-10. URL https://blog.aee.net/this-is-advanced-energy-flexible-alternating-current-transmission-systems.

[17] GE Grid Solutions, Series compensation systems, 2015, accessed: 2019-09-20. URL https://www.gegridsolutions.com/products/brochures/powerd_vtf/seriescompensation_gea12785c_lr.pdf.

[18] ABB, ABB to improve power supply and reliability in Brazil, 2018, accessed: 2019-09-20. URL https://new.abb.com/news/detail/10072/abb-to-improve-power-supply-and-reliability-in-brazil.

[19] S. Gerbex, R. Cherkaoui, A.J. Germond, Optimal location of multi-type FACTS devices in a power system by means of genetic algorithms, IEEE Trans. Power Syst. 16 (3) (2001) 537–544.

[20] Smart Wires, Inc., Overview of Smart Wires solutions, 2017, accessed: 2019-09-10. URL https://www.electranet.com.au/wp-content/uploads/ritt/2016/11/Smart-Wires-submission.pdf.

[21] M. Sahraei-Ardakani, S.A. Blumsack, Transfer capability improvement through market-based operation of series FACTS devices, IEEE Trans. Power Syst. 31 (5) (2015) 3702–3714.

[22] M. Sahraei-Ardakani, K.W. Hedman, Day-ahead corrective adjustment of FACTS reactance: A linear programming approach, IEEE Trans. Power Syst. 31 (4) (2015) 2867–2875.

[23] B. Stott, J. Jardim, O. Alsaç, DC power flow revisited, IEEE Trans. Power Syst. 24 (3) (2009) 1290–1300.

[24] T. Ding, R. Bo, F. Li, H. Sun, Optimal power flow with the consideration of flexible transmission line impedance, IEEE Trans. Power Syst. 31 (2) (2015) 1655–1656.

[25] M. Sahraei-Ardakani, K.W. Hedman, Computationally efficient adjustment of FACTS set points in DC optimal power flow with shift factor structure, IEEE Trans. Power Syst. 32 (3) (2016) 1733–1740.

[26] Y. Sang, M. Sahraei-Ardakani, M. Parvania, Stochastic transmission impedance control for enhanced wind energy integration, IEEE Trans. Sustain. Energy 9 (3) (2017) 1108–1117.

[27] M. Sahraei-Ardakani, Y. Sang, Discussion on linear modeling of variable reactance in "co-optimization of transmission expansion planning and TCSC placement considering the correlation between wind and demand scenarios", IEEE Trans. Power Syst. 33 (5) (2018) 5808–5809.

[28] M.B. Shafik, H. Chen, G.I. Rashed, R.A. El-Sehiemy, Adaptive multi objective parallel seeker optimization algorithm for incorporating TCSC devices into optimal power flow framework, IEEE Access 7 (2019) 36934–36947.

[29] IEEE 118-bus, 54-unit, 24-hour system, 2021, accessed: 2021-07-05. URL https://www.researchgate.net/file.PostFileLoader.html?id=568516485f7f71c9c68b456c&assetKey=AS%3A312690231185408%401451562568681.

[30] A.B. Birchfield, T. Xu, K.M. Gegner, K.S. Shetye, T.J. Overbye, Grid structural characteristics as validation criteria for synthetic networks, IEEE Trans. Power Syst. 32 (4) (2016) 3258–3265.

[31] ACTIVSg2000: 2000-bus synthetic grid on footprint of Texas, 2016, accessed: 2018-11-15. URL https://electricgrids.engr.tamu.edu/electric-grid-test-cases/activsg2000/.

[32] Y. Sang, M. Sahraei-Ardakani, Effective power flow control via distributed FACTS considering future uncertainties, Electr. Power Syst. Res. 168 (2019) 127–136.

[33] Y. Sang, M. Sahraei-Ardakani, Economic benefit comparison of D-FACTS and FACTS in transmission networks with uncertainties, in: 2018 IEEE Power & Energy Society General Meeting (PESGM), IEEE, 2018, pp. 1–5.

[34] Power systems test case archive, 2020, accessed: 2020-06-15. URL http://labs.ece.uw.edu/pstca/rts/pg_tcarts.htm.

[35] J. Jin, Y. Xu, A flow direction enforcing approach for economic dispatch with adjustable line impedance, in: 2017 IEEE Power & Energy Society General Meeting, IEEE, 2017, pp. 1–5.

CHAPTER 4

PARALLEL STOCHASTIC UNIT COMMITMENT WITH OPTIMAL FACTS OPERATION USING PROGRESSIVE HEDGING

The SUC often involves immense computational challenges, especially for larger systems or when using a more extensive set of scenarios. Variable-impedance FACTS adds to the computational burden with the binary variables and constraints. In previous research, decomposition methods, such as dual decomposition and progressive hedging, that facilitate parallelization in implementation have been proposed to address the computational efficiency issue of SUC. The effectiveness of such methods has not been studied under the presence of FACTS operations. The published article[1][2] presented in this chapter utilizes the progressive hedging algorithm to solve SUC that co-optimizes FACTS setpoints with generation dispatch. The results demonstrate substantial computational efficiency gains provided by parallelization.

---

[1]

[2]

Parallel Stochastic Unit Commitment with Optimal FACTS Operation Using Progressive Hedging

Xinyang Rui, *Student Member, IEEE*, and Mostafa Sahraei-Ardakani, *Member, IEEE*

***Abstract*—The increasing penetration of renewable generation poses challenges to grid operation, including the need for increased available transfer capability (ATC). The power flow control capability of flexible AC transmission system (FACTS) devices can enhance the transfer capability over the existing network, thus improving the utilization of renewable energy. To harness such benefits, it is essential to integrate FACTS operation into stochastic unit commitment (SUC), in which renewable generation uncertainties are explicitly modeled. Furthermore, to ensure the computational tractability of SUC with FACTS incorporated, it is vital to study the impacts of FACTS deployment on computational burden of the model. This paper proposes a SUC model with the consideration of optimal FACTS operation. The proposed model is solved using the progressive hedging (PH) algorithm. PH is also used to solve the original SUC model for comparison. Simulation results reveal that despite the increased computational complexity due to FACTS operation, PH is a valuable approach in ensuring that the proposed model can be solved efficiently.**

***Index Terms*—Stochastic unit commitment, renewable generation integration, power flow control, progressive hedging.**

NOMENCLATURE

Indices

g	generator
k	transmission line
n	bus
s	scenario
t	time period
w	wind farm

Parameters

η_{C}	Capacitive FACTS compensation level
η_{L}	Inductive FACTS compensation level
ν	Wind speed
ν_{cin}	Cut-in speed of wind turbines
ν_{cout}	Cut-out speed of wind turbines
ν_{rated}	Rated speed of wind turbines
ξ_s	Probability of scenario s
c_g	Linear cost of generator g
d_{nt}	Demand at bus n in period t
DT_g	Minimum down time of generator g
$f_k^{\max}$	Capacity of line k
M	A very large positive number
NL_g	No-load cost of generator g
ns	The number of scenarios
$p_g^{\max}$	Maximum generator output of generator g
$p_g^{\min}$	Minimum generator output of generator g
RD_g	Ramp-down limit of generator g
RU_g	Ramp-up limit of generator g
SU_g	Start-up cost of generator g
UT_g	Minimum up time of generator g
WG_{rated}	Rated wind turbine output
WG_{wts}	Output of wind farm w, in period t, scenario s

Sets

$\mathcal{F}$	Set of lines equipped with FACTS, $\mathcal{F} \subset K$
$G(n)$	Set of generators connected to bus n
G	Set of generators
K	Set of transmission lines
$l^+(n)$	Set of lines that are connected "to" bus n
$l^-(n)$	Set of lines that are connected "from" bus n
N	Set of buses
S	Set of scenarios
T	Set of time periods
$W(n)$	Set of wind farms connected to bus n

Variables

Δx_k	FACTS reactance adjustment on line k
$\theta_{k,\mathrm{fr},ts}$	Bus voltage angle at the "from" bus of line k, in period t, scenario s
$\theta_{k,\mathrm{fr}}$	Bus voltage angle at the "from" bus of line k
$\theta_{k,\mathrm{to},ts}$	Bus voltage angle at the "to" bus of line k, in period t, scenario s
$\theta_{k,\mathrm{to}}$	Bus voltage angle at the "to" bus of line k
f_{kts}	Active power flow on line k, in period t, scenario s
f_k	Active power flow on line k
p_{gts}	Active power output of generator g, in period t, scenario s
p_{wts}^{wind}	Utilized wind generation of wind farm w, in period t, scenario s
u_{gt}	Commitment of generator g in period t
v_{gts}	Start-up of generator g, in period t, scenario s
z_{kts}	Power flow direction on line k, in period t, scenario s

This research was supported by the National Science Foundation grant number 1756006. Xinyang Rui and Mostafa Sahraei-Ardakani are with the Department of Electrical and Computer Engineering, University of Utah, Salt Lake City, UT, 84112 USA e-mail: xinyang.rui@utah.edu mostafa.ardakani@utah.edu.

I. INTRODUCTION

UNCERTAINTY management in the day-ahead unit commitment (UC) is increasingly more critical for systems with high levels of renewable energy penetration [1]. Stochastic unit commitment (SUC) is a popular approach in power system operation for handling the uncertainties of renewable generation. In the SUC, uncertainties are modeled as scenarios, and the multi-stage stochastic program is solved to determine optimal schedule of generating units.

Because of the computational burden of stochastic programs, directly solving SUC in its extensive form (EF) is viewed as a very undesirable approach. Therefore, techniques such as decomposition are widely used to improve computational efficiency. Between the two main categories of decomposition methods, scenario-based decomposition techniques have an advantage over their stage-based counterparts in that sub-problem difficulty is more uniformly distributed [2]. Prominent scenario-based decomposition methods include dual decomposition, which is applied in [3], [4] to solve SUC problems, and progressive hedging (PH). Although PH was originally proposed in [5] for problems that involve only continuous variables, it has been successfully applied as a heuristic to solve mixed-integer stochastic programs [6] and used for power system-related models in previous research. PH was proposed as an efficient method to solve SUC in [7], where several techniques and heuristics in accelerating convergence were presented. These techniques and heuristics were further analyzed in [2]. An extensive analysis of applying PH to solve SUC is presented in [8]. In [9], the authors applied a Frank–Wolfe-based decomposition method in conjunction with the PH to solve stochastic security-constrained unit commitment (S-SCUC).

Another significant challenge in enabling higher levels of renewable energy penetration is the need for significantly more transmission capacity [10]. Insufficient available transfer capability (ATC) to accommodate renewable generation hinders its utilization. Among the options to increase the ATC, deployment of flexible AC transmission systems (FACTS) provides an efficient approach in comparison to the lengthy and expensive process of constructing new transmission lines. With the active power flow control capabilities, FACTS devices allow rerouting of power flows to avoid transmission bottlenecks, thus improving the utilization of renewable generation. However, the inclusion of FACTS potentially adds more computational complexity to the already computationally challenging SUC. Therefore, efficient algorithm is in demand to facilitate the solution process.

The benefits of FACTS in facilitating renewable generation integration has been investigated in several previous studies. In [11], the authors proposed a methodology that uses an optimal power flow model with FACTS devices to minimize wind power spillage. The combined impact of FACTS and real-time thermal ratings on improving wind energy utilization was studied in [12]. Many studies focused on the planning of FACTS installation in power systems with renewable generation integration [13]–[16]. Despite the extensive effort on studying the impact of FACTS on renewable generation penetration, research on SUC with FACTS operation has been very limited. In [10], a two-stage stochastic optimization model was proposed to study the effectiveness of FACTS in reducing operation cost and wind curtailment. However, no decomposition algorithm was used in the solution process.

With the growing renewable penetration in power systems, it is important to incorporate FACTS operation into SUC to harness the benefits of the power flow control capabilities in power system operation. Furthermore, given the computational challenge of SUC, it is vital to understand the impacts of FACTS operation on computational efficiency of SUC models. To fill this gap, this paper proposes a SUC model with FATCS operation. The PH algorithm is used to solve SUC with FACTS, and computational impacts of the application of PH and FACTS deployment are evaluated.

The rest of this paper is organized as follows: Section II presents the methodology, including FACTS device modeling, problem formulations, PH implementation, and the scenario generation method. Simulation studies are presented in Section III. Finally, conclusions are drawn in Section IV.

II. Methodology

A. FACTS Modeling

In this paper, we focus on variable-impedance FACTS devices, which offer power flow control capabilities by directly altering the apparent impedance of transmission lines. Prominent examples include the thyristor-controlled series compensator (TCSC) and the continuously variable series reactor (CVSR). A variable-impedance FACTS device in power flow models are modeled as a controllable reactance, and such modeling is presented in Fig. 1.

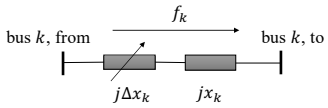

Fig. 1. Controllable reactance model of FACTS.

For a transmission line equipped with FACTS, the DC power flow equation is presented as follows:

$$f_k = -\frac{\theta_{k,\mathrm{to}} - \theta_{k,\mathrm{fr}}}{x_k + \Delta x_k}. \tag{1}$$

The operating range of the installed FACTS device is specified as:

$$-\eta_{\mathrm{C}} x_k \leq \Delta x_k \leq \eta_{\mathrm{L}} x_k. \tag{2}$$

In this paper, we set $\eta_{\mathrm{C}} = \eta_{\mathrm{L}} = 0.5$, which is a common setting for the TCSC according to previous research [17], [18].

Note that with Δx_k being a variable, (1) is nonlinear, which is very undesirable as the nonlinearity substantially increases the computational burden. To address this issue, a mixed-integer reformulation based on the big-M method was developed, which introduces binary variables to represent the flow direction on the transmission lines equipped with FACTS [19], [20]. The reformulation is presented in details as a part of problem formulation, presented in the following subsection.

B. Problem Formulations

The EF of the SUC model considering FACTS operation (SUC_FACTS) is presented as follows:

$$\textbf{SUC\_FACTS}: \quad \min \sum_{g\in G}\sum_{t\in T} NL_g u_{gt} + \sum_{g\in G}\sum_{t\in T}\sum_{s\in S}\xi_s(c_g p_{gts} + SU_g v_{gts}) \tag{3}$$

s.t.

$$u_{gt}p_g^{\min} \le p_{gts} \le u_{gt}p_g^{\max}, g \in G, t \in T, s \in S \quad (4)$$

$$0 \le p_{wts}^{\text{wind}} \le WG_{wts}, w \in W, t \in T, s \in S \quad (5)$$

$$-f_k^{\max} \le f_{kts} \le f_k^{\max}, k \in K, t \in T, s \in S \quad (6)$$

$$f_{kts} = -\frac{\theta_{k,\text{to},ts} - \theta_{k,\text{fr},ts}}{x_k}, k \notin \mathcal{F}, k \in K, t \in T, s \in S \quad (7)$$

$$\frac{\theta_{k,\text{fr},ts} - \theta_{k,\text{to},ts}}{(1+\eta_\text{L})x_k} - z_{kts}M \le f_{kts}, k \in \mathcal{F}, t \in T, s \in S \quad (8)$$

$$\frac{\theta_{k,\text{fr},ts} - \theta_{k,\text{to},ts}}{(1-\eta_\text{C})x_k} - (1-z_{kts})M \le f_{kts}, k \in \mathcal{F}, t \in T, s \in S \quad (9)$$

$$\frac{\theta_{k,\text{fr},ts} - \theta_{k,\text{to},ts}}{(1+\eta_\text{L})x_k} + (1-z_{kts})M \ge f_{kts}, k \in \mathcal{F}, t \in T, s \in S \quad (10)$$

$$\frac{\theta_{k,\text{fr},ts} - \theta_{k,\text{to},ts}}{(1-\eta_\text{C})x_k} + z_{kts}M \ge f_{kts}, k \in \mathcal{F}, t \in T, s \in S \quad (11)$$

$$\theta_{k,\text{to},ts} - \theta_{k,\text{fr},ts} \le z_{kts}M, k \in \mathcal{F}, t \in T, s \in S \quad (12)$$

$$\theta_{k,\text{to},ts} - \theta_{k,\text{fr},ts} \ge (z_{kts}-1)M, k \in \mathcal{F}, t \in T, s \in S \quad (13)$$

$$z_{kts} \in \{0,1\}, k \in \mathcal{F}, t \in T, s \in S \quad (14)$$

$$M > \max_{k \in \mathcal{F}}\{\frac{\eta_\text{C} + \eta_\text{L}}{1-\eta_\text{C}} f_k^{\max}\}, \quad (15)$$

$$\theta_{1,ts} = 0, t \in T, s \in S \quad (16)$$

$$\sum_{k \in l^+(n)} f_{kts} - \sum_{k \in l^-(n)} f_{kts} + \sum_{g \in G(n)} p_{gts} + \sum_{w \in W(n)} p_{wts}^{\text{wind}} = d_{nt}, n \in N, t \in T, s \in S \quad (17)$$

$$-RD_g \le p_{g,t+1,s} - p_{gts} \le RU_g, g \in G, t \in T, s \in S \quad (18)$$

$$\sum_{r=t-UT_g+1}^{t} v_{grs} \le u_{gt}, g \in G, t \ge UT_g, s \in S \quad (19)$$

$$\sum_{r=t+1}^{t+DT_g} v_{grs} \le 1 - u_{gt}, g \in G, t \le |T| - DT_g, s \in S \quad (20)$$

$$0 \le v_{gts} \le 1, g \in G, t \in T, s \in S \quad (21)$$

$$u_{gt} - u_{g,t-1} \le v_{gts}, g \in G, t \in T, s \in S \quad (22)$$

$$u_{gt} \in \{0,1\}, g \in G, t \in T. \quad (23)$$

The formulation presented above is a two-stage stochastic program. (3) is the objective function which includes first-stage costs and second-stage costs. The first-stage costs include only the no-load costs, which are associated with the first-stage variables u_{gt}. Note that u_{gt} only have generator and time period indices, meaning that they are not dependent on scenarios. Non-anticipativity is, thus, ensured. Second-stage costs are the expected summation of fuel costs and start-up costs in each scenario. (4) imposes the output limits on generators. (5) specifies the constraint on available wind power in each scenario. (6) are the capacity limits of transmission lines. DC power flow equations for lines not equipped with FACTS are presented in (7). Power flow equations for lines equipped with FACTS are reformulated to (8)–(14), with (15) specifying how the value of M can be set. (16) imposes constraints on the bus voltage angle at the reference bus. Nodal power balance constraints are presented in (17). (18) imposes ramping constraints on generators. (19) and (20) are the minimum up and down time constraints of generators. (21) and (22) are constraints on the start-up variables. Note that start-up variables can be relaxed from being binary to continuous variables as they are forced to take the limits in (21). Finally, (23) specifies that generator commitment variables are binary.

In the mixed-integer reformulation of (1)–(2) to (8)–(14), z_{kts} represents the power flow direction on line k. The equivalence between the value of z_{kts} and the flow direction are shown as follows:

$$z_{kts} = 0 \iff f_{kts} \ge 0, \quad (24)$$

$$z_{kts} = 1 \iff f_{kts} < 0. \quad (25)$$

The formulation of SUC without FACTS devices (referred to as SUC) is solved for comparison so that we can study the computational impact of FACTS operation. The formulation is presented as follows:

SUC :

$$\min \sum_{g \in G}\sum_{t \in T} NL_g u_{gt} + \sum_{g \in G}\sum_{t \in T}\sum_{s \in S} \xi_s (c_g p_{gts} + SU_g v_{gts}) \quad (26)$$

s.t.

$$f_{kts} = -\frac{\theta_{k,\text{to},ts} - \theta_{k,\text{fr},ts}}{x_k}, k \in K, t \in T, s \in S \quad (27)$$

$(4)-(6), (16)-(23)$.

C. Progressive Hedging

We use the PH algorithm presented in [2], [7] to solve the formulated models. When solving a stochastic program using PH, after the aforementioned scenario-based decomposition, first-stage variables are temporarily allowed to be dependent on scenarios [7]. Non-anticipativity is then restored through iteratively updating the multipliers [2]. To improve the convergence of PH when solving a mixed-integer program such as SUC, accelerating techniques are needed. In our implementation, the following techniques are utilized:

- Variable-specific ρ – The parameter ρ is important in the step of updating the multipliers in PH implementation. Properly choosing the value of ρ is crucial in facilitating PH convergence and ensuring solution quality [2]. In our simulation studies, ρ for each generator is set as $\rho_g = \alpha c_g$, where α is the scale factor. Such parameterization is referred to as "cost-proportional ρ" which is effective in assisting PH convergence [2];
- Variable-fixing – We fix the values of first-stage variables that have converged over the past β iterations [7].

The values of PH parameters in simulation studies are presented in Table I.

TABLE I
PH PARAMETER SETTING

Parameter	Value
α (ρ scale factor)	100
β (fixing iteration lag)	3
σ (convergence metric)	0.00001

PH is implemented using the mpi-sppy package, which uses Pyomo for mathematical programming and has a central feature of efficient and scalable parallelization [21]. In mpi-sppy, message passing interface (MPI) is used for parallelization [22].

D. Scenario Generation

In this paper, wind is used as the renewable energy source. We first generate wind speed scenarios, which are time series, then map them to the output of wind farms using the wind turbine model to create scenarios of wind power output. The method to generate wind speed time series is based on the methods in [3], [23], and the procedures are presented as follows:

- Fit an Inverse Gaussian (IG) distribution to the historical wind speed data;
- Transform the historical wind speed data into a normalized Gaussian time series using the marginal distribution function of the IG distribution;
- Fit an autoregressive (AR) model to the normalized Gaussian time series;
- Generate normalized Gaussian time series using the AR model;
- Un-transform the normalized wind speed time series to produce reasonable wind speed scenarios.

In this paper, we use historical wind speed data from Douglas County, Kansas. The data is obtained from [24]. The wind turbine model for determining the output based on wind speed is presented as follows [10]:

$$WG = \begin{cases} WG_{\text{rated}} \frac{\nu^3 - \nu_{\text{cin}}^3}{\nu_{\text{rated}}^3 - \nu_{\text{cin}}^3} & \text{if } \nu_{\text{cin}} \leq \nu < \nu_{\text{rated}} \\ WG_{\text{rated}} & \text{if } \nu_{\text{rated}} \leq \nu < \nu_{\text{cout}} \\ 0 & \text{otherwise} \end{cases} \quad (28)$$

Using this model, time series of wind power output of the wind farms can be generated. The probability of each scenario is assigned by solving an optimization problem with the objective of matching the statistical properties of the generated wind speed time series to that of the original continuous random variables as closely as possible [25].

III. Simulation Studies

The test system we use is area 1 of the RTS-96 system and the data is available at [26]. The following modifications are made to the system so that it is more suitable for studying the impact of FACTS devices:

1) The capacity of every line is reduced by 10%;
2) The capacity of the line with highest utilization, line 23, is further altered to 315 MW.

5 FACTS devices are located on the 5 lines that are utilized the most in the system. For wind generation integration, we add 3 wind farms each with rated output of 300 MW to the system. Both SUC and SUC_FACTS are solved using two methods: PH and directly solving the EF. The EFs and PH subproblems are solved using CPLEX 12.10 on a Intel Xeon Gold 6136 CPU with 128 GB RAM. EFs are solved with a MIPgap of 0.5%. For PH, the MIPgap is set as 1% for the first iteration, and reduced to 0.5% from the second iteration onward. The simulation results with 15 and 30 scenarios are presented in Tables II–V.

TABLE II
SUC_FACTS results ($ns = 15$)

Solution method	PH	EF
Cost ($)	744314.59	738774.13
Number of iterations	40	NA
Ave. total solution time (s)	43.64	319.35

TABLE III
SUC_FACTS results ($ns = 30$)

Solution method	PH	EF
Cost ($)	753239.66	748286.74
Number of iterations	43	NA
Ave. total solution time (s)	63.56	1295.79

TABLE IV
SUC results ($ns = 15$)

Solution method	PH	EF
Cost ($)	796121.91	788153.43
Number of iterations	27	NA
Ave. total solution time (s)	31.33	60.28

TABLE V
SUC results ($ns = 30$)

Solution method	PH	EF
Cost ($)	803122.70	799459.59
Number of iterations	44	NA
Ave. total solution time (s)	59.85	248.14

We first compare the total costs of SUC_FACTS and SUC, and calculate that on average a saving of 6.35% can be achieved. The results highlights the benefit of FACTS in improving renewable energy utilization.

Furthermore, we evaluate the computational efficiency improvement provided by applying PH. We use the total solution time as the measurement to calculate computational efficiency improvement, and results are presented in Table VI.

TABLE VI
Computational efficiency improvement by PH

Model (ns)	Comp. eff. imp.
SUC_FACTS (15)	632%
SUC_FACTS (30)	1939%
SUC (15)	92%
SUC (30)	315%

The results in Table VI reveal that, compared to directly solving the EF, PH significantly improves the computational efficiency, especially with FACTS operation considered. As mentioned previously, the incorporation of FACTS leads to increased computational complexity for power system operation models. We again use average total solution time as the measurement, and compare the results of SUC and SUC_FACTS to calculate the increased computational burden. The results are presented in Table VII.

TABLE VII
INCREASED COMPUTATIONAL BURDEN DUE TO FACTS

Solution method (ns)	**FACTS comp. burden**
EF (15)	430%
EF (30)	422%
PH (15)	39%
PH (30)	6%

It can be seen from Table VII that FACTS significantly increases computational burden when directly solving EFs. However, in comparison, the increased computational complexity due to FACTS operation is significantly less and much more reasonable with PH applied. SUC_FACTS only requires 6% more solution time than SUC when solved using PH with 30 sceanrios. The results in Tables VI–VII indicate that PH is a valuable, efficient approach for solving the proposed SUC_FACTS model. This is important for power system operation to utilize FACTS to facilitate renewable generation integration, and encouraging for the deployment of FACTS technology in the power grid in general.

Note that PH does lead to a certain level of suboptimality in our simulation results, which can be observed in the costs in Tables II–V. The average suboptimality in costs is 1.2%. The implementation of the PH algorithm is a trade-off between solution quality and computational efficiency [2], and we think that solution quality can be improved by further parameter tuning. Moreover, the suboptimaility in our simulation studies is insignificant compared to the computational efficiency improvement provided by PH.

IV. CONCLUSIONS

This paper developed a stochastic unit commitment model that co-optimizes FACTS set-point alongside generation dispatch, as a way to manage renewable energy uncertainty. To efficiently solve the proposed model, we applied the progressive hedging algorithm. Additionally, results of directly solving the extensive forms are presented for comparison. Simulation results on the RTS-96 system reveal that compared to directly solving the extensive form, applying progressive hedging reduces the computational time by 632% and 1939% with 15 and 30 scenarios. This is a rather significant computational efficiency improvement, which will assist in achieving tractability for larger systems. In addition, the results show that the increased computational complexity due to FACTS operation is much more manageable when using progressive hedging. Future work will involve testing the proposed model on larger systems with larger scenario sets.

REFERENCES

[1] J. Shi and S. S. Oren, "Stochastic unit commitment with topology control recourse for power systems with large-scale renewable integration," *IEEE Transactions on Power Systems*, vol. 33, no. 3, pp. 3315–3324, 2017.

[2] K. Cheung, D. Gade, C. Silva-Monroy, S. M. Ryan, J.-P. Watson, R. J.-B. Wets, and D. L. Woodruff, "Toward scalable stochastic unit commitment," *Energy Systems*, vol. 6, no. 3, pp. 417–438, 2015.

[3] A. Papavasiliou, S. S. Oren, and R. P. O'Neill, "Reserve requirements for wind power integration: A scenario-based stochastic programming framework," *IEEE Transactions on Power Systems*, vol. 26, no. 4, pp. 2197–2206, 2011.

[4] A. Papavasiliou and S. S. Oren, "Multiarea stochastic unit commitment for high wind penetration in a transmission constrained network," *Operations research*, vol. 61, no. 3, pp. 578–592, 2013.

[5] R. T. Rockafellar and R. J.-B. Wets, "Scenarios and policy aggregation in optimization under uncertainty," *Mathematics of operations research*, vol. 16, no. 1, pp. 119–147, 1991.

[6] J.-P. Watson and D. L. Woodruff, "Progressive hedging innovations for a class of stochastic mixed-integer resource allocation problems," *Computational Management Science*, vol. 8, no. 4, pp. 355–370, 2011.

[7] S. M. Ryan, R. J.-B. Wets, D. L. Woodruff, C. Silva-Monroy, and J.-P. Watson, "Toward scalable, parallel progressive hedging for stochastic unit commitment," in *2013 IEEE Power & Energy Society General Meeting*. IEEE, 2013, pp. 1–5.

[8] C. Ordoudis, P. Pinson, M. Zugno, and J. M. Morales, "Stochastic unit commitment via progressive hedging—extensive analysis of solution methods," in *2015 IEEE Eindhoven PowerTech*. IEEE, 2015, pp. 1–6.

[9] A. M. Palani, H. Wu, and M. M. Morcos, "A frank–wolfe progressive hedging algorithm for improved lower bounds in stochastic scuc," *IEEE Access*, vol. 7, pp. 99 398–99 406, 2019.

[10] Y. Sang, M. Sahraei-Ardakani, and M. Parvania, "Stochastic transmission impedance control for enhanced wind energy integration," *IEEE Transactions on Sustainable Energy*, vol. 9, no. 3, pp. 1108–1117, 2017.

[11] A. Nasri, A. J. Conejo, S. J. Kazempour, and M. Ghandhari, "Minimizing wind power spillage using an OPF with FACTS devices," *IEEE Transactions on Power Systems*, vol. 29, no. 5, pp. 2150–2159, 2014.

[12] A. Kapetanaki, V. Levi, M. Buhari, and J. A. Schachter, "Maximization of wind energy utilization through corrective scheduling and FACTS deployment," *IEEE Transactions on Power Systems*, vol. 32, no. 6, pp. 4764–4773, 2017.

[13] S. Galloway, I. Elders, G. Burt, and B. Sookananta, "Optimal flexible alternative current transmission system device allocation under system fluctuations due to demand and renewable generation," *IET generation, transmission & distribution*, vol. 4, no. 6, pp. 725–735, 2010.

[14] A. Elmitwally and A. Eladl, "Planning of multi-type FACTS devices in restructured power systems with wind generation," *International Journal of Electrical Power & Energy Systems*, vol. 77, pp. 33–42, 2016.

[15] A. Elmitwally, A. Eladl, and J. Morrow, "Long-term economic model for allocation of FACTS devices in restructured power systems integrating wind generation," *IET Generation, Transmission & Distribution*, vol. 10, no. 1, pp. 19–30, 2016.

[16] X. Zhang, D. Shi, Z. Wang, B. Zeng, X. Wang, K. Tomsovic, and Y. Jin, "Optimal allocation of series FACTS devices under high penetration of wind power within a market environment," *IEEE Transactions on power systems*, vol. 33, no. 6, pp. 6206–6217, 2018.

[17] Y. Ou and C. Singh, "Improvement of total transfer capability using TCSC and SVC," in *2001 Power Engineering Society Summer Meeting. Conference Proceedings (Cat. No. 01CH37262)*, vol. 2. IEEE, 2001, pp. 944–948.

[18] M. B. Shafik, H. Chen, G. I. Rashed, and R. A. El-Sehiemy, "Adaptive multi objective parallel seeker optimization algorithm for incorporating TCSC devices into optimal power flow framework," *IEEE Access*, vol. 7, pp. 36 934–36 947, 2019.

[19] T. Ding, R. Bo, F. Li, and H. Sun, "Optimal power flow with the consideration of flexible transmission line impedance," *IEEE Transactions on Power Systems*, vol. 31, no. 2, pp. 1655–1656, 2015.

[20] M. Sahraei-Ardakani and K. W. Hedman, "Day-ahead corrective adjustment of FACTS reactance: A linear programming approach," *IEEE Transactions on Power Systems*, vol. 31, no. 4, pp. 2867–2875, 2015.

[21] B. Knueven, D. Mildebrath, C. Muir, J. D. Siirola, J.-P. Watson, and D. L. Woodruff, "A parallel hub-and-spoke system for large-scale scenario-based optimization under uncertainty," 2020.

[22] mpi-sppy. [Online]. Available: https://mpi-sppy.readthedocs.io/en/latest/

[23] J. M. Morales, R. Minguez, and A. J. Conejo, "A methodology to generate statistically dependent wind speed scenarios," *Applied Energy*, vol. 87, no. 3, pp. 843–855, 2010.

[24] NREL. The wind prospector. [Online]. Available: https://maps.nrel.gov/wind-prospector/?aL=MlB4Hk%255Bv%255D%3Dt%26VMGtY3%255Bv%255D%3Dt%26VMGtY3%255Bd%255D%3D1&bL=clight&cE=0&lR=0&mC=40.21244%2C-91.625976&zL=4

[25] S. Jin, S. M. Ryan, J.-P. Watson, and D. L. Woodruff, "Modeling and solving a large-scale generation expansion planning problem under uncertainty," *Energy Systems*, vol. 2, no. 3, pp. 209–242, 2011.

[26] Power systems test case archive. [Online]. Available: http://labs.ece.uw.edu/pstca/rts/pg_tcarts.htm

CHAPTER 5

ADMM-BASED DISTRIBUTED DC OPTIMAL POWER FLOW WITH POWER FLOW CONTROL

This chapter presents a published article[1][2] focusing on integrating FACTS operation into the distributed DCOPF. The distributed DCOPF is formulated in response to a distributed structure of grid operations. Under such a structure, the grid consists of interconnected subsystems, each operating reasonably independently. Variables associated with transmission lines that connect neighboring subsystems need to converge following the global convergence of DCOPF. As shown in later chapters, transmission technologies can be deployed on such border transmission lines to facilitate energy flow between neighboring subsystems. The publication included in this chapter indicates that FACTS controllers can be smoothly integrated into the distributed DCOPF, which is solved using the alternating direction method of multipliers.

---

[1]

[2]

ADMM-Based Distributed DC Optimal Power Flow with Power Flow Control

Xinyang Rui
Department of Electrical and Computer Engineering
University of Utah
Salt Lake City, UT, USA
xinyang.rui@utah.edu

Mingxi Liu
Department of Electrical and Computer Engineering
University of Utah
Salt Lake City, UT, USA
mingxi.liu@utah.edu

Mostafa Sahraei-Ardakani
Department of Electrical and Computer Engineering
University of Utah
Salt Lake City, UT, USA
mostafa.ardakani@utah.edu

Thomas R. Nudell
Smart Wires Inc.
Durham, NC, USA
Tom.Nudell@smartwires.com

***Abstract*—This paper presents a new methodology of incorporating power flow controllers, specifically flexible AC transmission systems (FACTS), into distributed DC optimal power flow (DCOPF). The distributed DCOPF problems are then solved by the alternating direction method of multipliers (ADMM). Efficient modeling of the power flow control capabilities of prominent FACTS devices, such as the unified power flow controller (UPFC) and the static synchronous series compensator (SSSC), enables the seamless integration of FACTS into the ADMM-based distributed DCOPF, thus allowing FACTS operation to be co-optimized with generator dispatch under a distributed control paradigm for the power system. The proposed ADMM-based distributed DCOPF problem with FACTS devices are studied through simulations on a 6-bus system and a modified IEEE 118-bus system to verify its convergence to the optimal generator dispatch.**

***Index Terms*—Distributed DCOPF, ADMM, power flow control, FACTS devices.**

NOMENCLATURE

Indices

g	Index of generators
k	Index of transmission lines
n	Index of buses
u, v, m	Index of subsystems

Parameters

a_g, b_g, c_g	Quadratic cost function parameters of generator g
b_k	Susceptance of line k
d_n	Demand at bus n
$f_k^{\max}$	Capacity of line k
M	Total number of subsystems
n_k^{FACTS}	The number of modular FACTS devices per phase on line k
$p_g^{\max}$	Maximum active power output of generator g
$p_g^{\min}$	Minimum active power output of generator g
V_k^{inj}	Maximum FACTS voltage injection on line k
V^{mod}	Maximum voltage injection of a modular FACTS device
x_k	Reactance of line k

Sets

$\hat{K}$	Set of lines equipped with FACTS, $\hat{K} \subset K$
$\iota^+(n)$	Set of lines that are connected "to" bus n
$\iota^-(n)$	Set of lines that are connected "from" bus n
$G(n)$	Set of generators connected to bus n
G	Set of generators
K	Set of transmission lines
N	Set of buses

Variables

Δb_k	FACTS susceptance adjustment on line k
Δx_k	FACTS reactance adjustment on line k
$\theta_{k,\text{fr}}$	Bus voltage angle at the "from" bus of line k
$\theta_{k,\text{to}}$	Bus voltage angle at the "to" bus of line k
f_k	Active power flow on line k
p_g	Active power output of generator g

This research was supported by the National Science Foundation under grant number 1756006.

978-1-6654-9921-7/22/$31.00 ©2022 IEEE

I. INTRODUCTION

THE complexities of power system operation is increasing because of renewable energy penetration, power flow control technologies, demand response (DR) resources, etc. Moreover, the power grid is shifting towards a more distributed structure where independent entities are physically interconnected through transmission lines [1]. These factors cause difficulties for centralized control and operation of the power system. A more scalable, robust, and efficient alternative is the distributed control strategy [2], [3]. Therefore, the realization of solving power system operation models in a distributed manner is essential. One of the most important power system operation models is the optimal power flow (OPF), which minimizes the operation cost while considering system constraints. Power system operation requires OPF

problems to be solved frequently and efficiently. Previous studies have discussed the advantages of distributed OPF over the traditional centralized OPF. Distributed OPF has lower requirements on communication infrastructure as it limits the amount of information exchanged [4], which also helps improve cyber security in the smart grid. In addition, distributed OPF has shown performance superiority in solving complex problems over large-scale networks [5].

To better utilize the transmission flexibility provided by flexible AC transmission system (FACTS) devices under the distributed control scheme, it is critical to incorporate them into distributed OPF. The power flow control capabilities of FACTS devices are important for improving the operation efficiency and available transfer capability (ATC) of the power grid [6]. Series FACTS devices can provide power flow control capabilities through adjusting the impedance of transmission lines. Previous studies have proposed distributed DCOPF formulations with the incorporation of FACTS devices [3], [5]. However, only variable-impedance FACTS devices, for which a prominent example is the thyristor-controlled series compensator (TCSC), that directly provide continuous impedance adjustments, are studied. Therefore, there is a necessity to incorporate other types of FACTS devices into distributed OPF. Different types of series FACTS devices rely on different methods to alter the effective reactance of transmission lines [7]. Prominent FACTS devices such as the unified power flow controller (UPFC) and the static synchronous series compensator (SSSC), which are both widely studied and used power flow control technologies, use voltage injections to effectively emulate reactance adjustments. UPFC is versatile [8] and is regarded as the latest generation of FACTS device [9]. Furthermore, SSSC devices are gaining rapid adoption through a light-weight and easy-to-deploy modular technology commercialized by Smart Wires Inc. [10]. In this paper, we focus on incorporating these types of FACTS devices into distributed OPF. For the remainder of this paper, we use the term "FACTS" is used to specifically refer to them.

Among the optimization methods for solving distributed OPF, the alternating direction method of multipliers (ADMM) has been utilized by many studies in recent years because of its suitability for solving large-scale, distributed optimization problems [4], [11], [12]. Several previous studies have focused on using ADMM to solve a variety of distributed OPF models. In [13], the authors developed a fully distributed and robust algorithm for ACOPF based on ADMM. In [4], a consensus-based ADMM approach for solving DCOPF with DR is presented. DCOPF is an approximate model of ACOPF and is widely used in market applications [14]. The effect of communication delay in ADMM-based distributed DCOPF is studied in [15]. In [16], a learning-aided asynchronous ADMM is proposed to better utilize computational resources when solving distributed OPF. The authors in [17] proposed a privacy preserving ADMM-based DCOPF algorithm and provided analysis for potential privacy leakage.

In this paper, we propose a distributed DCOPF formulation using the efficient FACTS modeling developed in [7] for the incorporation of FACTS devices. The proposed distributed DCOPF with FACTS is solved using ADMM. To the best of the authors' knowledge, no existing literature focuses on solving distributed OPF with power flow control using ADMM.

The rest of this paper is organized as follows. Section II introduces the modeling of FACTS in DCOPF. The formulation and the algorithm of ADMM-based distributed DCOPF with FACTS is presented in Section III. In Section IV, the proposed model is studied through simulations on two different test systems. Finally, Section V concludes the paper.

II. Modeling of FACTS devices

In [7], linear modeling of various types of FACTS devices are presented for DC-based power system operation problems based on injection shift factors (ISF). The modeling of FACTS devices in this paper is adopted from [7], and is also equivalent to the DC model of SSSC presented in [18].

For a transmission line equipped with FACTS devices, the DC power flow equation is formulated as:

$$f_k = (b_k + \Delta b_k)(\theta_{k,\mathrm{to}} - \theta_{k,\mathrm{fr}}). \tag{1}$$

Alternatively, (1) can be formulated using reactance:

$$f_k = \frac{\theta_{k,\mathrm{fr}} - \theta_{k,\mathrm{to}}}{x_k + \Delta x_k}. \tag{2}$$

As mentioned previously, series FACTS devices provide power flow control capabilities through altering the apparent impedance of transmission lines. Therefore, Δb_k and Δx_k are variables, resulting in nonlinearity in both (1) and (2). The constraints on Δb_k and Δx_k are dependent on device type. SSSC alters the line reactance by injecting a voltage that is in quadrature with the line current [19]. The magnitude of the voltage injection is controllable. Similarly, UPFC also provides series compensation through a voltage injection. The difference between UPFC and SSSC devices in altering the line reactance is that the angle of the UPFC voltage injection is also controllable. The series device of UPFC can be regarded as an SSSC [20], and it provides the maximum series compensation in magnitude when the voltage injection is in quadrature with the line current [7]. Therefore, in this paper, UPFC and SSSC share the same modeling for their operating ranges regarding line reactance adjustments.

In [7], the variation bounds of $\Delta b_k(\theta_{k,\mathrm{to}} - \theta_{k,\mathrm{fr}})$ for a line k equipped with FACTS devices is derived, which is presented as follows:

$$-V_k^{\mathrm{inj}}|b_k| \le \Delta b_k(\theta_{k,\mathrm{to}} - \theta_{k,\mathrm{fr}}) \le V_k^{\mathrm{inj}}|b_k|. \tag{3}$$

Eqns. (1) and (3) are nonlinear, which is highly undesirable in terms of computational efficiency. Moreover, their nonconvexity hinders the application in ADMM, as ADMM becomes a local optimization method when applied to solve nonconvex problems [12]. To address these issues, equivalently to the FACTS nodal injection model presented in [21], a variable ϕ_k is introduced to substitute $\Delta b_k(\theta_{k,\mathrm{to}} - \theta_{k,\mathrm{fr}})$. Eqns. (1) and (3) are then reformulated as:

$$f_k = b_k(\theta_{k,\mathrm{to}} - \theta_{k,\mathrm{fr}}) + \phi_k, \tag{4}$$

$$-V_k^{\text{inj}}|b_k| \le \phi_k \le V_k^{\text{inj}}|b_k|. \tag{5}$$

To validate the substitution, the equivalence between the DCOPF problems before and after the introduction of ϕ_k needs to be proved. Therefore, we first present the formulation of the DCOPF problem with FACTS using the nonlinear DC power flow equation (1), which is shown as follows:

$$\begin{aligned}
&\mathrm{P}_1: \\
&\min \sum_{g\in G}(a_g p_g^2 + b_g p_g + c_g) && (6)\\
&\text{s.t.} \\
&(3); \\
&p_g^{\min} \le p_g \le p_g^{\max}, \forall g \in G; && (7)\\
&-f_k^{\max} \le b_k(\theta_{k,\text{to}} - \theta_{k,\text{fr}}) \le f_k^{\max}, \forall k \in K, k \notin \hat{K}; && (8)\\
&-f_k^{\max} \le (b_k + \Delta b_k)(\theta_{k,\text{to}} - \theta_{k,\text{fr}}) \le f_k^{\max}, \forall k \in \hat{K}; && (9)\\
&\sum_{k\in\iota^+(n)} b_k(\theta_{k,\text{to}} - \theta_{k,\text{fr}}) - \sum_{k\in\iota^-(n)} b_k(\theta_{k,\text{to}} - \theta_{k,\text{fr}}) \\
&+ \sum_{k\in\iota^+(n),k\in\hat{K}} \Delta b_k(\theta_{k,\text{to}} - \theta_{k,\text{fr}}) - \\
&\sum_{k\in\iota^-(n),k\notin\hat{K}} \Delta b_k(\theta_{k,\text{to}} - \theta_{k,\text{fr}}) && (10)\\
&= d_{nt} - \sum_{g\in G(n)} p_g, \forall n \in N.
\end{aligned}$$

Eqn. (6) is the quadratic objective function which minimizes the total fuel cost. (3) is the aforementioned bounds of the impact of FACTS devices on power flow and is included in the formulation. (7) enforces the generator output constraints. (8) and (9) are transmission line thermal capacity limit constraints for lines without and with FACTS respectively. (10) specifies the power balance at each bus in the system.

Then, the DCOPF problem after the variable substitution is needed for comparison. The formulation is presented as follows:

$$\begin{aligned}
&\mathrm{P}_2: \\
&\min \sum_{g\in G}(a_g p_g^2 + b_g p_g + c_g) && (11)\\
&\text{s.t.} \\
&(5), (8); \\
&-f_k^{\max} \le b_k(\theta_{k,\text{to}} - \theta_{k,\text{fr}}) + \phi_k \le f_k^{\max}, \forall k \in \hat{K}; && (12)\\
&\sum_{k\in\iota^+(n)} b_k(\theta_{k,\text{to}} - \theta_{k,\text{fr}}) - \sum_{k\in\iota^-(n)} b_k(\theta_{k,\text{to}} - \theta_{k,\text{fr}}) \\
&+ \sum_{k\in\iota^+(n),k\in\hat{K}} \phi_k - \sum_{k\in\iota^-(n),k\in\hat{K}} \phi_k && (13)\\
&= d_{nt} - \sum_{g\in G(n)} p_g, \forall n \in N.
\end{aligned}$$

Eqn. (5) is the aforementioned constraint on ϕ_k to enforce the operating range of FACTS. (12) specifies the thermal capacity limits on lines equipped with FACTS. (13) is the nodal balance constraints. Note that for modular FACTS (M-FACTS) devices, V_k^{inj} for line $k(k \in \hat{K})$ is related to the number of modules deployed on the line [7]:

$$V_k^{\text{inj}} = n_k^{\text{FACTS}} V^{\text{mod}}. \tag{14}$$

Therefore, the proposed model can be utilized for M-FACTS operation under the distributed control scheme.

Contradiction is used to prove the equivalence between P_1 and P_2. Suppose $\boldsymbol{\omega}^* = \{\boldsymbol{\theta}^*, \boldsymbol{p}^*, \boldsymbol{\Delta b}^*\}$ are the optimal solutions of P_1. Then, for a line $k(k \in \hat{K})$, we can calculate ϕ_k^* as:

$$\phi_k^* = \Delta b_k^*(\theta_{k,\text{to}}^* - \theta_{k,\text{fr}}^*). \tag{15}$$

Using (15) and $\boldsymbol{\omega}^*$, we can form a feasible solution $\hat{\boldsymbol{\omega}}^* = \{\boldsymbol{\theta}^*, \boldsymbol{p}^*, \boldsymbol{\phi}^*\}$. Apparently, $\hat{\boldsymbol{\omega}}^*$ is a feasible for P_2. Let $\Gamma(\cdot)$ denote the objective function in (6). We now make the assumption that P_1 and P_2 are not equivalent, which means that there exists a solution $\boldsymbol{\upsilon} = \{\boldsymbol{\theta}, \boldsymbol{p}, \boldsymbol{\phi}\}$ for P_2, where:

$$\boldsymbol{\Gamma}(\boldsymbol{p}) < \boldsymbol{\Gamma}(\boldsymbol{p}^*). \tag{16}$$

Again, for a line $k(k \in \hat{K})$, Δb_k can be calculated as:

$$\Delta b_k = \frac{\phi_k}{\theta_{k,\text{to}} - \theta_{k,\text{fr}}}. \tag{17}$$

Combining (17) with $\boldsymbol{\upsilon}$, a feasible solution for P_1, $\hat{\boldsymbol{\upsilon}} = \{\boldsymbol{\theta}, \boldsymbol{p}, \boldsymbol{\phi}\}$ can be formed. As $\boldsymbol{\omega}^*$ is the optimal solution for P_1, we have:

$$\boldsymbol{\Gamma}(\boldsymbol{p}^*) \le \boldsymbol{\Gamma}(\boldsymbol{p}). \tag{18}$$

Eqn. (16) contradicts (18), implying that the assumption of P_1 and P_2 are unequivalent is false. Because of the convexity and linearity in constraints, we use P_2 to further derive the distributed DCOPF with FACTS, as well as applying ADMM for solving the model.

III. ADMM-based Distributed DCOPF with FACTS

Following the approach in [4], DCOPF is reformulated to accommodate the application of ADMM. We use the decentralized ADMM with a central collector that handles the global variables [12]. Such approach is also utilized for distributed DCOPF in [22]. The power system is first divided into M subsystems. For each subsystem, there are local and coupling variables. Local variables are strictly only related to one subsystem. The other variables are all coupling variables. Each subsystem solves a subproblem independently and report the coupling variables to the central collector.

Coupling variables can be identified by examining the lines connecting different subsystems, which are referred to as boundary lines. Consider a boundary line k with node (k, fr) in subsystem v and (k, to) in subsystem u. Apparently, $\theta_{k,\text{fr}}$ and $\theta_{k,\text{to}}$ are both coupling variables. In addition, to locally solve the problems in v and u, these two variables need to be duplicated in the neighboring subsystem [4]. Thus, there are $\theta_{k,\text{fr}}$ and $\theta_{k,\text{to}}^v$ in v, as well as $\theta_{k,\text{to}}$ and $\theta_{k,\text{fr}}^u$ in u. The variables and their duplicates all are included in the full set of

coupling variables. A coupling variable and its duplicates are associated with the same global variable.

If FACTS devices are deployed on boundary line k, then ϕ_k is needed in both v and u to solve local problems in ADMM-based distributed DCOPF. Thus, ϕ_k^v and ϕ_k^u are coupling variables and are related to the same global variable. We can see that the previously presented FACTS modeling effectively facilitates the integration of FACTS in the ADMM-based distributed DCOPF. The general form consensus optimization [12] can be applied to formulate the ADMM-based distributed DCOPF. The formulation is presented as follows [4]:

$$\mathrm{P}_3:$$

$$\min \sum_{m=1}^{M} \mathcal{C}_m(\boldsymbol{x}_m) \tag{19}$$

s.t.

$$\boldsymbol{x}_m \in \xi_m, \forall m; \tag{20}$$

$$\tilde{\boldsymbol{x}}_m - \tilde{\boldsymbol{z}}_m = 0, \forall m. \tag{21}$$

Eqn. (19) is the objective function which is the summation of the cost for all subsystems. In (20), ξ_m is the feasible region for variables in subsystem m. Therefore, (20) specifies the constraints for local and coupling variables in P_2 for each subsystem. (21) specifies the relation between coupling variables and global variables. $\tilde{\boldsymbol{z}}_m$ is a linear function of the vector of global variables $\boldsymbol{z}$ [12].

The update rules of the ADMM are specified as [4], [12]:

$$\boldsymbol{x}_m^{j+1} = \underset{x_m \in \xi_m}{\operatorname{argmin}} (\mathcal{C}_m(\boldsymbol{x}_m) + \boldsymbol{\lambda}_m^{jT} \tilde{\boldsymbol{x}}_m + \frac{\rho}{2} \|\tilde{\boldsymbol{x}}_m^j - \tilde{\boldsymbol{z}}_m^j\|_2^2), \forall m; \tag{22}$$

$$z_h^{j+1} = \frac{\sum_{\mathcal{G}(m,w)=h} (\tilde{\boldsymbol{x}}_m^{j+1})_w}{\sum_{\mathcal{G}(m,w)=h} 1}, \forall h; \tag{23}$$

$$\boldsymbol{\lambda}_m^{j+1} = \boldsymbol{\lambda}_m^j + \rho(\tilde{\boldsymbol{x}}_m^{j+1} - \tilde{\boldsymbol{z}}_m^{j+1}), \forall m; \tag{24}$$

where $\boldsymbol{\lambda}_m^j$ is the vector of dual variables in iteration j. $\mathcal{G}$ in (23) denotes the relationship that coupling variables correspond to a global variable. In (22), the problems are solved locally in each subsystem. The stopping criteria are [4]:

$$\|\boldsymbol{r}_m^{j+1}\|_2^2 = \|\boldsymbol{\lambda}_m^{j+1} - \boldsymbol{\lambda}_m^j\|_2^2 \leq \epsilon_1, \forall m \tag{25}$$

$$\|\boldsymbol{s}^{j+1}\|_2^2 = \rho \|\boldsymbol{z}^{j+1} - \boldsymbol{z}^j\|_2^2 \leq \epsilon_2. \tag{26}$$

where ϵ_1 and ϵ_2 are the threshold values.

The algorithm is presented as follows [4]:

Algorithm 1 ADMM-based distributed OPF with FACTS

1: Initialize dual and global variables, set the threshold values for the stopping criterion;
2: Solve the optimization problem in (22) for each subsystem;
3: Subsystems report coupling variable values, which include voltage phase angles and FACTS power injections, to the central collector;
4: The central collector updates global variables and sends them back to the subsystems;
5: If stopping criteria are satisfied at all subsystems, stop the algorithm. Otherwise, update the dual variables in each subsystem and go back to step 2.

IV. Numerical Studies

The proposed model of ADMM-based distributed DCOPF with FACTS is tested in simulations on a 6-bus system as well as a modified IEEE 118-bus system. A two-way partition is applied to the 6-bus system and the 118-bus system is divided into 3 subsystems. Each iteration of ADMM is solved using IBM CPLEX 12.9 on a Intel Core i5 CPU with 8 GB of RAM.

For SSSC, we assume that each location of FACTS installation has a maximum voltage injection equivalent to two SmartValve 10-1800 modules installed, which is 11.32 kV [23]. Note that the M-FACTS devices are installed per phase, and the maximum voltage injection in real cases needs be multiplied by $\sqrt{3}$. The maximum voltage injection value is also used as the maximum voltage injection for UPFC devices.

A. 6-bus system results

The system data, presented in Table I-III, is taken from [4] with modifications.

TABLE I
Generator data of the 6-bus system

Unit	$p^{\min}$ (MW)	$p^{\max}$ (MW)	a	b	c
1	20	200	0.67	26.24	31.67
2	50	200	0.95	12.89	6.78

TABLE II
Transmission line data of the 6-bus system

Branch	From	To	x(p.u.)	$f^{\max}$ (MW)
1	1	2	0.6	150
2	1	3	0.6	50
3	2	4	0.1	150
4	3	5	0.1	150
5	4	5	0.1	150
6	1	6	0.1	150

TABLE III
Load data of the 6-bus system

Demand	Location (bus)	Load (MW)
1	3	150
2	4	150
3	6	10

Note that we changed the thermal limit of line 2 from 150 MW to 50 MW to increase the congestion in the system. The partition of the 6-bus system is shown in Table IV [4].

TABLE IV
PARTITION OF THE 6-BUS SYSTEM

Subsystem	Buses
1	1,6
2	2-5

FACTS devices are deployed on line 2 as it is a boundary line. The effectiveness of power flow control allows the cheaper generator 1 to produce more compared with the results obtained from DCOPF without FACTS. To verify that the ADMM-based distributed DCOPF converges to the optimal solution, the dispatch results are compared with the ones obtained from the DCOPF problem with nonlinear FACTS operating range. The full formulation is presented as follows:

$$\mathrm{P}_4:$$

$$\min \sum_{g\in G}(a_g p_g^2 + b_g p_g + c_g) \tag{27}$$

s.t.

(7);

$$-f_k^{\max} \le \frac{\theta_{k,\mathrm{fr}} - \theta_{k,\mathrm{to}}}{x_k} \le f_k^{\max}, \forall k \notin \hat{K}, k \in K; \tag{28}$$

$$-f_k^{\max} \le \frac{\theta_{k,\mathrm{fr}} - \theta_{k,\mathrm{to}}}{x_k + \Delta x_k} \le f_k^{\max}, \forall k \in \hat{K}; \tag{29}$$

$$-V_k^{\mathrm{inj}} \le \frac{\Delta x_k(\theta_{k,\mathrm{fr}} - \theta_{k,\mathrm{to}})}{x_k} \le V_k^{\mathrm{inj}}, \forall k \in \hat{K}; \tag{30}$$

$$\begin{aligned}&\sum_{k\in\iota^+(n),k\notin\hat{K}} \frac{\theta_{k,\mathrm{fr}} - \theta_{k,\mathrm{to}}}{x_k} - \sum_{k\in\iota^-(n),k\notin\hat{K}} \frac{\theta_{k,\mathrm{fr}} - \theta_{k,\mathrm{to}}}{x_k} \\ &+ \sum_{k\in\iota^+(n),k\in\hat{K}} \frac{\theta_{k,\mathrm{fr}} - \theta_{k,\mathrm{to}}}{x_k + \Delta x_k} \\ &- \sum_{k\in\iota^-(n),k\in\hat{K}} \frac{\theta_{k,\mathrm{fr}} - \theta_{k,\mathrm{to}}}{x_k + \Delta x_k} \\ &= d_n - \sum_{g\in G(n)} p_g, \forall n \in N.\end{aligned} \tag{31}$$

Eqn. (30) is the operating range regarding the effective reactance adjustment [7]. Because of its nonconvexity and nonlinearity in constraints, P_4 is solved using the IPOPT solver.

Suppose that $\boldsymbol{p}_4^*$ is the optimal dispatch obtained by solving P_4, and $\boldsymbol{p}_3^k$ is the dispatch reported by ADMM at iteration k, we can calculate the 2-norm estimated error (NEE) to show the convergence of ADMM to the optimal global generator dispatch as the iteration progresses. At iteration k, the NEE is calculated as:

$$NEE(k) = \sqrt{\frac{\sum_g((\boldsymbol{p}_4^*)_g - (\boldsymbol{p}_3^k)_g)^2}{|G|}} \tag{32}$$

where $|G|$ is the total number of generators in the system.

For the 6-bus system, ρ is set to be 600. Threshold values ϵ_1 and ϵ_2 are both set to be 0.001. ADMM converged after 27 iterations. Fig. 1 shows how the value of NEE changes as the algorithm progresses, which verifies the convergence of the proposed ADMM-based DCOPF to the same result as P_4.

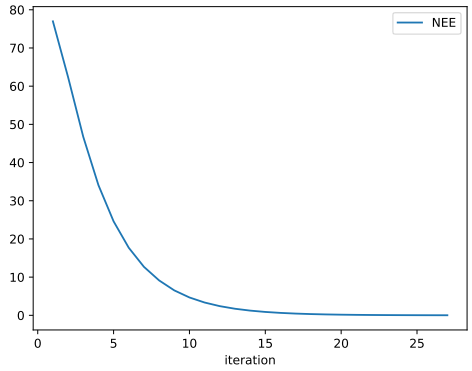

Fig. 1. NEE value of each iteration of ADMM-based DCOPF for the 6-bus system.

B. 118-bus system

The IEEE 118-bus test system data is available at [24], and modifications are made according to [25].The partition of the system is presented in Table V [4].

TABLE V
PARTITION OF THE 118-BUS SYSTEM

Subsystem	Buses
1	1-32, 113-115, 117
2	33-73, 116
3	74-112, 118

FACTS devices are deployed on boundary lines 39 and 112. The value of ρ is set to be 1750. Threshold values ϵ_1 and ϵ_2 are both set as 0.001. The algorithm converged after 301 iterations. The progression of NEE is presented in Fig. 2. From the NEE results we can see that, for the 118-bus system, the NEE approaches 0 as the algorithm progresses, which verifies the convergence of the proposed model to optimal generator dispatch.

C. Discussion

The first interesting observation is that using per unit (p.u.) values facilitates the convergence of ADMM. Most implementations of DC power flow are based on the per unit system. However, in practice, if the base of power is multiplied at each side of the constraints, we can directly solve for the real values through DCOPF. For simulation studies in this paper, such an approach leads to slow convergence of ADMM compared to

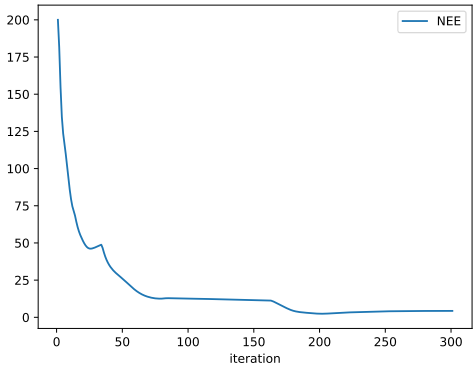

Fig. 2. NEE value of each iteration of ADMM-based DCOPF for the 118-bus system.

using p.u. values. If real values are used, ADMM takes more than 300 iterations to converge for the 6-bus system. For the 118-bus system, it could take more than 1500 iterations if ρ is not set very desirably. In addition, to achieve convergence within a reasonable number of iterations, ADMM requires a very large ρ value, e.g., $\rho > 50000$, for the 118-bus system.

Another observation is that the favorable ρ value of 20 in proposed by the authors of [4] is actually too small in our simulations and results in slow convergence.

V. Conclusions

In this paper, prominent series FACTS devices are integrated into the ADMM-based distributed DCOPF model. The developed model preserves the desirable feature of linearity and convexity of the original DCOPF problem, facilitating efficient co-optimization of FACTS point and generator dispatch under the distributed control scheme. The integration approach and the proposed model are validated by simulation studies conducted using different test systems. Simulation results shows the convergence of the ADMM algorithm when solving the proposed distributed DCOPF model.

Future research will include incorporating other types of series FACTS devices into the ADMM-based distributed DCOPF and modifying the ADMM algorithm to accommodate the computational challenges introduced by the modeling of certain types of FACTS devices.

References

[1] A. Kargarian, J. Mohammadi, J. Guo, S. Chakrabarti, M. Barati, G. Hug, S. Kar, and R. Baldick, "Toward distributed/decentralized DC optimal power flow implementation in future electric power systems," *IEEE Transactions on Smart Grid*, vol. 9, no. 4, pp. 2574–2594, 2016.

[2] J. Mohammadi, G. Hug, and S. Kar, "Role of communication on the convergence rate of fully distributed DC optimal power flow," in *2014 IEEE International Conference on Smart Grid Communications (SmartGridComm)*. IEEE, 2014, pp. 43–48.

[3] ——, "Fully distributed DC-OPF approach for power flow control," in *2015 IEEE Power & Energy Society General Meeting*. IEEE, 2015, pp. 1–5.

[4] Y. Wang, L. Wu, and S. Wang, "A fully-decentralized consensus-based ADMM approach for DC-OPF with demand response," *IEEE Transactions on Smart Grid*, vol. 8, no. 6, pp. 2637–2647, 2016.

[5] Q. Zhang and M. Sahraei-Ardakani, "Distributed dcopf with flexible transmission," *Electric Power Systems Research*, vol. 154, pp. 37–47, 2018.

[6] Y. Xiao, Y. Song, C.-C. Liu, and Y. Sun, "Available transfer capability enhancement using FACTS devices," *IEEE transactions on power systems*, vol. 18, no. 1, pp. 305–312, 2003.

[7] X. Rui, M. Sahraei-Ardakani, and T. R. Nudell, "Linear modelling of series FACTS devices in power system operation models," *IET Generation, Transmission & Distribution*, vol. 16, no. 6, pp. 1047–1063, 2022.

[8] J. Guo, M. L. Crow, and J. Sarangapani, "An improved upfc control for oscillation damping," *IEEE transactions on power systems*, vol. 24, no. 1, pp. 288–296, 2009.

[9] H. Cai, L. Yang, H. Wang, P. Song, and Z. Xu, "Application of unified power flow controller (UPFC) in Jiangsu power system," in *2017 IEEE Power & Energy Society General Meeting*. IEEE, 2017, pp. 1–5.

[10] Smart Wires Inc., "SmartValve™," 2022, accessed: 2022-07-10. [Online]. Available: https://www.smartwires.com/smartvalve/

[11] L. Yang, J. Luo, Y. Xu, Z. Zhang, and Z. Dong, "A distributed dual consensus ADMM based on partition for DC-DOPF with carbon emission trading," *IEEE Transactions on Industrial Informatics*, vol. 16, no. 3, pp. 1858–1872, 2019.

[12] S. Boyd, N. Parikh, E. Chu, B. Peleato, J. Eckstein *et al.*, "Distributed optimization and statistical learning via the alternating direction method of multipliers," *Foundations and Trends® in Machine learning*, vol. 3, no. 1, pp. 1–122, 2011.

[13] T. Erseghe, "Distributed optimal power flow using ADMM," *IEEE transactions on power systems*, vol. 29, no. 5, pp. 2370–2380, 2014.

[14] B. Stott, J. Jardim, and O. Alsaç, "Dc power flow revisited," *IEEE Transactions on Power Systems*, vol. 24, no. 3, pp. 1290–1300, 2009.

[15] J. Xu, H. Sun, and C. J. Dent, "ADMM-based distributed opf problem meets stochastic communication delay," *IEEE Transactions on Smart Grid*, vol. 10, no. 5, pp. 5046–5056, 2018.

[16] A. Mohammadi and A. Kargarian, "Learning-aided asynchronous admm for optimal power flow," *IEEE Transactions on Power Systems*, vol. 37, no. 3, pp. 1671–1681, 2021.

[17] E. Liu and P. Cheng, "Mitigating cyber privacy leakage for distributed DC optimal power flow in smart grid with radial topology," *IEEE Access*, vol. 6, pp. 79 181–7920, 2018.

[18] S. Galvani, B. Mohammadi-Ivatloo, M. Nazari-Heris, and S. Rezaeian-Marjani, "Optimal allocation of static synchronous series compensator (SSSC) in wind-integrated power system considering predictability," *Electric Power Systems Research*, vol. 191, p. 106871, 2021.

[19] X.-P. Zhang, C. Rehtanz, and B. Pal, *Flexible AC transmission systems: modelling and control*. Springer Science & Business Media, 2012.

[20] D. Sen and P. Acharjee, "Optimal line flows based on voltage profile, power loss, cost and conductor temperature using coordinated controlled upfc," *IET Generation, Transmission & Distribution*, vol. 13, no. 7, pp. 1132–1144, 2019.

[21] M. Sahraei-Ardakani and K. W. Hedman, "Computationally efficient adjustment of FACTS set points in DC optimal power flow with shift factor structure," *IEEE Transactions on Power Systems*, vol. 32, no. 3, pp. 1733–1740, 2016.

[22] M. Ma, L. Fan, and Z. Miao, "Consensus ADMM and proximal ADMM for economic dispatch and AC OPF with SOCP relaxation," in *2016 North American power symposium (NAPS)*. IEEE, 2016, pp. 1–6.

[23] Smart Wires Inc., "SmartValve™ 10-1800 v1.04," 2021, accessed: 2022-07-15. [Online]. Available: https://www.smartwires.com/download/20801/

[24] Department of Electrical Engneering, Unviersity of Washington. Power systems test case archive. [Online]. Available: https://labs.ece.uw.edu/pstca/pf118/pg_tca118bus.htm

[25] S. Blumsack, *Network topologies and transmission investment under electric-industry restructuring*. Carnegie Mellon University, 2006.

CHAPTER 6

IMPACT OF GET OPERATIONS ON THE RISK-LEVEL IN STOCHASTIC UNIT COMMITMENT

This chapter presents a risk-averse two-stage SUC model that integrates transmission system flexibilities provided by GETs. The proposed SUC model is utilized to study the impact of GET operations on the risk level in the day-ahead SUC. Numerical studies are conducted on a 6-bus system and a modified IEEE 24-bus system, with results showing that, while GETs effectively reduce the total cost, they can lead to undesirable high levels of unserved demand under extreme scenarios without risks-averse measures. Additionally, with risk management, the high-level load-shedding issue is effectively addressed by considering the conditional value at risk (CVaR).

6.1 Introduction

The penetration of renewable energy sources (RES) in the power grid is growing worldwide. The capacity of renewable generation increased by 9.6%, accounting for 83% of the total new generation capacity in 2022 [22]. The variable and intermittent nature of RES adds uncertainties to power system operation. The stochastic unit commitment (SUC) model is widely proposed to manage RES uncertainties using scenarios with different probabilities to represent renewable generation. SUC is a less conservative approach than its alternatives, such as robust optimization, as it engages an objective function of expectation minimization. Therefore, costly load-shedding events can occur under extreme scenarios with very low probabilities. Conditional value-at-risk (CVaR), widely used in financial risk management, has been integrated into power system operation models to manage potential load-shedding occasions. CVaR constraints are integrated into the two-stage SUC model presented in [20], which includes non-generation resources such as energy storage systems (ESS) and demand response (DR) programs. Ref. [2] utilizes CVaR to manage

risk in SUC decisions for isolated systems with high RES penetration. A risk-averse SUC model is presented in [43], which uses CVaR to manage loss-of-load risks under extreme scenarios. In [25], CVaR constraints are included in the SUC model for large-scale energy systems, considering day-ahead and intra-day electricity markets. A two-stage SUC model with weekly dispatched energy storage facilities is formulated in [5], which uses CVaR as the risk management method.

Transmission bottlenecks in the existing grid hinder the utilization of RES. Alleviating congestion and facilitating RES integration require upgrades to the transmission system. Adopting GETs that improve the utilization of the existing power grid is regarded as a vital approach to enhancing the available transfer capability (ATC). GETs include power flow control, DLR, and topology control. Power flow control can be accomplished by using FACTS devices, which are power electronic devices that can adjust the parameters of transmission lines. In addition, TS, which allows control of the breakers to open/close transmission lines [15], is utilized for topology control. GET operations have been integrated into SUC models to study the effectiveness in cost reduction and alleviating RES curtailment [35, 36, 28, 39]. The results are promising regarding enhancing transmission-side flexibility to facilitate the utilization of RES. Risk-averse constraints are also integrated into the SUC models, which include operations of GETs.

Studies on the impacts of GET operations on risk levels are relatively limited. The impact of FACTS devices on system risk in a deregulated market is studied in [6]. Reference [7] proposes a system risk curtailing method, which optimizes FACTS and wind farm placement in deregulated market environments to minimize risk. A CVaR-constrained optimal power flow (OPF) model is proposed in [41]. However, both studies use the more computationally demanding AC power flow constraints. As stochastic optimization is a widely used approach for power system operation under RES uncertainties, studies on GET operations in a CVaR-constrained two-stage SUC model are desirable. Moreover, the existing literature does not identify the potential impacts of GETs on risk, which is essential for the adoption of SUC solutions. This chapter shows that as more RES becomes accessible due to reduced congestion, especially under scenarios where renewable generation output is relatively abundant, the SUC solution includes fewer committed conventional generators. This may lead to load shedding under extreme scenarios where renewable generation

suddenly drops. However, since these scenarios occur at very low probabilities, overall cost savings are still achieved thanks to improved flexibility in the transmission system.

This chapter bridges the research gap by studying the impacts of various types of GETs on risk levels caused by RES integration. The contributions of this chapter are summarized as follows:

1. A SUC problem that incorporates CVaR constraints and GETs operations is formulated using the injection shift factors (ISFs); the formulated SUC model is then studied with two test systems where congestion is caused by RES penetration;

2. The potential for GET operation to increase the risk levels in SUC is discussed, emphasizing the necessity of risk management when co-optimizing GET set points in SUC models. The results that suggest a thorough analysis of the system is essential when planning GETs to fully harness their benefits.

The rest of this chapter is organized as follows. Problem formulation of the two-stage SUC model with GET operation constraints is presented in Section 6.2. Section 6.2 also shows the scenario generation and reduction methods for wind generation. Numerical studies are shown in Section 6.3. Finally, Section 6.4 presents the conclusions.

6.2 Methodology

To study the impact of GETs on the risk level, CVaR constraints and GET operating limits are integrated into the SUC model. The problem is formulated with DC power flow constraints using ISFs. Modeling techniques proposed by previous research [30, 31, 33] allow FACTS and TS to be represented by nodal power injections, thus enabling smooth integration into the ISF-based power system operation models. Prominent voltage source converter-based FACTS devices such as the static synchronous series compensator (SSSC) and the unified power flow controller (UPFC) are to study the effect of FACTS deployments as their modeling keeps the linearity of DC power flow without introducing extra binary variables [30]. As mentioned, time series scenarios are used to model uncertainty in the SUC models. Details about the scenario generation methods are presented later in this section.

6.2.1 Problem Formulation

The CVaR terms are added following the convention of [2]. The SUC model is first partially presented, excluding the constraints on GET operation, as follows:

$$\begin{aligned}&\min \beta\mathcal{CV} + (1-\beta)(\sum_{g\in G}\sum_{t\in T}(c_g^{\min}u_{gt} + c_g^{\mathrm{SU}}v_{gt} + c_g^{\mathrm{SD}}z_{gt} + \sum_{s\in S}\sum_{q\le Seg}\pi_s c_g^q p_{gts}^q)\\&+\sum_{s\in S}\sum_{n\in N}\sum_{t\in T}\pi_s c^{\mathrm{ls}} l_{nts}^{\mathrm{sh}})\end{aligned} \tag{6.1}$$

s.t.

$$\mathcal{CV} = \mathcal{V} + \frac{1}{1-\eta}\sum_{s\in S}\pi_s\zeta_s \tag{6.2}$$

$$\zeta_s \ge c_g^{\min}u_{gt} + c_g^{\mathrm{SU}}v_{gt} + c_g^{\mathrm{SD}}z_{gt} + \sum_{q\le Seg} c_g^q p_{gts}^q - \mathcal{V}, s\in S \tag{6.3}$$

$$\zeta_s \ge 0, s\in S \tag{6.4}$$

$$p_{gts} = u_{gt}\underline{p}_g + \sum_{q\le Seg} p_{gts}^q, g\in G, t\in T, s\in S \tag{6.5}$$

$$0 \le p_{gts}^q \le u_{gt}p_g^{q,\max}, q\le Seg, g\in G, t\in T, s\in S \tag{6.6}$$

$$0 \le p_{wts}^{\mathrm{wind}} \le \overline{W}_{wts}, w\in W, t\in T \tag{6.7}$$

$$-\overline{f}_k \le f_{kts} \le \overline{f}_k, k\in K, k\notin \tilde{K}\cup K^{\mathrm{DLR}}, t\in T, s\in S \tag{6.8}$$

$$\begin{aligned}f_{kts} = &\sum_{n\in N}\Phi_k^n(\sum_{g\in G(n)} p_{gts} + l_{nts}^{\mathrm{sh}} + \sum_{w\in W(n)} p_{wts} - d_{nt}\\&+\sum_{k\in\delta^+(n)\cap\tilde{K}}\Delta f_k - \sum_{k\in\delta^-(n)\cap\tilde{K}}\Delta f_k)\end{aligned} \tag{6.9}$$

$$\sum_{g\in G} p_{gts} + \sum_{w\in W} p_{wts}^{\mathrm{wind}} + \sum_{n\in N} l_{nts}^{\mathrm{sh}} = \sum_{n\in N} d_{nt}, t\in T, s\in S \tag{6.10}$$

$$-u_{g,t+1}RD_g - z_{gt}RD_g^{\mathrm{SD}} \le p_{g,t+1,s} - p_{gts} \le -u_{g,t+1}RU_g + v_{gt}RU_g^{\mathrm{SU}}, g\in G, t\in T \tag{6.11}$$

$$\sum_{r=t-UT_g+1}^{t} v_{gr} \le u_{gt}, g\in G, t\ge UT_g, \tag{6.12}$$

$$\sum_{r=t+1}^{t+DT_g} z_{gr} \le 1-u_{gt}, g\in G, t\ge DT_g, \tag{6.13}$$

$$0 \le v_{gt} \le 1, g\in G, t\in T, \tag{6.14}$$

$$0 \le z_{gt} \le 1, g\in G, t\in T, \tag{6.15}$$

$$u_{gt} - u_{g,t-1} = v_{gt} - z_{gt}, g\in G, t\in T \tag{6.16}$$

$$u_{gt}\in\{0,1\}, g\in G, t\in T. \tag{6.17}$$

The formulation presents a two-stage CVaR-based SUC framework. Details about notations and symbols are shown in Appendix B. First-stage decisions involve the com-

mitment, start-up, and shut-down status of conventional generators. Second-stage variables include generator outputs, nodal load shedding, and power flows. Due to the fast-response features of GETs, their operations are also modeled as second-stage variables. The objective function (6.1) minimizes the summation of CVaR $\mathcal{CV}$ and total expected cost (EC), with π_s denoting the probability of scenario s. Parameter β controls the level of risk management in the objective function. The first part of EC is the summation of no-load cost, start-up cost, shut-down cost, and production cost of generators. The second part is the load-shedding cost. Calculation of CVaR is shown in (6.2) with $\mathcal{V}$ denoting the value-at-risk (VaR). Constraints on the auxiliary variable ζ_s are shown in (6.3) and (6.4). Eqn. (6.5) specifies the total output of generators considering a linearized function with Seg segments and q denoting the index for each segment. The maximum active power output constraint of each segment is shown in (6.6), with p^q_{gts} denoting generator outputs in segment q. The constraints on wind farm outputs are presented in (6.7). Thermal capacity constraints for lines not equipped with GETs are shown in (6.8). The (partial) power flow is calculated using the ISF and nodal power injections, as shown in (6.9). System-wide power balance constraints are formulated as (6.10). Generator ramping constraints are shown in (6.11). The minimum up and down time constraints of generators are shown in (6.12) and (6.13). Both start-up and shut-down variables of a generator are modeled as continuous as they will converge to the limits shown in (6.14) and (6.15) in the solution. Generator commitment variables are binary as specified in (6.17).

6.2.2 FACTS Operating Constraints

The constraints on the FACTS nodal injection are shown as follows [30]:

$$-V_k^{\max}|b_k| \leq \Delta f_{kts} \leq V_k^{\max}|b_k|, k \in \tilde{K}, t \in T, s \in S \tag{6.18}$$

Note that for lines equipped with FACTS, the flow in (6.9) is only partial, and the thermal capacity constraints are formulated as follows:

$$-\overline{f}_k \leq f_{kts} + \Delta f_k \leq \overline{f}_k, k \in \tilde{K}, t \in T, s \in S. \tag{6.19}$$

6.2.3 TS Constraints

The ISF-based constraints on TS [31] are formulated as follows:

$$-M(1-y_{kts}) \leq \Delta f_{kts} \leq M(1-y_{kts}).k \in \tilde{K}, t \in T, s \in S \tag{6.20}$$

$$-y_{kts}\overline{f}_k \leq f_{kts} + \Delta f_{kts} \leq y_{kts}\overline{f}_k, k \in \tilde{K}, t \in T, s \in S, \tag{6.21}$$

where binary variable y_{kts} taking the value of 0 and 1 represents the open and closed statuses of line k, respectively.

6.2.4 DLR Constraints

The implementation of DLR requires detailed weather data, as the rating is affected by wind speed, wind direction, solar radiation, and ambient temperature [21]. In this chapter, a simplified method is adopted to model DLR. Lines with DLR implementation can increase their thermal capacities when the available wind energy is above a certain level, as a higher wind generation output means higher wind speed. The DLR settings are presented as follows:

$$\delta_{kts} = 1.05, k \in K^{\text{DLR}}, t \in T, s \in s, 250 \leq W_{ts} \leq 500, \tag{6.22}$$

$$\delta_{kts} = 1.25, t \in T, s \in S, k \in K^{\text{DLR}}, W_{ts} \geq 500. \tag{6.23}$$

The thermal capacity constraints are, thus, formulated as follows:

$$-\delta_{kts}\overline{f}_k \leq f_{kts} \leq \delta_{kts}\overline{f}_k, t \in T, s \in S, k \in K^{\text{DLR}}. \tag{6.24}$$

6.2.5 Scenario Generation and Reduction

For SUC models, scenarios are time series of the RES generation created to represent future uncertainties. Various methodologies to generate RES scenarios, including ARMA-based methods, have been used in the existing literature. The scenarios of available wind power production are generated using the *mape_maker* [16]. Scenarios are generated using the wind power data in the RTS-GMLC system [4]. A set of 2000 scenarios are generated initially to model the uncertainties. Larger sets of scenarios are more accurate in reflecting future uncertainties. However, they will lead to paramount computational complexity. Therefore, the fast-forward scenario reduction technique [19] is applied to reduce the set to contain 30 scenarios, which are employed in simulation studies.

Note that available wind generation in the scenarios can be immense for the scale of the test systems in Section 6.3. Therefore, multipliers are applied for the wind generators added to the systems.

6.3 Numerical Studies

Numerical case studies are conducted on two test systems, with details presented later in this section. Optimization problems are solved using CPLEX 22.10 on an Apple M2 Pro CPU with 16 GB of RAM. The optimality gap is set at 0.1% and is increased to 0.5% for the SUC model considering topology control in the 24-bus system due to higher computational complexity.

6.3.1 6-bus System

The 6-bus system data is taken from [40] and is modified in this chapter to change the congestion pattern. Demands on B2 and B3 are increased to 350 MW and 250 MW, respectively. Wind farms are added on buses B2 and B6, with their output being the scenarios multiplied by factors of 0.2 and 0.1, respectively. As mentioned previously, such factors are applied to make wind output comparable to conventional generation and demand in the system. Furthermore, a new generator, G4, is added at bus B3, with detailed parameters presented in Table 6.1. The thermal capacities of lines L2 and L5 are adjusted to 250 MW and 120 MW, respectively, to accommodate load changes and added wind generation. The cost of load shedding is set as \$5000/MW, and the confidence level for CVaR is 98%.

Four cases are studied to understand the impact of GETs on the risk level, each involving deploying one type of GET. Details of the GET implementations of each case are shown as follows:

- Case 0: no GETs;
- Case 1: FACTS devices are installed on transmission lines L4 and L5, each with a maximum magnitude of 0.1 pu for voltage injection.
- Case 2: Line L4 is switchable.
- Case 3: DLR is implemented on lines L2 and L4.

Simulation studies are first conducted with $\beta = 1^{-5}$, equivalent to solving risk-neutral SUC models. The results are presented in Figure 6.1. It can be seen that implementing each of the technologies leads to overall cost savings. However, GETs cause higher CVaR values.

The potential load-shedding events under each case, shown as follows, can also reflect the results of increased risk levels:

- Case 0: no load shedding under any scenario;
- Case 1: 1.45 MW, 10.17 MW, 29.85 MW, 8.99 MW load shed under scenarios 4, 5, 17, 25, respectively;
- Case 2: 20.67 MW load shed under scenario 17;
- Case 3: 6.25 MW, 16.25 MW, 1.76 MW, 14.85 MW, 2.57 MW load shed under scenarios 4, 5, 6, 17, 25, respectively.

The increased load shedding with implementing GETs is because of a less conservative first-stage solution. GET operation allows fewer conventional unit commitments as it enhances the utilization of wind generation, especially under scenarios with abundant wind resources and not in the tail end of the probability distribution of scenarios. This can be observed in the 6-bus system with the variation of schedules of generating unit G4 in each case, as shown in Table 6.2 where 0 and 1 represent the on and off statuses, respectively. Unit G4 commits in fewer periods with each type of GET deployment, thus leading to increased load shedding under extreme scenarios.

Furthermore, the risk-averse SUC with GETs is studied by setting the value of β to 0.1. The focus of the objective function now shifts towards CVaR minimization compared with the risk-neutral case. The EC and CVaR results of the four cases are presented in Fig 6.2. The results compared with the risk-neutral ones presented in Fig. 6.1 show that the risk control measure leads to increased EC, but only slightly. GET operations result in reduced EC and CVaR. Additionally, the risk-averse measure effectively eliminated all load-shedding events in any of the four cases.

The effectiveness of GETs in increasing RES penetration is demonstrated by the expected wind spillage (EWS) and expected wind spillage percentage (EWSP) shown in Tables 6.3 and 6.4. EWS and EWSP are calculated as follows:

$$EWS = \sum_{w \in W, t \in T, s \in S} \pi_s (\overline{W}_{wts} - p^{\text{wind}}_{wts}), \tag{6.25}$$

$$EWSP = \frac{EWS}{\sum_{w \in W, t \in T, s \in S} \pi_s \overline{W}_{wts}}. \tag{6.26}$$

Overall, the results show that GETs effectively enhance the utilization of RES based on the smaller EWSP and EWS values for cases involving GET deployments. GET operations still lead to higher wind generation utilization when β is set to 0.1. However, the risk-averse measure effectively controls the load-shedding events and reduces CVaR. It is worth noting that, due to the limited ramping capabilities of the conventional generators in the 6-bus system, a slightly lower EWS is shown in Table 6.4 compared to the results in Table 6.3, even though a higher EC is achieved with the risk control measure.

6.3.2 Modified IEEE 24-bus System

The IEEE 24-bus system [17] is employed in this chapter following the convention in [20]. The generation data from [26] is applied, while all other system data is from an updated version [27] of the IEEE 24-bus system. Shut-down costs of generators 1, 2, and 7 are changed to \$34. The minimum-up time of these generators is also changed to 2 as we are not considering fast start units in this study. The system is further modified by first increasing every load by 5%. Wind generation, rescaled by a factor of 0.3, is added at buses 11, 17, and 22. The thermal capacities of transmission lines 7, 16, and 27 are reduced to 175 MW, 175 MW, and 220 MW, respectively. The GET deployments are specified again in four cases:

- Case 0: no GET;
- Case 1: FACTS devices are installed on transmission lines 7, 16, and 27, each with a maximum magnitude of 0.1 pu for voltage injection.
- Case 2: line 33 is switchable.
- Case 3: DLR is implemented on lines 7, 16, and 27.

The CVaR and EC results are presented in Figure 6.3, showing that GET deployments lead to higher CVaR values while achieving cost reduction. Studies with risk-averse measures are again conducted with $\beta = 0.1$. The results are presented in Fig. 6.4, which again shows the effectiveness of the CVaR constraints in risk control.

The wind spillage results are shown in Tables 6.5 and 6.6. The smaller EWSP and EWS results in Cases 1, 2, and 3 show that, similar to the conclusion from the results for

the 6-bus system, GET operations help increase RES penetration. Comparison between Tables 6.5 and 6.6 show mixed results. A slight decrease in EWS can be seen for Case 2 with risk control measures, while other cases show increases in wind curtailment. Overall, the curtailment results for the 2 test systems reveal that a smaller EC is not necessarily correlated with higher RES utilization.

6.3.3 Discussion

The numerical results in this chapter reveal the potential effect of GET operation in increasing the risk level of SUC models. Certain key points can be implied by the results in this chapter, which are listed as follows.

- The deployment of GET is an effective method for *cost reduction*. However, it is subject to how the objective functions of power system operation models are formulated. This chapter reveals that when the emphasis of the objective shifts to CVaR optimization, GETs can be effective in risk management. Yet, negative impacts can occur when minimizing the total EC is the objective. Similar results are also presented in previous research regarding GET operations and emission reduction [24], which shows that GET can lead to increased carbon emissions while still achieving overall cost reduction.

- Risk-aversion measures increase the EC and overall RES utilization, again emphasizing the trade-off between cost reduction and reliability. The results from this chapter show that the increase in EC caused by CVaR regulation is minimal.

- This congestion pattern in simulation studies aligns with the observation in previous research that RES integration leads to increased congestion. However, the impact of GET implementations is subject to multiple factors, which include transmission system topology, congestion patterns, GET placements, RES locations, etc. Therefore, the results can differ regarding the effectiveness of GET operations under different circumstances. Thus, thorough planning processes and, potentially, regulation enforcement are vital for utilizing GETs.

6.4 Conclusion

This chapter discusses the impact of GETs on the risk level in SUC models. A CVaR-based SUC model is formulated with the injection shift factors and various types of GETs, each integrated into the model. Numerical studies reveal that GET operations can lead to increased risk levels in SUC without proper risk management measures while still providing savings in the total expected cost. Such an impact emphasizes the importance of risk management under high RES penetration. The results in this chapter can provide a valuable reference for system operators and industrial entities involved in the operations and planning processes of GETs.

Table 6.1. Parameters of G4

$\overline{p}$	$\underline{p}$	c^{SU}	c^{SD}	$\overline{p}^1$	$\overline{p}^2$	$\overline{p}^3$	RU	RD	RU^{SU}	RD^{SD}	c^1	c^2	c^3	$c^{\min}$
20	100	373.83	0	20	20	40	80	80	80	80	11.78	12.15	12.71	1349.63

Table 6.2. Unit commitment results of G4, $\beta = 1^{-5}$ (risk-neutral)

Case	**Hours 1-24**
0	0 0 0 0 0 0 0 0 1 1 1 1 1 1 1 1 1 1 1 1 1 0 0
1	0 0 0 0 0 0 0 0 0 0 0 1 1 1 0 0 1 1 1 1 1 1 0 0 0
2	0 0 0 0 0 0 0 0 0 0 0 0 0 0 0 0 0 0 0 1 1 0 0 0 0 0
3	0 0 0 0 0 0 0 0 0 0 0 1 1 1 1 1 1 1 1 1 1 1 1 0 0

Table 6.3. Wind spillage in the 6-bus system, $\beta = 1^{-5}$ (risk-neutral)

Case	**EWSP (%)**	**EWS (MW)**
0	26.09	2103.50
1	24.14	1933.49
2	25.43	2026.13
3	24.19	1941.33

Table 6.4. Wind spillage in the 6-bus system, $\beta = 0.1$ (risk-averse)

Case	EWSP (%)	EWS (MW)
0	26.09	2103.50
1	23.69	1912.03
2	24.54	1957.54
3	23.81	1923.84

Table 6.5. Wind spillage in the 24-bus system, $\beta = 1^{-5}$ (risk-neutral)

Case	EWSP (%)	EWS (MW)
0	16.31	4101.56
1	12.99	3258.01
2	13.84	3489.64
3	12.37	3113.99

Table 6.6. Wind spillage in the 24-bus system, $\beta = 0.1$ (risk-averse)

Case	EWSP (%)	EWS (MW)
0	16.85	4235.37
1	12.94	3252.37
2	13.84	3490.34
3	12.55	3168.65

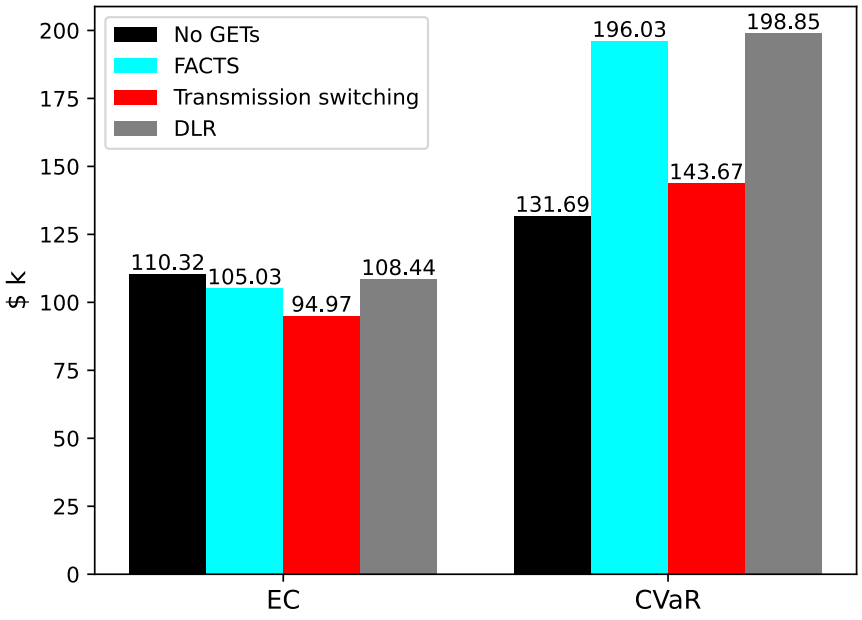

Figure 6.1. Comparison of EC and CVaR for the 6-bus system with the risk-neutral SUC ($\beta = 1^{-5}$)

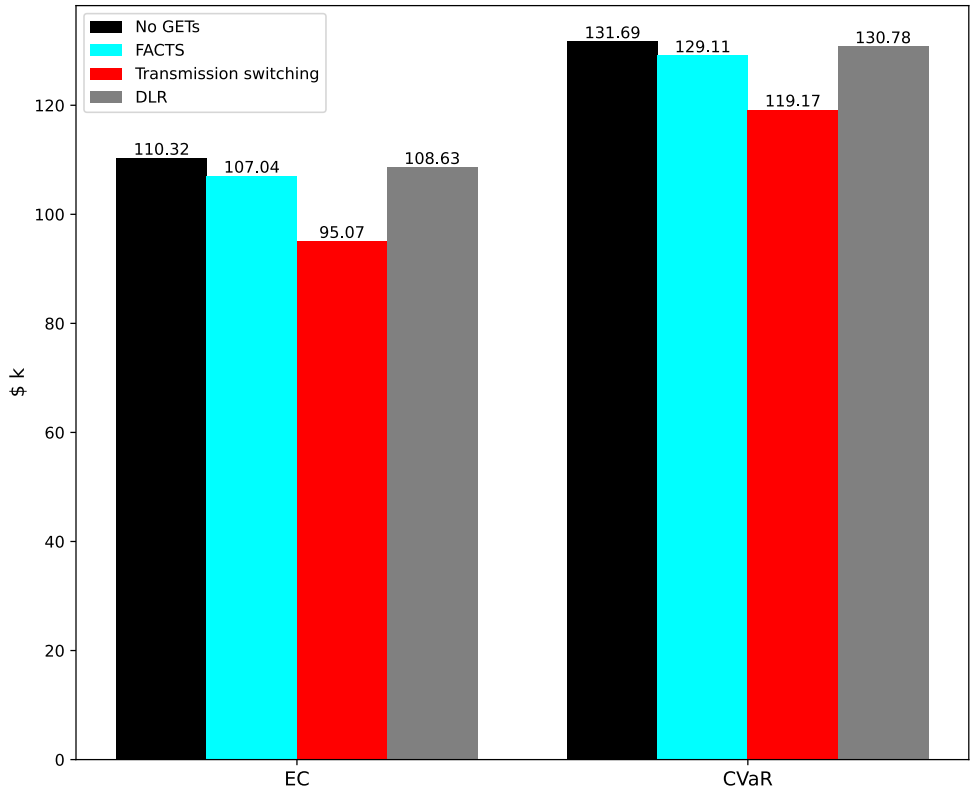

Figure 6.2. Comparison of EC and CVaR for the 6-bus system with the risk-averse SUC ($\beta = 0.1$)

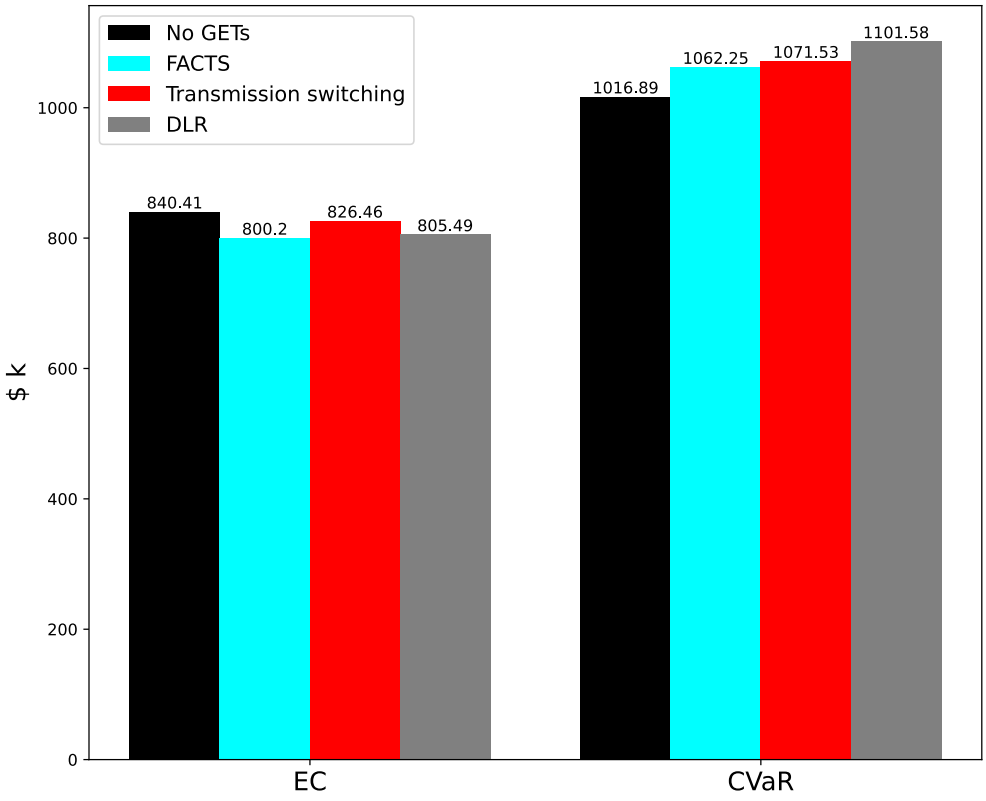

Figure 6.3. Comparison of EC and CVaR for the 24-bus system with the risk-neutral SUC ($\beta = 1^{-5}$)

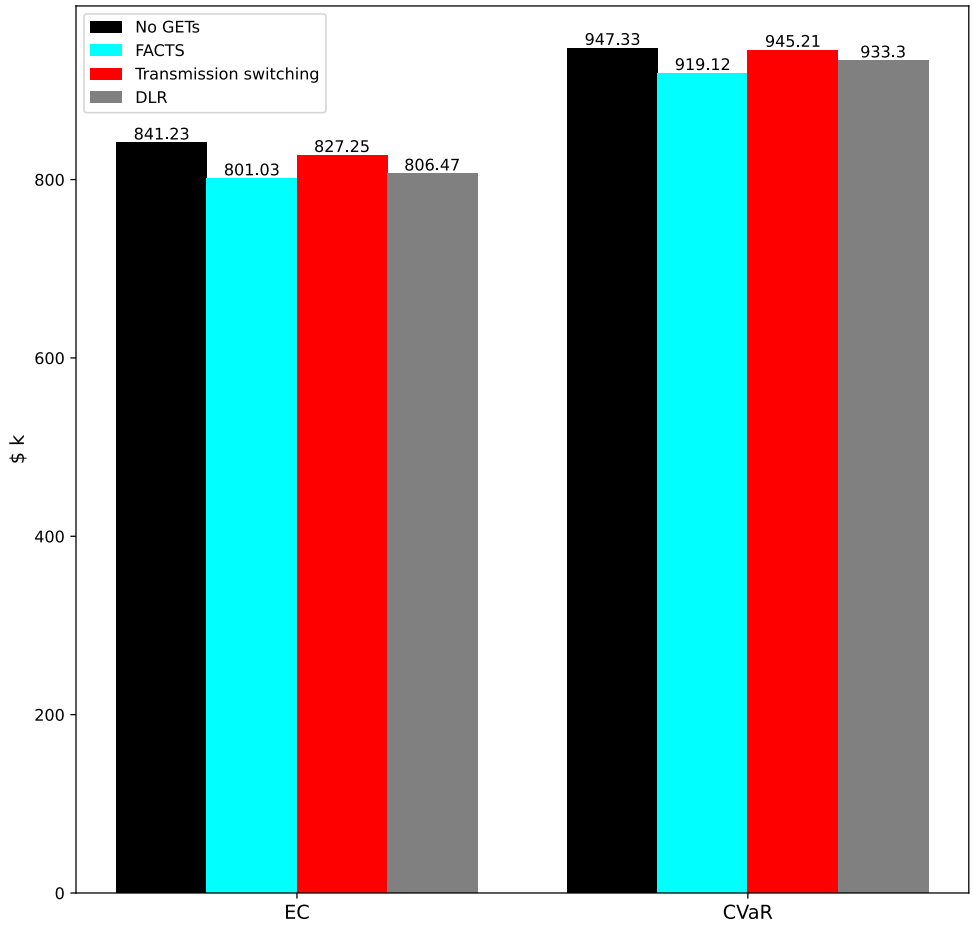

Figure 6.4. Comparison of EC and CVaR for the 24-bus system with the risk-averse SUC ($\beta = 0.1$)

CHAPTER 7

A SENSITIVITY-BASED METHOD FOR OPTIMAL PLACEMENT OF FACTS DEVICES

FACTS devices enable power flow control and improve the transfer capability over the existing power grid. Therefore, they can play a vital role in the future power grid in alleviating congestion and accommodating the growing penetration of RES. The effectiveness of FACTS deployment is highly dependent upon the placement of these devices in the power system. Optimizing the location of FACTS devices is a rather challenging problem. This chapter presents a fast and effective solution for the FACTS placement problem through a sensitivity-based method. The proposed method uses shadow prices from DC power flow to create ranking metrics for potential FACTS locations in the transmission system. The effectiveness of the proposed method is tested with simulation studies conducted on modified RTS-96 and IEEE 300-bus test systems. The results show that the sensitivity-based method can provide the most effective FACTS deployment locations for reducing dispatch costs.

7.1 Introduction

Effective utilization of FACTS technology highly depends on the location. Therefore, determining the optimal placement of FACTS devices in the transmission system is essential. FACTS allocation belongs to the family of expansion planning models that are computationally burdensome [8]. An effective approach to facilitate the optimal allocation of FACTS is to create an index list or ranking of transmission lines, providing favorable candidates for FACTS deployments. The solution space is, thus, effectively reduced after applying such methods [7], providing top candidates for more detailed analyses [42]. Depending on the purpose of FACTS deployments, the ranking of candidate locations has been developed by previous research based on various metrics or variables. For example, line outage sensitivity factors, locational marginal price (LMP) differences, and conges-

tion rent contributions are used in previous studies [18, 1] for optimal placement of the thyristor-controlled series compensator (TCSC). Sensitivity-based methods have also been developed for FACTS devices that are based on voltage source converters (VSC), such as the static synchronous series compensator (SSSC). The sensitivities are derived in previous studies [14, 12, 23] for SSSC operation based on various system performances, including bus voltages, line flow changes, line loadings, power losses, and load increases.

The existing literature, however, lacks a sensitivity-based placement method for prominent VSC-based FACTS devices that directly links total dispatch cost to the setpoint adjustments. A key application of FACTS is reducing overall generation dispatch costs via power flow control. This is especially essential for transfer capability enhancement, which helps improve the utilization of the growing renewable energy sources in the power grid. However, the methods in the existing literature mainly do not provide ranking metrics that reflect the effectiveness of FACTS operation in this vital aspect. Such sensitivities have been developed for FACTS that directly alter line reactance, such as the TCSC [42], but are lacking for devices such as the SSSC and the unified power flow controller (UPFC). These are prominent VSC-based devices for power flow control, with different operating principles for reactance adjustments and modeling in power system optimization problems compared to the TCSC. They provide various advantages and have been deployed for congestion alleviation purposes [13, 29]. Examples in the industry include the UPFC PLUS [37] by Siemens and the SmartValve by Smart Wires Inc. [38], with the latter having a modular design that allows extra operation flexibility through easier relocations. Therefore, it is essential to have a sensitivity-based allocation method for the VSC-based FACTS to enhance their utilization.

To fill such research gaps, this chapter contributes to the literature by presenting a simple, fast, and effective sensitivity-based placement method for prominent VSC-based FACTS devices such as the SSSC and the UPFC. This method utilizes the DC power flow modeling of such devices and computes the sensitivity of total dispatch cost to the FACTS setpoints. The sensitivities are employed to develop ranking metrics for FACTS deployment locations, providing the basis for the proposed method. The method presented in this chapter provides the following benefits and advantages.

1. The proposed method can facilitate planning for VSC-based FACTS for congestion

alleviation and cost reduction purposes, leading to improved utilization of the existing grid.

2. The proposed method is based on DC power flow, a linearized model of the more complicated AC power flow models. It provides better computational efficiency and is widely used in market-clearing software tools.

3. Derivation of the sensitivities utilizes the shadow prices from the dual solution of DCOPF, which are available from past data. They can be directly used without a need to change the operation software or strategies.

4. The DCOPF formulation based on ISFs provides better scalability than the $b - \theta$ formulation [34].

The remainder of this chapter is organized as follows. First, the derivation of sensitivities and the proposed method are presented in detail in Secion 7.2. Then, numerical studies, including both setup and results, are shown in Section 7.3, followed by a brief discussion on the scope of the proposed method. Finally, the conclusions of the Chapter are presented in Section 7.5.

7.2 Methodology

7.2.1 Sensitivities of Dispatch Cost to FACTS Setpoint Adjustment

This subsection presents the derivation of sensitivities of dispatch cost to FACTS setpoint adjustments. FACTS setpoint adjustments are regarded as perturbations to the DC power flow constraints. The impact of such perturbations can be derived using the dual variables of the DCOPF. Devices such as the SSSC and the UPFC use voltage injections to provide the function of power flow control. Therefore, the sensitivities linking cost reduction to the voltage injection can be used to evaluate the effectiveness of such devices, which provide the basis for the proposed optimal FACTS placement method.

The ISF-based DCOPF problem is formulated as follows:

$$(\mathbf{P1}:) \text{ minimize } TC = \sum_{s=1}^{\bar{s}} \mathbf{c}_s^{\mathrm{T}} \mathbf{p}_s \tag{7.1}$$

s.t.

$$\sum_{s=1}^{\bar{s}} \mathbf{p}_s = \mathbf{p}, \qquad (\boldsymbol{\alpha}) \tag{7.2}$$

$$\mathbf{f} = \boldsymbol{\Phi}(\mathcal{G}\mathbf{p} - \mathbf{d}), \qquad (\sigma) \tag{7.3}$$

$$-\mathbf{f}^{\max} \leq \mathbf{f} \leq \mathbf{f}^{\max}, \qquad (\boldsymbol{\beta}_-, \boldsymbol{\beta}_+) \tag{7.4}$$

$$\mathbf{0} \leq \mathbf{p}_s \leq \mathbf{p}_s^{\max}, 1 \leq s \leq \bar{s}, \qquad (\boldsymbol{\gamma}_s) \tag{7.5}$$

$$\mathbf{p}^{\min} \leq \mathbf{p}, \qquad (\boldsymbol{\delta}) \tag{7.6}$$

$$\mathbf{1}^{\mathrm{T}}(\mathcal{G}\mathbf{p} - \mathbf{d}) = 0. \qquad (\lambda) \tag{7.7}$$

In **P1**, the objective function (7.1) minimizes the total dispatch cost TC. The production of each generating unit is represented using $\bar{s}$ linearized segments, with $\boldsymbol{c}_s$ and $\boldsymbol{p}_s$ being the vectors of the linearized cost and production for segment s respectively. It is specified in (7.2) that the summation of productions in each segment equals the total generation of generating units $\boldsymbol{p}$. In (7.3), $\boldsymbol{f}$ is the vector of power flows and is calculated using the ISF matrix $\boldsymbol{\Phi}$ and nodal power injections. Productions of generators are projected to nodal injections using the generator location matrix $\mathcal{G}$, and $\boldsymbol{d}$ represents the loads at each node. The thermal limits of transmission elements are enforced in (7.4), with $\boldsymbol{f}^{\max}$ denoting the line capacity. The constraints on generator output are formulated in (7.5) and (7.6). The system-wide power balance constraint is shown in (7.7). The vectors of dual variables are presented in parentheses following the corresponding constraints.

FACTS operations lead to perturbations to (10.3) and (10.4), which can be presented as follows:

$$\mathbf{f} = \boldsymbol{\Phi}(\mathcal{G}\mathbf{p} - \mathbf{d} - \mathbf{A}^{\mathrm{T}}\boldsymbol{\Delta}\mathbf{f}), \qquad (\sigma) \tag{7.8}$$

$$-\mathbf{f}^{\max} \leq \mathbf{f} + \boldsymbol{\Delta}\mathbf{f} \leq \mathbf{f}^{\max}, \qquad (\boldsymbol{\beta}_-, \boldsymbol{\beta}_+) \tag{7.9}$$

where $\boldsymbol{\Delta f}$ represents the perturbations and $\boldsymbol{A}$ is the adjacency matrix. The value of the dual variables of **P1** are sensitivities of the total cost to the perturbation of the constraints. Therefore, the vector of the sensitivities of the total cost to FACTS setpoint change can be formulated as follows:

$$\boldsymbol{\zeta} = \boldsymbol{\beta}_-^* - \boldsymbol{\beta}_+^* - \mathbf{A}\boldsymbol{\Phi}^{\mathrm{T}}\sigma^*. \tag{7.10}$$

Note that * represents the optimal solution.

In addition, the following equation is formulated with the Karush–Kuhn–Tucker (KKT) conditions of **P1**:

$$\frac{\partial \mathcal{L}}{\partial \boldsymbol{f}} = (\boldsymbol{\beta}_+^* - \boldsymbol{\beta}_-^*) + \boldsymbol{\sigma}^* = \mathbf{0}, \tag{7.11}$$

where $\mathcal{L}$ is the LaGrangian function. Therefore, (7.10) can be further derived as follows:

$$\boldsymbol{\zeta} = (\mathbf{I} - \mathbf{A}\boldsymbol{\Phi}^{\mathrm{T}})(\boldsymbol{\beta}_-^* - \boldsymbol{\beta}_+^*), \tag{7.12}$$

where $\boldsymbol{I}$ is the identity matrix. It is revealed in (7.12) that the sensitivity vector is derived using the flowgate marginal prices (FMP) $\boldsymbol{\beta}_+^*$ and $\boldsymbol{\beta}_-^*$. Note that $\boldsymbol{\zeta}$ is equivalent to the susceptance prices in the $b-\theta$ DCOPF shown in [32].

VSC-based FACTS devices, as previously mentioned, use voltage injections to control power flows. Therefore, the sensitivities linking total cost reduction to FACTS voltage injection are needed. Suppose FACTS devices are installed on line k; the impact of FACTS operation is presented as follows [30]:

$$\Delta f_k = \pm V_k^{\mathrm{inj,pu}} b_k, \tag{7.13}$$

where $V_k^{\mathrm{inj,pu}}$ is the FACTS voltage injection in the per-unit (pu) value. Then, the sensitivity of the total cost to FACTS voltage injection is derived as follows:

$$-\frac{\partial TC^*}{\partial V_k^{\mathrm{inj,a}}} = -\frac{\partial TC^*}{\partial \Delta f_k}\frac{\partial \Delta f_k}{\partial V_k^{\mathrm{inj,pu}}}\frac{1}{V_k^{\mathrm{base}}} = \pm\frac{\zeta_k b_k}{V_k^{\mathrm{base}}}, \tag{7.14}$$

where $V_k^{\mathrm{inj,a}}$ is FACTS voltage injections on line k in the actual value and V_k^{base} is the base voltage level of transmission line k.

Optimal FACTS operation will lead to total cost reduction. SSSC and UPFC devices can inject voltages that can either lag or lead to the line current in phase angles, thus effectively achieving capacitive or inductive reactance adjustments. Therefore, we can use the following vector of sensitivities to determine the effectiveness of FACTS operation on each line:

$$\boldsymbol{\epsilon} = abs(\boldsymbol{b} \odot \boldsymbol{\zeta} \odot \hat{\boldsymbol{v}}), \tag{7.15}$$

where $\boldsymbol{b}$ is the vector of line susceptances, and $\hat{\boldsymbol{v}}$ is defined with each element shown as follows:

$$\hat{v}_k = \frac{1}{V_k^{\mathrm{base}}}. \tag{7.16}$$

In (7.15), $abs(\cdot)$ represents the operation of taking element-wise absolute values of a vector, and $\odot$ is the Hadamard product that takes the element-wise product of two vectors.

Transmission lines with a larger value of ϵ_k are more effective in reducing the total cost with voltage injections. Granted, $\boldsymbol{\epsilon}$ consists of sensitivity values that are more accurate with smaller perturbations. However, aggregating the sensitivities for different time periods involving different loading patterns can offset the potential inaccuracy.

7.2.2 Sensitivity-Based FACTS Placement Method and Verification

Based on the sensitivities presented in the previous subsection, the proposed optimal placement method consists of the following steps:

1. Obtain historical data and select typical time periods, e.g., weekly peak load hours;
2. Solve **P1** for each time period and obtain FMPs;
3. For each time period, calculate the sensitivity vector $\boldsymbol{\epsilon}$ using (7.15);
4. Calculate the aggregated sensitivities $\tilde{\boldsymbol{\epsilon}}$ following $\tilde{\boldsymbol{\epsilon}} = \sum_{t=1}^{T} \boldsymbol{\epsilon}_t$, with t denoting the time period;
5. Sort transmission lines based on vector $\tilde{\boldsymbol{\epsilon}}$ and report the top candidate lines with the largest values of $\tilde{\epsilon}_k$.

The aggregation allows the method to more accurately reflect the effectiveness of FACTS for the planning horizon as (7.15) provides sensitivities of single-hour operations. FACTS operations can offer more cost savings when a higher congestion level occurs. Peak load hours, thus, can be selected as representative time periods to calculate the sensitivities, as the system is heavily loaded and likely highly congested. This approach is applied in the simulations, presented in the next section. However, it is worth noting that for systems with changing loading patterns, e.g., different spatial loading in the morning and evening, the selected snapshots should represent all the essential congestion patterns.

7.3 Numerical Studies

To evaluate the effectiveness of the proposed method, it is tested on two different systems. Note that transformers are not considered for FACTS placement.

7.3.1 24-Bus System

Simulation studies are conducted using a modified RTS-96 system [17] (1 area) with 24 buses, 33 generating units, and 38 transmission elements. The system data is available at [9]. The 52 weekly peak load hours are used for calculating the sensitivities. Lines A7, A10, A25-2, and A22 have their thermal limits reduced to 200 MW, 105 MW, 300 MW, and 350 MW, respectively. Such modifications increase the congestion so that the system is more suitable for studying the impact of FACTS deployments.

An exhaustive search procedure is employed as a comparison to verify the effectiveness of the sensitivity-based method. A voltage injection is implemented at each transmission line with a maximum of 12 kV. The DCOPF problems with FACTS operation incorporated, formulated following [30], are then solved with daily peak load levels for the entire year. The transmission lines are then sorted based on the aggregated dispatch cost. Optimization problems are modeled with CVXPY [11] and solved using CPLEX 12.10.

The results are presented in Table 7.1, which show that the proposed method reports the same top 5 candidate lines as in the exhaustive search. Therefore, the results confirm the effectiveness of the sensitivity-based method.

7.3.2 300-Bus System

The proposed method is further tested using a modified IEEE 300-bus system [10]. The data is obtained from the PGlib IEEE 300-bus test case v21.07 [3]. Further modifications are made to the test system to increase congestion. Transmission elements No. 61, 101, 115, 137, 190, 349, 365, and 400 have their thermal limits reduced by 50%. Additionally, the thermal limit of elements No. 268 and 410 are reduced by 25% and 30%, respectively. The year-long load profile data from the RTS system is used for the 300-bus system.

Simulation results are shown in Table 7.2. Again, the top 20 candidate locations reported by the proposed method achieve the least production cost in the verification. The results again show that the sensitivity-based method effectively provides the top candidate locations with the highest cost savings. There exist three mismatches in the ranking. However, it is worth noting that the exhaustive search does involve substantially more time periods than when calculating the sensitivities.

7.4 Discussions

One of the critical benefits of FACTS deployment is facilitating RES integration in the power system. The simulation studies do not involve any RES integration. However, the developed method is generic and can be applied to different systems under various loading conditions. The sensitivities are based on total cost reduction, thus leading to better utilization of cheaper renewable generation if it is involved in the generation mix.

The sensitivity of one transmission line can be affected by FACTS operation in other locations. This means that accurately allocating multiple devices simultaneously may require further studies. However, the ranking can provide accurate guidance for placing one FACTS device. Moreover, the proposed method still provides a simple allocation scheme. It can serve as the basis for more complex allocation methods as it can effectively reduce the solution space, especially for larger systems.

7.5 Conclusion

This chapter presents a sensitivity-based method for the optimal placement of prominent VSC-based FACTS devices. This method provides a ranking of potential locations for FACTS deployment to reduce the dispatch cost. The ranking is based on the sensitivities calculated using the dual solution of the DCOPF. The sensitivity-based method is compared with an exhaustive search in simulation studies. The results show that the sensitivity-based method provides the most effective FACTS deployment locations for congestion alleviation. Furthermore, because the sensitivity-based method utilizes shadow prices from DCOPF, it offers substantial computational advantages and can be vital for further detailed analyses on FACTS allocation. The proposed method is an effective approach to facilitate the planning of FACTS devices to enhance the transfer capability of the power grid.

7.6 References

[1] N. Acharya and N. Mithulananthan, *Locating series FACTS devices for congestion management in deregulated electricity markets*, Electric Power Systems Research, 77 (2007), pp. 352–360.

[2] M. Asensio and J. Contreras, *Stochastic unit commitment in isolated systems with renewable penetration under CVaR assessment*, IEEE Transactions on Smart Grid, 7 (2015), pp. 1356–1367.

[3] S. Babaeinejadsarookolaee, A. Birchfield, R. D. Christie, C. Coffrin, C. DeMarco, R. Diao, M. Ferris, S. Fliscounakis, S. Greene, R. Huang, et al., *The power grid library for benchmarking AC optimal power flow algorithms*, arXiv preprint arXiv:1908.02788, (2019).

[4] C. Barrows, A. Bloom, A. Ehlen, J. Ikäheimo, J. Jorgenson, D. Krishnamurthy, J. Lau, B. McBennett, M. O'Connell, E. Preston, et al., *The ieee reliability test system: A proposed 2019 update*, IEEE Transactions on Power Systems, 35 (2019), pp. 119–127.

[5] G. E. Constante-Flores, A. J. Conejo, and R. M. Lima, *Stochastic scheduling of generating units with weekly energy storage: A hybrid decomposition approach*, International Journal of Electrical Power & Energy Systems, 145 (2023), p. 108613.

[6] A. Das, S. Dawn, S. Gope, and T. S. Ustun, *A strategy for system risk mitigation using facts devices in a wind incorporated competitive power system*, Sustainability, 14 (2022), p. 8069.

[7] S. Dawn, P. K. Tiwari, A. K. Goswami, and R. Panda, *An approach for system risk assessment and mitigation by optimal operation of wind farm and FACTS devices in a centralized competitive power market*, IEEE Transactions on Sustainable Energy, 10 (2018), pp. 1054–1065.

[8] R. A. de Araujo, S. P. Torres, J. Pissolato Filho, C. A. Castro, and D. Van Hertem, *Unified AC transmission expansion planning formulation incorporating VSC-MTDC, FACTS devices, and reactive power compensation*, Electric Power Systems Research, 216 (2023), p. 109017.

[9] Department of Electrical Engineering, University of Washington, *Power systems test case archive*.

[10] ——, *Power systems test case archive*.

[11] S. Diamond and S. Boyd, *CVXPY: A Python-embedded modeling language for convex optimization*, Journal of Machine Learning Research, (2016). To appear.

[12] N. Eghtedarpour and A. R. Seifi, *Sensitivity-based method for the effective location of sssc*, Journal of Power Electronics, 11 (2011), pp. 90–96.

[13] European Network of Transmission System Operators for Electricity (ENTSO-E), *Static Synchronous Series Compensator*. Last accessed 31 January 2024.

[14] X. Fang, J. H. Chow, X. Jiang, B. Fardanesh, E. Uzunovic, and A.-A. Edris, *Sensitivity methods in the dispatch and siting of FACTS controllers*, IEEE Transactions on Power Systems, 24 (2009), pp. 713–720.

[15] E. B. Fisher, R. P. O'Neill, and M. C. Ferris, *Optimal transmission switching*, IEEE Transactions on Power Systems, 23 (2008), pp. 1346–1355.

[16] G. Goujard, J.-P. Watson, and D. L. Woodruff, *Mape_maker: A scenario creator*, Energy Systems, (2020), pp. 1–27.

[17] C. Grigg, P. Wong, P. Albrecht, R. Allan, M. Bhavaraju, R. Billinton, Q. Chen, C. Fong, S. Haddad, S. Kuruganty, et al., *The IEEE reliability test system-1996. a report prepared by the reliability test system task force of the application of probability methods subcommittee*, IEEE Transactions on Power Systems, 14 (1999), pp. 1010–1020.

[18] H. Hashemzadeh and S. H. Hosseini, *Locating series FACTS devices using line outage sensitivity factors and particle swarm optimization for congestion management*, in 2009 IEEE Power & Energy Society General Meeting, IEEE, 2009, pp. 1–6.

[19] H. Heitsch and W. Römisch, *Scenario reduction algorithms in stochastic programming*, Computational optimization and applications, 24 (2003), pp. 187–206.

[20] Y. Huang, Q. P. Zheng, and J. Wang, *Two-stage stochastic unit commitment model including non-generation resources with conditional value-at-risk constraints*, Electric Power Systems Research, 116 (2014), pp. 427–438.

[21] International Renewable Energy Agency, *Dynamic line rating innovation landscape brief*, 2020.

[22] ——, *Record growth in renewables achieved despite energy crisis*, March 2023.

[23] D. Menniti and N. Sorrentino, *A new method for SSSC optimal location to improve power system available transfer capability*, in 2006 IEEE PES Power Systems Conference and Exposition, IEEE, 2006, pp. 938–945.

[24] O. Mirzapour, X. Rui, and M. Sahraei-Ardakani, *Transmission impedance control impacts on carbon emissions and renewable energy curtailment*, Energy, 278 (2023), p. 127741.

[25] M. Nobis, C. Schmitt, R. Schemm, and A. Schnettler, *Pan-european CVaR-constrained stochastic unit commitment in day-ahead and intraday electricity markets*, Energies, 13 (2020), p. 2339.

[26] E. Nycander, G. Morales-España, and L. Söder, *Security constrained unit commitment with continuous time-varying reserves*, Electric Power Systems Research, 199 (2021), p. 107276.

[27] C. Ordoudis, P. Pinson, J. M. Morales, and M. Zugno, *An updated version of the IEEE RTS 24-bus system for electricity market and power system operation studies*, Technical University of Denmark, 13 (2016).

[28] H. Park, Y. G. Jin, and J.-K. Park, *Stochastic security-constrained unit commitment with wind power generation based on dynamic line rating*, International Journal of Electrical Power & Energy Systems, 102 (2018), pp. 211–222.

[29] Power Engineering International, *Managing grid stability in the changing energy landscape*. Last accessed 22 January 2024.

[30] X. Rui, M. Sahraei-Ardakani, and T. R. Nudell, *Linear modelling of series FACTS devices in power system operation models*, IET Generation, Transmission & Distribution, 16 (2022), pp. 1047–1063.

[31] P. A. Ruiz, E. Goldis, A. M. Rudkevich, M. C. Caramanis, C. R. Philbrick, and J. M. Foster, *Security-constrained transmission topology control MILP formulation using sensitivity factors*, IEEE Transactions on Power Systems, 32 (2016), pp. 1597–1605.

[32] M. Sahraei-Ardakani and S. A. Blumsack, *Transfer capability improvement through market-based operation of series FACTS devices*, IEEE Transactions on Power Systems, 31 (2015), pp. 3702–3714.

[33] M. Sahraei-Ardakani and K. W. Hedman, *Day-ahead corrective adjustment of FACTS reactance: A linear programming approach*, IEEE Transactions on Power Systems, 31 (2015), pp. 2867–2875.

[34] ——, *Computationally efficient adjustment of FACTS set points in DC optimal power flow with shift factor structure*, IEEE Transactions on Power Systems, 32 (2016), pp. 1733–1740.

[35] Y. Sang, M. Sahraei-Ardakani, and M. Parvania, *Stochastic transmission impedance control for enhanced wind energy integration*, IEEE Transactions on Sustainable Energy, 9 (2017), pp. 1108–1117.

[36] J. Shi and S. S. Oren, *Stochastic unit commitment with topology control recourse for power systems with large-scale renewable integration*, IEEE Transactions on Power Systems, 33 (2017), pp. 3315–3324.

[37] Siemens Energy, *UPFC PLUS*. Last accessed 6 February 2023.

[38] Smart Wires Inc., *SmartValve^{TM}*, 2022. Accessed: 2022-07-10.

[39] F. Teng, R. Dupin, A. Michiorri, G. Kariniotakis, Y. Chen, and G. Strbac, *Understanding the benefits of dynamic line rating under multiple sources of uncertainty*, IEEE Transactions on Power Systems, 33 (2017), pp. 3306–3314.

[40] Q. Wang, Y. Guan, and J. Wang, *A chance-constrained two-stage stochastic program for unit commitment with uncertain wind power output*, IEEE Transactions on Power Systems, 27 (2011), pp. 206–215.

[41] L. You, H. Ma, and T. K. Saha, *A cvar-constrained optimal power flow model for wind integrated power systems considering transmission-side flexibility*, International Journal of Electrical Power & Energy Systems, 150 (2023), p. 109087.

[42] X. Zhang, D. Shi, Z. Wang, B. Zeng, X. Wang, K. Tomsovic, and Y. Jin, *Optimal allocation of series FACTS devices under high penetration of wind power within a market environment*, IEEE Transactions on Power Systems, 33 (2018), pp. 6206–6217.

[43] Y. Zhang, J. Wang, T. Ding, and X. Wang, *Conditional value at risk-based stochastic unit commitment considering the uncertainty of wind power generation*, IET Generation, Transmission & Distribution, 12 (2018), pp. 482–489.

Table 7.1. Ranking of transmission lines as FACTS placement candidates in the 24-bus system

Sensitivity-based method			**Exhaustive search**		
Rank	Line	Aggregated sensitivity	Rank	Line	Aggregated cost ($k)
1	A6	5619.62	1	A6	16,471
2	A26	4958.11	2	A26	16,483
3	A24	4030.39	3	A24	16,501
4	A2	2643.90	4	A2	16,534
5	A28	2509.40	5	A28	16,538

Table 7.2. Ranking of transmission lines as FACTS placement candidates in the 300-bus system

Sensitivity-based method			**Exhaustive search**		
Rank	Line	Aggregated sensitivity	Rank	Line	Aggregated cost ($k)
1	182	38751.30	1	182	123,372
2	177	30527.73	2	358	123,937
3	358	29867.46	3	174	123,937
4	174	29867.46	4	177	124,020
5	176	23868.22	5	176	124,326
6	239	11955.92	6	239	125,119
7	180	8883.84	7	180	125,329
8	181	8223.58	8	181	125,374
9	175	5999.24	9	175	125,531
10	357	5999.24	10	357	125,531
11	269	5589.76	11	269	125,545
12	309	5589.76	12	309	125,545
13	268	5589.76	13	268	125,545
14	201	3652.85	14	185	125,726
15	185	3174.28	15	183	125,760
16	183	2697.32	16	179	125,793
17	61	2303.66	17	178	125,793
18	179	2224.34	18	61	125,798
19	178	2224.34	19	201	125,811
20	111	1786.25	20	111	125,818

PART II

INCENTIVIZING GET INVESTMENTS AND OPTIMAL OPERATIONS

CHAPTER 8

A REVIEW OF ECONOMIC INCENTIVES FOR EFFICIENT OPERATION OF FLEXIBLE TRANSMISSION

Market integration of GETs is essential to fully utilize their benefits in facilitating the energy transition towards more RES. To obtain a more precise understanding of the problems regarding market mechanisms and incentives for GETs, this chapter presents a published review[1][2] of current market integration efforts by regulatory entities and the industry, as well as proposals in the existing literature on this topic. The review also discusses the challenges in this field, which provides directions for further studies, including the proposed market mechanisms shown later in this Chapter. It is worth noting that "flexible transmission" used in this chapter is an equivalent terminology to "grid-enhancing technologies".

---

[1]

[2]

A Review of Economic Incentives for Efficient Operation of Flexible Transmission

Xinyang Rui
Department of Electrical and Computer Engineering
University of Utah
Salt Lake City, UT, USA
xinyang.rui@utah.edu

Omid Mirzapour
Department of Electrical and Computer Engineering
University of Utah
Salt Lake City, UT, USA
omid.mirzapour@utah.edu

Brittany Pruneau
Department of Electrical and Computer Engineering
University of Utah
Salt Lake City, UT, USA
u1352355@utah.edu

Mostafa Sahraei-Ardakani
Department of Electrical and Computer Engineering
University of Utah
Salt Lake City, UT, USA
mostafa.ardakani@utah.edu

***Abstract*—The growing penetration of renewable energy requires upgrades to the transmission network to ensure the deliverability of renewable generation. As an efficient alternative to transmission expansion, flexible transmission technologies, whose benefits have been widely studied, can alleviate transmission system congestion and enhance renewable energy integration. However, under the current market structure, investments for these technologies only receive a regulated rate of return, providing little to no incentive for efficient operation. Additionally, a regulated rate of return creates an incentive for building more transmission lines rather than efficient utilization of the existing system. Therefore, investments in flexible transmission technologies remain rather limited. To facilitate the deployment of flexible transmission, improve system efficiency, and accommodate renewable energy integration, a proper incentive structure for flexible transmission technologies, compatible with the current market design, is vital. This paper reviews the current market-based mechanisms for various flexible transmission technologies, including impedance control, dynamic line rating, and transmission switching. This review pinpoints current challenges of the market-based operation of flexible transmission and provides insights for future endeavors in designing efficient price signals for flexible transmission operation.**

***Index Terms*—Flexible transmission, electricity markets, phase shifting transformers, power systems operation, reactance control, topology control, transmission investments.**

I. Introduction

As the electricity generation and consumption patterns are evolving towards carbon-free generation and electrified consumption worldwide, the transmission system needs upgrades to adapt to the new environment with increased penetration from renewable energy sources (RES). Enhancing renewable integration is essential for decarbonizing the power grid and achieving a carbon-neutral economy, which has been an important objective for countries worldwide. For example, the Biden administration has announced the goal of a net-zero greenhouse gas (GHG) emission economy by 2050 [1]. Increased levels of renewable energy penetration and growing demand for electrified consumption have led to new congestion patterns in the legacy transmission grid [2]. The geographic locations of renewable resources [3], [4] have added to the congestion in the transmission grid as they can be far away from load centers [5]. Therefore, the available transfer capability (ATC) needs enhancement to ensure the deliverability of intermittent and geographically dispersed renewable generation. Transmission expansion is an obvious approach to enhance ATC; however, building new transmission lines faces challenges such as lengthy permitting processes and lumpy investment discouraging investors from investing in this sector [6], [7].

On the other hand, flexible transmission technologies have been viewed by previous literature as an efficient alternative to transmission expansion for ATC procurement and streamlining renewable energ deployment through congestion relief in the transmission system [8]. Flexible transmission includes a range of technologies and operational methods that allow optimal utilization of current transmission infrastructure instead of considering transmission systems as fixed assets during operation. The adjustments that can provide flexibility in the transmission network include topology changes, reactance compensation, thermal rating adjustment, and nodal phase shift. Prominent flexible transmission technologies include series flexible transmission system (FACTS) devices, transmission switching, dynamic line rating (DLR), high-voltage direct-current (HVDC) lines, and phase-shifting transformers (PST). More detailed descriptions of these technologies are presented in later sections of the paper. An extensive body of literature has shown the potential benefits of implementing flexible transmission to alleviate congestion and facilitate renewable generation integration.

Despite the widely-studied benefits, flexible transmission

This research was supported by the National Science Foundation under grant number 2146531.

deployment in the existing power grid is still limited due to challenges such as the conservative investments in the transmission system, increased computational complexity of operation and planning models with flexible transmission, and lack of economic incentive. An important challenge hindering the implementation of flexible transmission is the lack of a proper market-based incentive structure for transmission assets in current electricity market designs. The most prevalent compensation scheme for transmission investment in several markets does not provide proper incentives for deploying and optimally operating flexible transmission technologies, as the owners receive only a regulated rate of return (RoR) compensation. This is due to the fact that transmission assets were operated as a part of the vertically integrated utilities (VIU) under government regulation. Following the restructuring of power systems, the VIUs disintegrated, and competitive markets were formed for electricity generation and retail. However, the transmission system remained regulated under the umbrella of natural monopoly. Independent System Operators/Regional Transmission Organizations (ISO/RTOs) were formed to manage wholesale energy and ancillary service markets, operate the transmission network, and plan transmission expansion. Extending the competition to the transmission sector has been a subject of interest since then. The merchant transmission model for compensating transmission investment through Financial Transmission Rights (FTR) has been investigated in several studies [9]–[12]. However, under realistic conditions, the benefits of this model are undermined due to stochastic characteristics of the transmission network and market participant behavior [9]. With the aforementioned demands for transmission system upgrades due to the steep growth of renewable generation and the need for higher grid resilience, the conventional cost-of-service regulation and monopoly transmission investment projects are insufficient for the changing electricity industry environment. The Federal Energy Regulatory Commission (FERC) Order 1000, issued in 2011, intends to bring competition to US transmission investment by removing barriers, stimulating more participation in transmission investment, and promoting decentralized transmission projects [13]. Several research endeavors have sought to find optimal investment in flexible transmission technologies in the market environment thereafter [14], [15]. A large portion of these efforts have focused on transmission expansion planning with flexible transmission technologies [16], [17]

A properly designed market structure facilitates flexible transmission deployment in the deregulated market. Previous literature has proposed different market structures and compensation schemes for flexible transmission. They are based on financial transmission rights or marginal value of flexible transmission operation in day-ahead markets. Regulatory entities and the industry has also pushed for performance-based market structures regarding flexible transmission. Nevertheless, further research is still needed to implement a well-designed market mechanism to harness the benefits of flexible transmission. This paper critically reviews the market structure and incentive proposals for flexible transmission to facilitate further research.

The rest of this paper is organized as follows: Section II presents an overview of flexible transmission technologies. Economic valuation and impacts of flexible transmission technologies are presented in Section III, followed by an overview of the proposed market-based incentive structures for flexible transmission operation and concluded by efforts and incentive mechanisms adopted by industry in various ISO/RTOs. The challenges for establishing efficient market mechanisms for flexible transmission are discussed in Section IV. Finally, conclusions are drawn in Section V, and guidelines for future research are presented.

II. Overview Flexible transmission Technologies

This section presents the functionalities of different flexible transmission technologies in the context of DC power flow. The basic formulation of the single-hour DC optimal power flow (DCOPF) is shown as follows:

$$\min \sum_{g\in G} c_g p_g \tag{1}$$

s.t.

$$p_g^{\min} \le p_g \le p_g^{\max}, g \in G; \tag{2}$$

$$-f_k^{\max} \le f_k \le f_k^{\max}, k \in K; \tag{3}$$

$$f_k = b_k(\theta_{k,\mathrm{to}} - \theta_{k,\mathrm{fr}}), k \in K; \tag{4}$$

$$\theta_1 = 0; \tag{5}$$

$$\sum_{k\in\delta^+(n)} f_k - \sum_{k\in\delta^-(n)} f_k + \sum_{g\in G(n)} p_g = d_n, n \in N, \tag{6}$$

where p_g is the active power output of generator g, f_k is the active power flow through transmission line k, and $\theta_{k,\mathrm{to}}$ and $\theta_{k,\mathrm{fr}}$ are the voltage angles at the end buses of line k. (1) is the objective function that minimizes the total generation cost, with c_g being the linear marginal cost of generator g. Generator capacity limits $p_g^{\max}$ and $p_g^{\min}$ are specified in (2). (3) defines the thermal limit constraint of transmission lines and $f_k^{\max}$ is the thermal limit of transmission line k. The DC power flow equation, with b_k being the susceptance of transmission line k, is presented in (4). (5) specifies the voltage angle at the reference bus. Finally, (6) is the power balance constraint at each system bus n.

Flexible transmission technologies can enhance operation efficiency and ATC by altering the constraints (3) and (4) in the DCOPF formulation presented above. There are four ways to alter these constraints mathematically: (i) controlling the phase angles in (4), (ii) adjusting the susceptance in (4), (iii) removing the constraints for a line (switching it out), and (iv) changing the limits in (3).

PSTs can provide controllability over $\theta_{k,\mathrm{to}}$ and $\theta_{k,\mathrm{to}}$ in (4), effectively enabling the power flow to be controlled [18]. This controllability can be integrated into the DCOPF formulation by introducing a new variable ϕ_k into the line flow constraint (4) to extend the feasible region to a wider area. This is shown in Fig. 1(a).

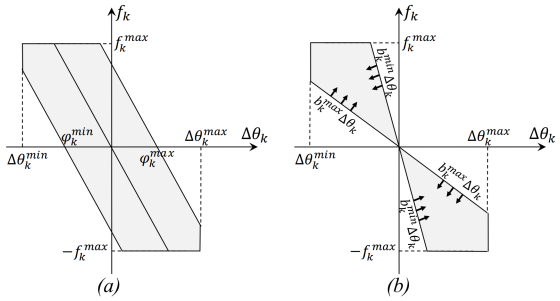

Fig. 1. Feasible region extension by: (a) phase shift (b) susceptance adjustment.

With the deployment of series FACTS devices, the reactance of transmission lines can be altered so that power flows can be rerouted to avoid transmission bottlenecks. Devices such as the thyristor-controlled series compensator (TCSC), the static synchronous series compensator (SSSC), and the unified power flow controller (UPFC) are widely studied in previous literature and have been deployed in actual industry applications. The TCSC directly adjust the line susceptance, making (4) a nonlinear equation. The UPFC and the SSSC use voltage injections to emulate susceptance adjustments. Techniques and modeling to efficiently incorporate series FACTS into power system operation models are presented in [19], [20]. The impact of reactance control from TCSC-type devices can be visualized through expanded feasible region as shown in Fig. 1(b).

With transmission switching, the status of the transmission elements can be altered so that power flow control functions are provided [21]. The formulations of (3) and (4) are changed, using the big-M method, with the introduction of binary variable z_k representing line switching [22]:

$$-f_k^{\max} z_k \le f_k \le f_k^{\max} z_k, k \in K; \quad (7)$$

$$f_k - b_k(\theta_{k,\mathrm{to}} - \theta_{k,\mathrm{fr}}) + (z_k - 1)M \le 0, k \in K; \quad (8)$$

$$f_k - b_k(\theta_{k,\mathrm{to}} - \theta_{k,\mathrm{fr}}) - (z_k - 1)M \ge 0, k \in K. \quad (9)$$

Transmission switching can also be considered as a discrete susceptance control, where the susceptance is adjusted to zero for a line that is switched out of the system. It is also worth noting that transmission switching can be performed utilizing existing assets [23], whereas line reactance and phase angle control require the installation of additional devices, which can involve hefty investments.

Under static line rating, the thermal limit $f_k^{\max}$ is a parameter, and traditionally the value is given with a conservative estimate. With DLR, $f_k^{\max}$ is dynamically updated based on monitoring of real-time weather conditions or communication of the actual conductor temperature. Thus, DLR enables the adoption of higher limits that will increase transmission system capacity [24].

As an alternative to AC transmission systems, HVDC systems are superior in some applications, including long-distance transmission, offshore renewable integration, and regional electricity market interconnections [25]. The unique controllability features that HVDC systems provide make them suitable for managing congestion and providing flexibility on the grid level [26].

III. Economic Valuation and Market Integration of Flexible Transmission

A. Quantification of Economic Value

The first step towards designing an efficient market-based scheme for flexible transmission technologies is quantifying the economic benefits of such technologies. This could be evaluated as social welfare enhancement or cost savings in markets with inelastic demand for electricity. Quantifying the benefits is essential for developing market structures to provide the correct incentives for the efficient operation of flexible transmission. A well-designed incentive structure will ensure that the flexible transmission owner benefit is aligned with social welfare improvement. In cases where the optimal direction of adjustment is not aligned with the owner's interest, the market-based scheme should provide compensation schemes for the owner to operate the device in the optimal direction.

The most common benefit of flexible transmission in the existing literature is dispatch cost reduction. Different levels of savings have been reported in various previous studies [22], [27], [28]. With recent developments in FACTS technology, modular lightweight versions are introduced to the flexible transmission market known as distributed/modular FACTS (D-FACTS or M-FACTS) with enhanced controllability and congestion management capabilities. Ref. [29] evaluates the operation cost savings provided by implementing FACTS and D-FACTS. The evaluation is carried out through a linearized optimal power flow model under different loading scenarios. The results show that the benefits of both FACTS and D-FACTS are higher than break-even costs. D-FACTS offers higher economic value than FACTS incurring cost savings of up to 2.55%.

TABLE I
Economic Valuation of Flexible Transmission Technologies

Technology	Implementation Cost	Operation Cost Savings
FACTS	Medium-High	up to 30% [29]
TS	Marginal	up to 25% [21], [22], [30]
HVDC	High	up to 50% [25], [26]
PST	Medium	∼12% [31]
DLR	Marginal	∼20% [28], [32]

Other types of benefits are also quantified by previous research. Ref. [30] evaluates the economic benefits of transmission switching providing both congestion alleviation and

reliability enhancement in the ISO-NE system. In [32], the authors conduct a case study to evaluate the economic benefits of implementing DLR to consumers by studying the electricity prices at both ends of a transmission bottleneck.

Overall, the literature suggests that deploying flexible transmission can provide various benefits, each of which should be quantified separately. These benefits are important in evaluating the performance of flexible transmission technologies and can be the basis for developing economic incentives and compensation mechanisms. The quantification of such benefits is summarized in Table I. This evaluation lays the foundation for efficient incentive design for market operation and further helps the investors with the right choice of technology.

B. Incentive Design and Market Integration

Although flexible transmission does not possess the same characteristics as bulk transmission expansion projects, they are still regulated as a part of transmission system upgrades and implemented upon ISO/RTO transmission upgrades requirement. This scheme, however, provides no incentive for investing in these technologies, and the deployment has been slow so far. Several compensation mechanisms have been proposed in recent studies to accelerate the proliferation of such technologies through performance-based incentives.

Financial transmission rights (FTRs) are risk-hedging tools designed to minimize the congestion price risk for forward contracts and are successfully implemented in various power markets [33]. In [34], a market structure, where owners of power flow controllers receive FTR allocations, is proposed to solve the lack of incentive problem under the existing market structure. The authors argued that additional FTRs should be assigned to FACTS device owners. Revenue adequacy and performance of the proposed mechanism are demonstrated on 2-bus and 3-bus systems. However, the difficulty in identifying which particular set of FTRs would correspond to a transmission expansion project, and the order in which projects are built affects the rights awarded can be a drawback for using FTR-style rights to compensate merchant transmission projects [35].

Besides directly using FTR allocation, several previous studies proposed marginal value or other metrics as a compensation mechanism for flexible transmission. It is argued in [36] that an important issue for using FACTS devices to manage congestion in the deregulated market is the compensation scheme for the utilization of FACTS devices and penalty for users to operate at their limits and addressed both in their proposed price scheme. Under such a scheme, FACTS device owners receive a regulated portion of the total cost savings incurred by their operation. They also receive a penalty from loads when the device is operating at its limits, which is proportional to the value of the Lagrangian dual variable associated with the FACTS operating constraints. However, the proposal is revenue inadequate and incompatible with wholesale energy market structures. Yet, the modeling of FACTS devices presented in this paper is still valuable. Ref. [37] seeks to address the positive externality problem in the transmission payment method proposed in [35]. In [35], each transmission element receives a payment equal to the active power flow multiplied by the locational marginal price (LMP) different at the two ends of the element. This creates a positive externality problem, where a flow on a line can increase due to the actions taken by another market player, but the line owner will receive the benefits, due to the increased flow. Ref. [37] alternatively proposes a sensitivity-based calculation of the marginal value of susceptance adjustment by variable-impedance FACTS devices. However, the mathematical proof of revenue adequacy is limited to the case that susceptance adjustment increases the flow on the line that the FACTS device is installed, which is when FACTS increases the absolute value of susceptance. An investment recovery scheme for FACTS devices is proposed in [38], which is based on the load and generator surplus increase due to FACTS deployment. Such a scheme can be utilized as a performance-based incentive for FACTS deployment. In [39], similar to the proposal in [35], a metric is introduced to identify the favorable candidate lines for transmission switching. Although this proposal is not intended for the market, it can be used to develop a compensation mechanism.

Besides the widely studied benefits of reducing the operation cost and facilitating renewable generation integration, the value of flexible transmission in transmission planning as an asset to provide investment flexibility and risk alleviation has also been explored by the existing literature. New transmission projects are capital-intensive and are, in most cases, irreversible. Technologies such as FACTS and PST can provide investment flexibility to avoid unfavorable transmission expansion plans due to uncertainty introduced by future integration of renewable generation [31], [40]. Simulation studies in [40] and [31] show the option value of flexible transmission in long-term transmission expansion projects. The results in [40] show that the option value provided by FACTS devices for deferment of new transmission line investments can be 12% of the net present value (NPV) of transmission expansion. It is shown in [31] that PSTs can bring the total value of £13.1 million (reducing investment cost from £5609 million to £5596 million) in investment cost reduction while providing the transmission expansion planning projects with enough flexibility to reduce uncertainty in investment decisions. However, no existing literature has incorporated such expansion strategies into a merchant transmission scheme.

C. Industry Practice and ISO/RTO Experience

The issues of a regulated RoR and the lack of incentives are known to regulatory entities such as FERC, the ISO/RTOs, and the industry. Over the years, there have been endeavors to make changes and facilitate the deployment of flexible transmission technologies. The U.S. Department of Energy, in a study conducted in the early 2000s, has highlighted the importance of a performance-based regulation (PBR) and revealed that the PBR in the UK led to congestion cost reduction in substantial amounts [41]. Ref. [41] also highlighted that the PBR scheme in the UK showed that incentives for enhanced

transmission system operations could have an important role in enhancing transmission operation efficiency, which includes increasing investment in innovative transmission technologies such as flexible transmission.

Studies regarding the benefits of flexible transmission have been conducted by ISO/RTOs as well. In [42], ISO New England (ISO-NE) discussed the value of implementing FACTS and HVDC in their system. Ref. [42] stated that because of the controllability of HVDC, it is attractive for merchant transmission line applications, and that opportunities for merchant FACTS and HVDC are open in New England. However, no performance-based compensation mechanism regarding merchant transmission projects is mentioned. It is also highlighted by the Pennsylvania-New Jersey-Maryland Interconnection (PJM) that precise control by HVDC makes it ideal for merchant transmission projects [43], with an example being the SOO Green HVDC link [44]. However, the mechanism is still being developed to incorporate inter-RTO HVDC links into the PJM capacity market to allow customers to benefit from increased competition, greater geographic and technological generation diversity, and the additional instantaneous control offered by dispatchable HVDC facilities [44].

In September 2021, FERC held the "Workshop to Discuss Certain Performance-based Ratemaking Approaches" [45]. With a focus on shared savings, this workshop was intended to stimulate the development of transmission technologies. The transmission technologies, or grid-enhancing technologies (GET) discussed at the workshop include flexible transmission technologies such as FACTS devices. The Shared Savings Proposal [46] made by Working for Advanced Transmission Technologies (WATT coalition) and AEE presented a compensation scheme, where 25% of the savings achieved by implementing transmission technologies are allocated. The proposal also presented a re-evaluation scheme that if the cost-benefit ratio of the project can satisfy the predefined requirement, the incentive will be awarded for the subsequent three years. Despite introducing a performance-based mechanism, this proposal does not have any information regarding making flexible transmission market participants. It also does not address how the compensations should be allocated if multiple projects are planned or carried out in the same time period.

IV. Challenges and Future Research

The existing proposals regarding market structures and incentives for flexible transmission provide important references and guidance for future developments on this topic. The following challenges in this field need to be addressed in future proposals.

- The existing proposals involve a variety of ways of providing incentives/compensations for flexible transmission. They involve shared savings, FTR allocations, as well as generation and load surpluses. Further investigations are needed for each scheme to determine the proper schemes for each technology in different scenarios. A more general compensation scheme for different technologies is desirable. Additionally, Previous studies mainly focused on continuous resources such as FACTS. More compensation mechanism proposals for other technologies are needed [47]. Notably, the discrete changes in the network topology have unpredictable impacts on locational marginal prices (LMP) and might create revenue inadequacy in current FTR markets [48]. Creating a market-compatible mechanism for accruing the economic benefits of optimal transmission switching remains an interesting research subject.
- Several previous studies use small systems which only have two to three buses to demonstrate the effectiveness of the proposed schemes. Numerical studies on larger systems or using real system data are preferable in future research.
- Mathematical proofs, regarding revenue adequacy and alignment of social welfare improvement with flexible transmission incentives, are key for the future development of market structures for flexible transmission.

V. Conclusions

This paper reviews the existing efforts to establish market structures and economic incentives to stimulate the adoption of flexible transmission technologies. Considering the technological advancements, the lack of performance-based compensation is a key obstacle to increasing the utilization of flexible transmission. Effective solutions to resolve this problem will be vital for enhancing the efficiency of power system operation, improving utilization of the existing transmission system, and ultimately facilitating renewable generation integration to achieve decarbonization targets. While the existing literature provides directions for future research, the problem remains unsolved. We do not yet have appropriate ways to provide incentives for flexible transmission operations.

References

[1] Department of Energy, "Biden-Harris Administration Launches $2.6 Billion Funding Programs To Slash Carbon Emissions," July 2022, accessed: 2022-11-20. [Online]. Available: https://www.energy.gov/articles/biden-harris-administration-launches-26-billion-funding-programs-slash-carbon-emissions

[2] A. Navon, P. Kulbekov, S. Dolev, G. Yehuda, and Y. Levron, "Integration of distributed renewable energy sources in israel: Transmission congestion challenges and policy recommendations," *Energy Policy*, vol. 140, p. 111412, 2020.

[3] M. Sengupta, Y. Xie, A. Lopez, A. Habte, G. Maclaurin, and J. Shelby, "The national solar radiation data base (NSRDB)," *Renewable and sustainable energy reviews*, vol. 89, pp. 51–60, 2018.

[4] M. Panahazari, M. Koscak, J. Zhang, D. Hou, J. Wang, and D. W. Gao, "A hybrid optimization and deep learning algorithm for cyber-resilient der control," in *2023 IEEE Power & Energy Society Innovative Smart Grid Technologies Conference (ISGT)*. IEEE, 2023, pp. 1–5.

[5] F. Monforti-Ferrario and M. P. Blanco, "The impact of power network congestion, its consequences and mitigation measures on air pollutants and greenhouse gases emissions. a case from germany," *Renewable and Sustainable Energy Reviews*, vol. 150, p. 111501, 2021.

[6] Y. Li, B. Hu, K. Xie, L. Wang, Y. Xiang, R. Xiao, and D. Kong, "Day-ahead scheduling of power system incorporating network topology optimization and dynamic thermal rating," *IEEE Access*, vol. 7, pp. 35 287–35 301, 2019.

[7] S. Lumbreras and A. Ramos, "The new challenges to transmission expansion planning. survey of recent practice and literature review," *Electric Power Systems Research*, vol. 134, pp. 19–29, 2016.

[8] F. H. Gandoman, A. Ahmadi, A. M. Sharaf, P. Siano, J. Pou, B. Hredzak, and V. G. Agelidis, "Review of FACTS technologies and applications for power quality in smart grids with renewable energy systems," *Renewable and sustainable energy reviews*, vol. 82, pp. 502–514, 2018.

[9] P. Joskow and J. Tirole, "Merchant transmission investment," *The Journal of industrial economics*, vol. 53, no. 2, pp. 233–264, 2005.

[10] A. Rubino and M. Cuomo, "A regulatory assessment of the electricity merchant transmission investment in eu," *Energy Policy*, vol. 85, pp. 464–474, 2015.

[11] P. Staudt and S. S. Oren, "Merchant transmission in single-price electricity markets with cost-based redispatch," *Energy Economics*, vol. 104, p. 105610, 2021.

[12] D. R. Biggar and M. R. Hesamzadeh, "Merchant transmission investment using generalized financial transmission rights," *Transmission Network Investment in Liberalized Power Markets*, pp. 323–351, 2020.

[13] Federal Energy Regulatory Commission, "Order no. 1000 - transmission planning and cost allocation," 2011, accessed: 2018-12-01. [Online]. Available: https://www.ferc.gov/electric-transmission/order-no-1000-transmission-planning-and-cost-allocation

[14] X. Zhang, D. Shi, Z. Wang, B. Zeng, X. Wang, K. Tomsovic, and Y. Jin, "Optimal allocation of series FACTS devices under high penetration of wind power within a market environment," *IEEE Transactions on power systems*, vol. 33, no. 6, pp. 6206–6217, 2018.

[15] H. Nourizadeh, A. Mosallanejad, and M. SetayeshNazar, "Optimal placement of fixed series compensation and phase shifting transformer in the multi-year generation and transmission expansion planning problem at the pool-based market for maximizing social welfare and reducing the investment costs," *IET Generation, Transmission & Distribution*, vol. 16, no. 15, pp. 2959–2976, 2022.

[16] C. Y. Tee and M. D. Ilić, "Toward valuing flexibility in transmission planning," *Power Grid Operation in a Market Environment: Economic Efficiency and Risk Mitigation*, pp. 219–249, 2016.

[17] B. F. Hobbs, Q. Xu, J. Ho, P. Donohoo, S. Kasina, J. Ouyang, S. W. Park, J. Eto, and V. Satyal, "Adaptive transmission planning: implementing a new paradigm for managing economic risks in grid expansion," *IEEE Power and Energy Magazine*, vol. 14, no. 4, pp. 30–40, 2016.

[18] J. Verboomen, D. Van Hertem, P. H. Schavemaker, W. L. Kling, and R. Belmans, "Phase shifting transformers: principles and applications," in *2005 International Conference on Future Power Systems*. IEEE, 2005, pp. 6–pp.

[19] M. Sahraei-Ardakani and K. W. Hedman, "Day-ahead corrective adjustment of FACTS reactance: A linear programming approach," *IEEE Transactions on Power Systems*, vol. 31, no. 4, pp. 2867–2875, 2015.

[20] X. Rui, M. Sahraei-Ardakani, and T. R. Nudell, "Linear modelling of series FACTS devices in power system operation models," *IET Generation, Transmission & Distribution*, vol. 16, no. 6, pp. 1047–1063, 2022.

[21] K. W. Hedman, R. P. O'Neill, E. B. Fisher, and S. S. Oren, "Optimal transmission switching with contingency analysis," *IEEE Transactions on Power Systems*, vol. 24, no. 3, pp. 1577–1586, 2009.

[22] E. B. Fisher, R. P. O'Neill, and M. C. Ferris, "Optimal transmission switching," *IEEE Transactions on Power Systems*, vol. 23, no. 3, pp. 1346–1355, 2008.

[23] K. W. Hedman, S. S. Oren, and R. P. O'Neill, "A review of transmission switching and network topology optimization," in *2011 IEEE power and energy society general meeting*. IEEE, 2011, pp. 1–7.

[24] E. Fernandez, I. Albizu, M. Bedialauneta, A. Mazon, and P. T. Leite, "Review of dynamic line rating systems for wind power integration," *Renewable and Sustainable Energy Reviews*, vol. 53, pp. 80–92, 2016.

[25] A. Alassi, S. Bañales, O. Ellabban, G. Adam, and C. MacIver, "HVDC transmission: Technology review, market trends and future outlook," *Renewable and Sustainable Energy Reviews*, vol. 112, pp. 530–554, 2019.

[26] A. Held, M. Ragwitz, F. Sensfuß, G. Resch, L. Olmos, A. Ramos, and M. Rivier, "How can the renewables targets be reached cost-effectively? policy options for the development of renewables and the transmission grid," *Energy Policy*, vol. 116, pp. 112–126, 2018.

[27] M. Sahraei-Ardakani and K. W. Hedman, "A fast LP approach for enhanced utilization of variable impedance based FACTS devices," *IEEE Transactions on Power Systems*, vol. 31, no. 3, pp. 2204–2213, 2015.

[28] F. Teng, R. Dupin, A. Michiorri, G. Kariniotakis, Y. Chen, and G. Strbac, "Understanding the benefits of dynamic line rating under multiple sources of uncertainty," *IEEE Transactions on Power Systems*, vol. 33, no. 3, pp. 3306–3314, 2017.

[29] Y. Sang and M. Sahraei-Ardakani, "Economic benefit comparison of D-FACTS and FACTS in transmission networks with uncertainties," in *2018 IEEE Power & Energy Society General Meeting (PESGM)*. IEEE, 2018, pp. 1–5.

[30] J. D. Lyon, S. Maslennikov, M. Sahraei-Ardakani, T. Zheng, E. Litvinov, X. Li, P. Balasubramanian, and K. W. Hedman, "Harnessing flexible transmission: corrective transmission switching for iso-ne," *IEEE Power and Energy Technology Systems Journal*, vol. 3, no. 3, pp. 109–118, 2016.

[31] I. Konstantelos and G. Strbac, "Valuation of flexible transmission investment options under uncertainty," *IEEE Transactions on Power systems*, vol. 30, no. 2, pp. 1047–1055, 2014.

[32] S. Uski, "Estimation method for dynamic line rating potential and economic benefits," *International Journal of Electrical Power & Energy Systems*, vol. 65, pp. 76–82, 2015.

[33] V. Sarkar and S. A. Khaparde, "A comprehensive assessment of the evolution of financial transmission rights," *IEEE Transactions on Power Systems*, vol. 23, no. 4, pp. 1783–1795, 2008.

[34] M. Sahraei-Ardakani, "Merchant power flow controllers," *Energy Economics*, vol. 74, pp. 878–885, 2018.

[35] R. P. O'Neill, E. B. Fisher, B. F. Hobbs, and R. Baldick, "Towards a complete real-time electricity market design," *Journal of Regulatory Economics*, vol. 34, no. 3, pp. 220–250, 2008.

[36] G. M. Huang and P. Yan, "Establishing pricing schemes for FACTS devices in congestion management," in *2003 IEEE Power Engineering Society General Meeting (IEEE Cat. No. 03CH37491)*, vol. 2. IEEE, 2003, pp. 1025–1030.

[37] M. Sahraei-Ardakani and S. A. Blumsack, "Transfer capability improvement through market-based operation of series FACTS devices," *IEEE Transactions on Power Systems*, vol. 31, no. 5, pp. 3702–3714, 2015.

[38] N. Mithulananthan and N. Acharya, "A proposal for investment recovery of FACTS devices in deregulated electricity markets," *Electric Power Systems Research*, vol. 77, no. 5-6, pp. 695–703, 2007.

[39] J. D. Fuller, R. Ramasra, and A. Cha, "Fast heuristics for transmission-line switching," *IEEE Transactions on Power Systems*, vol. 27, no. 3, pp. 1377–1386, 2012.

[40] G. Blanco, F. Olsina, F. Garces, and C. Rehtanz, "Real option valuation of FACTS investments based on the least square Monte Carlo method," *IEEE Transactions on power systems*, vol. 26, no. 3, pp. 1389–1398, 2011.

[41] S. Abraham, "National transmission grid study," USDOE Office of the Secretary of Energy, Washington, DC (United States), Tech. Rep., 2003.

[42] M. Henderson, D. Bertagnolli, and D. Ramey, "Planning HVDC and FACTS in New England," in *2009 IEEE/PES Power Systems Conference and Exposition*. IEEE, 2009, pp. 1–3.

[43] S. Frenkel, "Technology and Reliability Applications Overview," July 2020, accessed: 2022-11-20. [Online]. Available: https://www.pjm.com/-/media/committees-groups/task-forces/hvdcstf/2020/20200713/20200713-item-03-soo-green-a-technology-and-reliability-overview.ashx

[44] ——, "SOO Green HVDC Link," May 2020, accessed: 2022-11-20. [Online]. Available: https://www.pjm.com/-/media/committees-groups/committees/mrc/2020/20200522-hvdc/20200522-item-03-soo-green-hvdc-link-presentation.ashx

[45] Workshop to discuss certain performance-based ratemaking approaches. Accessed: 2022-11-19. [Online]. Available: https://www.ferc.gov/news-events/events/workshop-discuss-certain-performance-based-ratemaking-approaches-09102021

[46] WATT Coalition and AEE, "WATT Coalition and AEE savings proposal," September 2020, accessed: 2022-11-17. [Online]. Available: https://www.ferc.gov/media/shared-savings-proposal

[47] J. Li, F. Liu, Z. Li, C. Shao, and X. Liu, "Grid-side flexibility of power systems in integrating large-scale renewable generations: A critical review on concepts, formulations and solution approaches," *Renewable and Sustainable Energy Reviews*, vol. 93, pp. 272–284, 2018.

[48] K. W. Hedman, S. S. Oren, and R. P. O'Neill, "Optimal transmission switching: economic efficiency and market implications," *Journal of Regulatory Economics*, vol. 40, no. 2, pp. 111–140, 2011.

CHAPTER 9

AN INCENTIVE SCHEME FOR GRID-ENHANCING TECHNOLOGIES BASED ON THE SHAPLEY VALUE

A common performance-based approach for rewarding transmission system upgrade projects is to provide payoffs to investors based on the social welfare positives. However, a benefit allocation method is needed when there are multiple asset owners. The publication[1][2] presented in this chapter proposes an incentive scheme for GETs that regards GET deployments in a system as participants in a coalition game. Payoffs, the social welfare increases created by GET operation, are distributed to GET owners using an improved Shapley value. The improvement over the traditional Shapley value approach is based on market efficiency considerations, which resets the operating limits of GETs based on the grand coalition results to reflect the participants' contributions more accurately. The effectiveness of the proposed scheme in incentivizing GET investments is demonstrated by comparing it with a regulated RoR.

---

[1]

[2]

An Incentive Scheme for Grid-Enhancing Technologies Based on the Shapley Value

Xinyang Rui, *Student Member, IEEE,* Omid Mirzapour, *Student Member, IEEE,* and Mostafa Sahraei-Ardakani, *Member, IEEE*

***Abstract*—Modernization of the transmission system via deploying grid-enhancing technologies (GETs) is a cornerstone of future grid design. New congestion patterns necessitating renewable energy curtailment highlight the significance of GETs. Despite the wide acknowledgment of the importance and benefits of GETs, their deployment remains fairly limited. One important barrier is the lack of proper incentives for deployment and efficient operation of GETs. This paper designs an incentive scheme to compensate GETs, based on their performance in the intraday market. The rewards are determined based on the cost savings achieved by GETs operation and are allocated to market participants using the Shapley value. The proposed incentive scheme is tested with numerical studies on modified IEEE RTS 24-bus and IEEE 300-bus systems. Results confirm that the designed incentive is aligned with the system objective: GET owners are compensated when cost savings are achieved. The benefits of a performance-based payment scheme are threefold: (i) it promotes efficient operation of existing GETs, based on the state of the system, (ii) it attracts further GETs deployment, and (iii) moves the risk from ratepayers to the investors.**

***Index Terms*—Electricity market, grid-enhancing technologies, power flow control, transmission investment incentive, Shapley value, power system flexibility, transfer capability.**

NOMENCLATURE

Indices

i, j	GET owner
k	Transmission line
s	Segment of linearized generator cost functions

Parameters

$\overline{\mathbf{f}}$	Thermal capacities of transmission lines
$\overline{\mathbf{\Delta f}}$	GET nodal injections upper bounds
$\overline{\mathbf{p}}_s$	Maximum output of generator g in segment s
$\overline{I}_k$	Maximum current on line k
θ_k^{PST}	Maximum phase shift by PSTs on line k
$\underline{\mathbf{p}}$	Minimum output of generators
$\mathbf{0}$	Vector of zeros
$\mathbf{1}$	Vector of ones
$\mathbf{\Gamma}$	Generator placement matrix
$\mathbf{\Phi}$	Injection shift factor matrix
$\mathbf{\Psi}$	GET placement matrix
$\mathbf{A}$	Adjacency matrix
$\mathbf{c}_s$	Linear costs of generators in segment s
$\mathbf{d}$	Vector of nodal Demands
b_k	Susceptance of line k
C^{FACTS}	Cost of FACTS devices
C^{PST}	Cost of PSTs
S_k^{FACTS}	Rating of FACTS device on line k
V_k^{FACTS}	Maximum voltage injection by FACTS devices on line k

Variables

$\mathbf{\Delta f}$	GET nodal injections
$\mathbf{f}$	Active power flows
$\mathbf{p}$	Active power output of generators
$\mathbf{p}_s$	Active power output of generators in segment s

Xinyang Rui, Omid Mirzapour, and Mostafa Sahraei-Ardakani are with the Department of Electrical and Computer Engineering, University of Utah, Salt Lake City, UT, 84112 USA (e-mail: xinyang.rui@utah.edu; omid.mirzapour@utah.edu; mostafa.ardakani@utah.edu).

This research is supported by the National Science Foundation under Grant No. 2146531.

I. INTRODUCTION

THE transmission system needs upgrades to maintain the operational efficiency of the power grid and accommodate the growing penetration of variable renewable energy sources (vRES). Grid-enhancing technologies (GETs), with prominent examples including impedance control, phase angle control, topology control, and dynamic line rating (DLR), provide a fast and cost-effective alternative to the expensive and lengthy processes of constructing new transmission lines. While new transmission lines may be necessary, GETs can offer immediate transfer capability enhancement and postpone the need for new transmission. Despite the maturity of the technology and wide acceptance of GETs benefits, their deployment remains limited. One of the main challenges contributing to this under-deployment is the lack of incentives for the installation and efficient operation of GETs.

Currently, GETs are considered as a component of the monopoly transmission system. Thus, GETs are regulated and receive regulated payments that are not linked to performance [1]. Regulated rate of return (RoR) payments often create an incentive to maximize the investment, which would lead to a tendency to build more lines rather than operating the existing system more efficiently [2]. This is a major reason for under-utilization of GETs [3]. Even when GETs are adopted, there is no incentive for efficient operation of GETs, which requires frequent adjustment of GETs setpoint [1]. A more appealing alternative would be to provide GETs operators with performance-based incentives.

Previous studies have proposed performance-based incentives for transmission investments. A widely employed approach is rewarding transmission projects using the surplus improvements they generate to incentivize investments in the socially optimal direction [4]. Such methods are employed

in [5]–[9], where transmission expansion investors receive the social welfare positives created by their projects as a part of the payment. It is worth noting that the cost savings and social welfare improvements can be modeled as inelastic demand. Despite the research focusing on economic incentive design for transmission expansion investments, proposals on payoffs to GETs have been somewhat limited. Reference [10] proposes to use the social welfare change to recover the investments in flexible AC transmission system (FACTS) devices. A sensitivity-based payment scheme for operations of FACTS is proposed in [11], which uses the dual variable of the DC power flow equation as a payment factor. However, this method may be revenue inadequate and does not accurately reflect the cost savings produced by FACTS operations. A merchant market model is proposed in [1], where power flow controller (PFC) owners acquire financial transmission rights (FTR). FTR is a long-term right to congestion rent, as described in [12]. It serves several purposes, including hedging against spot market price volatility, financial management of access rights to the transmission grid in the deregulated environment, allocation of congestion rent, and providing the environment for additional auctions and bilateral contracts between market participants. In electricity markets, the initial FTRs are allocated based on the historical use of the transmission network by market players. The congestion rent collected from the spot market is distributed among market participants based on the share of FTRs obtained. These FTRs can be transferred in secondary markets so that different participant can tailor their FTRs based on the risk assessments [13]. Previous research has shown that GETs can improve the efficiency of FTR auctions and allow for more FTRs to be auctioned [14]. Therefore, part of the additional auctioned FTRs can be assigned to GET owners, with the hope that they can recover their investment in a competitive manner and help the liquidity of electricity markets [1]. FTRs can further be used to secure fundamental transmissions in market processes or infrastructure upgrades, which is also the case for GETs. For instance, [15] proposes an FTR model for transition from single-price electricity markets (as in the European Union) to nodal electricity market (as in PJM) without endangering consumer supply security or steep increases in electricity prices. The literature on allocating incremental FTRs to new GET projects to incentivize the deployment and optimal operation is, however, limited. Reference [14] has discussed that additional FTRs can be auctioned considering the role of FACTS devices in FTR markets but did not discuss how to allocate a share of these incremental FTRs to FACTS owners. Reference [1] has shown that FTR markets can be revenue adequate in the presence of FACTS if power flow directions are known and discussed that FACTS owners can request additional FTRs as long as it is feasible considering network constraints. Further research is required for a clear FTR allocation mechanism for FACTS owners. Since these challenges have not yet found appropriate solutions, FTR-based incentives for GETs cannot be readily developed and used.

The approach of using system benefits as compensations has recently attracted attention to designing incentives for GETs. The Working for Advanced Transmission Technologies (WATT) coalition proposed a shared savings incentive for GETs, which was a main topic at the workshop on performance-based rate-making hosted by the Federal Energy Regulatory Commission (FERC) [16], [17]. This proposal allows GET owners to receive a portion of the system-wide cost-saving benefits that they generate [18]. However, a key question remains: How should compensation be allocated to different GET owners? Often, multiple GETs operate within a single transmission system with the goal of minimizing the system-wide operating cost. While each asset contributes to this objective, it is not straightforward to calculate the benefits of GETs. More importantly, it is unclear how such benefits (if calculated) should be distributed to different GET owners. Additionally, technological advances in the field, such as the modular FACTS (M-FACTS) devices, e.g., the SmartValve [19] by Smart Wires Inc. and the UPFC PLUS [20] from Siemens, allow GET deployments in a more distributed manner. Therefore, it is essential to have a method to distribute the economic compensation fairly among market participants. In [5], the marginal contribution of each transmission expansion project to social welfare, which is used as a reward, is determined sequentially. However, such an approach can be subject to the order in which the projects are carried out.

This paper fills the research gap by proposing an incentive scheme for hourly operation for GETs, with a benefit allocation method to distribute the payoffs. The proposed method considers GET deployments from different owners and calculates the cost savings created by GETs in hourly operation, and payoff distribution is completed by utilizing the Shapley value [21], a concept from cooperative game theory. Furthermore, we propose an improved Shapley value calculation, which resets the operating limits of GETs based on the grand coalition results to ensure market efficiency. Details of the modification and its effectiveness are presented in later sections. The Shapley value is a key method that provides value distribution in coalition games [22]. In previous studies, Shapley-value-based methods have been utilized to allocate compensations to transmission investors [6] and demand-side consumers participating in demand response programs [23]. In [24], the revenue for generators that bid as a coalition is allocated using the Shapley value, and a similar application of the Shapley value is presented in [25]. Other power system-related applications of the Shapley value include transmission cost allocation [26], [27] and profit allocation for distributed energy resources [28]. GET-related applications of the Shapley value are very limited. In [29], profits are allocated to the owners of transmission lines, thyristor-controlled series capacitor (TCSC) devices, and distributed generators using the Shapley value. However, in this allocation scheme, the whole of social welfare is distributed while considering transmission owners as a participant in the coalition game, which leads to the under-evaluation of GET contributions. Furthermore, the model developed in [29] is based on nonlinear AC power flow equations, which is incompatible with existing market management software tools.

The proposed scheme assumes that GET owners receive compensations calculated in the intraday market (IDM). There are two reasons behind this implementation. First, with the

increasing penetration of the variable renewable energy, hourly optimal power flow (OPF) results can more accurately reflect the actual social welfare contributions of GET operations. Second, GETs, unlike transmission lines, need to adjust their setpoints frequently to facilitate efficient dispatch under different operating conditions. This is enabled by the fast-response features of the GETs. Granted, integrating GETs into energy management systems (EMS) is required to fully utilize their features and allow IDM participation. We show that the proposed scheme can be implemented using the models in the existing literature that co-optimize GET setpoints in power system operation. Moreover, this paper aims to show that the proposed scheme, with performance-based financial compensations, is a desirable approach to incentivize GET investments. As mentioned previously, the current common approach for transmission investment recovery is through regulated RoRs. Therefore, The payoffs to GET owners are compared with ones achieved under a regulated RoR to confirm the effectiveness of the proposed scheme.

The main contributions of this paper are summarized as follows:

- An incentive scheme for the optimal operation of GETs is proposed, which allows owners to receive financial compensation for the socially optimal adjustment of their GETs' setpoints. The payoffs are calculated in the IDM, allowing the benefits of GETs to be more accurately captured, which is also in line with their flexibility. The Shapley value is utilized to allocate the benefits fairly to GET owners. The proposed scheme is based on system operation models compatible with existing EMS. To the best of our knowledge, this paper is the first paper to thoroughly study the effectiveness of a game-theory-based method in providing incentives to GETs.
- The proposed scheme employs an improved Shapley value approach, which not only considers the players' participation in coalitions but also reflects their actual contribution based on the results of the grand coalition. This design is intended to ensure market efficiency.

The rest of this paper is organized as follows: the proposed payment scheme is presented in Section II; Section III presents simulations studies on two test systems; Finally, Section IV concludes the paper.

II. Methodology

In this paper, we propose calculating the financial compensation to GET owners based on hourly dispatch results. This section first presents the problem formulation of (DC optimal power flow) DCOPF with GET operation, followed by a brief introduction of the Shapley value. Detailed steps of the proposed incentive scheme are then presented.

Including GETs in power system operation models increases the computational complexity. Various models have been proposed in previous research to efficiently co-optimize the setpoints of different GETs in power system operation [30]–[34]. In this paper, prominent voltage source converter-based FACTS (VSC-FACTS) devices, such as the static synchronous series compensator (SSSC) and the UPFC, and phase-shifting transformers (PSTs) are used to study the proposed incentive scheme. Both technologies are well-studied in the existing literature and have seen developments and deployments in the industry. Moreover, their modeling using the nodal injection model [31] helps preserve the linearity of DCOPF. Additionally, such modeling regards the GET adjustments to transmission grid parameters as nodal power injections, which helps preserve the original topology of the system and allows the injection shift factors (ISFs) to be used without changes. Devices such as the variable-impedance FACTS devices are beyond the scope of this paper. However, we expect similar results for these devices.

A. Co-optimizing GET operation in DCOPF

The DCOPF formulation with ISFs involving GET operations is shown as follows:

$$(\mathbf{P1}:)\ \text{minimize}\ \Pi = \sum_{s=1}^{\bar{s}} \mathbf{c}_s^{\mathrm{T}} \mathbf{p}_s \tag{1}$$

s.t.

$$\sum_{s=1}^{\bar{s}} \mathbf{p}_s = \mathbf{p}, \tag{2}$$

$$\mathbf{0} \le \mathbf{p}_s \le \mathbf{p}_s^{\max}, 1 \le s \le \bar{s}, \tag{3}$$

$$\underline{\mathbf{p}} \le \mathbf{p}, \tag{4}$$

$$\mathbf{f} = \mathbf{\Phi}(\mathbf{\Gamma}\mathbf{p} - \mathbf{d} - \mathbf{A}^{\mathrm{T}}\mathbf{\Psi}\mathbf{\Delta}\mathbf{f}), \tag{5}$$

$$-\overline{\mathbf{f}} \le \mathbf{f} + \mathbf{\Psi}\mathbf{\Delta}\mathbf{f} \le \overline{\mathbf{f}}, \tag{6}$$

$$\mathbf{1}^{\mathrm{T}}\mathbf{p} - \mathbf{1}^{\mathrm{T}}\mathbf{d} = 0, \tag{7}$$

$$-\overline{\mathbf{\Delta f}} \le \mathbf{\Delta}\mathbf{f} \le \overline{\mathbf{\Delta f}}, \tag{8}$$

The objective of the DCOPF is to minimize total production cost, as shown in (1). A piece-wise linearized model is adopted for production cost functions for the generating units. Equation (2) specifies that the sum of the output in each linearized segment is equal to the total output of a generator. The generator output upper bounds of each segment are shown in (3). Minimum output requirements for generators are presented in (4). In (5), the ISF matrix calculates power flows based on nodal power injections, which consist of generator outputs, demands, and GET nodal injections. Power flows are bounded by line thermal limits, as shown in (6). The system-wide active power balance constraint is shown in (7). The constraints on GET nodal injections are specified in (8), with the elements of $\overline{\mathbf{\Delta f}}$ presented as follows for the VSC-FACTS devices [33]:

$$\overline{\Delta f}_k = V_k^{\mathrm{FACTS}} |b_k|. \tag{9}$$

The modeling in (9) can be used for prominent VSC-FACTS devices. The bounds of PST nodal injections are shown as follows [35]:

$$\overline{\Delta f}_k = \theta_k^{\mathrm{PST}} |b_k|. \tag{10}$$

Note that the PST and the VSC-FACTS share similar modeling, as seen from (9) and (10). Thus, the constraints (8) represent the operation of both types of technology.

B. The Shapley Value

The Shapley value is a widely used game theory method to allocate benefits or costs among players forming a coalition. The allocation is based on the marginal contribution of each player to all possible coalitions it participates in. The calculation of the Shapley value for player i, denoted as $\phi(i)$, is shown as follows:

$$\phi(i) = \sum_{\mathcal{S} \subseteq \mathcal{N} \setminus i} \frac{|\mathcal{S}|!(n - |\mathcal{S}| - 1)!}{n!} (v(\mathcal{S} \cup \{i\}) - v(\{\mathcal{S}\})), \quad (11)$$

where $\mathcal{N} = \{1, 2, ..., n\}$ is the grand coalition which consists of the complete set of players, and $\mathcal{S}$ is a set of players not included i in the game. Additionally, $v(\cdot)$ denotes the characteristic function, which represents the value of a coalition.

The Shapley value provides a fair and unique distribution solution [27]. Additionally, essential features of the Shapley value that are related to the application in this paper are presented as follows [23]:

- Efficiency: the entirety of benefits is distributed to all the players in the grand coalition, as shown in (12).

$$\sum_{i \in \mathcal{N}} \phi(i) = v(\mathcal{N}); \quad (12)$$

- Symmetry: two players receive equal rewards if they contribute equally, which is presented as follows [36]:

$$\text{if } v(\{i\} \cup \mathcal{S}) = v(\{j\} \cup \mathcal{S}), \quad (13)$$
$$\text{then } \phi(i) = \phi(j). \quad (14)$$

C. Shapley value-based incentives for GETs operations

The incentive scheme for GET owners is considered a coalition game, with the characteristic function being the cost savings achieved by GETs operations. In the proposed scheme, players are GET owners who invested in deploying GETs in the power grid. Each player can own assets at one or multiple locations. Players in this coalition game are assumed to be obligated by contracts to adjust the setpoints of their devices according to the results of power system operation models.

The characteristic function of a coalition is the cost savings they achieve, which is presented as follows:

$$\begin{aligned} v(\mathcal{S}) &= \mathbf{P1}\{\mathcal{F}(\emptyset)\} - \mathbf{P1}\{\mathcal{F}(\mathcal{S})\} \\ &= \mathbf{P1}\{\mathbf{0}\} - \mathbf{P1}\{\mathcal{F}(\mathcal{S})\}, \end{aligned} \quad (15)$$

where $\mathbf{P1}\{\cdot\}$ denotes the objective function value when solving $\mathbf{P1}$ with a vector representing the operating limits of GETs. $\mathcal{F}(\cdot)$ represents a function that maps a coalition of players to the corresponding operating constraints. Therefore, $\mathbf{P1}\{\mathbf{0}\}$ represents a base case where the DCOPF is solved with no GET operation, and (15) calculates the cost savings achieved by coalition $\mathcal{S}$.

Certain GET deployments may not operate at their full limits, particularly when the system congestion level is low. Therefore, to improve market efficiency, the proposed scheme is designed with steps to accurately measure the marginal contribution of each participant in the grand coalition $\mathcal{N}$. Such design is further discussed in Section III.

The incentive scheme is presented as follows:

1) For the current hour in the IDM, get $\mathbf{P1}\{\mathbf{0}\}$;
2) Solve $\mathbf{P1}\{\mathcal{F}(\mathcal{N})\}$;
3) Check if all the operating constraints (8) are binding in step 2. If yes, go to step 5. If no, continue to step 4;
4) Reset GET operating ranges using the values from step 2;
5) Calculate the cost savings for each coalition using (15);
6) Calculate the Shapley values using (11);
7) Use Shapley values calculated in step 6 as payoffs to GET owners for this hour.
8) Accumulate the results of step 7 for the whole contract length.

We assume that the GET owners are under the obligations of contracts, and payoffs are settled by accumulating each IDM payoff after the contracts conclude. For example, GET owners can receive payoffs annually. However, with the advances in the GET designs, more flexibilities in the planning process are granted, allowing more options in the payoff cycles. This will be further discussed in Section III.

III. Case Studies

Numerical case studies are conducted on modified IEEE RTS 24-bus [37] and IEEE 300-bus [38] test systems. The systems are modified to increase congestion, in order to generate reasonable levels of cost savings through GET operations. The 24-bus system is modified following a similar approach presented in [39]. A total of 480 MW of load is shifted from buses 14, 15, 19, and 20 to bus 13, with load at each bus then increased by 5%. The capacities of lines A21, A22, A25-1, and A25-2 are all reduced by 50%. For the IEEE 300-bus system, we use the OPF case from PGlib [40]. The 300-bus system is further modified by reducing the thermal capacities of a group of transmission elements (lines and transformers) under heavy utilization. The thermal capacities of elements 61, 91, 101, 115, 137, 365, and 395 are all reduced by 50%. Additionally, element 268 has its thermal capacity reduced by 25%. For the case studies on the 300-bus system, we consider GET owners that own a group of GET devices. Maximum voltage injections of VSC-FACTS devices are specified in per-unit (pu) values, and the actual values are dependent on the rating of the transmission line where the devices are deployed. The PSTs are assumed to have a maximum angle adjustment of 10 degrees [35].

Note that simulation studies in this paper focus on the operation aspect, and the optimal allocation of GETs is beyond its scope. However, different allocation policies (APs) of GETs are employed to reveal the effect of planning on benefit distribution, with detailed results in the following subsections. DCOPF problems are modeled using CVXPY [41] and solved with CPLEX 22.10 on an Apple M2 Pro CPU with 16 GB of RAM.

A. IDM examples

1) IDM Case 1: We consider three GET owners who have invested in the system, with their corresponding GET deployments shown as follows:

- **GET Owner 1**: One VSC-FACTS device deployed at line A21 which has a maximum voltage injection of 0.05 pu.
- **GET Owner 2**: One PST device deployed on line A22.
- **GET Owner 3**: One VSC-FACTS device deployed at line A25-1 with a maximum voltage injection of 0.1 pu.

GETs, in this case, are deployed on three of the most utilized lines in the system. This is a commonly used engineering judgment in previous studies for FACTS placement [10], [32], [39] and is referred to as AP1 in this paper. The system is operating under peak load.

Following the incentive scheme presented in Section II, we first get the result of the grand coalition, which is shown in Table I.

TABLE I
GRAND COALITION RESULTS OF CASE 1

GET owner	Location	Type	Setpoint (MW)	Binding?
1	A21	FACTS	51.55	Y
2	A22	PST	66.68	N
3	A25-1	FACTS	-63.16	Y

It can be seen from Table I that the PST on Line A22 is not operating at its maximum. Therefore, to accurately capture the marginal contributions, this setpoint is used in calculating the characteristic function values for other coalitions as the new operating range for this device.

The Shapley value results are presented in Table II. The sum of the Shapley value is equal to the total cost savings achieved by the grand coalition, thus reflecting the desirable feature of efficiency for the Shapley value.

TABLE II
SHAPLEY VALUE RESULTS OF CASE 1

GET Owner	Shapley value ($)
1	1498.83
2	1958.40
3	43.61

2) IDM Case 2: We again consider three GET owners in this case, with their assets listed as follows:

- **GET owner 1**: One VSC-FACTS device deployed at line A23 which has a maximum voltage injection of 0.05 pu;
- **GET owner 2**: One PST device deployed on line A28;
- **GET owner 3**: One VSC-FACTS device deployed at line A18 with a maximum voltage injection of 0.1 pu.

The results for Case 1 show that the VSC-FACTS device on the transmission line A25-1 provides a very marginal contribution to congestion alleviation. In Case 2, AP2, which is based on the susceptance price [11], is employed. The sensitivity obtained from DCOPF dual solutions reflects the impact of GET operation on cost savings. Again, the DCOPFs are solved assuming a peak load hour. The grand coalition of the three devices achieved a cost-saving of $12,364, with detailed results presented in Table III.

In Case 2, all the GET operating constraints are binding, thus allowing the step of resetting operating bounds to be skipped. The Shapley value results are shown in Table IV.

TABLE III
GRAND COALITION RESULTS OF CASE 2

GET owner	Location	Type	Setpoint (MW)	Binding?
1	A23	FACTS	-84.75	Y
2	A28	PST	-758.84	Y
3	A18	FACTS	208.33	Y

TABLE IV
SHAPLEY VALUE RESULTS OF CASE 2

Device ID	Shapley value ($)
1	1625.47
2	8122.30
3	2616.68

Note that the result of Case 2 shows that the game presented in this paper is not necessarily superadditive, which is different from some of the profit allocation schemes in previous studies, such as [28]. The superadditivity can be affected by the allocation of GETs, as shown in this paper. Non-superadditivity means that each GET deployment reward, based on Shapley value, is not guaranteed to be any more than the compensation received when acting alone. However, the GET owners receive subsidies for the socially optimal operation of their assets, incentivizing them to participate and stay in the grand coalition.

B. Annualized return and comparison with regulated RoR

To study the effectiveness of the proposed method in incentivizing investments in GETs, numerical studies are conducted to estimate the potential annualized returns based on the Shapley value, which are then compared to RoRs.

1) IEEE RTS 24-bus system: Simulation studies are first conducted using the IEEE RTS 24-bus system. The year-long hourly load profile data is obtained from [37]. Typical days from each season are selected following the approach in [42]. Summer is represented by the fourth, fifth, and sixth days of week 25, whereas the fourth, fifth, and sixth days of week 51 are used to represent winter. The fourth, fifth, and sixth days of week 11 represent spring and fall, as the two seasons have similar load profiles. The total of 72-hour DCOPF problems is solved, and the returns for each GET owner are calculated using the Shapley value. We then use such results to approximate the annualized Shapley value (ASV) return of GETs. The results are shown in Tables V-VI.

TABLE V
SEASONAL AND ANNUALIZED RETURN RESULTS FOLLOWING AP1 IN THE 24-BUS SYSTEM

GET owner	1	2	3
72h return (Spring & Fall) ($k)	0.284	0.406	0.003
72h return (Summer) ($k)	45.582	86.818	0.590
72h return (Winter) ($k)	48.011	78.189	0.952
ASV ($M)	2.864	5.044	0.047

The returns under a regulated RoR are calculated based on the investment cost (IC). Therefore, to compare the payoffs of the proposed scheme and that of a regulated RoR, ICs for

TABLE VI
SEASONAL AND ANNUALIZED RETURN RESULTS FOLLOWING AP2 IN THE 24-BUS SYSTEM

GET owner	1	2	3
72h return (Spring & Fall) ($k)	0.170	0.261	0.261
72h return (Summer) ($k)	18.526	114.705	65.607
72h return (Winter) ($k)	36.268	183.278	95.995
ASV ($M)	1.677	9.080	4.931

GETs are calculated. The cost of VSC-FACTS device is set at $C^{\text{FACTS}} = \$150/\text{kVA}$ [2]. The ratings of the VSC-FACTS devices are calculated as follows [43]:

$$S_k^{\text{FACTS}} = V_k^{\text{FACTS}} \overline{I}_k. \tag{16}$$

The current in (16) can be approximated using the following DC power flow approximation in the per-unit system:

$$\overline{I}_k^{\text{pu}} = \overline{f}_k^{\text{pu}}. \tag{17}$$

Then, the current in the actual value is calculated using the following equation:

$$\overline{I}_k = \overline{I}_k^{\text{pu}} I^{\text{base}} = \overline{f}_k^{\text{pu}} S^{\text{base}} / V^{\text{base}}. \tag{18}$$

The IC of a VSC-FACTS device installed on line k is then calculated as follows:

$$C_k^{\text{FACTS}} = C^{\text{FACTS}} S_k^{\text{FACTS}} \tag{19}$$

Similarly, the calculation of the PST investment cost on line k is presented as follows [35]:

$$C_k^{\text{PST}} = C^{\text{PST}} S_k = \overline{f}_k C^{\text{PST}} \tag{20}$$

The value of C^{PST} are vastly different in previous studies [35], [44], varying from 10$/kVA to 100$/kVA. Therefore, we estimate the IC of PSTs in this paper using the CAISO project [45] as a reference. This project involves the deployment of a PST on an 800MVA-rated transmission line, with the installation cost estimated between $55M to $68M. The value of C^{PST} is set at 76.875$/kVA.

The IC of each GET deployment is shown in Table VII. Additionally, Table VII presents the annualized regulated revenue (ARR), assuming 10% regulated RoR [46] and an interest rate of 6%, provided to the GET owners. Previous studies have made various assumptions regarding the lifespan of the devices, varying from 5 to 30 years [35], [47]–[50]. The lifespan of devices is set at 15 years in this paper.

TABLE VII
INVESTMENT COST FROM GET OWNERS IN THE 24-BUS SYSTEM

GET owner	1	2	3
IC under AP1($M)	1.875	11.096	3.750
IC under AP2($M)	3.750	22.192	7.500
ARR under AP1($M)	0.212	1.257	0.424
ARR under AP2($M)	0.425	2.513	0.849

The comparison between the ARR and the annualized return under the proposed scheme for each GET deployment is presented in Fig 1 and Fig 2.

The results show a significant payoff increase under the proposed scheme compared to a regulated RoR for five of the six GET owners in the two cases. GET owner 3 in Case 1 receives a meager payoff as the GET deployment makes a minimal contribution to the cost savings. The results show that the payoffs are performance-based and are affected by the planning of GETs. The results will be further discussed in the following subsection.

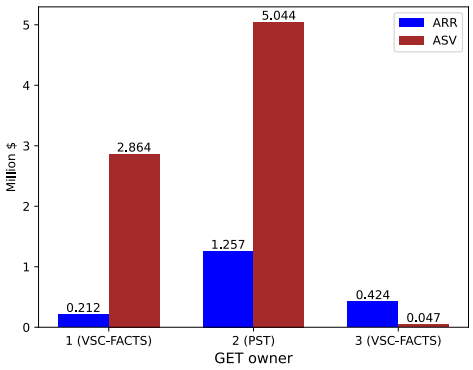

Fig. 1. Comparison between RoR and the proposed scheme under AP1 in the 24-bus system

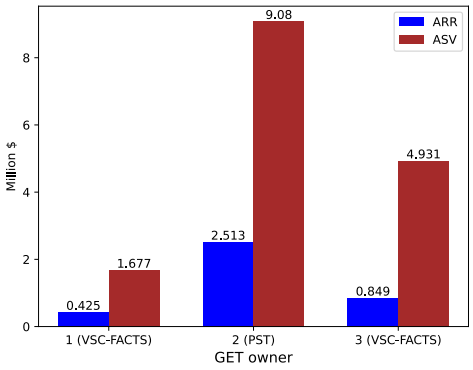

Fig. 2. Comparison between RoR and the proposed scheme under AP2 in the 24-bus system

2) IEEE 300-bus system: The proposed scheme is further studied with simulations conducted on a modified IEEE 300-bus system. In this case, we consider three GET owners, with their GET assets presented as follows:

- **GET owner 1**: Three VSC-FACTS devices deployed at lines 91, 182, and 358. Each device has a maximum voltage injection of 0.1 pu.
- **GET owner 2**: One VSC-FACTS device deployed at line 177 with a maximum voltage injection of 0.05 pu. Two VSC-FACTS devices deployed at lines 105 and 178, each

having a maximum voltage injection of 0.1 pu.

- **GET owner 3**: Two PSTs deployed at lines 83 and 180.

Note that the locations of GET deployments are selected following AP2, which is shown to be more effective in previous subsections.

The results of 72-hour returns and ASVs are shown in Table VIII, and the IC of each GET owner is presented in Table IX. The comparison between ASV and ARR is shown in Fig. 3.

TABLE VIII
SEASONAL AND ANNUALIZED RETURN RESULTS IN THE 300-BUS SYSTEM

GET owner	1	2	3
72h return (Spring & Fall) ($k)	284.853	125.488	112.744
72h return (Summer) ($k)	377.727	168.751	151.426
72h return (Winter) ($k)	432.178	183.468	170.853
ASV ($M)	41.963	18.347	16.661

TABLE IX
INVESTMENT COST FROM GET OWNERS IN THE 300-BUS SYSTEM

GET owner	1	2	3
IC($M)	5.625	6.563	22.192
ARR($M)	0.637	0.743	2.513

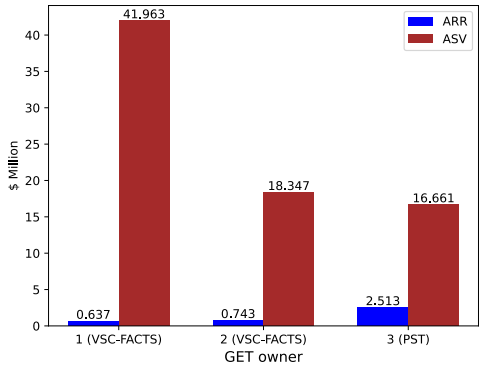

Fig. 3. Comparison between RoR and the proposed scheme in the 300-bus system

The results show that, for the IEEE 300-bus system, the proposed scheme provides massively more financial compensation to GET owners compared to the regulated RoR. The proposed scheme outperforms the regulated RoR even more for the IEEE RTS 24-bus system. This is mainly because of two reasons. First, the IEEE 300-bus system is much larger and has a higher value of flexibility congestion cost (FCC), at peak load hour, of $28,562 compared to the FCC of $15,464. The FCC is the cost reduction that can be achieved if all the DC power flow constraints are relaxed in DCOPF, essentially turning the transmission system into a transportation network. Second, the IEEE 300-bus system still has a fair level of congestion under light loading conditions. The IEEE RTS 24-bus system bears no congestion cost with a load factor of 0.6, whereas, under such circumstances, a congestion cost of $14,106 still exists for the IEEE 300-bus system. This allows the GET owners to get considerable returns for GET operations in the spring and fall seasons. The results further illustrate how the proposed scheme can effectively provide incentives for GET owners, as more financial returns can be achieved with their investments in a larger system with more congestion.

C. Discussions

1) Effectiveness of performance-based schemes: The comparisons between the proposed scheme and a regulated RoR emphasize the effectiveness of a performance-based method. The GET deployments contributing significantly to the cost savings will receive higher returns, and the proposed scheme is much more attractive than the RoR. However, the rewards are insignificant for devices that only marginally contribute to cost savings, e.g., the VSC-FACTS on line A25-1 under AP1 and the VSC-FACTS on line 23 under AP2 in the 24-bus system. The returns can be even less than a regulated RoR, if GET does not contribute much to system efficiency. Such results also emphasize the importance of adequately planning GET deployments. The case studies in this paper are all examples only involving power system operations. Rigorous planning studies should be conducted to determine the optimal allocations of GETs, and ineffective projects should be discarded. In other words, ineffective GETs in our simulation studies should not be built in the first place; the reason for their inclusion in simulation studies is to precisely show that the developed compensation method is able to correctly allocate little compensation to ineffective installations.

2) Planning flexibilities of GETs: The results show that the ASVs are much smaller in the spring and fall when the systems generally endure low congestion. This also means that GET assets are likely over-planned during these seasons. This issue can be addressed by the recent developments in the mobile deployments of FACTS devices [51], which provide even more operational flexibility. Mobile deployment can allow GET owners to gain even more payoffs during these seasons, as their devices can be redeployed to systems with a different congestion pattern or contribute to other projects, such as overload alleviation.

3) Market efficiency design: As mentioned in Section II, the proposed scheme resets the operating range of GET deployments when the operation constraints are not binding. This ensures that the Shapley value return is calculated based on the actual setpoint of the technologies rather than their full operating ranges. The results of the following numerical study illustrate the effectiveness of this step. Suppose in the IEEE RTS 24-bus system, the VSC-FACTS of GET owner 1 now has a maximum voltage injection of 0.1 pu. The difference in the payoffs provided by the improved Shapley value compared to the traditional Shapley value approach is shown in Fig. 4. The results reveal that if the traditional Shapley value approach is adopted, GET owner 1 can receive a payoff that almost doubles its contribution to the grand coalition with more investments. However, the extra investments only provide $0.006M social welfare positives. Essentially, the over-investment from GET owner 1, while providing minimal contributions to the surplus,

still grants a high RoR considering the IC. This is also hurting the interests of the other GET owners, as shown in Fig. 4. This reveals the potential market inefficiency of applying the traditional Shapley value.

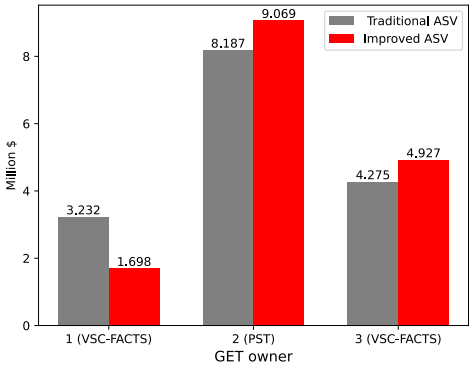

Fig. 4. Comparison between improved and traditional Shapley value methods

This design of the proposed scheme is essential to ensure proper planning for GET deployments. Investors and system operators will be inclined to plan GETs in sufficient yet not wasteful magnitudes. Furthermore, if the power flow or congestion pattern varies due to changes to the system, GET owners will intend to adjust their deployments, especially with the developments in the modular and relocatable design of the technologies, as mentioned previously.

4) Future directions: The proposed scheme allocates all social welfare changes to GET owners in the IDM. However, the percentage of the allocation could be different depending on the design of the incentive scheme. Additionally, the scheme presented in this paper does not consider one aspect of the benefit of GETs, which is cost savings related to the no-load and start-up costs of conventional generators in the DAM clearing process. Such topics will be further studied in future work. It is also worth noting that, as seen from (11), Shapley value calculation requires the characteristic functions for 2^n possible coalitions. This poses computational challenges to grid operation models, especially when the number of players is large. Proposals in the existing literature on improving computational efficiency focus on using sampling methods to estimate Shapley values [23], [52], [53]. Finding an efficient approach to calculate the Shapley value is beyond the scope of this paper and will be addressed in future work.

IV. Conclusion

The utilization of GETs in the power system is hindered by the lack of proper incentives both for their deployment and efficient operation. This paper presents a payoff scheme in the IDM based on the improved Shapley value to incentivize investments in GETs. The social welfare enhancements created by GET deployments are allocated to the GET owners as financial compensation for their investments. To improve market efficiency, the Shapley value is modified to accurately reflect the contributions of GETs deployments. The proposed scheme is analyzed through simulation studies conducted on the modified IEEE RTS 24-bus and 300-bus systems and compared with the returns under a regulated rate of return. The results show that a performance-based incentive scheme is highly effective in rewarding investments in GETs and, thus, can be expected to facilitate their deployments to enhance the utilization of the existing grid.

References

[1] M. Sahraei-Ardakani, "Merchant power flow controllers," *Energy Economics*, vol. 74, pp. 878–885, 2018.

[2] U.S. Department of Energy, "Grid Enhancing Technologies - A Case Study on Ratepayer Impact - February 2022," U.S. Department of Energy, 2022, Executive Summary. [Online]. Available: https://www.energy.gov/sites/default/files/2022-04/Grid%20Enhancing%20Technologies%20-%20A%20Case%20Study%20on%20Ratepayer%20Impact%20-%20February%202022%20CLEAN%20as%20of%20032322.pdf

[3] Jay Caspary, "The Role for Grid-Enhancing Technologies," January 2022, Accessed: 2023-07-25. [Online]. Available: https://www.esig.energy/the-role-for-grid-enhancing-technologies/

[4] D. E. Sappington and D. S. Sibley, "Regulating without cost information: The incremental surplus subsidy scheme," *International Economic Review*, pp. 297–306, 1988.

[5] P. Staudt and S. S. Oren, "Merchant transmission in single-price electricity markets with cost-based redispatch," *Energy Economics*, vol. 104, p. 105610, 2021.

[6] J. Contreras, G. Gross, J. M. Arroyo, and J. I. Muñoz, "An incentive-based mechanism for transmission asset investment," *Decision Support Systems*, vol. 47, no. 1, pp. 22–31, 2009.

[7] I. Vogelsang, "Can simple regulatory mechanisms realistically be used for electricity transmission investment? the case of hrgv," *Economics of Energy & Environmental Policy*, vol. 7, no. 1, pp. 63–88, 2018.

[8] D. Khastieva, S. Mohammadi, M. R. Hesamzadeh, and D. Bunn, "Optimal transmission investment with regulated incentives based upon forward considerations of firm and intermittent resources with batteries," *IEEE Transactions on Power Systems*, vol. 36, no. 5, pp. 4420–4434, 2021.

[9] M. R. Hesamzadeh, J. Rosellón, S. A. Gabriel, and I. Vogelsang, "A simple regulatory incentive mechanism applied to electricity transmission pricing and investment," *Energy Economics*, vol. 75, pp. 423–439, 2018.

[10] N. Mithulananthan and N. Acharya, "A proposal for investment recovery of FACTS devices in deregulated electricity markets," *Electric Power Systems Research*, vol. 77, no. 5-6, pp. 695–703, 2007.

[11] M. Sahraei-Ardakani and S. A. Blumsack, "Transfer capability improvement through market-based operation of series FACTS devices," *IEEE Transactions on Power Systems*, vol. 31, no. 5, pp. 3702–3714, 2015.

[12] W. W. Hogan, "Financial transmission rights: point-to point formulations," in *Financial Transmission Rights: Analysis, Experiences and Prospects*. Springer, 2012, pp. 1–48.

[13] V. Sarkar and S. A. Khaparde, "A comprehensive assessment of the evolution of financial transmission rights," *IEEE Transactions on Power Systems*, vol. 23, no. 4, pp. 1783–1795, 2008.

[14] X. Wang, Y. Song, Q. Lu, and Y. Sun, "Optimal allocation of transmission rights in systems with facts devices," *IEE Proceedings-Generation, Transmission and Distribution*, vol. 149, no. 3, pp. 359–366, 2002.

[15] F. Kunz, K. Neuhoff, and J. Rosellón, "Ftr allocations to ease transition to nodal pricing: An application to the german power system," *Energy Economics*, vol. 60, pp. 176–185, 2016.

[16] FERC, "Workshop to discuss certain performance-based ratemaking approaches," Accessed: 07-25-2023. [Online]. Available: https://www.ferc.gov/news-events/events/workshop-discuss-certain-performance-based-ratemaking-approaches-09102021

[17] WATT Coalition, "FERC Deep Dive on Performance Incentives Raises Few Challenges, No Alternatives," accessed: 08-01-2023. [Online]. Available: https://watt-transmission.org/ferc-deep-dive-on-performance-incentives-raises-few-challenges-no-alternatives/

[18] WATT Coalition, "Frequently Asked Questions about a shared savings incentive for Grid Enhancing Technologies," 2022, Accessed: 2023-07-25. [Online]. Available: https://watt-transmission.org/resources-2/shared-savings-faq/

[19] Smart Wires Inc., "SmartValve™," 2022, accessed: 2022-07-10. [Online]. Available: https://www.smartwires.com/smartvalve/

[20] Siemens Energy, "UPFC PLUS," last accessed 6 February 2023. [Online]. Available: https://assets.siemens-energy.com/siemens/assets/api/uuid:c1fb5690-e885-4c7c-972d-a2449fded8ac/two-pager-layout-se.pdf?ste_sid=67453f9c227e7d13f675ea824b9d3cd4

[21] L. S. Shapley, "Cores of convex games," *International journal of game theory*, vol. 1, pp. 11–26, 1971.

[22] A. A. Raja and S. Grammatico, "Online coalitional games for real-time payoff distribution with applications to energy markets," *IEEE Transactions on Energy Markets, Policy and Regulation*, 2023.

[23] G. O'Brien, A. El Gamal, and R. Rajagopal, "Shapley value estimation for compensation of participants in demand response programs," *IEEE Transactions on Smart Grid*, vol. 6, no. 6, pp. 2837–2844, 2015.

[24] I. T. Emami, H. A. Abyaneh, H. Zareipour, and A. Bakhshai, "A novel simulation-based method for assessment of collusion potential in wholesale electricity markets," *Sustainable Energy, Grids and Networks*, vol. 24, p. 100405, 2020.

[25] R. Oleksijs, A. Sauhats, and B. Olekshii, "Generator cooperation in district heating market considering open electricity market," in *2020 IEEE 61th International Scientific Conference on Power and Electrical Engineering of Riga Technical University (RTUCON)*. IEEE, 2020, pp. 1–6.

[26] P. Rathore, G. Agnihotri, B. Khan, and G. Naidu, "Transmission usage and cost allocation using shapley value and tracing method: A comparison," *Electrical and Electronics Engineering: An International Journal (ELELIJ)*, vol. 3, pp. 11–29, 2014.

[27] M. Kristiansen, F. D. Muñoz, S. Oren, and M. Korpås, "A mechanism for allocating benefits and costs from transmission interconnections under cooperation: A case study of the north sea offshore grid," *The Energy Journal*, vol. 39, no. 6, 2018.

[28] F. Fang, S. Yu, and M. Liu, "An improved shapley value-based profit allocation method for chp-vpp," *Energy*, vol. 213, p. 118805, 2020.

[29] D. Rashmi and S. Sivasubramani, "A game theoretic approach for profit allocation considering dg and facts devices," in *2021 IEEE 2nd International Conference on Smart Technologies for Power, Energy and Control (STPEC)*. IEEE, 2021, pp. 1–6.

[30] T. Ding, R. Bo, F. Li, and H. Sun, "Optimal power flow with the consideration of flexible transmission line impedance," *IEEE Transactions on Power Systems*, vol. 31, no. 2, pp. 1655–1656, 2015.

[31] M. Sahraei-Ardakani and K. W. Hedman, "Day-ahead corrective adjustment of FACTS reactance: A linear programming approach," *IEEE Transactions on Power Systems*, vol. 31, no. 4, pp. 2867–2875, 2015.

[32] ——, "A fast LP approach for enhanced utilization of variable impedance based FACTS devices," *IEEE Transactions on Power Systems*, vol. 31, no. 3, pp. 2204–2213, 2015.

[33] X. Rui, M. Sahraei-Ardakani, and T. R. Nudell, "Linear modelling of series FACTS devices in power system operation models," *IET Generation, Transmission & Distribution*, vol. 16, no. 6, pp. 1047–1063, 2022.

[34] X. Rui and M. Sahraei-Ardakani, "A successive flow direction enforcing algorithm for optimal operation of variable-impedance FACTS devices," *Electric Power Systems Research*, vol. 211, p. 108171, 2022.

[35] X. Zhang, D. Shi, Z. Wang, B. Zeng, X. Wang, K. Tomsovic, and Y. Jin, "Optimal allocation of series FACTS devices under high penetration of wind power within a market environment," *IEEE Transactions on Power Systems*, vol. 33, no. 6, pp. 6206–6217, 2018.

[36] F. Pourahmadi, M. Fotuhi-Firuzabad, and P. Dehghanian, "Application of game theory in reliability-centered maintenance of electric power systems," *IEEE Transactions on Industry Applications*, vol. 53, no. 2, pp. 936–946, 2016.

[37] C. Grigg, P. Wong, P. Albrecht, R. Allan, M. Bhavaraju, R. Billinton, Q. Chen, C. Fong, S. Haddad, S. Kuruganty *et al.*, "The IEEE reliability test system-1996. a report prepared by the reliability test system task force of the application of probability methods subcommittee," *IEEE Transactions on Power Systems*, vol. 14, no. 3, pp. 1010–1020, 1999.

[38] Department of Electrical Engineering, University of Washington. Power systems test case archive. [Online]. Available: http://labs.ece.uw.edu/pstca/pf300/pg_tca300bus.htm

[39] Y. Sang, M. Sahraei-Ardakani, and M. Parvania, "Stochastic transmission impedance control for enhanced wind energy integration," *IEEE Transactions on Sustainable Energy*, vol. 9, no. 3, pp. 1108–1117, 2017.

[40] S. Babaeinejadsarookolaee, A. Birchfield, R. D. Christie, C. Coffrin, C. DeMarco, R. Diao, M. Ferris, S. Fliscounakis, S. Greene, R. Huang *et al.*, "The power grid library for benchmarking AC optimal power flow algorithms," *arXiv preprint arXiv:1908.02788*, 2019.

[41] S. Diamond and S. Boyd, "CVXPY: A Python-embedded modeling language for convex optimization," *Journal of Machine Learning Research*, 2016, to appear. [Online]. Available: https://stanford.edu/~boyd/papers/pdf/cvxpy_paper.pdf

[42] Y. Sang and M. Sahraei-Ardakani, "The interdependence between transmission switching and variable-impedance series facts devices," *IEEE Transactions on Power Systems*, vol. 33, no. 3, pp. 2792–2803, 2017.

[43] N. G. Hingorani and L. Gyugyi, *FACTS Concept and General System Considerations*, 2000, pp. 1–35.

[44] A. L. Ara, A. Kazemi, and M. Behshad, "Improving power systems operation through multiobjective optimal location of optimal unified power flow controller," *Turkish journal of Electrical Engineering and Computer sciences*, vol. 21, no. 7, pp. 1893–1908, 2013.

[45] CAISO, "APPENDIX F: Description and Functional Specifications for Transmission Facilities Eligible for Competitive Solicitation," February 2014, accessed: 07-30-2023. [Online]. Available: https://www.caiso.com/Documents/AppendixFDraft2013-2014TransmissionPlan.pdf

[46] "The mechanics of rate of return regulation," accessed: 07-31-2023. [Online]. Available: https://www.e-education.psu.edu/eme801/node/531

[47] I. Zunnurain, Y. Sang, P. Mandal, M. Velez-Reyes, and J. Espiritu, "Improving the resilience of large-scale power systems using distributed static series compensators," *International Journal of Electrical Power & Energy Systems*, vol. 145, p. 108702, 2023.

[48] A. C. Bekkala, "Analysis and synthesis of smart wires in an electric power system," Ph.D. dissertation, University of Minnesota, 2018.

[49] F. B. Alhasawi and J. V. Milanovic, "Techno-economic contribution of facts devices to the operation of power systems with high level of wind power integration," *IEEE Transactions on Power Systems*, vol. 27, no. 3, pp. 1414–1421, 2012.

[50] A. Alabduljabbar and J. Milanović, "Assessment of techno-economic contribution of facts devices to power system operation," *Electric Power Systems Research*, vol. 80, no. 10, pp. 1247–1255, 2010.

[51] K. F. Krommydas, A. C. Stratigakos, C. N. Dikaiakos, G. P. Papaioannou, M. G. Jones, and G. C. McLoughlin, "A novel modular mobile power flow controller for real-time congestion management tested on a 150kv transmission system," *IEEE Access*, vol. 10, pp. 96 414–96 426, 2022.

[52] Q. Yu, J. Xie, X. Chen, K. Yu, L. Gan, and L. Chen, "Loss allocation for radial distribution networks including dgs using shapley value sampling estimation," *IET Generation, Transmission & Distribution*, vol. 13, no. 8, pp. 1382–1390, 2019.

[53] S. Maleki, "Addressing the computational issues of the shapley value with applications in the smart grid," Ph.D. dissertation, University of Southampton, 2015.

Xinyang Rui Xinyang Rui received his M.Sc. in Electrical Engineering from the University of Kansas. He is currently a Ph.D. candidate in the Department of Electrical and Computer Engineering at the University of Utah. His research interests include power system operation and planning, electricity markets, and grid-enhancing technologies.

Omid Mirzapour Omid Mirzapour received both B.Sc. and M.Sc. in Electrical Engineering from Sharif University of Technology. Since 2019 he has been pursuing a Ph.D. degree in the Department of Electrical and Computer Engineering at the University of Utah. His research is focused on market-based incentives for deployment of grid-enhancing technologies.

Mostafa Ardakani is an associate professor in the department of electrical and computer engineering at the University of Utah. His research focuses on power systems optimization, power systems resilience, interdependent infrastructure networks, energy economics and policy, and energy justice. Dr. Sahraei-Ardakani holds a Ph.D. degree in Energy Engineering from the Pennsylvania State University as well as a B.S. and an M.S. degree in Electrical Engineering from University of Tehran. Prior to joining the University of Utah, he worked as a postdoctoral scholar at Arizona State University. Dr. Ardakani is a recipient of 2022 NSF CAREER award.

CHAPTER 10

A REVENUE-ADEQUATE MARKET DESIGN FOR GETS

GETs are expected to be vital for upgrading the transmission system to accommodate higher levels of penetration from RES. Proper financial incentives are key to facilitating the deployment of GETs. This chapter presents a market model based on co-optimizing GET setpoints alongside generation dispatch in power system operation. The dual variables associated with GET constraints serve as the marginal price for GET operation. GET owners receive payments based on this marginal price and GET setpoints. A proof of revenue adequacy for the proposed market design is presented. Simulation studies on two IEEE test cases show that the market design is effective in rewarding efficient GET operation and results in payments that are substantially higher than those from a regulated rate of return. The results suggest that the adoption of a market design, similar to what is presented in this chapter, for GETs can lead to proliferation and bring unprecedented levels of efficiency to transmission network utilization.

10.1 Introduction

The transmission system needs upgrades to alleviate congestion and accommodate the increasing penetration from RES. GETs provide an efficient alternative to constructing new transmission lines to enhance the grid's transfer capability. GETs include a range of hardware and software tools that improve the utilization of the existing system [25]. Prominent examples of GETs include FACTS devices, PSTs, DLR, and TS [14]. These technologies can alter key transmission parameters and alleviate transmission system constraints to facilitate more cost-efficient generation dispatch and pave the way for a cleaner electricity sector with reduced carbon emission [13].

Despite the relative maturity of the technology, GET adoption remains rather limited [20]. One of the significant obstacles hindering GET deployments is the lack of proper

financial incentives. GETs are currently treated as a part of a regulated monopoly transmission network. Similar to any other prudent transmission investment, GETs will also receive a regulated RoR. This structure creates a preference towards larger projects, from the investor's perspective, negatively affecting GET deployment [11, 16].

To overcome this challenge, several performance-based incentive mechanisms have been proposed to incentivize GET investments. One method proposed to allocate financial transmission rights (FTRs) to GET investors [20]. The FTRs would enable the investors to collect market-based payments or trade the allocated rights in long-term markets, including FTR auctions and secondary markets [18]. However, the FTR's downside is the loose link between the revenue allocation and real-time operation of GETs in the short-term markets. Therefore, there will be a need for additional processes to ensure efficient operation in real time.

The second key approach is to reward transmission investments with the benefits they create. Previous studies have proposed such an approach as a performance-based incentive for transmission expansion projects [10, 4]. However, proposals regarding GET investments are relatively limited. In [15], FACTS investments are rewarded with surplus increases they create. One major proposal regarding the GET incentives is the shared-savings incentives proposed by the WATT Coalition [26] in recent years. Under this proposal, asset owners receive a portion of the savings created by GET deployments. Ref. [15] presents a method that uses the benefits of FACTS operation as financial compensation for investments, with benefits measured by changes in generation and demand surpluses, as well as congestion rent. A clear drawback of such proposed methods is that a base case solution, without considering GETs, is required to calculate the savings generated by GETs, which can lead to extra computational burden. Moreover, the allocation of savings to multiple GETs may not be straightforward.

A third approach is to calculate a marginal price signal for transmission projects based on the dual solution of power system operation problems. Transmission infrastructure is viewed as a resource, and the dual variables serve as measurements of marginal value. An example of this approach is the use of flowgate marginal price (FMP) to compensate transmission companies [2, 17, 9]. A proposal for GETs is presented in [21], where the authors use the dual variable associated with the DC power flow equation, referred to as the

susceptance price, to compute a price signal for variance-impedance FACTS devices. The approach is computationally efficient and straightforward. However, a major drawback is that revenue adequacy cannot be guaranteed.

Co-optimizing GET operations with generation dispatch is essential for the full realization of their benefits. Various modeling techniques are developed in the literature that facilitate the integration of GETs into power system operation models [19]. These models must be included in energy and market management systems (EMS/MMS) to adjust GET setpoints and incorporate their influence in the market-clearing process. Therefore, a desirable approach would be to calculate a price signal for GETs alongside the locational marginal price, which is used to settle generation revenue and load payment. This chapter fills the research gap by proposing a market design for two main types of GETs: VSC-based series FACTS and PSTs. The proposed market design rewards asset owners based on a price signal. This price is obtained from the dual solution of DCOPF, co-optimizing GET operation, and measures the marginal value of GET operations. The DCOPF model in this chapter fully considers the operation constraints of GETs. The approach leading to the proposed market design can be demonstrated by Fig 10.1.

The main contributions of this chapter are summarized as follows:

1. To incentivize efficient GET investments and optimal operations, this chapter proposes a market design that provides payoffs to GET owners based on marginal prices associated with GET revenue constraints. It allows full market integration of GET operations by settling the payoffs simultaneously with other payments for generation, load, and transmission.

2. Revenue adequacy of the proposed market design is proved by showing that the total congestion rent is sufficient to cover GETs payments and prior transmission commitments.

This chapter considers prominent GETs that provide power flow control capabilities with linear models. Linear GET models are compatible with the existing market operation software, making the implementation straightforward. The proposed market design aligns incentives with performance, where every profitable investment will require efficient planning and operation.

10.2 Market Design

Based on the linear modeling presented in the previous section, the DCOPF problem with ISFs considering GET operation is formulated as follows:

P0 :

$$\text{minimize } \mathbf{c}^{\mathrm{T}}\mathbf{p} \tag{10.1}$$

s.t.

$$\mathbf{p}^{\min} \leq \mathbf{p} \leq \mathbf{p}^{\max}, \qquad (\boldsymbol{\alpha}^{-}, \boldsymbol{\alpha}^{+}) \tag{10.2}$$

$$\mathbf{f} = \boldsymbol{\Phi}(\boldsymbol{\Gamma}\mathbf{p} - \mathbf{d} - \mathbf{A}^{\mathrm{T}}\boldsymbol{\Psi}\boldsymbol{\Delta}\mathbf{f}), \qquad (\boldsymbol{\sigma}) \tag{10.3}$$

$$-\mathbf{f}^{\max} \leq \mathbf{f} + \boldsymbol{\Psi}\boldsymbol{\Delta}\mathbf{f} \leq \mathbf{f}^{\max}, \qquad (\boldsymbol{\beta}^{-}, \boldsymbol{\beta}^{+}) \tag{10.4}$$

$$\mathbf{1}_g^{\mathrm{T}}\mathbf{p} - \mathbf{1}_n^{\mathrm{T}}\mathbf{d} = 0, \qquad (\lambda) \tag{10.5}$$

$$-\boldsymbol{\Delta}\mathbf{f}^{\max} \leq \boldsymbol{\Delta}\mathbf{f} \leq \boldsymbol{\Delta}\mathbf{f}^{\max}, \qquad (\boldsymbol{\tau}^{-}, \boldsymbol{\tau}^{+}) \tag{10.6}$$

The vectors shown in parenthesis are the dual variables associated with the corresponding constraints. Details of certain matrices in P0 are shown in Appendix A. The objective function (10.1) minimizes the total production cost. Constraints on generating unit outputs are presented in (10.2). The impact of nodal power injection on power flows is calculated using ISFs as shown in (10.3). Eqn. (10.4) enforces the thermal capacity constraints on transmission lines. System-wide power flow balance is shown in (10.5). Finally, GET operating ranges are shown in (10.6).

Dual variables $\boldsymbol{\tau}^{-}$ and $\boldsymbol{\tau}^{+}$ can be used as marginal prices for GETs, and they measure the marginal amount of savings in total production cost achieved by changing the GET operating limits, shown in (10.6), by incremental increases. Therefore, in the proposed market design, the GET revenues are formulated as follows:

$$GR_i = ({\tau^{+}}_i^{*} - {\tau^{+}}_i^{*})\Delta f_i^{*}, \tag{10.7}$$

$$TGR = \sum GR_i = (\boldsymbol{\tau}^{+^{*}} - \boldsymbol{\tau}^{-^{*}})^{\mathrm{T}}\boldsymbol{\Delta}\mathbf{f}^{*}. \tag{10.8}$$

Note that the $*$ denotes optimality. Eqn. (10.7) is consistent with the market clearing process with DCOPF, where marginal prices are utilized for settling payments. The formu-

lation of GET revenues has some desirable properties presented with the lemmas below.

Lemma 1: GET revenues are non-negative.

Proof: According to complementary slackness, for GET deployment i, the following equations can be derived:

$$\tau^{+*}_i(\Delta f^*_i - \Delta f^{\max}_i) = 0, \tag{10.9}$$

$$\tau^{-*}_i(\Delta f^{\max}_i + \Delta f^*_i) = 0. \tag{10.10}$$

Therefore, (10.7)-(10.8) can be alternatively shown as:

$$GR_i = (\tau^{+*}_i + \tau^{-*}_i)\Delta f^{\max}_i, \tag{10.11}$$

$$TGR = (\boldsymbol{\tau}^{+*} + \boldsymbol{\tau}^{-*})^{\mathrm{T}}\boldsymbol{\Delta}\mathbf{f}^{\max}. \tag{10.12}$$

Additionally, dual feasibility states that:

$$\tau^{+*}_i \geq 0, \tag{10.13}$$

$$\tau^{-*}_i \geq 0. \tag{10.14}$$

Therefore, using the equations above, GET revenues satisfy the following inequalities:

$$GR_i \geq 0, \tag{10.15}$$

$$TGR \geq 0. \tag{10.16}$$

Lemma 1 is, thus, proved.

Lemma 2: GR_i is zero when GET operating constraint of deployment i is not binding.

Proof: If (10.6) is not binding for GET deployment i, then based on (10.9)-(10.10), we have:

$$\tau^{+*}_i = \tau^{-*}_i = 0, \tag{10.17}$$

$$GR_i = 0. \tag{10.18}$$

Lemma 2 means GETs not operating at limits do not collect payments. This is justified as GETs have zero or negligible operating costs. GETs not operating at a limit implies that the assets do not contribute to congestion reduction and, thus, are not valuable in that particular system state. Therefore, the asset should not collect payment. Only in such circumstances will a GET installation receive a non-zero payment. Only when the asset is operating at a limit can we conclude that it has contributed to an efficient dispatch

and additional capacity would be desired. This property of the proposed market design helps to ensure market efficiency regarding GET planning, as redundant investment in GET deployments likely results in zero payoffs.

Lemma 3: GET revenues will not exceed the savings created by GET operations.

Proof: Consider the following optimization problem:

$$\text{P1}:$$

$$\text{minimize } \mathbf{c}^{\mathrm{T}}\mathbf{p} \tag{10.19}$$

$$\text{s.t.}$$

$$(10.2), (10.3), (10.4), (10.5)$$

$$-\mathbf{0} \leq \boldsymbol{\Delta} f \leq \mathbf{0}, \qquad (\boldsymbol{\tau}_1^-, \boldsymbol{\tau}_1^+) \tag{10.20}$$

P1 is equivalent to a base case DCOPF that does not include GETs. The LaGrange dual problems of P0 and P1 are presented as follows:

$$\tilde{\text{P0}}:$$

$$\begin{aligned}\text{maximize } q(\gamma) = &-\boldsymbol{\alpha}^{+\mathrm{T}}\mathbf{p}^{\max} + \boldsymbol{\alpha}^{-\mathrm{T}}\mathbf{p}^{\min} + \sigma^{\mathrm{T}}\boldsymbol{\Phi}\mathbf{d} \\ &- \lambda\mathbf{1}_n^{\mathrm{T}}\mathbf{d} - \boldsymbol{\beta}^{+\mathrm{T}}\mathbf{f}^{\max} - \boldsymbol{\beta}^{-\mathrm{T}}\mathbf{f}^{\max} \\ &- \boldsymbol{\tau}^{+\mathrm{T}}\boldsymbol{\Delta}\mathbf{f}^{\max} - \boldsymbol{\tau}^{-\mathrm{T}}\boldsymbol{\Delta}\mathbf{f}^{\max}\end{aligned} \tag{10.21}$$

$$\text{s.t.}$$

$$(\boldsymbol{\alpha}^- - \boldsymbol{\alpha}^+) - \boldsymbol{c} + \boldsymbol{\Gamma}^{\mathrm{T}}\boldsymbol{\Phi}^{\mathrm{T}}\sigma - \lambda\mathbf{1}_g \leq \mathbf{0} \tag{10.22}$$

$$(\boldsymbol{\beta}^+ - \boldsymbol{\beta}^-) + \sigma = \mathbf{0} \tag{10.23}$$

$$\boldsymbol{\Psi}^{\mathrm{T}}(\boldsymbol{\beta}^+ - \boldsymbol{\beta}^-) + \boldsymbol{\Psi}^{\mathrm{T}}\mathbf{A}\boldsymbol{\Phi}^{\mathrm{T}}\sigma + (\boldsymbol{\tau}^+ - \boldsymbol{\tau}^-) = \mathbf{0} \tag{10.24}$$

$$
\begin{aligned}
&\tilde{\text{P}}1: \\
&\text{maximize } q_1(\gamma) = -{\boldsymbol{\alpha}^+}^{\text{T}}\mathbf{p}^{\max} + {\boldsymbol{\alpha}^-}^{\text{T}}\mathbf{p}^{\min} + \boldsymbol{\sigma}^{\text{T}}\boldsymbol{\Phi}\mathbf{d} \\
&- \lambda\mathbf{1}_n^{\text{T}}\mathbf{d} - {\boldsymbol{\beta}^+}^{\text{T}}\mathbf{f}^{\max} - {\boldsymbol{\beta}^-}^{\text{T}}\mathbf{f}^{\max} \\
&\text{s.t.} \\
&(10.22), (10.23), (10.24).
\end{aligned} \tag{10.25}
$$

In the two optimization problems shown above, $q(\cdot)$ and $q_1(\cdot)$ denote the dual objectives and γ represents the dual variables. Let γ^* and γ_1^* represent the sets of dual variables of P0 and P1 at optimality, respectively. Based on strong duality, the savings can be derived using the difference between the dual optimal objectives of P0 and P1. Therefore, Lemma 3 can be equivalently presented as the following inequality:

$$TGR = ({\boldsymbol{\tau}^+}^* + {\boldsymbol{\tau}^-}^*)^{\text{T}}\boldsymbol{\Delta}\mathbf{f}^{\max} \leq q_1(\gamma_1^*) - q(\gamma^*). \tag{10.26}$$

To prove (10.26), we first further derive its right-hand side as:

$$q_1(\gamma_1^*) - q_1(\gamma^*) + ({\boldsymbol{\tau}^+}^* + {\boldsymbol{\tau}^-}^*)^{\text{T}}\boldsymbol{\Delta}\mathbf{f}^{\max}. \tag{10.27}$$

Therefore, Lemma 3 can be proved if the following inequality holds:

$$q_1(\gamma^*) \leq q_1(\gamma_1^*). \tag{10.28}$$

As shown in the problem formulations, $\tilde{\text{P}}1$ and $\tilde{\text{P}}0$ share the same constraints and, thus, the same feasible region. Therefore, $\gamma*$ is within the feasible region of $\tilde{\text{P}}1$. Additionally, $\tilde{\text{P}}1$ is a maximization problem with γ_1^* being the optimal solution. Therefore, (10.28) is proved, which also proves Lemma 3. Lemma 3 ensures that the proposed market design does not *over-compensate* GET operations.

10.3 Revenue adequacy

Revenue adequacy implies that GET revenues in the market can be settled among participants without side payments. A mathematical proof of revenue adequacy is presented in this section to show that the congestion rent can cover the total GET revenue under the proposed market design.

The following equation can be formulated based on strong duality:

$$q(\gamma^*) = \mathbf{c}^{\mathrm{T}}\mathbf{p}^*. \tag{10.29}$$

For the rest of this section, mathematical derivations are based on optimal solutions of the primal and dual problems, and the $*$ sign is omitted for simplicity. LMPs are presented as follows:

$$\tilde{\boldsymbol{\lambda}}^{\mathrm{T}} = \boldsymbol{\sigma}^{\mathrm{T}}\boldsymbol{\Phi} - \lambda\mathbf{1}_n^{\mathrm{T}}. \tag{10.30}$$

Eqn. (10.29) can be reformulated to:

$$\begin{aligned} &\boldsymbol{\sigma}^{\mathrm{T}}\boldsymbol{\Phi}\mathbf{d} - \lambda\mathbf{1}_n^{\mathrm{T}}\mathbf{d} - (\mathbf{c}^{\mathrm{T}}\mathbf{p} + \boldsymbol{\alpha}^{+\mathrm{T}}\mathbf{p}^{\max} - \boldsymbol{\alpha}^{-\mathrm{T}}\mathbf{p}^{\min}) \\ &= \boldsymbol{\beta}^{+\mathrm{T}}\mathbf{f}^{\max} + \boldsymbol{\beta}^{-\mathrm{T}}\mathbf{f}^{\max} + \boldsymbol{\tau}^{+\mathrm{T}}\boldsymbol{\Delta}\mathbf{f}^{\max} + \boldsymbol{\tau}^{-\mathrm{T}}\boldsymbol{\Delta}\mathbf{f}^{\max}. \end{aligned} \tag{10.31}$$

Based on complementary slackness, the right-hand side of (10.31) is further reformulated as:

$$(\boldsymbol{\beta}^+ - \boldsymbol{\beta}^-)^{\mathrm{T}}(\mathbf{f} + \boldsymbol{\Psi}\boldsymbol{\Delta}\mathbf{f}) + (\boldsymbol{\tau}^+ - \boldsymbol{\tau}^-)^{\mathrm{T}}\boldsymbol{\Delta}\mathbf{f}. \tag{10.32}$$

The KKT conditions of P2 implies that:

$$\frac{\partial\mathcal{L}}{\partial\boldsymbol{p}} = (\boldsymbol{\alpha}^+ - \boldsymbol{\alpha}^-) + \boldsymbol{c} - \boldsymbol{\Gamma}^{\mathrm{T}}\boldsymbol{\Phi}^{\mathrm{T}}\boldsymbol{\sigma} + \lambda\mathbf{1}_g = 0. \tag{10.33}$$

Then, we have the following equation:

$$\boldsymbol{p}^{\mathrm{T}}(\boldsymbol{\Gamma}^{\mathrm{T}}\boldsymbol{\Phi}^{\mathrm{T}}\boldsymbol{\sigma} - \lambda\mathbf{1}_g) = \boldsymbol{p}^{\mathrm{T}}(\boldsymbol{\alpha}^+ - \boldsymbol{\alpha}^- + \boldsymbol{c}) = \mathbf{c}^{\mathrm{T}}\mathbf{p} + \boldsymbol{\alpha}^{+\mathrm{T}}\mathbf{p}^{\max} - \boldsymbol{\alpha}^{-\mathrm{T}}\mathbf{p}^{\min} \tag{10.34}$$

Generator revenue can be, then, derived as:

$$\begin{aligned} &(\boldsymbol{\Gamma}\boldsymbol{p})^{\mathrm{T}}(\boldsymbol{\sigma}^{\mathrm{T}}\boldsymbol{\Phi} - \lambda\mathbf{1}_n^{\mathrm{T}})^{\mathrm{T}} = \boldsymbol{p}^{\mathrm{T}}\boldsymbol{\Gamma}^{\mathrm{T}}\boldsymbol{\Phi}^{\mathrm{T}}\boldsymbol{\sigma} - \lambda\boldsymbol{p}^{\mathrm{T}}\boldsymbol{\Gamma}^{\mathrm{T}}\mathbf{1}_n \\ &= \boldsymbol{p}^{\mathrm{T}}(\boldsymbol{\Gamma}^{\mathrm{T}}\boldsymbol{\Phi}^{\mathrm{T}}\boldsymbol{\sigma} - \lambda\mathbf{1}_g) = \mathbf{c}^{\mathrm{T}}\mathbf{p} + \boldsymbol{\alpha}^{+\mathrm{T}}\mathbf{p}^{\max} - \boldsymbol{\alpha}^{-\mathrm{T}}\mathbf{p}^{\min} \end{aligned} \tag{10.35}$$

Therefore, (10.31) can be rewritten as:

$$\mathbf{d}^{\mathrm{T}}\tilde{\boldsymbol{\lambda}} - (\boldsymbol{\Gamma}\boldsymbol{p})^{\mathrm{T}}\tilde{\boldsymbol{\lambda}} = (\boldsymbol{\beta}^+ - \boldsymbol{\beta}^-)^{\mathrm{T}}(\mathbf{f} + \boldsymbol{\Psi}\boldsymbol{\Delta}\mathbf{f}) + (\boldsymbol{\tau}^+ - \boldsymbol{\tau}^-)^{\mathrm{T}}\boldsymbol{\Delta}\mathbf{f}. \tag{10.36}$$

Additionally, the total congestion rent (TCR) is formulated as follows:

$$
\begin{aligned}
TCR &= \tilde{\lambda}\mathbf{A}^{\mathrm{T}}(\mathbf{f}+\mathbf{\Psi}\mathbf{\Delta f}) = -(\sigma^{\mathrm{T}}\mathbf{\Phi}-\lambda\mathbf{1}_n^{\mathrm{T}})\mathbf{A}^{\mathrm{T}}(\mathbf{f}+\mathbf{\Psi}\mathbf{\Delta f}) \\
&= -\sigma^{\mathrm{T}}\mathbf{\Phi}\mathbf{A}^{\mathrm{T}}(\mathbf{f}+\mathbf{\Psi}\mathbf{\Delta f}) = [(\boldsymbol{\beta}^{+}-\boldsymbol{\beta}^{-})^{\mathrm{T}}\mathbf{\Psi}+(\boldsymbol{\tau}^{+}-\boldsymbol{\tau}^{-})^{\mathrm{T}}]\mathbf{\Delta f}-\sigma^{\mathrm{T}}\mathbf{\Phi}\mathbf{A}^{\mathrm{T}}\mathbf{f} \\
&= [(\boldsymbol{\beta}^{+}-\boldsymbol{\beta}^{-})^{\mathrm{T}}\mathbf{\Psi}+(\boldsymbol{\tau}^{+}-\boldsymbol{\tau}^{-})^{\mathrm{T}}]\mathbf{\Delta f}-\sigma^{\mathrm{T}}\mathbf{\Phi}\mathbf{A}^{\mathrm{T}}\mathbf{\Phi}(\mathbf{\Gamma p}-\mathbf{d}-\mathbf{A}^{\mathrm{T}}\mathbf{\Psi}\mathbf{\Delta f}) \\
&= [(\boldsymbol{\beta}^{+}-\boldsymbol{\beta}^{-})^{\mathrm{T}}\mathbf{\Psi}+(\boldsymbol{\tau}^{+}-\boldsymbol{\tau}^{-})^{\mathrm{T}}]\mathbf{\Delta f}-\sigma^{\mathrm{T}}\mathbf{\Phi}(\mathbf{\Gamma p}-\mathbf{d}-\mathbf{A}^{\mathrm{T}}\mathbf{\Psi}\mathbf{\Delta f}) \\
&= [(\boldsymbol{\beta}^{+}-\boldsymbol{\beta}^{-})^{\mathrm{T}}\mathbf{\Psi}+(\boldsymbol{\tau}^{+}-\boldsymbol{\tau}^{-})^{\mathrm{T}}]\mathbf{\Delta f}-\sigma^{\mathrm{T}}\mathbf{f} \\
&= [(\boldsymbol{\beta}^{+}-\boldsymbol{\beta}^{-})^{\mathrm{T}}\mathbf{\Psi}+(\boldsymbol{\tau}^{+}-\boldsymbol{\tau}^{-})^{\mathrm{T}}]\mathbf{\Delta f}+(\boldsymbol{\beta}^{+}-\boldsymbol{\beta}^{-})^{\mathrm{T}}\mathbf{f} \\
&= (\boldsymbol{\beta}^{+}-\boldsymbol{\beta}^{-})^{\mathrm{T}}(\mathbf{f}+\mathbf{\Psi}\mathbf{\Delta f})+(\boldsymbol{\tau}^{+}-\boldsymbol{\tau}^{-})^{\mathrm{T}}\mathbf{\Delta f}
\end{aligned}
\tag{10.37}
$$

The derivation of (10.37) uses Lemma 4, which is shown below, along with its proof.

Lemma 4: the following equation regarding the ISF matrix and the incidence matrix holds:

$$\mathbf{\Phi}\mathbf{A}^{\mathrm{T}}\mathbf{\Phi} = \mathbf{\Phi}. \tag{10.38}$$

Proof: Lemma 4 is proved if the following equation holds:

$$\mathbf{\Phi}^{\mathrm{T}}\mathbf{A}\mathbf{\Phi}^{\mathrm{T}} = \mathbf{\Phi}^{\mathrm{T}}. \tag{10.39}$$

Let $|N|$ and $|K|$ denote the total number of buses and branches in the system, respectively. Bus $|N|$ is set as the reference bus without losing genericity. Then, by definition, $\mathbf{\Phi}$ is presented as follows:

$$\mathbf{\Phi}_{|K|\times|N|} = \left[\begin{array}{c:c} \mathbf{\Phi'}_{|K|\times(|N|-1)} & \mathbf{0} \end{array}\right], \tag{10.40}$$

where $\mathbf{\Phi}'$ is the reduced ISF matrix developed by removing column $|N|$ of $\mathbf{\Phi}$. Elements in column $|N|$ of $\mathbf{\Phi}$, which is the column associated with the reference bus, are all zeroes as shown in (10.40). Based on DC power flow, matrix $\mathbf{\Phi'}$ is calculated using the following equation:

$$\mathbf{\Phi'} = \mathbf{B}_{\text{branch}}\mathbf{A'}\mathbf{B'}^{-1}, \tag{10.41}$$

Next, the development of each of the matrices on the right-hand side of (10.41) is presented. $\mathbf{B}_{\text{branch}_{|K|\times|K|}}$ is a diagonal matrix with the diagonal elements being the susceptance of the

lines. The reduced incidence matrix $\mathbf{A}'$ is developed by removing the column associated with the reference bus from $\mathbf{A}$. The relationship between $\mathbf{A}$ and $\mathbf{A}'$ is shown as follows:

$$\mathbf{A}' = \left[\begin{array}{c:c} \mathbf{A} & \mathbf{a}'_{|N|} \end{array} \right]. \tag{10.42}$$

Matrix $\mathbf{B}'_{(|N|-1)\times(|N|-1)}$ can be developed from the admittance matrix [1] $\mathbf{Y}_{|N|\times|N|}$ by first constructing $\mathbf{B}$ with neglecting the resistances and removing the imaginary units, as shown in (10.43). Note that $\mathbf{Y}$ does not have shunt terms.

$$\mathbf{Y} = j\mathbf{B}. \tag{10.43}$$

Then, the column and row associated with the reference bus in $\mathbf{B}$, which are bus $|N|$ and column $|N|$ in this case, are removed. As the calculation of matrix $\mathbf{\Phi'}$ involves the inverse of $\mathbf{B}'$, its invertibility is discussed. The rank of matrix $\mathbf{Y}$ is shown as follows [12, 24]:

$$\text{rank}(\mathbf{Y}) = |N| - 1. \tag{10.44}$$

Therefore, the rank of matrix $\mathbf{B}$ can be determined using (10.43):

$$\text{rank}(\mathbf{B}) = \text{rank}(\mathbf{Y}) = |N| - 1. \tag{10.45}$$

Based on how $\mathbf{B}'$ is developed form $\mathbf{B}$, the following equation can be formulated:

$$\mathbf{B}' = \tilde{\mathbf{I}}^{\mathrm{T}}\mathbf{B}\tilde{\mathbf{I}}, \tag{10.46}$$

where $\tilde{\mathbf{I}}$ is defined as follows:

$$\tilde{\mathbf{I}}_{|N|\times(|N|-1)} = \left[\begin{array}{c:c} \mathbf{I}_{(|N-1|)\times(|N-1|)} \\ \mathbf{0}^{\mathbf{T}} \end{array} \right]. \tag{10.47}$$

The following can be then formulated using the Frobenius inequality:

$$\text{rank}(\mathbf{B}') \geq \text{rank}(\tilde{\mathbf{I}}^{\mathrm{T}}\mathbf{B}) + \text{rank}(\mathbf{B}\tilde{\mathbf{I}}^{\mathrm{T}}) - \text{rank}(\mathbf{B}) \tag{10.48}$$

$$= 2\text{rank}(\tilde{\mathbf{I}}^{\mathrm{T}}\mathbf{B}) - \text{rank}(\mathbf{B}), \tag{10.49}$$

where $\text{rank}(\tilde{\mathbf{I}}^{\mathrm{T}}\mathbf{B})$ satisfies the following inequality based on the Sylvester's rank inequality:

$$\text{rank}(\tilde{\mathbf{I}}^{\mathrm{T}}\mathbf{B}) \geq \text{rank}(\tilde{\mathbf{I}}^{\mathrm{T}}) + \text{rank}(\mathbf{B}) - |N| = |N| - 2. \tag{10.50}$$

The equality in the "$\geq$" in (10.50) holds if and only if the following equation is satisfied [23]:

$$\tilde{\mathbf{I}}^{\mathrm{T}}\mathbf{B} = \mathbf{O}, \tag{10.51}$$

where **O** represents the zero matrix. Apparently, the equation above does not hold as the diagonal elements of **B** are non-zero. Therefore, the rank of $\tilde{\mathbf{I}}^{\mathrm{T}}\mathbf{B}$ satisfies the inequality shown as follows:

$$|N| - 1 \geq \mathrm{rank}(\tilde{\mathbf{I}}^{\mathrm{T}}\mathbf{B}) > |N| - 2, \tag{10.52}$$

which determines that $\mathrm{rank}(\tilde{\mathbf{I}}^{\mathrm{T}}\mathbf{B})$ is $|N| - 1$. Applying this result in (10.48) leads to:

$$\begin{aligned} \mathrm{rank}(\mathbf{B}') &\geq 2\mathrm{rank}(\tilde{\mathbf{I}}^{\mathrm{T}}\mathbf{B}) - \mathrm{rank}(\mathbf{B}) \\ &= 2(|N| - 1) - (|N| - 1) \\ &= |N| - 1. \end{aligned} \tag{10.53}$$

Therefore, $\mathbf{B}'$ is full rank and invertible. Eqn. (10.41) can, therefore, be reformulated as:

$$\mathbf{A'}^{\mathrm{T}}\mathbf{\Phi'}\mathbf{B} = \mathbf{A'}^{\mathrm{T}}\mathbf{B}_{\mathrm{branch}}\mathbf{A}'. \tag{10.54}$$

Let $\boldsymbol{S}$ denote the right-hand side of (10.54), we then have:

$$\boldsymbol{S} = \begin{bmatrix} \tilde{\mathbf{a}'}_1 & \tilde{\mathbf{a}'}_2 & \dots & \tilde{\mathbf{a}'}_{|K|} \end{bmatrix} \begin{bmatrix} b_1 & 0 & \dots & 0 \\ 0 & b_2 & \dots & 0 \\ \vdots & & \ddots & \vdots \\ 0 & \dots & & b_{|K|} \end{bmatrix} \begin{bmatrix} \tilde{\mathbf{a}'}_1^{\mathrm{T}} \\ \tilde{\mathbf{a}'}_2^{\mathrm{T}} \\ \vdots \\ \tilde{\mathbf{a}'}_{|K|}^{\mathrm{T}} \end{bmatrix} = \sum_{i=1}^{|K|} b_i \tilde{\mathbf{a}'}_i \tilde{\mathbf{a}'}_i^{\mathrm{T}}. \tag{10.55}$$

Then, a series of matrices is defined as follows:

$$\boldsymbol{X}_i = b_i \tilde{\mathbf{a}'}_i \tilde{\mathbf{a}'}_i^{\mathrm{T}}, i = 1, 2, \dots, |K|. \tag{10.56}$$

Based on the definition of **A**, elements of matrix $\boldsymbol{X}$ in this series can be shown as follows:

$$(\boldsymbol{X}_k)_{ij} = \begin{cases} b_k & \text{if } i = j \;\&\; i, j \in \{\mathrm{to}(k), \mathrm{fr}(k)\} \\ -b_k & \text{if } i \neq j \;\&\; i, j \in \{\mathrm{to}(k), \mathrm{fr}(k)\} \\ 0 & \text{else} \end{cases} \tag{10.57}$$

$\boldsymbol{S}$, as shown in (10.55), is the summation of matrices $\boldsymbol{X}$. Therefore, its elements can be shown as follows:

$$z_k \in \{0, 1\}, \tag{10.58}$$

$$\text{if } i = j:$$

$$S_{ij} = \sum_{k=1}^{|K|} z_k b_k, z_k = 1 \text{ iff } i \in \{\mathrm{to}(k), \mathrm{fr}(k)\}, \tag{10.59}$$

$$\text{if } i \neq j:$$

$$S_{ij} = \sum_{k=1}^{|K|} -z_k b_k, z_k = 1 \text{ iff } i, j \in \{\mathrm{to}(k), \mathrm{fr}(k)\}, \tag{10.60}$$

which is exactly how matrix $\mathbf{B}$ is defined. Therefore, we have proved that:

$$\mathbf{A'}^{\mathrm{T}}\mathbf{\Phi'}\mathbf{B'} = \mathbf{B'}. \tag{10.61}$$

Eqn. (10.61) is equivalent to:

$$\mathbf{\Phi'}^{\mathrm{T}}\mathbf{A'} = \mathbf{I}. \tag{10.62}$$

Then, calculation of $\mathbf{\Phi}^{\mathrm{T}}\mathbf{A}$ can be shown as follows:

$$\mathbf{\Phi}^{\mathrm{T}}\mathbf{A} = \left[\begin{array}{c} \mathbf{\Phi'}^{\mathrm{T}} \\ \hdashline \mathbf{0}^{\mathrm{T}} \end{array}\right] \left[\begin{array}{c:c} \mathbf{A'} & \mathbf{a'}_{|N|} \end{array}\right] = \left[\begin{array}{c:c} \mathbf{I} & \mathbf{\Phi'}^{\mathrm{T}}\mathbf{a'}_{|N|} \\ \hdashline \mathbf{0}^{\mathrm{T}} & 0 \end{array}\right]. \tag{10.63}$$

The left-hand side of (10.39) can be calculated using (10.40) and (10.63) as follows:

$$\begin{aligned} \mathbf{\Phi}^{\mathrm{T}}\mathbf{A}\mathbf{\Phi}^{\mathrm{T}} &= \left[\begin{array}{c:c} \mathbf{I} & \mathbf{\Phi'}^{\mathrm{T}}\mathbf{a'}_{|N|} \\ \hdashline \mathbf{0}^{\mathrm{T}} & 0 \end{array}\right] \left[\begin{array}{c} \mathbf{\Phi'}^{\mathrm{T}} \\ \hdashline \mathbf{0}^{\mathrm{T}} \end{array}\right] \\ &= \left[\begin{array}{c} \mathbf{I}\mathbf{\Phi'}^{\mathrm{T}} \\ \hdashline \mathbf{0}^{\mathrm{T}} \end{array}\right] = \left[\begin{array}{c} \mathbf{\Phi'}^{\mathrm{T}} \\ \hdashline \mathbf{0}^{\mathrm{T}} \end{array}\right] = \mathbf{\Phi}^{\mathrm{T}}. \end{aligned} \tag{10.64}$$

Therefore, (10.39) holds, which proves Lemma 4.

Finally, Eqn. (10.36) can be interpreted as:

$$TLP - TPR = TCR = TTR + TGR. \tag{10.65}$$

Equation (10.65) shows that GET revenue is part of the congestion rent and can be covered by the load payment without the need for any side payments. Therefore, the revenue adequacy of the proposed market design is proved. It is also shown that under the proposed structure, existing financial transmission obligations, such as FTRs, can be covered through the total transmission revenue calculated using FMPs.

10.4 Numerical Studies

Numerical studies are carried out on the IEEE RTS 24-bus system [8] and the IEEE 118-bus system, with results presented in this section. The test systems are modified with increased congestion levels to better demonstrate the effectiveness of GET implementations with sizable savings. GET placement is determined following an engineering judgment that chooses lines with higher susceptance price values. It is worth noting that this study focuses on operation, and optimal GET allocation is beyond the scope of the paper. The proposed market design is illustrated through numerical results. Furthermore, the GET owners' annual revenues in the proposed market mechanism are compared

with regulated returns. Results in this aspect show the effectiveness of the proposed method in incentivizing GET investments. Optimization problems are set up in Python with CVXPY [6] and solved using CPLEX 22.10.

10.4.1 24-Bus System

The IEEE 24-bus system data is obtained from [5]. The system is modified by reducing the thermal capacities of lines under high utilization to increase congestion. Modifications to the capacities of certain transmission branches are shown in Table 10.2. GET placement in the 24-bus system is shown in Table 10.1.

The proposed market design is first implemented in a single-hour operation case with peak load to validate the mathematical derivations and demonstrate revenue adequacy. The results are presented in Table 10.3. Furthermore, Figure 10.3 indicates that the aggregate revenue equals total load payments.

Annualized returns of GET owners are estimated following the method in [22], which selects representative days of different seasons to calculate seasonal returns. This method uses Thursday, Saturday, and Sunday as representative days of a week and selects weeks 11, 25, and 51 as typical weeks of spring, summer, and winter, respectively. Note that the 11th week also represents autumn, as it has a similar load profile as spring. Hourly GET revenues are calculated using (10.8) with DCOPF results of the 216 representative time periods and provide the basis to obtain the estimated annual market revenue (AMR) under the proposed market design.

The AMR results are compared with the annual regulated revenue (ARR) under RoR. To obtain ARR, we first calculate the device cost of the VSC-based FACTS as follows:

$$C_i^{\text{FACTS}} = S_i^{\text{FACTS}} C^{\text{FACTS}} = V_k^{\text{FACTS}} I_k^{\max}, \tag{10.66}$$

where FACTS ratings are calculated using the equation below [7]:

$$S^{\text{FACTS}} = V_k^{\text{FACTS}} \bar{I}_k \approx V_k^{\text{FACTS}} f_k^{\max}. \tag{10.67}$$

The calculation of the PST cost is shown as follows [27]:

$$C_i^{\text{PST}} = C^{\text{PST}} S_{k(i)} = f_{k(i)}^{\max} C^{\text{PST}}. \tag{10.68}$$

The unit costs of SSSC and PST devices, C^{FACTS} and C^{PST}, are set at \$150/kVA and \$100/kVA, respectively [28, 27]. The ARR is calculated assuming a 10% RoR (110% gross return) and

an interest rate of 6%. Additionally, the lifespan of the devices is considered to be 15 years. The comparison between the AMR and the ARR for the 24-bus system is presented in Figure 10.4. The results show that under the proposed market design, revenues of both GET deployments are much higher than regulated returns based on investment costs. This demonstrates the effectiveness of the proposed market design in incentivizing GET investments.

10.4.2 300-Bus System

This part of the numerical studies is conducted to test the effectiveness of the proposed market design on a larger system, with more options for installation locations. GET deployments are increased and consist of different types of technologies. The system data is obtained from the IEEE 300-bus test case v23.07 in the IEEE PES power grid library (PGlib) [3]. Again, certain highly utilized braches have their thermal capacities reduced to increase congestion in the system. The modifications are shown in the Table 10.4. GET allocation in the 300-bus system is presented in Table 10.5.

AMR and ARR results are obtained following the same approach for the 24-bus system and are shown in Figure 10.5. Again, the results show that for each of the GET deployments, AMR is much higher than ARR. GET investors will collect much more revenue under the proposed market design than under a RoR.

It is worth noting that the GET revenues of each deployment display a disparity. This is due to certain locations being much more effective than others regarding GET placement. Additionally, the deployments at different locations can belong to the same asset owner, and the summation of their revenues will be the total revenue of the owner.

10.5 Conclusion

Proper incentives are vital to increasing GET deployments in the power grid for transfer capability enhancements. This chapter presents a market design that provides financial compensation to GET operations. The proposed mechanism is simple, straightforward, and based on integrating GETs in power system operation models. GET revenues under the proposed structure are calculated using the marginal prices associated with GET operation constraints and are settled along with generation dispatch. Simulation studies

show that GET owners can collect a fair amount of revenues significantly higher than the regulated returns. The proposed market design is expected to provide significant incentives to GET investments. Future research will focus on integrating other types of GETs with nonlinear modeling into the proposed market design.

10.6 References

[1] *The DC Power Flow Equations*. Accessed: 2024-04-29.

[2] V. Asgharian and M. Abdelaziz, *A low-carbon market-based multi-area power system expansion planning model*, Electric Power Systems Research, 187 (2020), p. 106500.

[3] S. Babaeinejadsarookolaee, A. Birchfield, R. D. Christie, C. Coffrin, C. DeMarco, R. Diao, M. Ferris, S. Fliscounakis, S. Greene, R. Huang, et al., *The power grid library for benchmarking AC optimal power flow algorithms*, arXiv preprint arXiv:1908.02788, (2019).

[4] J. Contreras, G. Gross, J. M. Arroyo, and J. I. Muñoz, *An incentive-based mechanism for transmission asset investment*, Decision Support Systems, 47 (2009), pp. 22–31.

[5] Department of Electrical Engineering, University of Washington, *Power systems test case archive*.

[6] S. Diamond and S. Boyd, *CVXPY: A Python-embedded modeling language for convex optimization*, Journal of Machine Learning Research, (2016). To appear.

[7] P. O. Dorile, D. R. Jagessar, and R. A. McCann, *Techno-economic assessment of voltage stability improvement using sssc and statcom in a wind-dominated power system*, in 2021 IEEE Kansas power and energy conference (KPEC), IEEE, 2021, pp. 1–6.

[8] C. Grigg, P. Wong, P. Albrecht, R. Allan, M. Bhavaraju, R. Billinton, Q. Chen, C. Fong, S. Haddad, S. Kuruganty, et al., *The IEEE reliability test system-1996. a report prepared by the reliability test system task force of the application of probability methods subcommittee*, IEEE Transactions on Power Systems, 14 (1999), pp. 1010–1020.

[9] R. Hemmati, R.-A. Hooshmand, and A. Khodabakhshian, *Coordinated generation and transmission expansion planning in deregulated electricity market considering wind farms*, Renewable Energy, 85 (2016), pp. 620–630.

[10] M. R. Hesamzadeh, J. Rosellón, S. A. Gabriel, and I. Vogelsang, *A simple regulatory incentive mechanism applied to electricity transmission pricing and investment*, Energy Economics, 75 (2018), pp. 423–439.

[11] Jay Caspary, *The Role for Grid-Enhancing Technologies*, January 2022. Accessed: 2023-07-25.

[12] A. M. Kettner and M. Paolone, *On the properties of the power systems nodal admittance matrix*, IEEE Transactions on Power Systems, 33 (2018), pp. 1130–1131.

[13] O. Mirzapour, X. Rui, and M. Sahraei-Ardakani, *Transmission impedance control impacts on carbon emissions and renewable energy curtailment*, Energy, 278 (2023), p. 127741.

[14] ——, *Grid-enhancing technologies: Progress, challenges, and future research directions*, Electric Power Systems Research, 230 (2024), p. 110304.

[15] N. Mithulananthan and N. Acharya, *A proposal for investment recovery of FACTS devices in deregulated electricity markets*, Electric Power Systems Research, 77 (2007), pp. 695–703.

[16] K. Rebane, K. Siegner, and S. Toth, *Cheaper, Cleaner, Faster - Four strategies utility regulators can use to accelerate new renewables interconnection.*, July 2023. Accessed: 02-27-2024.

[17] J. H. Roh, M. Shahidehpour, and Y. Fu, *Market-based coordination of transmission and generation capacity planning*, IEEE Transactions on Power Systems, 22 (2007), pp. 1406–1419.

[18] X. Rui, O. Mirzapour, B. Pruneau, and M. Sahraei-Ardakani, *A review of economic incentives for efficient operation of flexible transmission*, in 2023 North American Power Symposium (NAPS), IEEE, 2023, pp. 1–6.

[19] X. Rui, M. Sahraei-Ardakani, and T. R. Nudell, *Linear modelling of series FACTS devices in power system operation models*, IET Generation, Transmission & Distribution, 16 (2022), pp. 1047–1063.

[20] M. Sahraei-Ardakani, *Merchant power flow controllers*, Energy Economics, 74 (2018), pp. 878–885.

[21] M. Sahraei-Ardakani and S. A. Blumsack, *Transfer capability improvement through market-based operation of series FACTS devices*, IEEE Transactions on Power Systems, 31 (2015), pp. 3702–3714.

[22] Y. Sang and M. Sahraei-Ardakani, *The interdependence between transmission switching and variable-impedance series facts devices*, IEEE Transactions on Power Systems, 33 (2017), pp. 2792–2803.

[23] N. Thome, *Inequalities and equalities for $\ell = 2$ (sylvester), $\ell = 3$ (frobenius), and $\ell > 3$ matrices*, Aequationes mathematicae, 90 (2016), pp. 951–960.

[24] D. Turizo and D. K. Molzahn, *Invertibility conditions for the admittance matrices of balanced power systems*, IEEE Transactions on Power Systems, 38 (2023), pp. 3841–3853.

[25] U.S. Department of Energy, *Grid Enhancing Technologies - A Case Study on Ratepayer Impact - February 2022*. U.S. Department of Energy, 2022. Executive Summary.

[26] WATT Coalition, *Frequently Asked Questions about a shared savings incentive for Grid Enhancing Technologies*, 2022. Accessed: 2023-07-25.

[27] X. Zhang, D. Shi, Z. Wang, B. Zeng, X. Wang, K. Tomsovic, and Y. Jin, *Optimal allocation of series FACTS devices under high penetration of wind power within a market environment*, IEEE Transactions on Power Systems, 33 (2018), pp. 6206–6217.

[28] I. Zunnurain, Y. Sang, P. Mandal, M. Velez-Reyes, and J. Espiritu, *Improving the resilience of large-scale power systems using distributed static series compensators*, International Journal of Electrical Power & Energy Systems, 145 (2023), p. 108702.

Table 10.1. GET allocation in the 24-bus system

GET	Location	Type	Operating limit
1	A23	FACTS	0.05 pu
2	A27	PST	0.03 pu

Table 10.2. Modifications to the 24-bus system

Brach No.	Capacity reduction (%)
A7,A21	50
A23, A27	60

Table 10.3. Results of the single-hour case

TLP	TPR	TTR	TGR
$168.252K	$124.427K	$37.065K	$6.765K

Table 10.4. Modifications to the 300-bus system

Brach No.	Capacity reduction (%)
61, 91, 101	60
115, 137, 365, 395	50
268	40

Table 10.5. GET allocation in the 300-bus system

GET	Location	Type	Operating limit
1	61	PST	10 degrees
2	91	PST	10 degrees
3	105	FACTS	0.03 pu
4	177	FACTS	0.03 pu
5	182	FACTS	0.03 pu
6	358	FACTS	0.03 pu

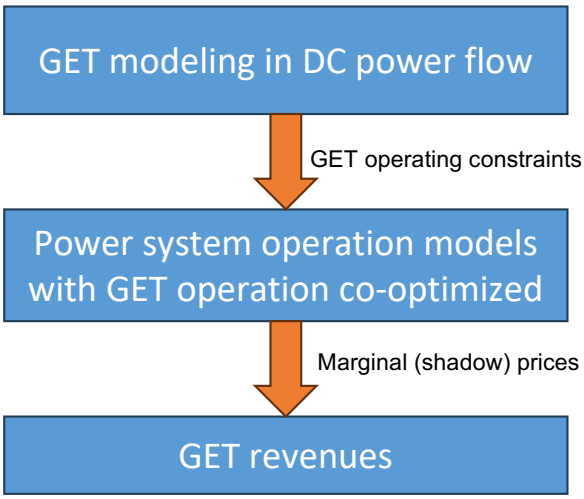

Figure 10.1. GET revenues in electricity markets considering GET operations

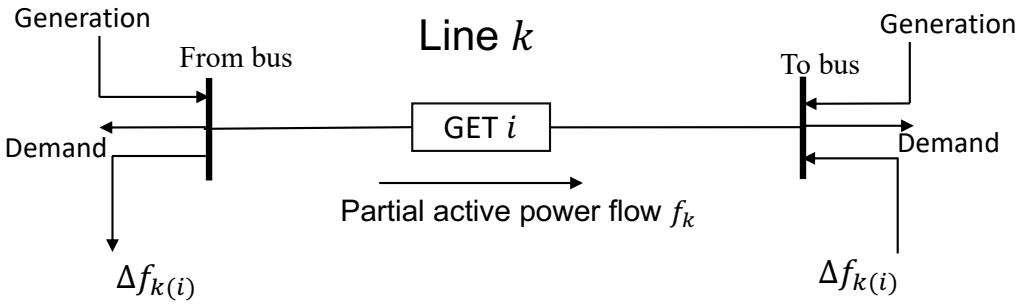

Figure 10.2. Nodal power injection model of GETs

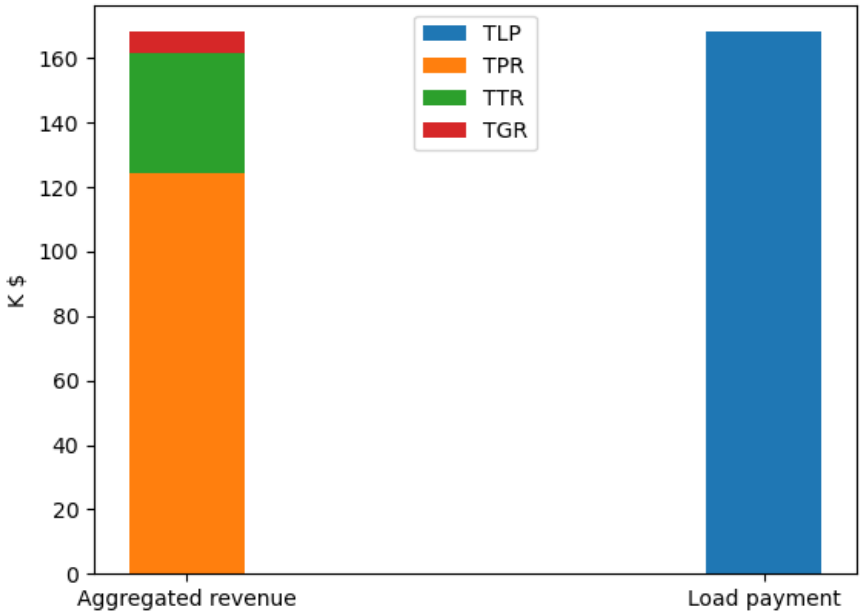

Figure 10.3. Comparison between revenues and load payments

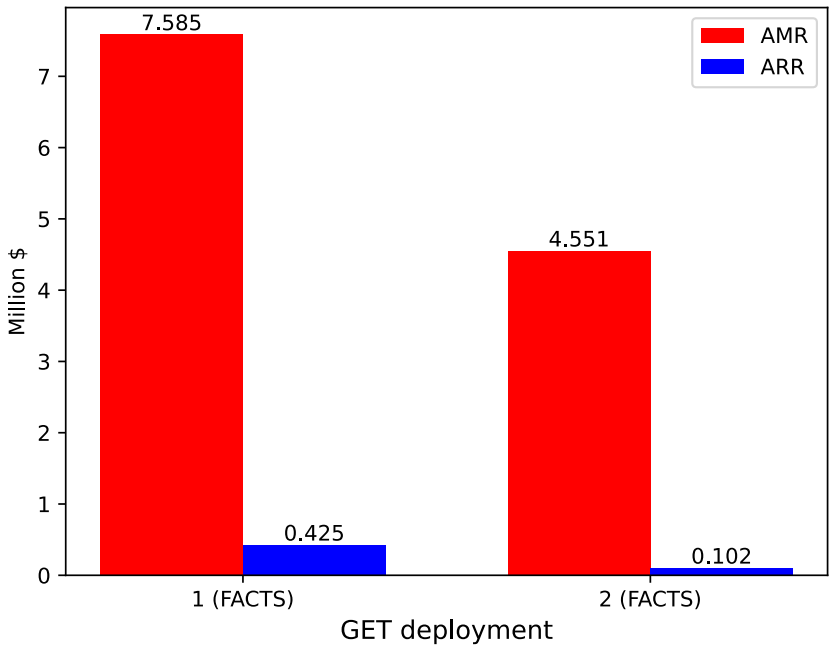

Figure 10.4. Comparison between AMR and ARR for GETs in the 24-bus system

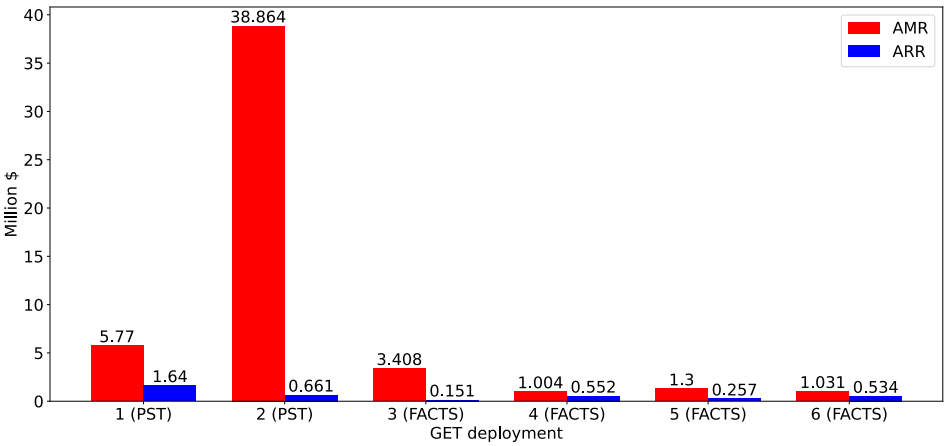

Figure 10.5. Comparison between AMR and ARR for GETs in the 300-bus system

CHAPTER 11

CONCLUSIONS AND FUTURE DIRECTIONS

This dissertation presents models, algorithms, and market mechanisms that will facilitate the deployment of grid-enhancing technologies (GETs) in the transmission grid. In this chapter, the conclusions and a discussion on future research are presented.

11.1 Conclusions

This dissertation focuses on tackling key challenges hindering the deployment of GETs in the power grid. The main focus of studies presented in Chapters 2-7 is on modeling and solution techniques that facilitate the integration of GETs into power system optimization. Chapter 2 presents models of various FACTS technologies that accurately reflect the operating principles of the technologies in DC power flow. Series FACTS rely on different methods to achieve series compensation. The results show that the operating ranges of different types of series FACTS devices can be modeled using linear or mixed-integer linear formulations, thus facilitating integration into the existing market management tools and ensuring computational efficiency when co-optimizing FACTS operation in power system operation and planning models. Chapter 2 highlights the importance of the perspective of not solely regarding series compensation as reactance adjustments but from the point of nodal injection modeling. The models also provide the basis for other studies presented in this dissertation. Chapter 3 presents the successive flow direction enforcing (SFDE) algorithm developed for the optimal operation of variable-impedance FACTS devices. The SFDE algorithm extends the application of the flow direction enforcing to UC models. The numerical results show that the SFDE algorithm addresses the potential suboptimality issue of using the flow direction results from a base case model. It also maintains computational efficiency superiority over directly solving DCOPF or UC models with mixed-integer FACTS constraint formulations. Chapters 4-6 presents the studies on GET operations in complex optimization problems. Results in Chapter 4 show that FACTS

operation adds immense computational burden to the already challenging SUC problem. However, such computational challenges can be effectively tackled by the parallelization of the progressive hedging algorithm. Chapter 5 shows that the modeling presented in Chapter 2 allows smooth integration of series FACTS into the ADMM-based distributed DCOPF. The result is essential for optimal FACTS operation in a distributed control scheme when they are placed on lines that transfer energy between neighboring subsystems. GET operations are further studied in a risk-averse two-stage SUC model in Chapter 6, with results showing that GETs can potentially lead to increased risk of unserved load, stressing the importance of risk control measures. The case studies in this chapter are the first in the literature to reveal such an effect and serve as an essential reference for GET operation. In Chapter 7, a sensitivity-based method for FACTS placement is developed based on the modeling shown in Chapter 2 and shadow prices from the DCOPF dual solution. This method can facilitate the often complex optimization process of FACTS planning. Overall, this part of the thesis advances the research on incorporating GETs into power system operation and planning. The results are essential tools for the full utilization of GETs under various circumstances.

This dissertation also proposes market mechanisms to provide financial incentives to GET investments. They both follow a performance-based approach while using different methods to calculate payoffs to GETs. Chapter 9 shows an incentive scheme that uses an improved Shapley value method to distribute benefits, which are the social welfare positives created by GET operations, to GET owners. The improved Shapley value resets the GET operating limits based there setpoints to reflect the contributions accurately, thus enhancing market efficiency. In Chapter 10, a revenue-adequate market design is presented, which uses dual variables of GET operation constraints as marginal prices. Mathematical proof shows that the proposed method is revenue-adequate, meaning that GET revenues are part of the congestion rent. Both proposed mechanisms are compared with a regulated RoR, with results demonstrating the superiority of offering performance-based financial compensation to asset owners.

11.2 Future Directions

This dissertation addresses several critical issues regarding integrating GETs into grid operation and planning while providing the basis for studies to further advance research on GET-related topics. Several challenges can be tackled by future research to facilitate the application of the methodologies proposed in this dissertation.

11.2.1 Planning of GETs

Effective utilization of GETs requires proper allocation, which involves placement and sizing, in the transmission systems. Planning of GETs is a widely studied topic in the existing literature. However, the performance-based market mechanisms can add complexities to the problem. The optimal allocation of GETs is commonly formulated in a centralized manner considering the social welfare positives and investment costs. Under the proposed market mechanisms, GET owners will consider their potential payoffs as there is a disparity in the effectiveness of GET operations at different locations. Therefore, the planning process can become a bilevel optimization problem. This is an essential topic for GETs and should be further studied in future research.

11.2.2 Computational Efficient Calculation of Shapley Values

The Shapley value provides a fair benefit distribution approach and is the foundation of the incentive scheme shown in Chapter 9. However, determining the Shapley value requires calculating the characteristic function for 2^n coalitions. This leads to computation complexity issues when there is a large group of participants in the coalition game. Therefore, an efficient method to calculate or estimate the Shapley values is an essential topic for future studies.

11.2.3 Integration of GETs into the Proposed Market Design

The market design presented in Chapter 10 is demonstrated with a DCOPF formulation considering two prominent types of GETs, VSC-based FACTS and PSTs. These power flow control technologies can be represented with a unified linear constraint formulation, allowing convenient derivation of revenues based on shadow prices. However, other types of GETs follow different modeling approaches, with some involving integer variables. Future research should focus on integrating various GETs into the proposed market design and

derive their shadow-price-based revenues. The mathematical derivations in Chapter 10 provide the basis for future developments, which can be facilitated by flow direction enforcement.

APPENDIX A

DETAILS OF MATRICES

In this appendix, we show the construction of some of the matrices in Chapter 10 by showing detailed definitions of their elements.

First, the incidence matrix $\mathbf{A}$:

$$\mathbf{A}_{kn} = \begin{cases} 1 & \text{if } n = \text{to}(k) \\ -1 & \text{if } n = \text{fr}(k) \\ 0 & \text{else} \end{cases}, \quad n \in N, k \in K. \tag{A.1}$$

Second, the generator location matrix $\mathbf{\Gamma}$:

$$\mathbf{\Gamma}_{ng} = \begin{cases} 1 & \text{if } n(g) = n \\ 0 & \text{else} \end{cases}, \quad n \in N, g \in G. \tag{A.2}$$

Finally, the GET placement matrix $\mathbf{\Psi}$:

$$\mathbf{\Psi}_{ki} = \begin{cases} 1 & \text{if } k(i) = k \\ 0 & \text{else} \end{cases}, \quad k \in K, i \in \mathcal{G}. \tag{A.3}$$

APPENDIX B

NOTATION AND SYMBOLS FOR CHAPTER 6

Table B.1. Notation and symbols for Chapter 6

Sets and indices	
S, T	Sets of time periods and scenarios
N,G,K, W	Sets of buses, generators, transmission branches, and wind farms
$G(n)$	Set of generators connected to bus n
$W(n)$	Set of wind farms connected to bus n
K^{DLR}	Set of transmission lines equipped with DLR
$\tilde{K}$	Set of transmission lines equipped with FACTS or TS
$\delta^+(n)$,$\delta^-(n)$	Sets of branches connected "to" and "from" bus n
n,g,k, w	Indices of buses, generators, transmission branches, and wind farms
t	Index of time periods
s	Index of scenarios
Parmeters	
Φ_k^n	ISF of branch k regarding bus n
c^{ls}	Load shedding cost
$c_g^{\min}$	Cost of minimum output of generator g
d_{nt}	Demand at bus n in time period t
c_g^q,	Linear cost of generator g in segment q
$\overline{p}_g$, $\underline{p}_g$	Generator output limits
$\overline{f}_k$	Thermal capacity of transmission branch k
$p_g^{q,\max}$	Maximum output of generator g in segment q
δ_{kts}	DLR factor on line k, in time period t, under scenario s
c_g^{SU}, c_g^{SU}	Startup and shutdown costs of generator g
UT_g, DT_g	Minimum up and minimum down time of generator g
RD_g, RD_g^{SD}	Ramp-down limits of generator g
RU_g, RU_g^{SU}	Ramp-up limits of generator g
Variables	
p_{gts}	Output of generator g in time period t under scenario s
p_{wts}^{wind}	Output of wind farm w in time period t under scenario s
l_{nts}^{sh}	Load shedding at bus n in time period t under scenario s
f_{kts}	(Partial) power flow of branch k in time period t under scenario s
Δf_{kts}	GET nodal injection of branch k in time period t under scenario s
v_{gt}, z_{gt}	Startup, and shutdown variables of generator g in time period t
u_{gt}	Unit commitment variable of generator g in time period t

APPENDIX C

NOTATION AND SYMBOLS FOR CHAPTER 10

Table C.1. Notation and symbols for Chapter 10

Sets	
$\mathcal{G}$	Set of GET deployments
N,G,K	Sets of buses, generators, and transmission branches
Indices	
n, g, k	Indices of buses, generators, and transmission branches
i	Index of GET deployments
$k(i)$	Index of transmission line k with GET i deployed
to(k), to(k)	"to" and "from" buses of transmission branch k
Parmeters	
$V_i^{\max}$	Maximum FACTS voltage injection
$\theta_i^{\max}$	Maximum PST angle adjustment
$\mathbf{d}$	Vector of nodal Demands
$\mathbf{c}$	Vector of linear costs of generators
$\mathbf{p}^{\min}$, $\mathbf{p}^{\max}$	Minimum and maximum output of generators
$\mathbf{\Delta f}^{\max}$,$\mathbf{\Delta f}^{\min}$	GET nodal injection upper and lower bounds
$\mathbf{A}$	Incidence matrix
$\mathbf{\Phi}$	Injection shift factor matrix
$\mathbf{\Psi}$	GET placement matrix
$\mathbf{\Gamma}$	Generator location matrix
C_i^{FACTS}, C_i^{PST}	Device costs of FACTS and PST
S_i^{FACTS}	FACTS device rating
S_k	Transmission line rating
Variables	
$\mathbf{p}$	Vector of generator outputs
$\mathbf{f}$	Vector of (partial) power flows
$\mathbf{\Delta f}$	GET nodal injection
$\boldsymbol{\beta}^+$, $\boldsymbol{\beta}^-$	Flowgate marginal prices
$\boldsymbol{\alpha}^+$, $\boldsymbol{\alpha}^-$	Generator capacity prices
$\boldsymbol{\tau}^+$, $\boldsymbol{\tau}^-$	GET marginal prices
TGR	Total GET revenue
TTR	Total transmission revenue
TPR	Total production revenue
TLP	Total load payment